Novel roles of matrix metalloproteinase-2 in myocardial oxidative stress injury

by

Brandon Ying-How Chan

A thesis submitted in partial fulfillment of the requirements for the degree of

Doctor of Philosophy

Department of Pharmacology
University of Alberta

ABSTRACT

Matrix metalloproteinase-2 (MMP-2) is a zinc-dependent protease that proteolyzes numerous substrates both inside and outside the cell when activated during oxidative stress. However, the full gamut of MMP-2 substrates in myocardial oxidative stress injury is largely unknown. This thesis investigates novel targets of MMP-2 and the effect of MMP inhibitors in two cardiac pathologies associated with increased oxidative stress: anthracycline cardiotoxicity and ischemia-reperfusion injury.

Oxidative stress is one of the major mechanisms of anthracycline cardiotoxicity. I showed that treating cardiomyocytes with the anthracycline doxorubicin enhanced cellular oxidative stress and concomitantly increased MMP-2 levels/activity. Doxorubicin enhanced MMP-2 activity in cardiomyocytes by two means: i) oxidative stress increased the levels and activity of 72 kDa MMP-2 and ii) oxidative stress triggers the de novo expression of N-terminal truncated MMP-2. Doxorubicin also increased the levels of MMP-2 secreted into the conditioned medium. Doxorubicin-induced cardiomyocyte injury was associated with reduced troponin I, SERCA2a, and phospholamban protein levels. However, MMP inhibitors did not prevent the loss of these proteins as doxorubicin reduced their expression at a transcriptional level.

Anthracycline cardiotoxicity is associated with extracellular matrix remodeling and myofilament lysis. Mice treated with doxorubicin exhibited cardiac contractile dysfunction and left ventricular remodeling in vivo. Ultrastructural analysis of the left ventricle showed that doxorubicin caused significant sarcomeric degeneration including myofilament lysis, reduced sarcomere lengths, and damage to the Z-disc and M-line. Doxorubicin also caused cardiac titin proteolysis and interstitial fibrosis. This was accompanied by increased MMP-2 levels/activity in

the heart and increased MMP-2 localization in the sarcomere and mitochondria. I demonstrated that mice treated with two orally available MMP inhibitors ameliorated doxorubicin-induced cardiac contractile dysfunction by attenuating titin proteolysis, interstitial fibrosis, and/or left ventricular remodeling.

Junctophilin-2 is a structural protein which tethers the T-tubule to the sarcoplasmic reticulum to allow for coordinated calcium-induced calcium release in cardiomyocytes. Junctophilin-2 proteolysis and intracellular calcium overload are implicated in myocardial ischemia-reperfusion injury. I found that degradation of junctophilin-2 in isolated rat hearts subject to ischemia-reperfusion injury contributes to cardiac contractile dysfunction. Furthermore, inhibition of MMP-2 prevented junctophilin-2 proteolysis and improved the recovery of cardiac contractile function during ischemia-reperfusion. In vitro degradation assays revealed that junctophilin-2 is susceptible to proteolysis by MMP-2 and this was prevented by MMP inhibition. I showed for the first time that MMP-2 is co-localized to junctophilin-2 in the Z-disc region of the sarcomere.

In summary, these studies show that MMP-2 plays an important role in the initiation and propagation of acute and chronic oxidative stress injury to the heart. Activation of MMP-2 by oxidative stress causes adverse remodeling of the intracellular and extracellular matrices. More importantly, these studies demonstrate the cardioprotective effects of MMP inhibitors in vivo and ex vivo against cardiac pathologies associated with increased oxidative stress. MMP inhibitors may be a potential therapeutic strategy to prevent cardiovascular disease.

PREFACE

This thesis is an original work by Brandon Chan. The research project of which this thesis is a part of received research ethics approval from the University of Alberta Animal Care and Use Committee, "MMP-2 in cardiovascular health and disease", AUP 00000329, Dr. Richard Schulz, Principal Investigator.

A portion of Chapter 1 of this thesis has been published in a book chapter as Chan BYH, Roczkowsky R, Ilarraza R, Schulz R. Matrix metalloproteinase-2 (2018). Matrix metalloproteinase-2. In: *Encyclopedia of Signaling Molecules, 2nd Edition*. S. Choi (ed.). Springer, Cham. Pp. 2996-3005. A portion of Chapter 2 of this thesis has been published as Chan BYH, Roczkowsky R, Moser N, Poirier M, Hughes BG, Ilarraza R, Schulz R. "Doxorubicin induces de novo expression of N-terminal truncated MMP-2 in cardiac myocytes," *Canadian Journal of Physiology and Pharmacology*, 2018;96(12):1238-45.

Dedicated to my parents and family,

for their love, support, and sacrifices

ACKNOWLEDGEMENTS

First and foremost, I would like to thank my supervisor *Dr. Richard Schulz* for his mentorship and giving me the opportunity to realize my passion. Your guidance and advice helped mold me into the critical thinking scientist that I am today. Your unwavering spirit during times of adversity has forever inspired me to never give up.

I would also like to thank members of the Schulz lab, past and present, for their help in my studies. In particular, a special thank you to *Mathieu Poirier* and *Andrej Roczkowsky* for their lifelong friendship. I would not have been able to accomplish this without your teamwork and dedication through the years. I would also like to thank *Dr. Javier Garcia* for always challenging me to take great leaps and *Nils Moser* for his technical assistance in the cardiomyocyte study.

I would like to thank *Dr. Henk Granzier* and members of his lab for their hospitality at the University of Arizona and introducing me to the field of titin biology. Thank you to *Donna Beker* for performing the echocardiography for the in vivo mouse study. Thank you *Woo Jung Cho* for teaching and helping me with electron microscopy.

I would like to thank my supervisory committee members *Dr. Jason Dyck*, *Dr. James Hammond*, and *Dr. John Mackey*. Your advice and feedback have been invaluable throughout the course of my training.

I am thankful to the Women and Children's Health Research Institute, the Faculty of Medicine and Dentistry, and Novartis Pharmaceuticals Canada for their funding support.

My deepest gratitude goes to my parents, *Alex* and *Diana Chan*. Your unconditional love since the very beginning is the reason why I can chase my goals and realize my dreams. To my sister, *Amanda Chan*, the best role model anyone could ask for. Thank you for your continued

support and encouragement. Finally, I thank my girlfriend, *Mary Zhang*, who has been my source of strength throughout this journey.

TABLE OF CONTENTS

LIST OF TABLES

LIST OF FIGURES

LIST OF ABBREVIATIONS

ANOVA	analysis of variance
AP-1	activated protein -1
APMA	4-aminophenyl mercuric acetate
BCA	bicinchoninic acid
B2M	beta-2-microglobulin
CXCL1	chemokine (C-X-C) motif ligand 1
DAPI	4',6-diamidino-2-phenylindole
DMEM	Dulbecco's modified Eagle medium
DMSO	dimethyl sulfoxide
Doxy	doxycycline
IC_{50}	concentration of antagonist or inhibitor which in inhibits 50% of measure response
IL-6	interleukin-6
IR	ischemia-reperfusion
JPH	junctophilin
kDa	kilodalton
LDH	lactate dehydrogenase
miR	micro ribonucleic acid
MMP	matrix metalloproteinase
MORN	membrane occupation and recognition nexus
MT-MMP	membrane-type matrix metalloproteinase
NRVM	neonatal rat ventricular myocytes

NTT-MMP-2	N-terminal truncated matrix metalloproteinase-2
PBS	phosphate buffered saline
PEVK domain	proline-glutamate-valine-lysine domain
qPCR	quantitative polymerase chain reaction
RBM20	ribonucleic acid binding motif 20
PVDF	polyvinylidene difluoride
RIPA	radioimmunoprecipitation assay
RNA	ribonucleic acid
ROI	region of interest
RONS	reactive oxygen and nitrogen species
SDS-PAGE	sodium dodecyl sulfate polyacrylamide gel electrophoresis
SEM	standard error of the mean
SERCA	sarco/endoplasmic reticulum calcium ATPase
TBS-T	Tris-Tween buffered saline
TIMP	tissue inhibitor of metalloproteinases

CHAPTER 1

GENERAL INTRODUCTION

A portion of this chapter is published in a book chapter:

Chan BYH, Roczkowsky R, Ilarraza R, Schulz R. Matrix metalloproteinase-2 (2018). Matrix metalloproteinase-2. In: *Encyclopedia of Signaling Molecules, 2nd Edition*. S. Choi (ed.). Springer, Cham. Pp. 2996-3005.

1.1 Introduction to matrix metalloproteinases

In 1962, Gross and Lapiere detected collagen degrading activity secreted from the tail of tadpoles undergoing metamorphosis[1]. This discovery surprised many as the native triple-helical configuration of collagen was unusually resistant to proteolysis by a wide variety of neutral proteases including trypsin and chymotrypsin[2]. This collagenolytic activity was later attributed to matrix metalloproteinases[3], a family of zinc and calcium-dependent endopeptidases that collectively play an important role in degrading components of the extracellular matrix[4].

Nearly two decades after the discovery of MMP-1, Liotta et al[5] reported proteolytic activity secreted from an invasive murine tumor that was capable of degrading basement membrane type IV collagen. It was not until 1988 that this 72 kDa protease was sequenced and identified as MMP-2, also known as type IV collagenase or gelatinase A[6]. This provided an important leap in our understanding of MMP-2 as it revealed characteristics of its proteolytic and extracellular substrate specificity profile which includes gelatin, laminin, fibronectin, and type IV and V collagen[7].

Initially, only extracellular matrix proteins were investigated as potential MMP-2 substrates, as MMPs in general were believed to be secreted and function exclusively in the extracellular space. This paradigm has since then been unequivocally challenged as subsequent studies have identified a plethora of non-matrix extracellular and intracellular substrates of MMP-2[8-10]. These seminal discoveries revealed the important roles of MMPs in long-term processes at the extracellular matrix and short-term processes inside the cell that underlie a vast range of physiological and pathological conditions.

1.1.1 Classification

To date, there are 25 members of the MMP family, 23 of which are found in humans[11, 12]. MMPs are subcategorized into five classes based on their primary sequence, extracellular substrate specificity, and cellular localization: collagenases (MMP-1, MMP-8, MMP-13), gelatinases (MMP-2, MMP-9), stromelysins (MMP-3, MMP-10, MMP-11, MMP-12), matrilysins (MMP-7 and MMP-26), membrane type (MT)-MMPs (MT1-MMP through MT6-MMP), and nonclassified MMPs[13, 14]. However, this nomenclature is highly arbitrary. Many MMPs no longer suit these categories given their broader biological roles in proteolyzing additional substrates to the ones they were originally named after. In addition to their canonical roles in remodeling the extracellular matrix, MMPs are now recognized to target non-matrix substrates both outside and inside the cell[8, 10, 11]. Our improved understanding of MMP biology contests whether 'matrix' should be removed as a descriptor of this class of metalloproteases.

1.1.2 Biosynthesis and structure

MMPs are generally synthesized as zymogens or inactive precursors. MMPs consist of a removable N-terminal signal sequence that allows the protease to be translocated to the endoplasmic reticulum for subsequent secretion from the cell. Next to the signal sequence is a hydrophobic propeptide domain consisting of three α-helices which shield the catalytic domain. The catalytic domain of MMPs consists of five β-sheets, three α-helices, and a conserved zinc-binding motif (HEXXHXXGXXH) with three histidines coordinating the catalytic zinc. Outside of the catalytic site, MMPs also contain an additional zinc-binding site and at least two calcium binding sites which facilitate proper folding of the enzyme[15, 16]. The catalytic domain is connected to a hemopexin-like domain by a flexible hinge region. The crystal structure of human MMP-2 is depicted in Fig. 1.1. MT-MMPs contain either a transmembrane domain or a

glycosylphosphatidylinositol moiety at the C-terminus that anchors the protein at the plasma membrane.

In humans, the MMP-2 gene contains 13 exons and spans 27.9 kilobases of the q12.2 region in chromosome 16. MMP-2 is translated as an inactive 72 kDa zymogen consisting of five structural domains: a removal N-terminal pre-domain containing a secretory signal peptide (aa 1-29), an autoinhibitory pro domain (aa 30-109), a catalytic zinc domain (aa 110-435), a hinge region and a hemopexin domain (aa 466-660, Figure 1.2)[15]. In its zymogen form, the catalytic zinc coordinates with the conserved Cys102 residue in the propeptide domain which renders it inactive. Unlike other MMPs, the gelatinases (MMP-2 and MMP-9) contain three fibronectin type II repeats within the catalytic domain, which allow for the binding and cleavage of type IV collagen or gelatin (denatured collagen)[15]. Additional substrate specificity is conferred by the hemopexin domain, which is linked to the catalytic domain via the hinge region. The hemopexin domain is also critical for the proteolytic activation of MMP-2 (discussed in Section 1.2.2).

To date, at least four additional isoforms of MMP-2 have been identified including an extracellular isoform and three distinct intracellular isoforms[17, 18]. These isoforms are illustrated in Figure 1.2 and are discussed in detail in Section 1.2.

1.2 Regulation of MMP-2 activity

MMPs are tightly regulated through each step from the gene to their processing to a bioactive protease to avoid aberrant proteolytic activity. Likewise, MMP-2 activity is regulated at transcriptional and post-translational levels involving transcription factors, zymogen activation, endogenous inhibitors and post-translational modifications.

1.2.1 Transcriptional regulation

MMP-2 was originally believed to be a constitutively expressed protease due to its ubiquitous expression in tissues and almost all cells and the absence of a canonical TATA box in the MMP-2 proximal promoter[19]. However, it has since then become evident that MMP-2 expression is tightly regulated through a complex transcriptional regulatory network under both physiological and pathophysiological conditions. Bergman et al[20] demonstrated that the binding of activating protein-1 (AP-1) transcription factors Fra1 and JunB to a functional AP-1 site regulates MMP-2 transcription in cardiomyocytes and fibroblasts. Under hypoxic conditions, Fra1-JunB and FosB-JunB heterodimers bind to the functional AP-1 site to drive MMP-2 transcription[20]. In accordance to this, increased binding of FosB-JunB heterodimers to the intrinsic MMP-2 promoter was found to enhance MMP-2 transcription and translation following myocardial oxidative stress injury[21]. A number of additional transcription factors have since been found to bind to elements in the MMP-2 promoter including AP-2[22], Sp1[22], Sp3[22], PU1[23], YB-1[24], p53[25], Stat3[26], and NF-κB[27]. In coordination with these transcription factors, MMP-2 transcription can be driven by a variety of specific inflammatory cytokines, hormones, and growth factors including endothelin-1, interleukin 1β, angiotensin II, tumor necrosis factor-α, estrogen, and progesterone [20, 21, 28, 29].

The MMP-2 proximal promoter lacks a canonical TATA box and is composed of a relatively GC-rich region that adjoins multiple transcriptional start locations[30]. In silico analysis revealed a high probability of an alternative promoter, induced by oxidative stress, within the first intron of the MMP-2 gene[18]. Transcription within the first intron of the MMP-2 gene generates a 5'-truncated MMP-2 transcripts and initiates translation at Met77 within the second exon[18]. This N-terminal truncated MMP-2 (NTT-MMP-2) isoform is devoid of the first 76 amino acids, which includes the entire secretory signal sequence and two of the three α-helices that make up the

propeptide domain (Figure 1.2)[18]. The remaining propeptide domain does not shield the zinc-containing catalytic site, rendering the NTT-MMP-2 isoform intracellular and proteolytically active[18]. Expression of NTT-MMP-2 was found to induce mitochondria-nuclear stress signalling through the activation of NFAT and NF-κB signaling cascades and expression of a highly defined innate immunity transcriptome[18]. The intracellular localization of NTT-MMP-2 is discussed in Section 1.3.5.

Multiple transcript variants have been reported in several members of the MMP family including MMP-8[31], MMP-13[32], MT3-MMP[33], and MT5-MMP[34]. Transcript variants are generated by alternative RNA splicing, a process in which exons from pre-mRNA are reconnected in multiple ways. A single gene can produce multiple protein isoforms resulting from translating different mature mRNA transcripts. Transcript variants may alter the activity, subcellular localization, and/or tissue distribution of a protein. Ali et al[17] identified an MMP-2 splice variant devoid of the first 50 amino acids which lacks the canonical MMP-2 secretory signal sequence (Figure 1.2). Thus, the MMP-2 splice variant is not targeted for secretion and remains intracellular[17]. Further investigation is needed to determine whether the MMP-2 splice variant is proteolytically active inside cells.

1.2.2 Post-translational regulation

Generally, nascent MMP-2 enters the endoplasmic reticulum where the signal peptide is removed and the protease is packaged into vesicles at the Golgi complex for secretion. The 72 kDa MMP-2 zymogen docks outside the cell membrane where it is proteolytically activated by forming a ternary complex with tissue inhibitor of metalloproteinase-2 (TIMP-2) and MT1-MMP (Figure 1.3)[35, 36]. TIMP-2 inhibits active MT1-MMP by binding to its N-terminal domain, preventing the intermolecular activation of MT1-MMP and subsequent accumulation of active MT1-MMP[35].

TIMP-2 anchors the 72 kDa MMP-2 zymogen outside the cell membrane by forming a non-covalent bond to the hemopexin domain. MT1-MMP then removes a portion of the propeptide domain of MMP-2 by hydrolyzing the Asn56-Leu57 peptide bond[36]. Partial processing of the propeptide domain disrupts the interaction between the Cys102 residue and catalytic zinc, exposes the catalytic site, and renders the MMP-2 intermediate partially active. Other active MMPs then cleave the remainder of the propeptide domain by hydrolyzing the Asn109-Tyr110 peptide bond, yielding an active, extracellular 64 kDa MMP-2 isoform.

In addition to the canonical activation of MMPs by proteolytic mechanisms, MMP activity is also regulated by non-proteolytic mechanisms. MMP-1, MMP-8, and MMP-9 zymogens were first shown to be activated by the pro-oxidant peroxynitrite without requiring the proteolytic removal of the propeptide domain[37, 38]. Low concentrations of peroxynitrite (1 to 10 μM), in the presence of cellular glutathione, results in the S-glutathiolation of a critical cysteine residue within PRCGVPD sequence of the propeptide domain[38]. The PRCGVPD sequence is highly conserved across all members of the MMP family. This post-translational modification disrupts the interaction between the catalytic zinc and the thiolate moiety within the PRCGVPD sequence, rendering the MMP catalytically active[38]. Like MMP-1, MMP-8, and MMP-9, 72 kDa MMP-2 is also activated intracellularly under conditions of increased oxidative stress via post-translational modification without the proteolytic removal of the propeptide domain[39]. In the presence of peroxynitrite and cellular glutathione, the interaction between the Cys102 residue in the propeptide domain and the catalytic zinc is disrupted[39]. This reaction triggers the S-glutathiolation of the Cys102 residue which alters the conformation of MMP-2, exposing the catalytic zinc, forming an active, intracellular 72 kDa S-glutathiolated MMP-2 (Figure 1.3)[39].

MMP-2 activity is also negatively regulated by phosphorylation. This was first demonstrated in MMP-2 secreted from human fibrosarcoma cells whereby treatment with alkaline phosphatase significantly increased MMP-2 activity[40]. Human MMP-2 has at least five phosphorylation sites: Ser32, Ser160, Thr250, Tyr271, and Ser365[40]. These phosphorylation sites are located within the collagen binding domain and the catalytic cleft (Figure 1.3), which are directly involved in substrate recognition and turnover. In silico analysis of the MMP-2 amino acid sequence predicted that MMP-2 is likely phosphorylated by protein kinase A, protein kinase C, and glycogen synthase kinase 3β[40]. Indeed, protein kinase C and protein kinase CK2 directly phosphorylate MMP-2 and decrease its activity in vitro[40, 41]. In accordance to this, okadaic acid, a serine/threonine phosphatase inhibitor, decreased MMP-2 activity by preventing its dephosphorylation in the isolated rat heart[42]. However, the protein kinases and phosphatases which regulate the phosphorylation status and activity of MMP-2 in vivo remain unknown.

Activation of 72 kDa MMP-2 zymogen is also modulated by homodimerization. MMP-2 can form homodimers through an intermolecular disulfide bond between two MMP-2 molecules at Cys102[43]. MMP-2 homodimerization is reduction-sensitive, calcium dependent, and independent of protein kinase C-mediated phosphorylation of MMP-2[43]. Homodimerization of MMP-2 was found to enhance thrombin-mediated activation of the 72 kDa MMP-2 zymogen[43].

1.2.3 Tissue inhibitors of metalloproteinases

MMP activity is tightly regulated by a family of endogenous inhibitors called tissue inhibitor of metalloproteinases (TIMPs). The TIMP family is comprised of four members (TIMP-1, TIMP-2, TIMP-3, and TIMP-4), all of which are cysteine rich proteins characterized by two domains. TIMPs are composed of a large N-terminal domain responsible for MMP inhibition and a smaller C-terminal domain, stabilized by three disulfide bonds[44]. TIMPs bind to the catalytic site

of MMPs in a 1:1 stoichiometric ratio, thereby inhibiting MMP activity[45]. It was initially believed that each TIMP inhibited specific members of the MMP family, but it is now known that all TIMPs can inhibit each member of the MMP family with different selectivity[12, 46]. TIMP-1, TIMP-2, and TIMP-3 are expressed in most mammalian tissues including the heart. TIMP-1 expression is modulated by several factors including angiotensin II[47] and pro-inflammatory cytokines[48]. TIMP-2 expression in the heart is considered constitutive[48], but is unique such that it has a dual role in inhibiting MMP-2 and facilitating its proteolytic activation, as described in Section 1.2.2. TIMP-3, which has a broad spectrum MMP inhibitory profile, is localized exclusively in the extracellular matrix through its interaction with heparan sulfate and sulfated proteoglycans[49]. Loss of TIMP-3 in the myocardium causes excessive degradation of the extracellular matrix and activation of inflammatory cytokines in heart failure[50]. Compared to the other TIMPs, TIMP-4 has a more restricted localization. TIMP-4 is expressed in the heart[51] and platelets[52]. Within cardiomyocytes, TIMP-4 is localized in the intracellular space with MMP-2 in the thin filaments[51]. Secretion of TIMP-4 from cardiomyocytes during oxidative stress injury causes an imbalance in the intracellular MMP-2/TIMP-4 ratio resulting in enhanced intracellular MMP-2 activity[51]. It is also important to note that peroxynitrite can directly inactivate TIMP-1[53] and TIMP-4[54].

1.2.4 Small molecule MMP inhibitors

Since the discovery of MMPs nearly 60 years ago, it has been established that MMPs play an important role in remodeling the extracellular matrix in both physiological and pathological processes including wound healing, cellular proliferation, inflammation, and cancer metastasis to name a few. Approximately three decades ago, many pharmaceutical companies invested in the development of broad spectrum MMP inhibitor drugs for anticancer and anti-inflammatory drug discovery. These first generation hydroxamate MMP inhibitors were designed on the basis of zinc

chelators. Pan-MMP inhibitors such as batimastat[55] and marimastat[56, 57] showed excellent anticancer efficacy in tumor cells and animal models such that drug development progressed to clinical trials. However, these first generation MMP inhibitors failed in late-stage anticancer clinical trials as they did not inhibit micro-metastasis and caused unexpected and dose-limiting musculoskeletal pain[56, 57]. The first hypothesis explaining musculoskeletal syndrome was based on the lack of selective MMP inhibition, particularly adverse side effects from inhibiting essential MMPs such as type 1 collagenase MMP-1[58]. This was attributed to the lack of knowledge in MMP biology as these pan-MMP inhibitors were developed prior to the identification of all the MMPs. At the time, it was not known which MMPs were implicated in cancer and which essential MMPs should not be inhibited. Secondly, musculoskeletal syndrome may be attributed to off-target metal ion chelation and non-selective inhibition of non-MMP metalloproteinases such as adamalysins and tumor necrosis factor-α-converting enzyme also known as a disintegrin and metalloproteinase[59, 60]. Since then, our understanding of the intracellular/extracellular localization, activation, and function of each MMP have significantly improved. Given that only certain MMPs are implicated in various diseases, including cancer and heart disease, adjusting the structure of MMP inhibitors to impart selectivity for certain MMPs should achieve great clinical impact in cancer chemotherapy[61].

Lessons learned from these early MMP inhibitor programs have fostered the development of new MMP inhibitors with greater potency, selectivity, and cell penetrance including ONO-4817 and ARP-100. ONO-4817 is a selective MMP inhibitor as it has nearly no inhibitory activity for other proteases (chymotrypsin, plasmin) up to 100 μM[62]. ONO-4817 is also the most potent MMP-2 inhibitor having subnanomolar affinity for MMP-2 with K_i of 0.7 nM (MMP-2), 42 nM (MMP-3), 2500 nM (MMP-7), 2 nM (MMP-9), and 1 nM (MMP-13)[62]. ONO-4817 is also an MMP-1

sparring MMP inhibitor as its K_i for MMP-1 is in the micromolar range[62]. Thus far, ONO-4817 has demonstrated beneficial effects against IR injury in the heart, kidney, and lungs[63-65]. ARP-100 is the most selective MMP gelatinase inhibitor available to date, having a K_i of 12 nM (MMP-2), 200 nM (MMP-9), and over 50 μM (MMP-1 and MMP-7)[66]. However, it has not been determined whether these inhibitors are protective against other cardiac pathologies associated with increased oxidative stress.

One particular class of MMP inhibitors that has clinical utility are some members of the tetracycline class of antibiotics. Golub et al[67] first recognized that certain tetracyclines such as doxycycline and minocycline possess MMP inhibitory properties by virtue of their ability to chelate zinc, resulting in conformational changes to the protease. In fact, the minimal effective plasma concentration of doxycycline for MMP inhibition is about five times lower than that required for antimicrobial effects[68]. In addition to its MMP inhibitory properties, doxycycline and chemically modified tetracyclines, which are devoid of antimicrobial activity, have been shown to reduce MMP-2 expression at a transcriptional level in human skin keratinocytes[69]. To date, doxycycline is the only MMP inhibitor approved by Health Canada and the U.S. Food and Drug Administration and is administered orally in the treatment of periodontitis[70] and rosacea[71]. Interestingly, doxycycline is a poor MMP-1 inhibitor, which may explain the absence of musculoskeletal syndrome in patients[72]. In a recent phase II clinical trial (TIPTOP)[73], doxycycline was administered for seven days immediately following percutaneous coronary intervention in patients with myocardial infarction. Doxycycline was found to attenuate adverse cardiac remodeling compared to placebo in a six month follow up[73]. Given its well-defined safety profile and clinical efficacy, doxycycline is an attractive drug in preclinical and clinical studies for the treatment of conditions in which MMPs are activated.

1.3 MMP-2 inside and outside the cell

Since its discovery as a type IV collagenase over 35 years ago, the field of MMP-2 biology has significantly grown. The full gamut of MMP-2 substrates under physiological and pathophysiological conditions continues to grow rapidly[11]. Beyond the extracellular matrix, a plethora of non-extracellular matrix proteins have been identified as targets of MMP-2, both inside and outside the cell (Figure 1.4).

1.3.1 MMP-2 in the extracellular space

The extracellular matrix provides the physical scaffold for cells to maintain tissue architecture. The extracellular matrix also regulates cell signaling by binding a plethora of cytokines and growth factors, and creating microenvironments. MMPs degrade membrane bound proteins which in turn influence cellular growth, proliferation, and migration. Collagen is the most abundant fibrous protein component of the extracellular matrix. Although not classified as a collagenase, MMP-2 can degrade type IV, V, VII, and X collagen. As suggested by its original name of gelatinase A, MMP-2 cleaves gelatin. Glycoproteins such as fibronectin and laminin, which form the basement membrane of cells, have also been added to the large list of extracellular matrix targets of MMP-2[74, 75].

MMP-2 cleaves other extracellular targets beyond extracellular matrix proteins. MMP-2 was shown to regulate vascular function by activating big-endothelin and calcitonin-gene-related peptide by proteolysis[76, 77]. MMP-2 also regulates inflammatory response by cleaving monocyte chemoattractant protein-3[78]. MMP-2 mobilizes growth factors and cell signaling by proteolytic release of non-matrix extracellular proteins. MMP-2 has been shown to cleave vascular endothelial growth factor from its inhibitory complex, which consists of connective tissue growth factor and

heparin affin regulatory peptide[79]. MMP-2 has also been shown to activate latent transforming growth factor-β and inactivate interleukin-1β[80, 81].

1.3.2 MMP-2 in the sarcomere

Rouet-Benzineb et al[82] first detected gelatinolytic (MMP-2 and MMP-9) activity by in situ zymography in the ventricles of patients with dilated cardiomyopathy. A subsequent study by Coker et al[83] then showed positive MMP-2 staining consistent with sarcomeric structure in adult human cardiomyocytes without commenting on it. In 2002, Wang et al[84] using immunogold electron microscopy revealed that MMP-2 has a distinct sarcomeric staining pattern in rat hearts and was found in highly purified thin myofilament fractions prepared from the ventricle. Using confocal microscopy, MMP-2 was found colocalized with the thin filament regulatory protein, troponin I. Purified troponin I was tested for its susceptibility to cleavage by MMP-2 in vitro and was rapidly proteolyzed in a concentration-dependent manner within 20 min of incubation[84]. In hearts subjected to oxidative stress injury by ischemia and reperfusion, increased MMP-2 activity was associated with cleavage of troponin I and reduced contractile function, an effect which was prevented with MMP inhibitors[84]. This marked the first clear-cut evidence of the intracellular localization and biological action of MMP-2, which greatly expanded our understanding of its effects beyond the extracellular matrix.

In a subsequent study using a combined pharmaco-proteomics approach, myosin light chain-1 was identified as another target of MMP-2 in the heart[85]. Immunogold electron microscopy localized MMP-2 to the A-band of the sarcomere, consistent with the distribution and localization of myosin light chain-1[85]. Furthermore, MMP-2 activity was detected in purified thick filament preparations from isolated rat hearts[85]. Titin, the molecular spring of the sarcomere, was also identified as a target of MMP-2 in acute myocardial ischemia-reperfusion injury[63].

Immunostaining of MMP-2 revealed distinct colocalization of MMP-2 and titin to the Z-disc region of the sarcomere[63]. Ischemic-reperfused rat hearts exhibited increased titin degradation and reduced titin immunostaining, an effect which was prevented by MMP inhibitors[63]. These seminal studies demonstrate that MMP-2 directly affects cardiac contractile function at the level of the sarcomere by targeting troponin I, myosin light chain-1, and titin.

1.3.3 MMP-2 in the cytoskeleton

MMP-2 also targets the cytoskeletal proteins α-actinin[86] and dystrophin[87]. Isolated rat hearts infused with peroxynitrite showed reduced levels of myocardial α-actinin and impaired contractile function as a result of increased MMP-2 activity[86]. Dystrophin is a key linker protein that connects the extracellular matrix through the cell membrane via dystroglycans, to the sarcolemma. As a consequence of cardiac ischemia-reperfusion injury, increased MMP-2 activity resulted in dystrophin proteolysis, an effect that was prevented by ischemic preconditioning, a treatment which attenuates oxidative stress-induced MMP-2 activity[88]. It is also important to mention that desmin, another intermediate filament protein, is susceptible to proteolysis by MMP-2 in vitro[86]. Whether this takes place in vivo remains an open question.

1.3.4 MMP-2 in the nucleus

The nucleus consists of a proteinaceous matrix that resembles the extracellular matrix and supports various nuclear processes. Kwan et al[89] identified that MMP-2 possesses a nuclear localization sequence, which suggests that it may be transported to the nucleus. The nuclear localization sequence is encoded in the C-terminus of MMP-2, making it easily accessible for receptors to transport MMP-2 through the nuclear pore. In addition to MMP-2, many other MMPs encode a nuclear localization sequence[90]. MMPs have been hypothesized to cleave transcription

factors[91, 92], proteolyze proteins involved in DNA repair, such as poly-ADP-ribose polymerase[89, 93], and regulate mitotic events in the nucleus[94]. Immunogold electron microscopy localized MMP-2 to the nucleus of cardiomyocytes[89]. Poly-ADP-ribose polymerase-1 is susceptible to proteolysis by MMP-2 in vitro[89]. Nuclear MMP-2 may have a protective role by preventing excessive poly-ADP-ribose polymerase activity, the latter which could exhaust energy stores in the cell. Recent work from the Schulz lab has also localized MMP-2 to the nucleolus in human osteosarcoma cells.

1.3.5 MMP-2 in the mitochondria

In 2002, MMP-2 was also found to be localized in the mitochondria in cardiomyocytes by immunogold electron microscopy[84]. However, the substrates and functions of MMP-2 in mitochondria were not yet understood. Subsequent research from Lovett's group determined that the NTT-MMP-2 isoform is primarily mitochondrial and is expressed in cells following oxidative stress injury[18]. The mitochondrial fraction prepared in this study also contained a portion of the endoplasmic reticulum that is bound to the mitochondria, known as the mitochondria-associated membrane. Further investigation determined that the majority of 72 kDa MMP-2 is localized to the mitochondria-associated membrane, while a smaller but also significant proportion resides in the mitochondria[95]. Calreticulin, a mitochondria-associated membrane resident calcium regulatory protein, is susceptible to proteolysis by MMP-2 in vitro, suggesting MMP-2 in the mitochondria-associated membrane may have an indirect role on mitochondrial function[95]. Using siRNA and 2D SDS-PAGE techniques, several mitochondrial enzymes involved in energy production were predicted as targets of MMP-2 including ATP synthase beta subunit, 2-oxoglutarate dehydrogenase complex, cytochrome c oxidase subunit 5A, electron transfer flavoprotein subunit beta, and NADH dehydrogenase 1 alpha subcomplex subunit 5[96]. Taken together, MMP-2 may play an important role in mitochondria by regulating energy metabolism.

1.3.6 MMP-2 in the sarcoplasmic reticulum

Recent work from our lab has demonstrated that MMP-2 is localized in the sarcoplasmic reticulum and is responsible for the rapid degradation of sarco/endoplasmic reticulum calcium ATPase-2a (SERCA2a) in acute myocardial IR injury[97]. Different experimental approaches provided strong evidence for the localization of MMP-2 activity in the sarcoplasmic reticulum. First, SERCA2a was proteolyzed in rat hearts subjected to IR, an effect that was prevented by MMP inhibition[97]. Second, sarcoplasmic reticulum-enriched microsomes prepared from isolated rat hearts contained abundant MMP-2 activity by gelatin zymography[97]. Finally, a combination of in silico analysis and in vitro degradation assays revealed that SERCA2a embedded in proteoliposomes is susceptible to proteolysis by MMP-2[97]. Though the role of MMP-2 in the sarcoplasmic reticulum is still early in investigation, the evidence provided thus far suggests it may play an important role in intracellular calcium homeostasis.

1.4 Titin

In 2010, Ali et al[63] identified titin as a novel target of intracellular MMP-2 in acute myocardial IR injury. Titin is the largest mammalian protein encoded by a single gene *TTN*[98] and is expressed in smooth and striated muscle cells[99, 100]. Titin functions as a scaffold and molecular spring, which are integral for sarcomere structure and function.

1.4.1 Titin isoforms in the heart

Titin spans the half-sarcomere with its N- and C-terminus localized at the Z-disc and M-line, respectively (Figure 1.5). Titin is composed of highly conserved inextensible regions and spliced extensible regions. The extensible region, located in the I-band, is subject to multiple splicing pathways resulting in two adult cardiac titin isoforms N2B and N2BA[98], which are

approximately 3.0 and 3.3 MDa, respectively (Figure 1.5). The extensible region of these two cardiac isoforms composes of tandem immunoglobulin (Ig) domains, proline-glutamate-valine-lysine (PEVK) domain, and N2B-unique sequence domains[98] (Figure 1.5). Titin exon microarrays have also identified a large fetal cardiac titin isoform (>3.6 MDa) that disappears during postnatal development[101]. The N2B-unique sequence is cardiac specific[99]. Titin in skeletal muscle cells only express the N2A element[98]. Splice factor RNA binding motif protein 20 (RBM20) dictates titin's spring composition by splicing the N2A element to produce the N2BA or N2B isoform[102-104]. Mammals co-express N2BA and N2B titin within a single sarcomere. Each thick filament binds to six titin molecules with varying N2BA to N2B ratios between mammalian species. Larger mammals such as humans express approximately equal amounts of N2BA and N2B titin (N2BA:N2B $\approx$ 1) whereas smaller mammals such as mice express higher levels of N2B (N2BA:N2B $\approx$ 0.2) in the heart.

1.4.2 Titin regulates myocardial passive force

As the molecular spring of the sarcomere, each element in titin's extensible I-band region has a distinct elastic property. Upon sarcomere stretch, tandem Ig domains are initially extended followed by the PEVK element and N2B-unique sequences[105, 106]. Extension of this region generates a passive force which pulls Z-discs together to restore slack sarcomere length. Titin is a major determinant of myocardial passive force at any sarcomere length. Titin establishes the lower limit of sarcomere length. Only when titin is fully extended does extracellular matrix collagen contribute equally with titin to myocardial passive force. At a given sarcomere length, titin isoform compliance is determined by the fractional extension of its extensible region[107]. N2B titin generates a larger passive force than N2BA titin because it requires a larger fractional extension as a result of its shorter extensible region[108]. Higher N2B expression in smaller mammals allows

rapid ventricular filling during diastole to accompany their higher heart rates. Consequently, the balance of N2BA:N2B titin co-expression directly affects myocardial contractility at the level of the cardiomyocyte[109, 110].

1.4.3 Titin regulates sarcomeric structure

Titin binds to many sarcomeric proteins and functions as a scaffold for sarcomere assembly. One characteristic of striated muscle is the equally spaced Z-discs which divide individual sarcomeres. X-ray crystallography studies revealed the palindromic assembly of titin between adjacent sarcomeres[111]. The N-termini of adjacent titin molecules interconnect with titin-capping protein T-cap at the Z-disc[111]. The C-termini of titin from opposite sarcomeres overlap within the M-line, stabilized by M-line proteins[112, 113]. At the Z-disc, titin-capping protein T-cap functions as an adaptor protein to anchor the sarcoplasmic reticulum[114] and T-tubule[115] in proximity to the sarcomere. The sarcomere is further stabilized by the titin-α-actinin complex at the Z-disc[116, 117].

Titin is hypothesized to function as a sarcomeric ruler to maintain sarcomere length and regulate myofilament assembly[118]. In the absence of titin, filament-crossbridge interactions are highly unstable. Titin binds to the thin filament via actin from the Z-disc to the extensible I-band region via Z repeats and PEVK element[119-121]. The passive forces from adjacent titin molecules stabilize the A-band and M-line during contraction. Towards the C-terminus, the A-band region of titin is linear and consists of eleven super-repeats. Each super-repeat comprises of regularly spaced fibronectin-3 domains separated by Ig domains which bind to myosin[122, 123]. Myosin alone cannot regulate the length of its self-assembly in vitro. These findings suggest titin plays an important role in regulating sarcomeric structure and assembly of the thick and thin filaments.

1.4.4 Cardiac titinopathies

Alterations in myocardial passive force and titin isoform expression have been found in the left ventricle of patients with dilated cardiomyopathy (DCM)[124, 125]. Patients with DCM exhibited elevated levels of the more compliant N2BA isoform than the stiffer N2B isoform[125]. The severity of diastolic dysfunction was directly proportional to the N2BA to N2B expression ratio[124, 125]. Several studies have reported titin degradation in human heart diseases associated with increased oxidative stress. Loss of titin and disorganization is characterized in ischemic heart failure in humans[126, 127]. However, the protease responsible for this is unclear. Titin degradation products have also been detected in the plasma of patients with Chagas disease, an infectious disease that can cause cardiomyopathy[128]. Others have reported titin degradation in vitro in adult rat cardiomyocytes treated with anthracyclines[129]. The Schulz lab found that titin is proteolyzed by MMP-2 in acute myocardial IR injury in isolated rat hearts[63]. These studies suggest that titin proteolysis and alterations in isoform expression can directly impair myocardial contractility.

1.5 Junctophilin

Junctophilins (JPH) are a family of structural proteins that are critical in the formation of junctional membrane complexes in excitatory cells[130]. Junctional membrane complexes are specialized subcellular structures which couple ion channels at the transverse tubules (T-tubules) to those on the endoplasmic reticulum at the Z-disc (Figure 1.6)[131, 132]. There are four known JPH isoforms, each are distributed in different types of excitable tissue. JPH-1 is the major isoform expressed in skeletal muscle with low levels also found in the heart[130]. JPH-2 is the predominant isoform in the heart and in cardiomyocytes[130]. JPH-3 and JPH-4 are found in neuronal tissue and T-cells, respectively[130, 133]. Given that MMP-2 and JPH-2 are both enriched at the Z-disc in

cardiomyocytes[63, 131], JPH-2 may be targeted by MMP-2 in conditions associated with increased MMP-2 activity.

1.5.1 JPH-2 structure

Each JPH isoform consists of three domains: an N-terminal domain with high affinity for the plasma membrane, a cytosolic domain, and a C-terminal hydrophobic transmembrane domain (Figure 1.6). Human JPH-2 consists of 696 amino acids, corresponding to a molecular weight of 75 kDa. Its apparent molecular weight in gel electrophoresis is 97 kDa, likely due to post-translational modifications[134, 135]. JPH-2 has eight membrane occupation and recognition nexus (MORN) motifs in the amino-terminal region, which interact with the phospholipids sphingomyelin and phosphatidylcholine in the plasma membrane[130, 132]. Next to the MORN motifs is the cytosolic domain which consists of an alpha helix and divergent region. The α-helix domain spans the majority of the junctional space and maintains uniform spacing between the plasma membrane and sarcoplasmic reticulum[132]. The divergent region is highly conserved across species and its sequence is unique between isoforms[136]. The function of the isoform specific divergent region remains unknown. The C-terminus of JPH-2 is defined by a hydrophobic transmembrane domain that anchors it to the sarcoplasmic reticulum[130].

1.5.2 JPH-2 and calcium-induced calcium release

Myocardial contractility depends on the process of excitation-contraction coupling within cardiomyocytes. This mechanism is responsible for converting an action potential to the mechanical contraction of the heart and is tightly controlled by the concentration of intracellular calcium[137]. A depolarizing potential activates voltage gated sodium channels along the invaginations of the plasma membrane or T-tubules[138]. Extracellular calcium then enters via

voltage-gated L-type calcium channels, increasing the concentration of intracellular calcium from ~100 nM to ~20 μM[139]. This influx of calcium triggers a large release of calcium from the sarcoplasmic reticulum via type 2 ryanodine receptors to activate mechanical cross-bridge formation and cardiomyocyte contraction[138, 140]. This process, termed calcium-induced calcium release, only propagates if T-tubules are closely positioned to the terminal cisternae of the sarcoplasmic reticulum network[141, 142]. JPH-2 anchors T-tubules across a ~12 nm junctional cleft to the sarcoplasmic reticulum, providing the structural basis for coordinated calcium-induced calcium release in cardiomyocytes[130, 143].

1.5.3 JPH-2 in heart disease

T-tubule distention is a common type of ultrastructural remodeling seen in hypertrophic, dilated, and ischemic cardiomyopathies, and aortic valvular disease[144]. In addition to T-tubule distention, the number of T-tubules is also markedly reduced[145]. Damage to the T-tubule-sarcoplasmic reticulum junction is a major cause of desynchronized calcium-induced calcium release and impaired myocardial contractility in heart failure[145]. Indeed, loss of JPH-2 is a common denominator in patients with dilated or ischemic cardiomyopathy[145]. Decreased JPH-2 levels were attributed to upregulation of miR-24, the only known endogenous negative regulator of JPH-2 expression[145]. Acute, conditional, cardiac knockdown of JPH-2 in mice was associated with systolic dysfunction and enhanced mortality[146]. Temporal reduction in JPH-2 levels was accompanied with increased thickness of the left ventricular posterior wall and cardiac contractility in pressure-overloaded rats[147, 148]. This highlights that loss of JPH-2 is an early event in compensatory hypertrophy before the development of overt heart failure[148].

Loss of JPH-2 was also reported in murine models of acute myocardial IR injury[134, 135]. Although JPH-2 degradation products were not detected in the heart without the addition of

exogenous calpain or calcium, in vitro degradation assays did reveal a calpain cleavage site at Arg565/Thr566 of JPH-2. This cleavage site produced ~75 kDa N-terminal and ~15 kDa C-terminal degradation products[134]. Loss of JPH-2 in the heart was prevented with the calpain inhibitor MDL-28170[134]. A previous study from the Schulz lab demonstrated that MDL-28170 also possesses MMP-2 inhibitory properties[149], raising the question as to which protease actually targets JPH-2 in acute myocardial IR injury.

1.6 Cancer chemotherapy-induced cardiotoxicity

Cancer is the second leading cause of global mortality[150]. Early detection and advancements in the treatment of cancer have significantly improved the survival of cancer patients[151]. However, cancer therapies including cytotoxic chemotherapies, molecular targeted therapies, and radiation therapy all cause heart injury and can lead to heart failure in some patients[151, 152]. In fact, long-term risk of death caused by chemotherapy-induced cardiovascular complications outweighs that of tumor recurrence[153-155]. Ewer and Lippman[156] classified two types of chemotherapy-induced cardiotoxicity. Type I is irreversible dysfunction and is associated with dose-dependent myocardial injury. Type II cardiotoxicity is reversible upon termination of treatment and the injury is not dose-dependent.

Anthracyclines such as doxorubicin (DXR), daunorubicin, and epirubicin are a class of topoisomerase inhibitors that are highly effective in the treatment of solid and hematologic cancers[157]. Approximately 30% of breast cancers, 60% of childhood cancers, and up to 70% of lymphomas are treated with anthracycline-containing chemotherapeutic regimens[158]. Anthracyclines can cause acute toxicity during treatment in some cases, but the majority of cases are irreversible and develop after the termination of treatment[159, 160]. Anthracycline cardiotoxicity

is also dose-dependent[161]. Because of this serious side effect, the lifetime cumulative dose of DXR has been reduced from 600 mg/m^2 to approximately 400 mg/m^2 [162]. Despite this, 10-25% of cancer patients develop asymptomatic left ventricular dysfunction and 1-5% of cancer patients develop heart failure upon taking anthracyclines[163]. Consequently, understanding the mechanisms of anthracycline cardiotoxicity will help develop novel adjuvant therapies to prevent heart injury in patients undergoing cancer treatment.

1.6.1 Mechanisms of anthracycline cardiotoxicity

Anthracyclines including DXR cause a plethora of ultrastructural changes within the cardiomyocyte. This is characterized by myofilament disorganization, fragmentation of the mitochondrial network, nucleolar shrinkage, and distention of the sarcoplasmic reticulum and T-tubules[164, 165]. These ultrastructural alterations are a consequence of the deleterious effects of DXR on the cardiomyocyte at a molecular level.

The mechanism of anthracycline cardiotoxicity is multifactorial. It has been proposed that DXR causes heart injury by generating reactive oxygen and nitrogen species (RONS) via topoisomerase-IIβ and/or redox cycling[166-169]. In cancer cells, anthracyclines intercalate DNA and inhibit topoisomerase II. This arrests cancer cell growth by inhibiting the synthesis of macromolecules and results in cell death. However, anthracyclines also affect non-cancer cells and trigger changes in the transcriptome and enhance the generation of RONS in cardiomyocytes[169]. Cardiomyocytes are susceptible to DXR-induced oxidative damage due to the volume of mitochondria, a major source and target of RONS[170]. The quinone moiety of DXR is susceptible to reduction by a number of oxidoreductases including NADH dehydrogenase of mitochondrial complex I[171]. NADH dehydrogenase converts DXR into a more reactive semiquinone, initiating redox cycling, and induces the formation of RONS[171]. RONS such as peroxynitrite then cause

membrane damage via lipid peroxidation in cardiomyocytes[172].

Impaired calcium handling and disruption of excitation-contraction coupling in cardiomyocytes are also implicated in anthracycline cardiotoxicity[173, 174]. DXR reduces the levels of critical calcium regulatory proteins such as SERCA2a and type 2 ryanodine receptors in cardiomyocytes[175]. Hanna et al[176] found that doxorubicinol, the metabolite of DXR, directly binds to SERCA2a and inhibits its ability to sequester calcium into the sarcoplasmic reticulum. This reduces the capacity of the sarcoplasmic reticulum to release sufficient calcium during calcium-induced calcium release for cardiomyocyte contraction. Doxorubicinol also activates type 2 ryanodine receptors and depletes the sarcoplasmic reticulum of calcium into the cytosol[176], resulting in intracellular calcium overload.

DXR damages the contractile apparatus within the cardiomyocyte. DXR reduces a number of sarcomeric proteins including α-actin, myosin light chain, myosin heavy chain, tropomyosin, troponin I, troponin C, and titin at transcriptional and/or post-translational levels[129, 177]. Titin proteolysis was detected in DXR-treated adult rat cardiomyocytes, an effect that was prevented with the calpain inhibitor ALLN[129], which also possesses MMP inhibitory properties[149]. However, titin proteolysis has not been determined in anthracycline cardiotoxicity in vivo.

1.6.2 MMPs in anthracycline cardiotoxicity

Adverse cardiac remodeling in anthracycline cardiotoxicity is initiated by a number of acute and chronic alterations to the extracellular matrix including fibrosis[178]. MMPs were then hypothesized to play an important role in the pathogenesis of anthracycline cardiotoxicity by remodeling the extracellular matrix. Within 24 hr, a single dose of DXR was found to increase MMP-2 and MMP-9 mRNA expression in the heart, induce vacuolization in cardiomyocytes, and

remodel the left ventricle[179]. This study also found that increased MMP-2 expression was associated with a significant increase in peroxynitrite in DXR-treated H9C2 cardiomyoblasts[166]. Furthermore, Spallarossa et al[180] determined that DXR activates MMP-2 and MMP-9, independent of TIMPs, via two distinct redox dependent signaling pathways. MMP-2 is activated via the pJNK/NAD(P)H oxidase cascade, whereas MMP-9 is activated by the MAP kinase p38[180].

Similarly, MMP activation occurs in chronic anthracycline cardiotoxicity. Myocardial MMP-1, MMP-2, MMP-9, and MT1-MMP are activated in pigs treated with DXR over five weeks[181]. Activation of these MMPs contributed to interstitial fibrosis, cardiomyocyte dropout, and reduced structural integrity of collagen[181]. The levels and activities of these MMPs are not only enhanced in the myocardium but also in the plasma. Elevated levels of MMP-2 and MMP-9 activity were found in the plasma of DXR-treated rats eight weeks after the end of DXR treatment[182]. These studies suggest MMP-2 activation is an early event in DXR cardiotoxicity and contributes to adverse cardiac remodeling after the termination of treatment.

1.6.3 Treatment of anthracycline cardiotoxicity

The current treatment recommendation is to withdraw chemotherapy if: 1) left ventricular ejection fraction decreases by >5% and drops below 50%, and the patient exhibits symptomatic left ventricular dysfunction; or 2) left ventricular ejection fraction decreases by 10%, drops below 50%, and patient exhibits asymptomatic left ventricular dysfunction[183]. Patients are then treated with conventional heart failure pharmacotherapy, a combination of angiotensin-converting-enzyme (ACE) inhibitors and β-blockers[183]. Chemotherapy resumes only if the ejection fraction improves to at least 45%, otherwise chemotherapy is discontinued[183].

Several clinical trials have tested the prophylactic effects of angiotensin II receptor

antagonists (PRADA[184]) and ACE inhibitors with β-blockers (OVERCOME[185], MANTICORE 101[186]) in cancer patients. The PRADA trial determined that candesartan, but not metoprolol, improved left ventricular ejection fraction in breast cancer patients treated with anthracycline-containing regimens[184]. However, the decline in left ventricular ejection fraction did not reach clinical significance[184]. The OVERCOME trial found that enalapril and carvedilol ameliorated chemotherapy-induced decline in ejection fraction, prevented the incidence of heart failure, and reduced the risk of mortality in patients with hematological cancers[185]. The MANTICORE 101 trial proved that perindopril and bisprolol prevented an overall decline in ejection fraction but did not prevent adverse cardiac remodeling, as measured by left ventricular end-systolic volume and left ventricular mass, in breast cancer patients[186]. These seminal studies show that heart failure pharmacotherapy has beneficial effects on acute left ventricular dysfunction, but also highlight its inability to prevent cardiac remodeling.

1.7 Myocardial ischemia-reperfusion injury

Ischemic heart disease is the leading cause of mortality and disability worldwide[187]. Acute coronary syndrome is the most common form of ischemic heart disease[187]. It occurs when an atherosclerotic plaque on a coronary artery erodes or ruptures and leads to the formation of a thrombus[188]. This ultimately reduces or even blocks the supply of oxygenated blood to a region of the heart, which can lead to cell death and extensive tissue damage. Immediate reperfusion of the heart using thrombolytic therapy or percutaneous coronary intervention greatly limits myocardial infarct size, left ventricular systolic dysfunction, and onset of heart failure[188]. However, reperfusion causes additional injury to the heart[187]. Although the pathophysiological mechanisms have long been investigated, there is still no effective therapy to treat myocardial ischemia-reperfusion (IR) injury.

1.7.1 Pathophysiology of myocardial IR injury

Oxidative stress and intracellular calcium overload are two major mechanisms of reperfusion injury[187]. Reperfusion of the ischemic myocardium causes a burst of RONS biosynthesis including peroxynitrite[189]. Under physiological conditions, the majority of basal superoxide generated by cellular metabolism is scavenged by superoxide dismutase and only a small amount reacts with nitric oxide to form peroxynitrite[190]. However, reperfusion of an ischemic myocardium causes maximal nitric oxide production, favoring the formation of peroxynitrite[189]. This rapidly generates a burst of peroxynitrite within the first seconds to minutes of reperfusion in the heart, which causes lipid peroxidation[191], activation of intracellular proteases[192], and damage to critical proteins[193]. This results in cardiac contractile dysfunction[189] and cell death[194].

Intracellular calcium overload occurs when the ischemic myocardium is reperfused[187, 195]. Ischemia induces an accumulation of intracellular sodium, hydrogen and calcium ions, culminating in myocardial acidosis[195, 196]. Reperfusion rapidly restores the myocardium to physiological pH and paradoxically causes more injury[195]. This activates the Na^+-H^+ exchanger, which exchanges H^+ for extracellular Na^+, thereby increasing intracellular sodium[197-199]. Under physiological conditions, the Na^+-Ca^{2+} exchanger takes up sodium to pump calcium out of the cell. However, under pathological conditions, accumulation of intracellular sodium reduces the sodium gradient and causes an influx of calcium[199, 200]. Intracellular calcium overload activates calcium-dependent proteases[201] and the formation of the mitochondrial permeability transition pore[202].

1.7.2 MMP-2 in myocardial IR injury

The burst of peroxynitrite within the first seconds to minutes of reperfusion[189] leads to a rapid release of MMP-2 from the heart[192]. Interestingly, the amount of MMP-2 activity released

into the perfusate increased proportionally with the duration of ischemia[192]. Peroxynitrite not only directly activates MMP-2 by post-translational modification[39], but also inactivates TIMPs[53, 54]. Furthermore, TIMP-4 is released into the perfusate during reperfusion, causing an imbalance which favors increased MMP-2 activity[51]. Release of MMP-2 activity may be a protective mechanism of the heart to counter intracellular MMP-2 activation[8]. During IR injury, activated MMP-2 proteolyzes troponin I, myosin light chain-1, and titin, thus impairing cardiac contractile function[63, 84, 85]. In silico mapping of MMP-2 cleavage sites in N2B titin revealed multiple putative sites within the I-band region near the N-terminus of titin[63]. Immunohistochemistry experiments showed reduced titin immunostaining near the Z-disc region of cardiomyocytes in IR hearts, which was prevented with an MMP inhibitor[63]. Loss in cardiac contractile function in IR injury was ameliorated with MMP-2 inhibition by preventing the degradation of sarcomeric proteins[63, 84, 85].

1.7.3 Therapeutic strategies for myocardial IR injury

Although there are no clinical interventions to attenuate reperfusion injury in the heart, there are several emerging therapeutic strategies. A number of studies suggest that ischemic postconditioning improves the recovery of cardiac function[203-205]. Ischemic postconditioning, done by reperfusing the heart intermittently in intervals, mitigates oxidative stress injury[206]. However, the results from clinical studies are mixed[207, 208]. A multicenter randomized clinical trial (DANAMI-3-iPOST) found that ischemic postconditioning did not improve the clinical outcome of patients undergoing percutaneous coronary intervention[209]. In experimental studies, lowering the temperature of the myocardium during ischemia can limit infarct size and heart injury by reducing the metabolic demand and inflammatory response[187, 210]. A multicenter clinical trial (CHILL-MI) found that adjunct therapeutic hypothermia to percutaneous coronary intervention lowered the incidence of heart failure in patients with early anterior ST-segment elevation

myocardial infarction, but did not reduce infarct size[211]. Lastly, pharmacological agents such as cyclosporin A[212, 213] and exenatide[214, 215] exhibit cardioprotective effects by preserving mitochondrial function and metabolism. A multicenter, double-blinded, randomized trial, however, determined that cyclosporine A did not improve clinical outcomes compared to placebo in patients with anterior ST-segment elevation myocardial infarction undergoing percutaneous coronary intervention[216]. The failure of these clinical trials highlight the importance of improving our understanding of the mechanisms of myocardial IR injury in order to develop effective therapeutic strategies.

1.8 Overall thesis hypothesis

Activation of intracellular MMP-2 is an early event in both acute and chronic myocardial oxidative stress injury. MMP-2 contributes to cardiac contractile dysfunction by remodeling the extracellular matrix and proteolyzing intracellular substrates including titin in anthracycline cardiotoxicity or IR injury. JPH-2 is proteolyzed by MMP-2 upon its activation during acute myocardial IR injury. Pharmacological inhibition of MMP-2 activity attenuates cardiac dysfunction by preventing adverse extracellular and/or intracellular matrix remodeling in acute or chronic myocardial oxidative stress injury.

1.9 Thesis objectives

1.9.1 Doxorubicin induces de novo expression of N-terminal truncated MMP-2 in cardiac myocytes (Chapter 2)

Oxidative stress plays a fundamental role in the anthracycline-induced cardiomyocyte injury and in the activation of MMP-2. Loss of intracellular proteins such as myosin light chain-1,

troponin I, and SERCA2a have been reported in anthracycline cardiotoxicity. These proteins have been identified as targets of MMP-2 in acute myocardial oxidative stress injury in the setting of IR. However the role of MMP-2 in anthracycline-induced loss of sarcomeric and sarcoplasmic reticular proteins has not been investigated. Therefore, the objective of this chapter is to determine whether intracellular MMP-2 is activated in anthracycline-treated cardiomyocytes and which intracellular proteins are potential targets of MMP-2 under this condition.

1.9.2 Matrix metalloproteinase inhibitors attenuate doxorubicin cardiotoxicity by preventing intracellular and extracellular matrix remodeling (Chapter 3)

Anthracycline cardiotoxicity is characterized by cardiac dysfunction, adverse cardiac remodeling, activation of MMPs, and proteolysis of myofilament proteins. Titin, the molecular spring of the sarcomere, is a major determinant of the Frank-Starling mechanism of the heart. Loss of titin has been reported in isolated cardiomyocytes acutely exposed to anthracyclines. However, the protease responsible for titin proteolysis in anthracycline cardiotoxicity remains unclear. The objective of this chapter is to examine the role of MMP-2 and the effect of MMP inhibitors as a prophylaxis against titin proteolysis, extracellular matrix remodeling, and cardiac dysfunction in an in vivo model of anthracycline cardiotoxicity in mice.

1.9.3 Junctophilin-2 is a target of matrix metalloproteinase-2 in myocardial ischemia-reperfusion injury (Chapter 4)

JPH-2 is a structural membrane protein that tethers the T-tubules to the sarcoplasmic reticulum to allow for coordinated calcium-induced calcium release in cardiomyocytes. Reduced myocardial contractility is associated with T-tubule disruption and JPH-2 degradation in heart failure and acute myocardial IR injury. Both MMP-2 and JPH-2 are localized near the Z-disc

region of the cardiac sarcomere. It is not known whether IR-induced JPH-2 degradation is attributed to enhanced MMP-2 activity. The objective of this chapter is to determine whether JPH-2 is proteolyzed by MMP-2 in isolated working rat hearts subjected to IR injury.

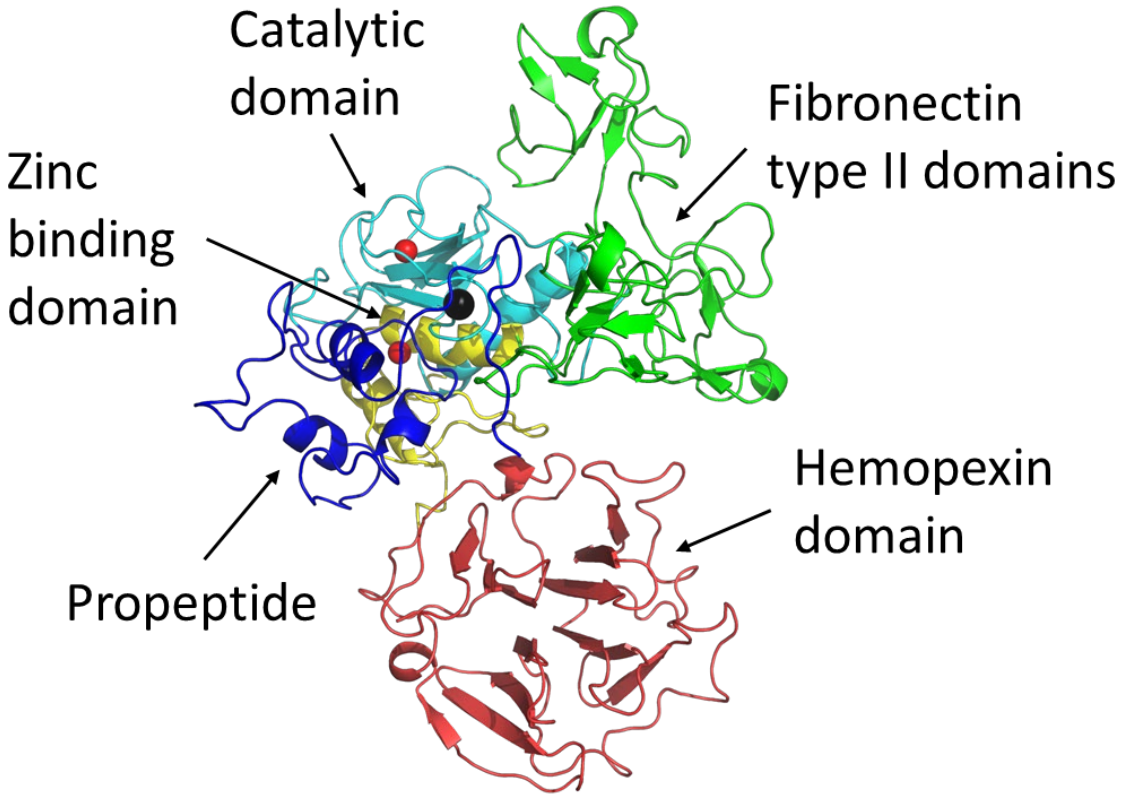

Figure 1.1: Crystal structure and structural domains of human MMP-2. The crystal structure was obtained from a mutant MMP-2 carrying a p.E404A mutation. The MMP-2 zymogen consists of a propeptide domain (three α-helices), a catalytic domain (five β-strands and three α-helices), three fibronectin type II domains, a zinc-binding domain, and a hinge region connected to a hemopexin domain (two four-stranded, antiparallel β-sheets). MMP-2 binds to zinc ion (black) in the catalytic site and two calcium ions (red) outside of the catalytic site. The PDB ID for human full-length MMP-2 is 1GXD. Adapted from Morgunova et al[15].

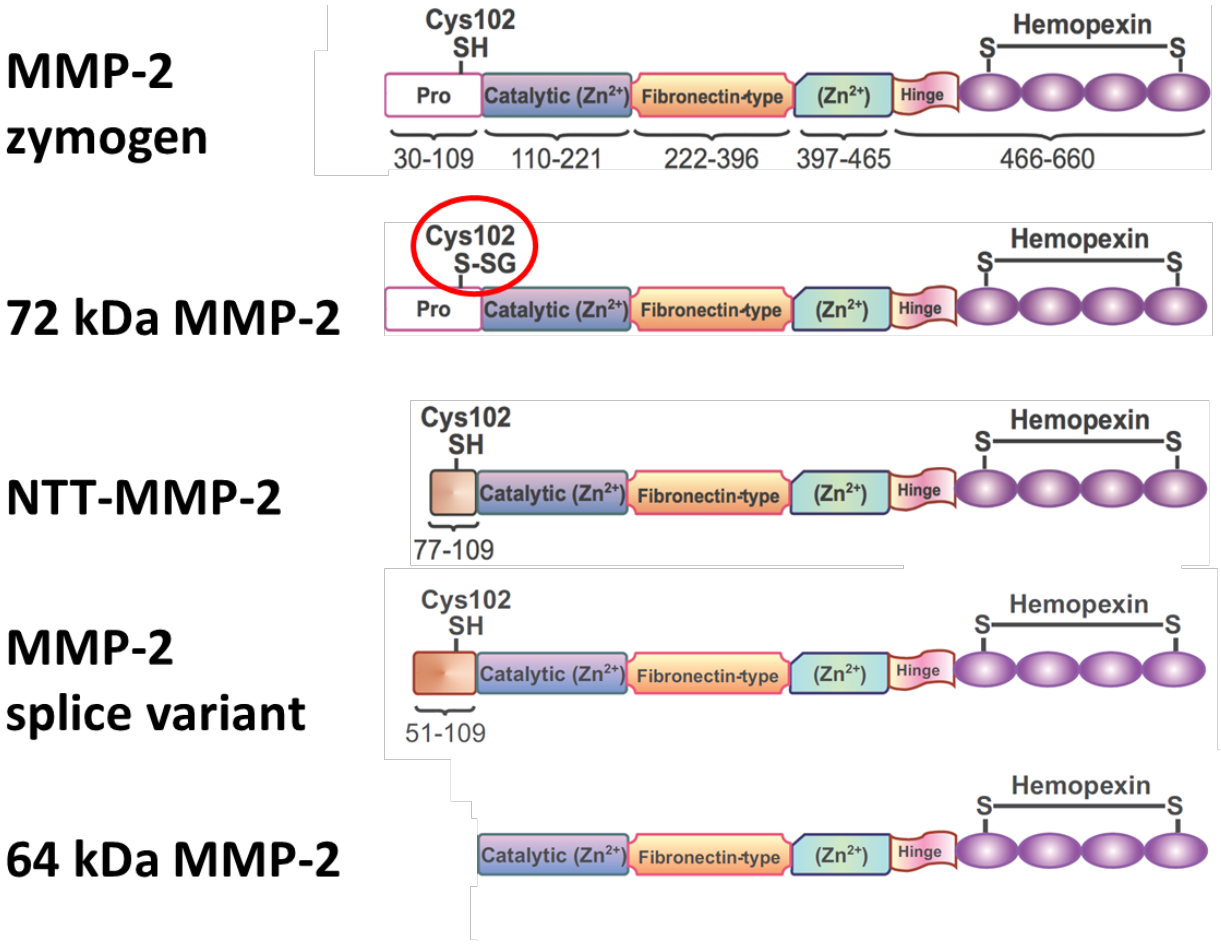

Figure 1.2: Intracellular and extracellular MMP-2 isoforms. Human MMP-2 is synthesized as a zymogen which consists of a propeptide domain (aa 30-109), a catalytic domain (aa 110-221), fibronectin type II domains (aa 222-396), a zinc-binding domain (aa 397-465), and a hinge region connected to a hemopexin domain (aa 466-660). There are three known intracellular MMP-2 isoforms: 1) 72 kDa S-glutathiolated MMP-2, 2) NTT-MMP-2, and an MMP-2 splice variant (also known as NTT_{50}-MMP-2). 64 kDa MMP-2 is found in the extracellular matrix where it is formed following the proteolytic removal of its pro-domain.

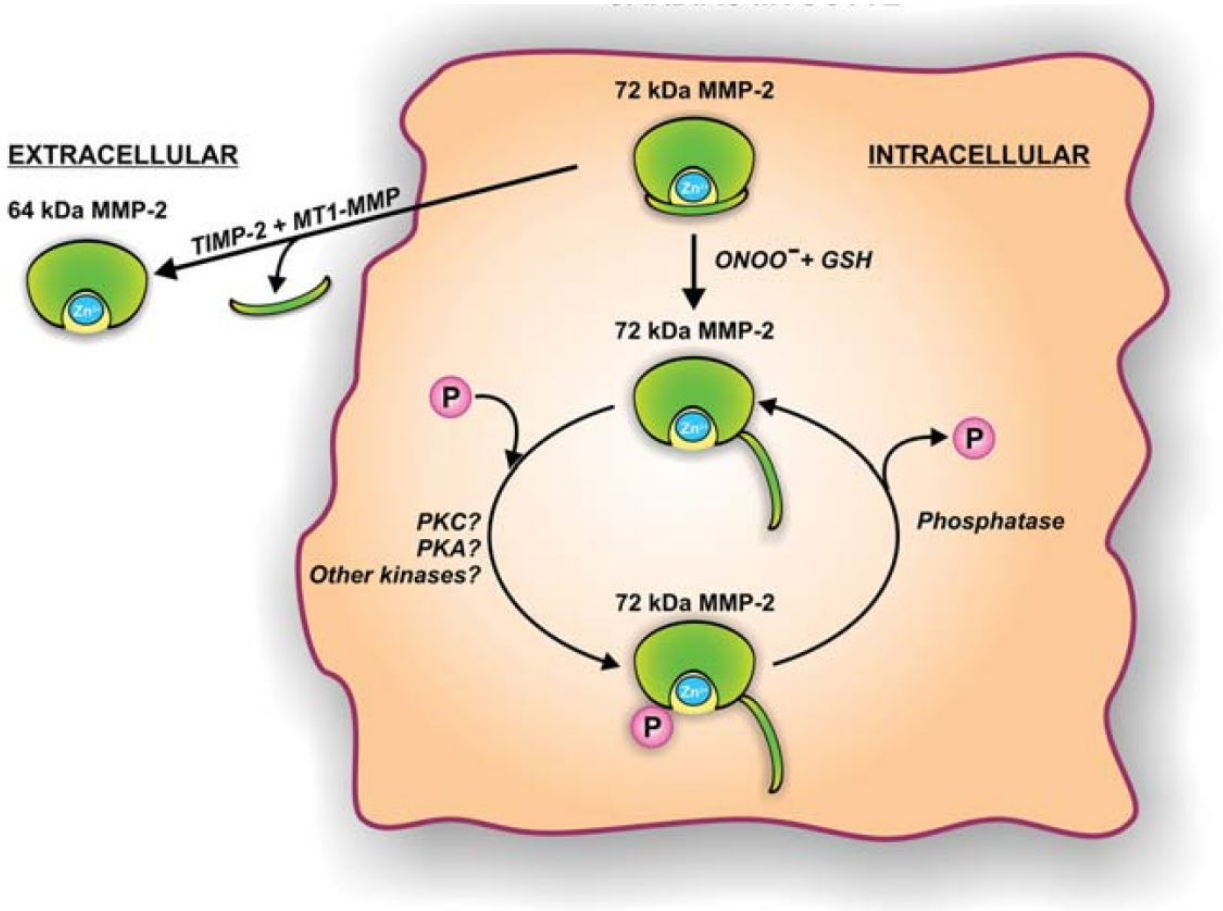

Figure 1.3: Post-translational regulation of extracellular and intracellular MMP-2 activity. MMP-2 is canonically activated in the extracellular matrix by TIMP-2 and MT1-MMP involving the proteolytic removal of the MMP-2 propeptide domain. Intracellular MMP-2 is activated by peroxynitrite via S-glutathiolation of the Cys102 in the propeptide domain, causing a conformational change that renders it enzymatically active. MMP-2 activity can also be regulated by reversible phosphorylation by protein kinases and phosphatases. Adapted from Kandasamy et al[217].

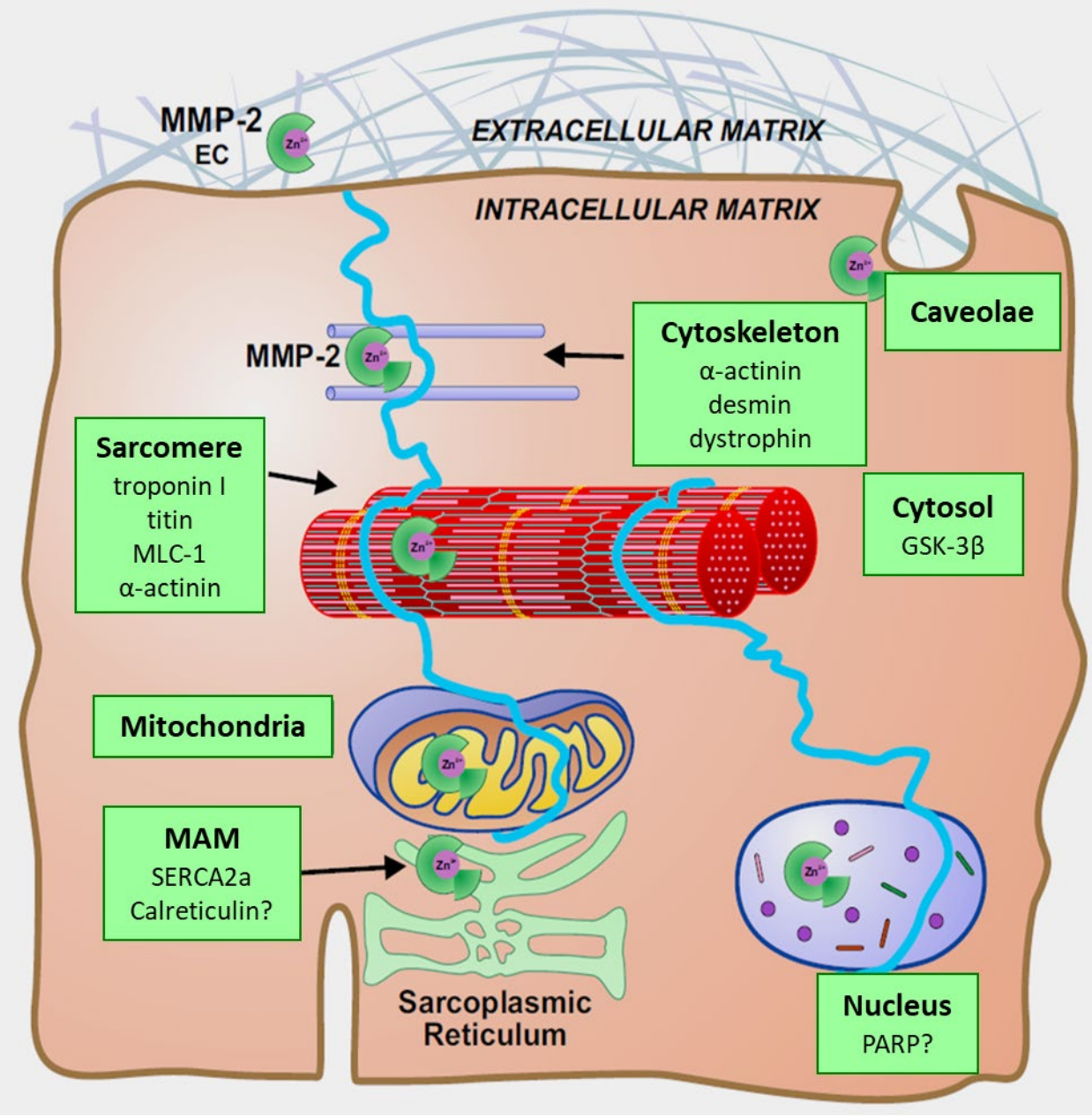

Figure 1.4: Confirmed and potential intracellular targets of MMP-2. MMP-2 is localized to several subcellular locales including the sarcomere, cytoskeleton, nucleus, mitochondria and mitochondria-associated membrane (MAM), sarcoplasmic reticulum, and caveolae. Confirmed intracellular MMP-2 substrates are identified in the boxes near the subcellular organelle which they are located and putative targets are denoted with a question mark. Adapted from Hughes & Schulz[218].

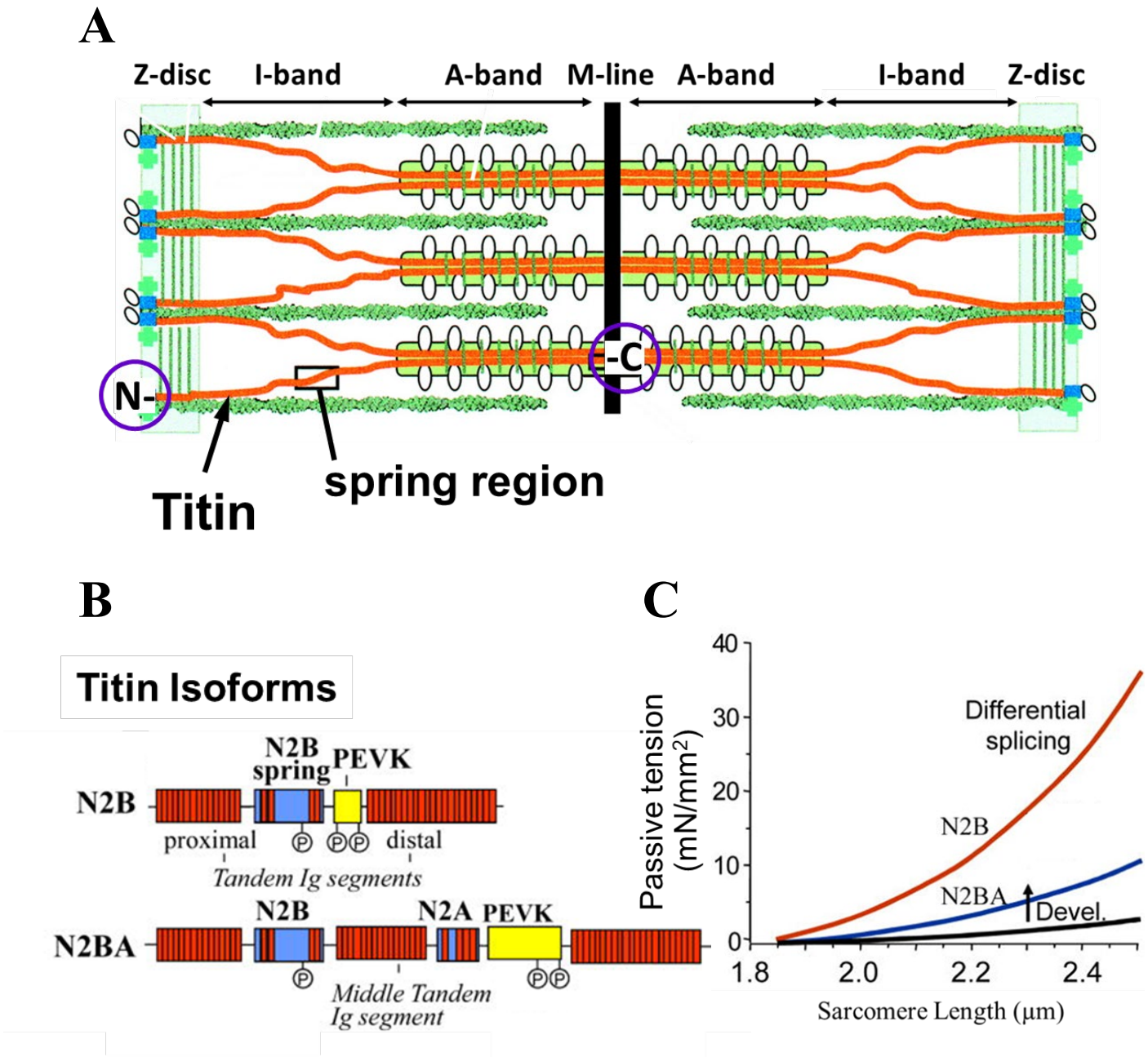

Figure 1.5: Cardiac titin in the sarcomere. (A) Titin spans the half-sarcomere from the Z-disc (N-terminus) to the M-band (C-terminus). Titin consists of a spring region (within the I-band region) and inextensible regions near the Z-disc and in the A-band region where it binds to actin and myosin, respectively. (B) The spring region is composed of tandem immunoglobulin segments (red), an N2B element (blue), an N2A element (blue), and a PEVK domain (yellow). Splicing of the N2A element dictates the expression of N2B or N2BA titin. (C) N2B titin exhibits greater passive tension than N2BA titin. Adapted from LeWinter & Granzier[98].

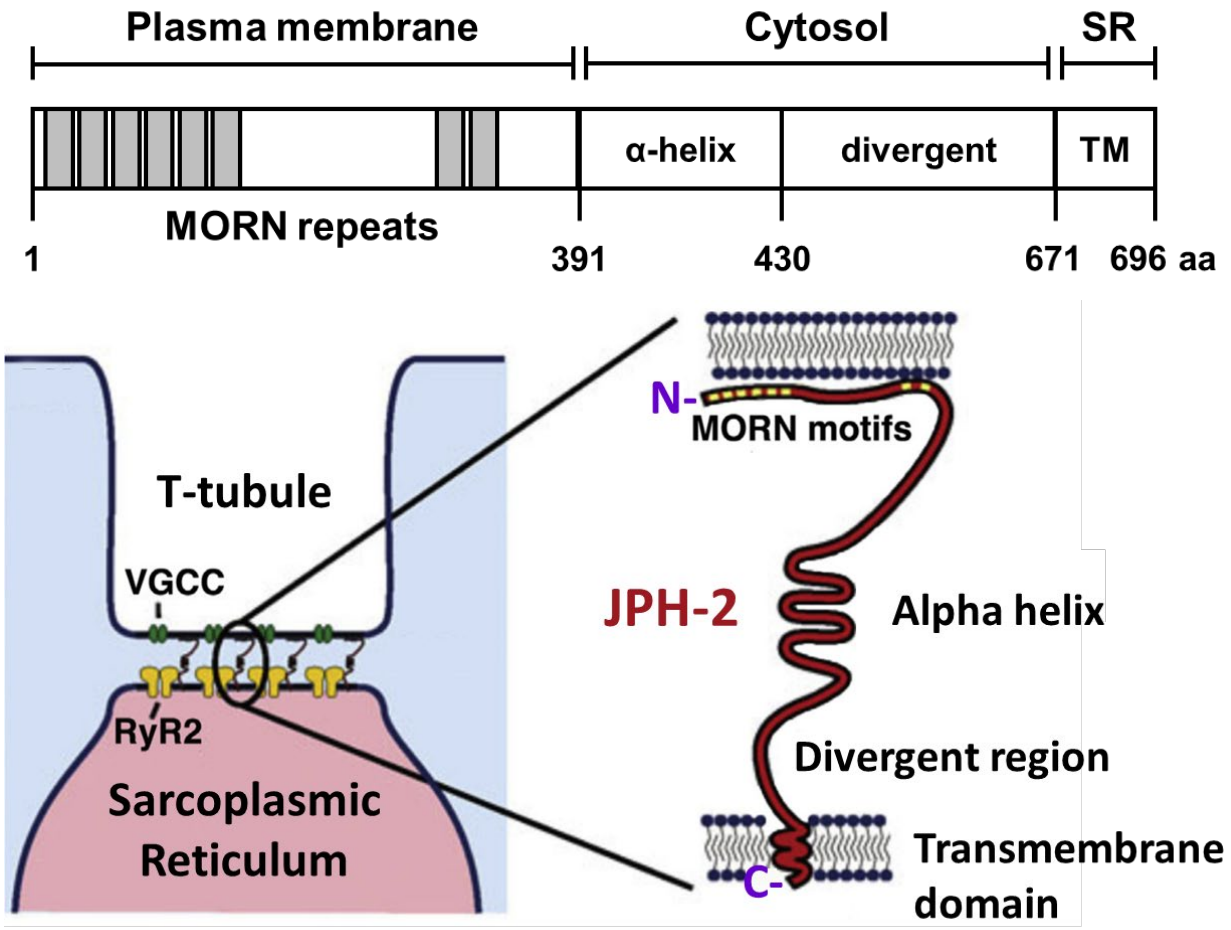

Figure 1.6: The structural domains of human JPH-2 within the cardiomyocyte. JPH-2 is localized within the junctional membrane complex and tethers the T-tubule to the sarcoplasmic reticulum. This junction brings voltage-gated calcium channels (VGCC) within ~12 nm of type 2 ryanodine receptors (RyR2). JPH-2 consists of four domains: eight MORN motifs (aa 1-390) which interact with the plasma membrane, an alpha helix domain (aa 391-429), a divergent region (aa 430-670), and a transmembrane domain (TM) at the sarcoplasmic reticulum (aa 671-696). Adapted from Quick et al[219].

CHAPTER 2

Doxorubicin induces de novo expression of N-terminal truncated MMP-2 in cardiac myocytes

A portion of this chapter is published in:

Chan BYH, Roczkowsky R, Moser N, Poirier M, Hughes BG, Ilarraza R, Schulz R. Doxorubicin induces de novo expression of N-terminal truncated MMP-2 in cardiac myocytes. *Canadian Journal of Physiology and Pharmacology*. 2018;96(12):1238-45.

2.1 Introduction

The therapeutic utility of many anticancer drugs, including anthracyclines such as doxorubicin (DXR), is hampered by their serious cardiotoxic side effects[151, 168]. Current efforts to prevent heart failure by lowering the lifetime cumulative dose of DXR compromise cancer therapy and fail to prevent heart injury, as the drug can damage cardiac myocytes even after a single dose[220]. Consequently, new strategies are needed to prevent heart injury in DXR chemotherapy. However, few, if any, have been successful because the mechanism by which DXR injures cardiac myocytes remains incompletely understood.

The detrimental effects of DXR on cardiac myocytes are believed to be primarily initiated by increased oxidative stress through the production of reactive oxygen and nitrogen species[166, 168, 169]. However, several studies using drugs to reduce oxidative stress have either failed to prevent DXR cardiotoxicity or increase the risk of secondary malignancies[167, 221, 222], likely due to their inability to target specific reactive oxygen and nitrogen species or additional mechanisms involved in myocardial dysfunction. DXR cardiotoxicity is also associated with loss of sarcomeric proteins[129, 177, 223], impaired calcium homeostasis[173, 174], and mitochondrial dysfunction[224, 225]. These adverse effects may be consistent with the consequences of activating matrix metalloproteinase-2 (MMP-2), an abundant extra- and intracellular protease in the heart[218]. In fact, a single dose of DXR was reported to increase MMP-2 protein levels in adult rat hearts[226]. However, the expression and activity of intracellular MMP-2 isoforms in DXR-exposed cardiac myocytes have not been elucidated and their proteolytic targets are unknown.

Full length MMP-2 (72 kDa) is a zinc-dependent protease involved in many physiological and pathological processes in the heart[9, 218]. MMP-2 activity was initially found to directly contribute to heart failure and injury[227-229] by remodeling extracellular matrix proteins. Cardiac

specific overexpression of MMP-2 in mice caused severe systolic dysfunction, myofilament lysis, fibrosis, and cardiac myocyte dropout[230]. However, subsequent discovery of the subcellular localization of at least two intracellular MMP-2 isoforms in cardiac myocytes expanded its pathological roles, particularly in oxidative stress-induced heart injury[84]. Full length MMP-2 can be activated by peroxynitrite via S-glutathiolation of a critical cysteine residue in its N-terminal propeptide domain[39]. Oxidative stress also triggers the transcription of an alternative promoter in the first intron of the *Mmp2* gene to generate NTT-MMP-2 which is devoid of a signal sequence and part of its inhibitory propeptide domain, rendering it proteolytically active[18]. NTT-MMP-2 was first discovered in cardiac myocytes subjected to hypoxia and is primarily mitochondrial[18, 231]. Mice with cardiac-specific expression of NTT-MMP-2 developed progressive heart failure not involving myofilament lysis but myocardial inflammation and cell death[231]. Whether DXR triggers expression of NTT-MMP-2 in cardiac myocytes is unknown.

Activation of intracellular MMP-2 plays an important role in pathophysiology of oxidative stress-induced heart injury as it is able to proteolyze many specific sarcomeric proteins, including troponin I[84], myosin light chain-1[85], α-actinin[86], and titin[63]. Cleavage of sarcomeric proteins by MMP-2 contributes to acute cardiac contractile dysfunction in myocardial ischemia-reperfusion injury[84]. MMP inhibitors improved the recovery of cardiac contractile function by preventing the degradation of sarcomeric proteins[63, 84, 192].

Depressed calcium transients are also characteristic of DXR-induced cardiomyocyte injury[175, 232-234]. This has been attributed to T-tubule damage and alterations in L-type calcium channel activity, suggesting the sarcolemma is targeted[235]. Others have reported that sarco/endoplasmic reticulum calcium ATPase-2a (SERCA2a) and its protein levels, but not mRNA expression, are decreased in the heart[175]. SERCA2a activity is tightly regulated by its

binding partner phospholamban[236, 237] to maintain the concentration of intracellular calcium at ~100 nM, allowing cardiomyocytes to relax during diastole. Decreased protein levels independent of transcriptional alterations may be a result of post-translational degradation by sarcoplasmic reticulum resident proteases. Phospholamban, the main negative regulator of SERCA2a activity[236, 237], is particularly susceptible to proteolytic cleavage as its cytoplasmic domain is intrinsically disordered. Although the intracellular targets of MMP-2 have been mostly investigated in the sarcomere, it is also localized to the cytoskeleton[86], nuclei[238], caveolae[239], mitochondria[18, 95], and the mitochondria-associated membrane (MAM)[95]. Activation of MMP-2 under pathophysiological conditions including increased oxidative stress caused by anthracyclines may result in impaired calcium handling by cleaving SERCA2a and/or phospholamban.

In the present study, I describe the activation of full length MMP-2 and *de novo* expression of NTT-MMP-2 in DXR-treated neonatal rat cardiac myocytes. Despite the upregulation of two distinct intracellular MMP-2 isoforms, this did not result in the proteolysis of specific sarcomeric and sarcoplasmic reticulum proteins as DXR decreases their expression independently of MMP-2. Given that there is abundant MMP-2 in the mitochondria and MAM, I performed some preliminary investigation on the effect of DXR on mitochondrial MMP-2 in neonatal rat cardiac myocytes.

2.2 Methods

All experiments involving animals in this study were approved by the University of Alberta Institutional Animal Care and Use Committee and performed in accordance to the *Guide to the Care and Use of Experimental Animals* published by the Canadian Council on Animal Care (AUP protocol number 329).

2.2.1 Isolation of neonatal rat ventricular myocytes

Neonatal rat ventricular myocytes (NRVM) were isolated from 1-2 day old Sprague-Dawley rats. Rat pups were euthanized by decapitation. The hearts were immediately excised and rinsed free of blood by agitation in ice cold phosphate buffered saline (PBS). The ventricles were minced with scissors. The minced tissue was then digested in PBS containing 0.1% w/v collagenase type II, 0.05% w/v trypsin, and 0.025% w/v DNase (all from Worthington Biochemical Corp, Lakewood, NJ) with agitation at 37°C for 20 min. Following the first digestion, 20 mL of DMEM/F-12 (Sigma-Aldrich, St. Louis, MO) containing 20% fetal bovine serum (Gibco, Gaithersburg, MD) was added to the digested ventricular tissue and then centrifuged at 200 g at room temperature for 1 min. The supernatant was discarded and the pellet was subsequently resuspended in collagenase/trypsin/DNase-PBS buffer for a second digestion at 37°C for 30 min. The suspension was then centrifuged at 200 g at room temperature for 1 min to pellet any undigested tissue. This pellet was further digested with collagenase/trypsin/DNase-PBS buffer at 37°C for 30 min. All supernatant fractions were then pooled and centrifuged at 500 g at room temperature for 7 min. The resulting pellet was resuspended in 50 mL of DMEM/F-12 media containing 10% fetal bovine serum and filtered through a cell strainer (BD Biosciences, San Jose, CA) and plated on 150 mm Nunclon dishes (Thermo Fisher Scientific, Waltham, MA) for 2 hr to remove fibroblasts, which preferentially adhere to dishes before cardiomyocytes. After a 2 hr pre-plating incubation, NRVM in the medium were collected and plated onto fresh dishes (as per Section 2.2.2 below). An aliquot of cells in the medium were stained with Trypan blue (Sigma-Aldrich) and NRVM were counted using a hemocytometer.

2.2.2 Cell culture

NRVM from 10 pup hearts were pooled and plated onto either 6-well plates (Corning, Corning, NY) at a density of 1.2×10^5 cells/cm^2 or onto 24-well plates (Corning) containing sterile glass cover slips (#1.5, 12 mm diameter, Electron Microscopy Sciences, Hatfield, PA) in DMEM/F-12 (Thermo Fisher Scientific) containing 10% fetal bovine serum. Cells were maintained at 37°C for 2 days prior to experiments. Human fibrosarcoma HT1080 cells (American Type Culture Collection, Manassas, VA) were also seeded onto 6-well plates at a density of 1.2×10^5 cells/cm^2 in DMEM (Gibco) containing 10% fetal bovine serum at 37°C.

2.2.3 Cell treatment with MMP inhibitors

All cell experiments were conducted under serum-free conditions. Cells were washed once with PBS and the medium was replaced with serum-free DMEM/F12. Stock solutions of the selective MMP-2 inhibitor ARP-100 (in DMSO, Cayman Chemical, Ann Arbor, MI), the gelatinase (MMP-2 and MMP-9) selective MMP inhibitor ONO-4817 (in DMSO, Ono Pharmaceutical Co., Osaka, Japan), and doxorubicin hydrochloride (in Nanopure H_2O, DXR, Sigma-Aldrich) were prepared (10, 10, and 3.45 mM, respectively). NRVM and HT1080 cells were treated with DMSO (vehicle, maximum 0.01% v/v) or DXR (0.5 μM) with or without MMP inhibitors ARP-100 or ONO-4817 (1 μM each). Cells were treated at 37°C for 2, 6, 12, or 24 hr. Cell conditioned media was collected and then centrifuged at 10,000 g at 4°C for 10 min. The supernatant was collected to measure cell viability and levels of secreted MMP-2. Cells were lysed with radioimmunoprecipitation assay (RIPA) buffer (150 mM NaCl, 1% IGEPAL CA-630, 0.5% sodium deoxycholate, 0.1% SDS, 50 mM Tris, pH 8.0) containing 1% proteinase inhibitor cocktail (P8340, Sigma-Aldrich) for 5 min at 4°C. Cell lysates and conditioned media were centrifuged (10,000 g, 10 min, 4°C) to remove cellular debris.

2.2.4 Measurement of protein concentration

Protein concentrations for all cell lysate samples were measured using a bicinchoninic acid assay (Sigma-Aldrich). Bovine serum albumin (BSA, Thermo Fisher Scientific), diluted in double distilled H_2O (ddH_2O), was used as a protein standard to produce a calibration curve between 31.25-1000 μg/mL. Cell lysates were diluted in ddH_2O to a ratio of 1:2. 10 μL of diluted BSA standard or cell lysate sample were loaded per well in a clear 96-well plate. Copper (II) sulfate solution was then mixed with bicinchoninic acid at a ratio of 1:50. 200 μL of this solution was added to each well and then incubated at 37°C for 30 min. Absorbance at 420 nm was then measured using a UVmax Kinetic microplate reader (Molecular Devices, San Jose, CA). SoftMax Pro (v 5.2C) was used to acquire and analyze the data from the plate reader.

2.2.5 Cell viability

To measure cell viability, lactate dehydrogenase (LDH) release was measured in freshly collected conditioned media as an index of cell necrosis using a CytoTox-ONE Homogeneous Membrane Integrity assay kit (Promega, Madison, WI). A positive lysis control was prepared by incubating a 35 mm dish of NRVM in culture medium with lysis buffer. LDH activity was measured by adding 50 μL of CytoTox-ONE reagent to 50 μL of conditioned media in a Costar 96 half-area well black plate (Corning). The plate was then agitated for 10 min at room temperature to allow thorough mixing. Fluorescence intensity (λ_{ex} 560 nm, λ_{em} 590 nm) from the production of resorufin was measured a Synergy H4 multi-well fluorescence plate reader (BioTek, Winooski, WT).

2.2.6 Cellular oxidative stress

Aconitase, a mitochondrial enzyme that converts citrate to isocitrate, is inactivated directly

by RONS including peroxynitrite[240] and thereby was used to estimate oxidative stress[240, 241]. Aconitase activity from NRVM lysates was measured spectrophotometrically using a microplate assay kit (Abcam, Cambridge, UK) which measures absorbance upon formation of the intermediate cis-aconitate from citrate. In brief, 10 µg of cell lysate protein diluted in aconitase preservation solution was incubated with 200 µL of assay buffer at room temperature for 30 min. The increase in absorbance at 240 nm was measured over 30 min. Aconitase activity was determined by the difference in optical density before and after the incubation divided by the incubation time.

2.2.7 Gelatin zymography

10 µg of cell lysate protein or 10 µL of cell conditioned media were diluted in RIPA buffer and nonreducing loading buffer (see Appendix). Samples were separated on 8% polyacrylamide Tris-tricine gels co-polymerized with 2 mg/mL porcine gelatin (G8150, Sigma-Aldrich). 2 µL of HT1080 cell conditioned media were run on each gel as an MMP-2 and MMP-9 standard. Samples were electrophoresed at 100 V for 80 min. Gels were then washed with 2.5% (v/v) Triton X-100 (Fisher Scientific, Ottawa, ON) in H_2O with gentle agitation, three times (20 min each), to remove the SDS and allow refolding of the gelatinases. The gels were then incubated in zymographic activity buffer (50 mM Tris-HCl, 150 mM NaCl, 5 mM $CaCl_2 \cdot 2H_2O$, and 0.05% NaN_3, pH 7.6) for 18 hr at 37°C. Following incubation, the gels were stained with 0.05% Coomassie Brilliant Blue G-250 for 3 hr and then destained in 4% methanol:8% acetic acid solution for 24 hr. The gels were scanned using a GS-800 densitometer (Bio-Rad, Hercules, CA) and quantified using ImageJ.

2.2.8 Western blot analysis

Cell lysate samples (10 µg protein each) were diluted in RIPA buffer and 6x Laemmli

buffer. Samples were heat denatured at 95°C for 5 min and separated on 10% polyacrylamide gels by electrophoresis at 100 V for 80 min. For the determination of phospholamban, 4 µg of protein was loaded onto 16% Tris-tricine polyacrylamide gels. Proteins were wet transferred onto polyvinylidene difluoride (PVDF) membranes (0.2 µm pore size, Bio-Rad) at 100 V for 1 hr at 4°C. Membranes were then blocked with 5% (w/v) skim milk powder (Carnation, Markham, ON) in Tris-buffered saline (0.1 M NaCl, 0.01 M Tris-base, pH 7.4) with 0.1% Tween 20 (TBS-T) for 2 hr at room temperature. Membranes were then immunoblotted with primary monoclonal antibodies, diluted in 5% (w/v) skim milk in TBS-T, against α-actinin (MAB1682, EMD Millipore, Burlington, MA), MMP-2 (ab92536, Abcam), TIMP-3 (sc-30075, Santa Cruz, Dallas, TX), TIMP-4 (ab58425, Abcam), troponin I (MA1040, iPOC, Toronto, ON), SERCA2a (ab137020, Abcam), and phospholamban (ab2865, Abcam) overnight at 4°C. Loading controls were conducted by splitting PVDF membranes to immunoblot for GAPDH (2118S, Cell Signaling Technology, Danvers, MA) overnight at 4°C or staining the polyvinylidene membrane with 0.25% Coomassie Brilliant Blue R-250 at room temperature for 15 min.

The next day, membranes were washed in TBS-T 5 times (7 min each) to remove any unbound primary antibodies. The membranes were then probed with an appropriate secondary antibody, either horseradish peroxidase conjugated goat anti-rabbit (CLCC42007, Cedarlane, Burlington, ON) or goat anti-mouse (CLCC30007, Cedarlane) diluted in 5% (w/v) skim milk in TBS-T, for 1 hr at room temperature. Residual secondary antibodies were washed from the membranes with 5 washes of TBS-T (7 min each). Protein bands were visualized using chemiluminescent detection reagent Clarity ECL western substrate (Bio-Rad) and exposed to autoradiography film. Films were developed using an Optimax X-Ray film processor and scanned with a Bio-Rad GS-800 densitometer. Bands were then quantified using ImageJ.

2.2.9 RNA quantification by quantitative PCR

Total cellular RNA was extracted from NRVM using TRIzol (Invitrogen) according to the manufacturer's instructions. RNA quality and concentration was assessed using a NanoDrop ND8000 spectrophotometer (Thermo Fisher Scientific). Reverse transcription was performed after DNase I treatment, using SuperScript II Reverse Transcriptase and Oligo(dT) (Invitrogen, Carlsbad, CA); controls where reverse transcriptase was omitted were included to confirm absence of genomic DNA contamination. Samples were processed in triplicate by qPCR using SYBR Green I Master Mix (Roche Diagnostics, Risch-Rotkreuz, Switzerland) in a LightCycler 480 System (Roche Diagnostics) with 40 cycles (30 sec each of denaturation, annealing, and extension). C_q values and melt curves were analyzed with LightCycler 480 software v1.5.1.

Primers were designed and optimized for *Rattus norvegicus* using the PrimerQuest Tool (Integrated DNA Technologies, Coralville, IA). Sequences for the designed primers and amplicon sizes are presented in Table 2.1. *Gapdh* was used as a reference gene as it showed the highest stability index compared to those for β-actin and 18S rRNA (data not shown). To generate standards for quantification I obtained PCR products by endpoint PCR and purified them from agarose gels using the NucleoSpin Gel & PCR Clean-up Kit (Macherey-Nagel, Düren, Germany). Purified products were quantified and sequenced. As standards for qPCR, I used serial $\log_{10}$ dilutions ranging from 1×10^2 to 1×10^6 copies of each PCR product. qPCR target C_q values were used to calculate copy numbers using the standard curve, normalized against *Gapdh*, and are reported as fold-copy numbers compared to *Gapdh*. A schematic diagram of the primer sets used to detect full length *Mmp2* and NTT-*Mmp2* is illustrated in Fig. 2.1. The mRNA copy number for total *Mmp2*, which includes full length *Mmp2* and NTT-*Mmp2*, was measured using Primer Set 2 which targets exons 2 and 3 in *Mmp2*. The copy number for full length *Mmp2* was determined

using Primer Set 1 which targets exons 1 and 2. The copy number for NTT-*Mmp2* was calculated by the difference between total *Mmp2* copy number and full length *Mmp2* copy number.

2.2.10 Immunocytochemistry

After 24 hr exposure of NRVM cultured on coverslips to DXR or DMSO vehicle, culture medium was replaced with serum-free DMEM-F12 containing 500 nM MitoTracker Deep Red FM (Invitrogen) and incubated at 37°C for 30 min. NRVM were then washed with PBS (3x) for 5 min before being fixed with 3.2% paraformaldehyde (Electron Microscopy Sciences) in PBS for 15 min at room temperature. NRVM were then washed with PBS (3x) for 5 min. Fixed NRVM were then permeabilized with 0.1% (v/v) Triton X-100 in PBS for 10 min at room temperature. NRVM were blocked with 5% donkey serum in PBS-T (PBS containing 0.1% Tween 20) for 1 hr at room temperature. Blocking was performed by placing the cover slips in a humidified chamber (large 150 mm petri dish containing a layer of parafilm on top of filter paper soaked in water). NRVM were simultaneously incubated with the diluted primary antibodies MMP-2 ab92536 (1:50, Abcam) and troponin I MA1040 (1:200, iPOC) in blocking buffer (5% donkey serum in PBS-T) overnight at 4°C in a humidified chamber. The next day, cover slips were washed with PBS (3x) at room temperature for 10 min each in 24-well plates. The cover slips were transferred back into the humidified chamber for secondary antibody incubation. Donkey anti-rabbit IgG conjugated to Alexa Fluor 488 (A21206, Invitrogen) and goat anti-mouse IgG conjugated to Alexa Fluor 546 (A11030, Invitrogen) were diluted 1:1000 in blocking buffer and applied onto cells for 1 hr at room temperature. Cover slips were washed with PBS (3x) for 10 min each in 24-well plates. NRVM were stained with DAPI (1 µg/mL in PBS, D9542, Sigma-Aldrich) for 1 min at room temperature. Cover slips were washed with PBS (3x) before mounting onto glass slides with Vectashield hardset mounting medium (Vector Laboratories, Burlingame, CA).

2.2.11 Laser scanning confocal microscopy

NRVM were imaged on a Leica SP5 laser scanning confocal microscope (Leica, Wetzlar, Germany) within 2 days after cover slips were mounted onto glass slides. Cells were visualized using a 63x 1.2 water immersion lens. The bandwidth of emission was determined by theoretical values calculated by Thermo Fisher Scientific Fluorescence Spectra Viewer software to eliminate cross-contamination of signals. The channel settings used were: Channel 1 - DAPI, Diode laser (20% power), λ_{ex} = 405 nm, λ_{em} = 425-500 nm; Channel 2 - Alexa 488, Argon ion laser (20% power), λ_{ex} = 488 nm, λ_{em} = 508-540 nm; Channel 3 - Alexa 546, Green HeNe laser (25% power), λ_{ex} = 543, λ_{em} = 563-630 nm; and Channel 4 - MitoTracker Deep Red, Red HeNe laser (25% power), λ_{ex} = 633 nm, λ_{em} = 653-750 nm. Images from each channel were acquired sequentially by frame. Control NRVM were imaged first. The focus was set using the epifluorescence lamp (Hg arc lamp). The focal plane was adjusted with the 405 nm laser under 512x512 pixel resolution. The gain was optimized for each channel by changing the lookup table to ensure no saturation. The offset was also adjusted for each channel to darken the outline of the cells. The resolution was set to 2048x2048 pixels with 6 frame averaging to capture the image. Once the control NRVM were imaged, NRVM treated with DXR were imaged using the same settings used for control NRVM. Last, the secondary antibodies alone control were imaged at the same settings set for control NRVM to detect any signal caused by non-specific binding.

2.2.12 Determining the localization of MMP-2 in mitochondria

NRVM image files acquired on the Leica microscope (LIF) were opened using ImageJ FIJI. Region of interests (ROIs) were traced around each cardiomyocyte. A single NRVM was traced using Channel 3 (Alexa 546, anti-troponin I) using the polygon selection tool on Image J. After the cell was traced, it was saved as an ROI. The background was subtracted on ImageJ.

Colocalization analysis was determined using the Coloc 2 plugin on ImageJ. Channel 1: Alexa 488 (MMP-2) and Channel 2: MitoTracker Deep Red FM. The Costes threshold regression was selected. Point Spread Function and Costes randomisations were set to 3.0 and 15, respectively. Mander's M_1 and M_2 coefficients were determined. Mander's M_1 (above threshold of channel 2) and Mander's M_2 (above threshold of channel 1) were averaged between 3 cells per group per isolation. The analysis of three separate cell isolations and three myocytes per isolation gave a sample size of 3 with a total of 9 cells analyzed.

2.2.13 Statistical analysis

An individual result (a single biological replicate) corresponds to the NRVM cultured from a single isolation of cells pooled from the hearts of 10 pups. Results are expressed as mean ± S.E.M. and were analyzed for statistical comparison with Prism 7.01 (GraphPad Software, San Diego, CA), using one-way ANOVA followed by Tukey's *post-hoc* test or two-way ANOVA followed by Bonferroni *post-hoc* test, as appropriate. $p<0.05$ was used as the criterion for statistical significance.

2.3 Results

2.3.1 DXR induces necrosis in tumor cells but not in NRVM after 24 hr

I used a concentration of DXR (0.5 μM) which is within the concentration range seen in the blood 6 hr after administrating DXR in chemotherapy patients[242]. To confirm that this concentration of DXR induced tumor cell death, I treated HT1080 cells with 0.5 μM DXR for 24 hr and measured cell necrosis by LDH release. DXR caused cell death in HT1080 cells after 24 hr compared to control, confirming that the concentration used kills tumor cells (Fig. 2.2A). In marked contrast, DXR did not cause NRVM cell death for up to 24 hr. However, 36 and 48 hr

DXR exposure increased NRVM cell death to 15 and 50%, respectively (Fig. 2.2B).

2.3.2 DXR increases oxidative stress in NRVM

Aconitase is directly inactivated by peroxynitrite, a RONS that is generated during oxidative stress. To confirm that DXR enhances cellular oxidative stress, particularly the generation of peroxynitrite, I compared aconitase activities of lysates from control and DXR-treated NRVM. Indeed, DXR increased oxidative stress in NRVM, seen by a 57% and 62% reduction in aconitase activity after 12 hr and 24 hr, respectively, relative to control (Fig. 2.3).

2.3.3 DXR increases intracellular MMP-2 levels and activity in NRVM

I next examined the effect of DXR on intracellular MMP-2 protein level and activity in NRVM lysates (in the absence of cell necrosis) by western blot and gelatin zymography. DXR increased MMP-2 protein levels in a time-dependent manner, up to 239 ± 20% of control after 12 hr, which remained elevated at 24 hr (Fig. 2.4A). MMP-2 activity from control cells appeared as a single 72 kDa band, with no evidence of other gelatinolytic activities, including 64 kDa MMP-2 (formed following proteolysis of 72 kDa MMP-2 by an MMP-14/TIMP-2 dependent process at the cell membrane) (Fig. 2.4B), or MMP-9. DXR treatment resulted in a significant, time-dependent increase in full length MMP-2 activity which also peaked at 12 hr (311 ± 40% of control, and remained elevated at 24 hr (287 ± 30% of control) (Fig. 2.4B). MMP inhibitors ARP-100 and ONO-4817 had no effect on MMP-2 protein levels in control and DXR-exposed cells (Fig. 2.4C). ARP-100 nor ONO-4817 affected activity in control cells but significantly attenuated the DXR-induced increase in MMP-2 activity (Fig. 2.4D).

2.3.4 DXR increases the levels and activity of secreted MMP-2

To determine whether DXR alters the abundance of secreted MMP-2, MMP-2 levels and

activity in the conditioned media were measured by western blot and gelatin zymography, respectively. DXR increased secreted MMP-2 protein levels by nearly fourfold (Fig. 2.5A). This increase in protein levels corresponded to an increase in MMP-2 activity by over fourfold (Fig. 2.5B). As expected, MMP inhibitors ARP-100 and ONO-4817 did not affect the abundance in secreted MMP-2 protein levels but attenuated the activity of secreted MMP-2 to control (Fig. 2.5A,B). Activity from a lower molecular weight gelatinase was also detected in the conditioned media. However, this gelatinolytic activity was unchanged between groups. This secreted ~35 kDa gelatinase could be attributed to the catalytic domain of MMP-2, given that there is no detectable MMP-9 activity in the conditioned media.

2.3.5 DXR upregulates NTT-MMP-2 and full-length MMP-2 mRNA expression

To better understand which intracellular MMP-2 isoforms are activated by DXR, I measured the effect of DXR on total *Mmp2*, full length *Mmp2*, and NTT-*Mmp2* mRNA expression. DXR increased total *Mmp2* mRNA levels in a time-dependent manner, up to 580% of control after 24 hr (Fig. 2.6A). 24 hr DXR exposure increased full length *Mmp2* and NTT-*Mmp2* mRNA levels by 680% and 560%, respectively (Fig. 2.6B,C). By comparing the copy numbers of full length *Mmp2* and NTT-*Mmp2* to total *Mmp2*, I determined the proportion of each MMP-2 isoform that constitute total *Mmp2*. In both control and DXR-treated NRVM, 88% of total *Mmp2* encodes the NTT-MMP-2 isoform and the remaining 12% is expressed as full length MMP-2 (Fig. 2.6D).

2.3.6 The effect of DXR on TIMP levels in NRVM

The activity of both intracellular and extracellular MMP-2 is post-translationally regulated by TIMPs. I measured the levels of TIMP-4, an abundant intracellular TIMP isoform found in cardiomyocytes[51], in NRVM lysates. However, TIMP-4 levels were not affected by DXR with or

without MMP inhibitors (Fig. 2.7). TIMP-3, the primary extracellular TIMP isoform, was not detectable in the NRVM lysates nor in the cell conditioned media (data not shown, n=6).

2.3.7 Potential sarcomeric targets of MMP-2 in NRVM

In adult rat hearts undergoing oxidative stress injury, intracellular MMP-2 proteolyzes the sarcomeric proteins troponin I[84] and α-actinin[86], thereby impairing cardiac muscle contractility[84]. I assessed the levels of these proteins in NRVM exposed to DXR for 24 hr. DXR treatment had no effect on α-actinin levels (Fig. 2.8A), whereas it caused a 40% decrease in troponin I which was not prevented by ARP-100 and ONO-4817 (Fig. 2.8B). Lower molecular weight bands, suggestive of proteolytic cleavage, were not detected for either protein. ARP-100 and ONO-4817 alone had no effect on troponin I (Fig. 2.8B). Troponin I mRNA (*Tnni3*) expression was then evaluated by qPCR. 24 hr DXR treatment nearly abolished *Tnni3* expression by 95% relative to control NRVM (Fig. 2.8C). These results indicate that the DXR-induced decrease in troponin I in NRVM occurs at a transcriptional level, and that, under these conditions, the DXR-induced up-regulation of MMP-2 does not directly result in increased troponin I proteolysis.

2.3.8 Putative targets of MMP-2 in the sarcoplasmic reticulum

To identify potential targets of MMP-2 in the sarcoplasmic reticulum, I measured the levels of SERCA2a and phospholamban in control and DXR-treated NRVM. DXR reduced SERCA2a (Fig. 2.9A) and phospholamban (Fig. 2.9B) protein levels in NRVM lysates by ~40% compared to control. However, ARP-100 and ONO-4817 did not restore the levels of SERCA2a and phospholamban. Coomassie Blue was used as a loading control as GAPDH was not sensitive enough for the amount of lysate protein analyzed due to the abundance of SERCA2a and phospholamban protein in NRVM lysates.

2.3.9 DXR decreases SERCA2a and phospholamban mRNA expression in NRVM

Since pharmacological inhibition of MMP-2 did not restore the levels of SERCA2a and phospholamban, I measured the mRNA expression of *Atp2a2* and *PLN*, which encode for SERCA2a and phospholamban, respectively, to determine whether DXR downregulates their expression. 24 hr DXR treatment reduced *Atp2a2* expression by 70% relative to control NRVM (Fig. 2.10A). DXR also reduced the expression of *PLN* by 40% relative to control NRVM (Fig. 2.10B). These results indicate that DXR downregulates the expression of *Atp2a2* and *PLN*, resulting in reduced SERCA2a and phospholamban protein levels, independent of increased MMP-2 activity.

2.3.10 The subcellular localization of MMP-2 in DXR-treated NRVM

Both 72 kDa MMP-2 and NTT-MMP-2 are also found in the mitochondria[18, 95]. Although there is abundant 72 kDa MMP-2 in the mitochondria, its levels are more enriched in the MAM[95]. Since DXR increased the expression of both 72 kDa MMP-2 and NTT-MMP-2, I performed immunocytochemistry to determine the subcellular distribution of MMP-2 in NRVM. NRVM were loaded with DAPI, MitoTracker Red, and an anti-MMP-2 antibody to label nuclei, mitochondria, and MMP-2, respectively. A control where the primary antibody is omitted and only the secondary antibody was used showed an absence of non-specific binding in control (Fig. 2.11A) and DXR-treated NRVM (Fig. 2.11B). Nuclei (Fig. 2.11C,D), mitochondria (Fig. 2.11E,F), and MMP-2 (Fig. 2.11G,H) were visualized in control and DXR-treated NRVM. Mitochondria were clustered around the nucleus and distributed throughout the cytosol in control NRVM (Fig. 2.11A,E). In DXR-treated NRVM, mitochondria remained clustered around the nuclei however its distribution in the cytosol was markedly reduced compared to control NRVM (Fig. 2.11B,F). After merging the individual images of MMP-2 and mitochondria, I found that MMP-2 was localized in

the mitochondria (co-localization seen in yellow) and cytosol in control and DXR-treated NRVM (Fig. 2.11I,J). Using Mander's overlap coefficient to analyze the mitochondrial localization of MMP-2, I found that MMP-2 was localized in mitochondria in control NRVM (Fig. 2.11I,K). Co-localization of MMP-2 in the mitochondria was reduced and redistributed to the cytosol in DXR-treated NRVM (Fig. 2.11J,L).

2.4 Discussion

In this study, I demonstrated that DXR used at a clinically relevant concentration increases intracellular MMP-2 protein levels and activity detectable in neonatal cardiac myocytes. For the first time I identified the intracellular MMP-2 isoforms stimulated by DXR in cardiac myocytes as full length MMP-2 was upregulated and accompanied by the *de novo* expression of NTT-MMP-2. In contrast to my hypothesis that MMP-2 would proteolyze sarcomeric proteins α-actinin and/or troponin I, I found no changes in the former while the reduction in troponin I was independent of MMP-2 activity.

DXR enhanced oxidative stress in NRVM, measured as a reduction in aconitase activity, was concurrent with increased MMP-2 activity in cell lysates. DXR enhances the generation of reactive oxygen-nitrogen species including peroxynitrite in cardiac myocytes[166] and myocardium[243]. Oxidative stress activates intracellular MMP-2 by three primary mechanisms. Firstly, peroxynitrite reacts with full length MMP-2 which causes the S-glutathiolation of a critical cysteine residue in its autoinhibitory domain[39]. This post-translational modification exposes the catalytic zinc site and renders the enzyme proteolytically active[39]. Secondly, oxidative stress also increases the biosynthesis of full length MMP-2 by enhancing the binding of AP-1 to the *Mmp2* gene promoter[21]. Thirdly, it also can trigger the *de novo* expression of NTT-MMP-2 via an

alternate transcription start site located within the first intron[18]. I found that DXR increased the mRNA expression for both full length *Mmp2* and NTT-*Mmp2*. Our results reveal that DXR increases MMP-2 activity in cardiac myocytes by upregulating these two intracellular isoforms. Interestingly, NTT-*Mmp2* constituted almost 90% of total *Mmp2* expression in both control and doxorubicin treated cells. It remains unclear why control NRVM express NTT-MMP-2. It is likely that the harsh process of isolating NRVMs via enzymatic digestion followed by serum starvation during cell treatment enhances cellular oxidative stress even in control cells.

In addition to increased MMP-2 activity detectable in NRVM lysates, DXR also increased secreted 72 kDa MMP-2 levels and activity in the conditioned media. I did not detect 64 kDa MMP-2 in the conditioned media, suggesting that MMP-2 was not proteolytically activated by MMP-14/TIMP-2 in the extracellular matrix. This is consistent with our previous work which showed that increased oxidative stress (by ischemia-reperfusion injury) stimulates 72 kDa MMP-2 secretion in isolated and perfused rat hearts[192]. Increased secretion of MMP-2 likely contributes to adverse myocardial extracellular matrix remodeling in chronic DXR cardiotoxicity[244].

Increased intracellular MMP-2 activity and myofibrillar disorganization occur in several heart pathologies associated with increased oxidative stress[63, 84, 86]. In myocardial ischemia-reperfusion injury, MMP-2 localized to the Z-disc region of the sarcomere[63] proteolyzes sarcomeric proteins including troponin I[84], α-actinin[86], and titin[63]. DXR cardiotoxicity is associated with a loss of sarcomeric proteins including α-actin, titin, troponin I, myosin light chain 2, and myosin binding protein C[129, 177, 245]. However, it is unknown whether this loss occurs at a transcriptional level or post-translationally via proteolysis. DXR caused a reduction in cellular troponin I without detectable degradation products which was not attenuated with two different selective MMP inhibitors. Although troponin I has been identified as a MMP-2 substrate in

myocardial ischemia-reperfusion injury in adult rat hearts, it is possible that MMP-2 is not localized to troponin I in NRVM exposed to DXR. Recent work has determined that NTT-MMP-2 is, in part, localized to subsarcolemmal mitochondria. Given that 90% of the MMP-2 mRNA expressed in NRVM is NTT-MMP-2, our findings that MMP inhibitors did not prevent DXR-induced reduced troponin I levels are consistent with previous reports that upregulation of NTT-MMP-2 does not result in myofilament lysis[246]. To test whether DXR triggers compensatory TIMP expression, I measured the levels of TIMP-4, the most abundant TIMP in the heart[247] and which is localized within cardiomyocytes[51], in NRVM lysates. However TIMP-4 levels were unaffected by DXR in the presence or absence of MMP inhibitors, ruling out the possibility that enhanced intracellular TIMP may have blocked troponin I and α-actinin proteolysis by MMP-2. Instead, I found that a significant reduction in troponin I mRNA may account for its reduced protein level.

MMP-2 is also localized to the mitochondria-associated membrane, a specialized region of the sarcoplasmic reticulum, in NRVM[95]. Preliminary work from our lab showed that MMP-2 protein and activity are detected in purified sarcoplasmic reticulum fractions from an adult rat heart[97]. However, its precise role in the sarcoplasmic reticulum is unknown. I investigated two sarcoplasmic reticulum proteins, SERCA2a and phospholamban, which are susceptible to proteolysis in myocardial oxidative stress injury[248, 249]. Degradation of these proteins was prevented by calpain inhibitors. It has since then been demonstrated that the calpain inhibitors ALLN and MDL-28170 used in these studies are also MMP inhibitors[149]. I found that DXR reduced SERCA2a and phospholamban protein levels in NRVM, an effect that could not be rescued with MMP inhibition. I then found that DXR reduced *Atp2a2* and *PLN* mRNA expression, resulting in decreased protein levels. My results suggest the loss of troponin I, SERCA2a, and phospholamban in DXR-treated NRVM are due to transcriptional down-regulation.

Since both 72 kDa MMP-2 and NTT-MMP-2 are localized in the mitochondria, I determined the effect of DXR on the subcellular localization of MMP-2 in NRVM. I found that MMP-2 was co-localized in the mitochondria in control NRVM. This is consistent with previous work[95, 231] which localized 72 kDa MMP-2 and NTT-MMP-2 in the mitochondria. Interestingly, the proportion of MMP-2 localized to the mitochondria was significantly decreased in DXR-treated NRVM. The mechanism of this redistribution of MMP-2 from the mitochondria to the cytosol remains unclear. It is possible that MMP-2 is secreted from the mitochondria through the mitochondrial permeability transition pore, which is formed by DXR-induced increased oxidative stress[164, 250].

In conclusion, I have shown that the anthracycline DXR activates full length MMP-2 and triggers increased expression of NTT-MMP-2 in neonatal rat cardiac myocytes. DXR-induced activation of MMP-2 was successfully attenuated by selective MMP inhibitors. I found that troponin I, SERCA2a, and phospholamban protein levels were reduced in an MMP-independent manner as a result of transcriptional down-regulation. Preliminary work revealed that DXR caused MMP-2 to redistribute from the mitochondria to the cytosol. Given the known ability of MMP-2 to degrade intracellular proteins with significant pathophysiological consequences, it will be important to identify the roles and proteolytic targets of MMP-2 at its subcellular locales in anthracycline cardiotoxicity. For example, in addition to the sarcomere, MMP-2 and NTT-MMP-2 are also compartmentalized in the mitochondria, MAM, and nucleus[18, 95, 238, 246]. Understanding the role of MMP-2 in cardiac myocytes may reveal new strategies for effective cancer chemotherapy without comprising heart function.

Table 2.1: Primer sequences for qPCR in NRVM.

Gene	Forward Primer Sequence (5'-3')	Reverse Primer Sequence (5'-3')	Amplicon size (bp)
Gapdh	AACTTTGTGAAGCTCATTTCCTGGTATG	GGGTGGTCCAGGGTTTCTTACTC	110
Mmp2 exons 1-2	GCCCTCTGCGGGTTCTCTGC	TTGCAACTCTCCTTGGGGCAGC	163
Mmp2 exons 2-3	TGACCAGAACACCATCGAGACC	AGTGGAGTTACGTCGCTCCATAC	204
Tnni3	CCATTCTCTACCTCTGGAGATCAGC	TTCTGGAGGCGGAGATCTTAGAC	164
Atp2a2	CCTTGCTGGAACTTGTGATCGAG	TCAGCGTTTCTCTCCTGCCATAC	196
PLN	TGTGACGATCACAGAAGCCAAGG	GATAGCCGAGCGAGTAAGGTATTGG	166

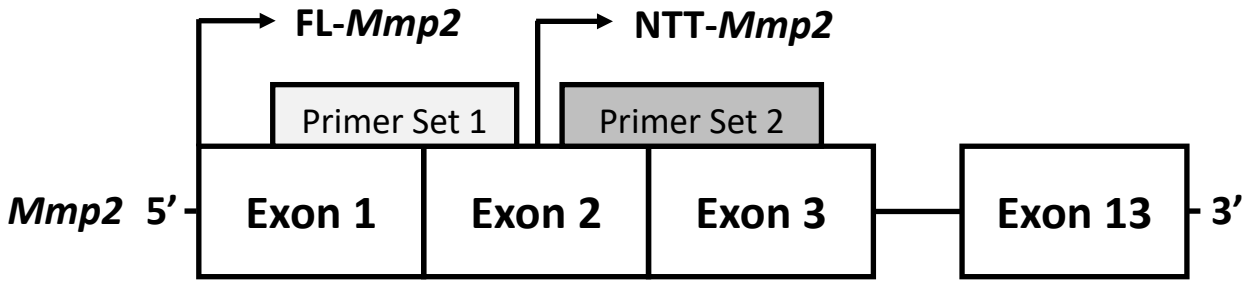

Figure 2.1: Schematic diagram of the primers used to detect full length (FL)- *Mmp2* and NTT-*Mmp2* in NRVM lysates. The mRNA copy number for total *Mmp2* (FL-*Mmp2* + NTT-*Mmp2*) was measured using Primer Set 2 which targets exons 2 and 3 in the *Mmp2* gene. The copy number for FL-*Mmp2* was detected using Primer Set 1 which targets exons 1 and 2. The copy number for NTT-*Mmp2*, which lacks exon 1, was calculated by the difference between total *Mmp2* copy number (Primer Set 1) and FL-*Mmp2* copy number (Primer Set 2).

A

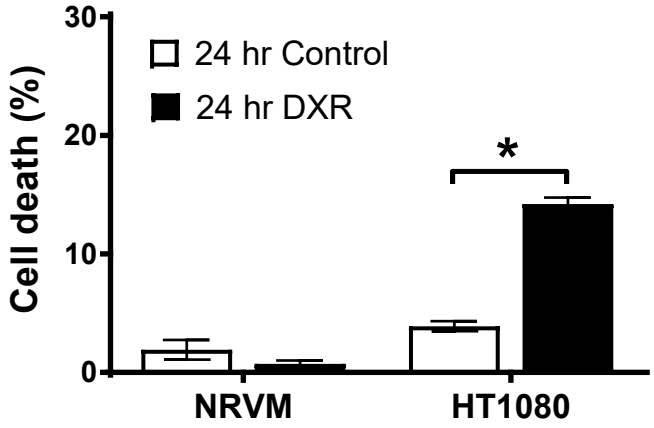

B

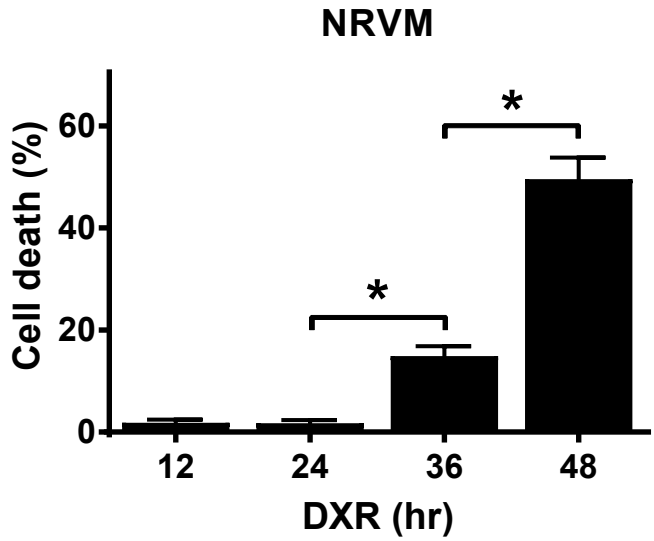

Figure 2.2: Doxorubicin (DXR) induces necrosis in tumor cells but not in NRVM after 24 hr. (A) DXR (0.5 μM, 24 hr) caused cell death in human fibrosarcoma HT1080 cells but not in NRVM (n=8). * $p<0.05$ by two-way ANOVA followed by Bonferroni's post hoc test. (B) DXR (0.5 μM) caused significant cell death in NRVM only after 36 hr or longer exposure (n=5). * $p<0.05$ by one-way ANOVA followed by Tukey's post hoc test. Bar graphs represent mean ± S.E.M.

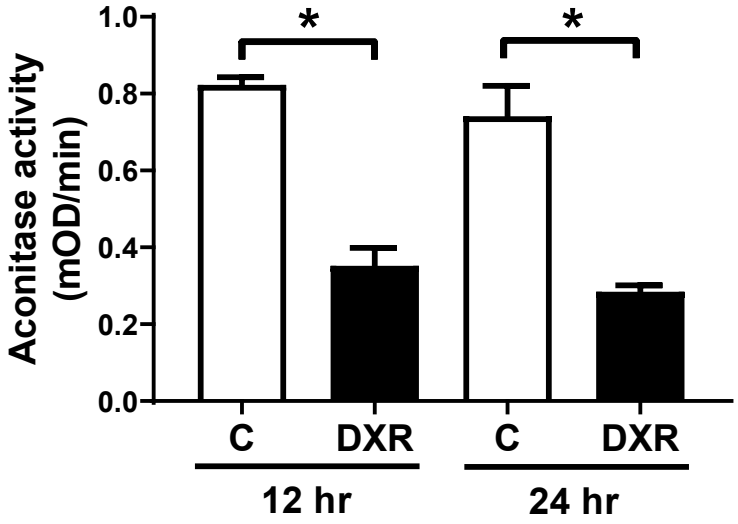

Figure 2.3: DXR significantly enhances cellular oxidative stress in NRVM at 12 and 24 hr, as measured by a reduction in aconitase activity (n=4). * $p<0.05$ by two-way ANOVA followed by Bonferroni's post hoc test. Bar graphs represent mean ± S.E.M.

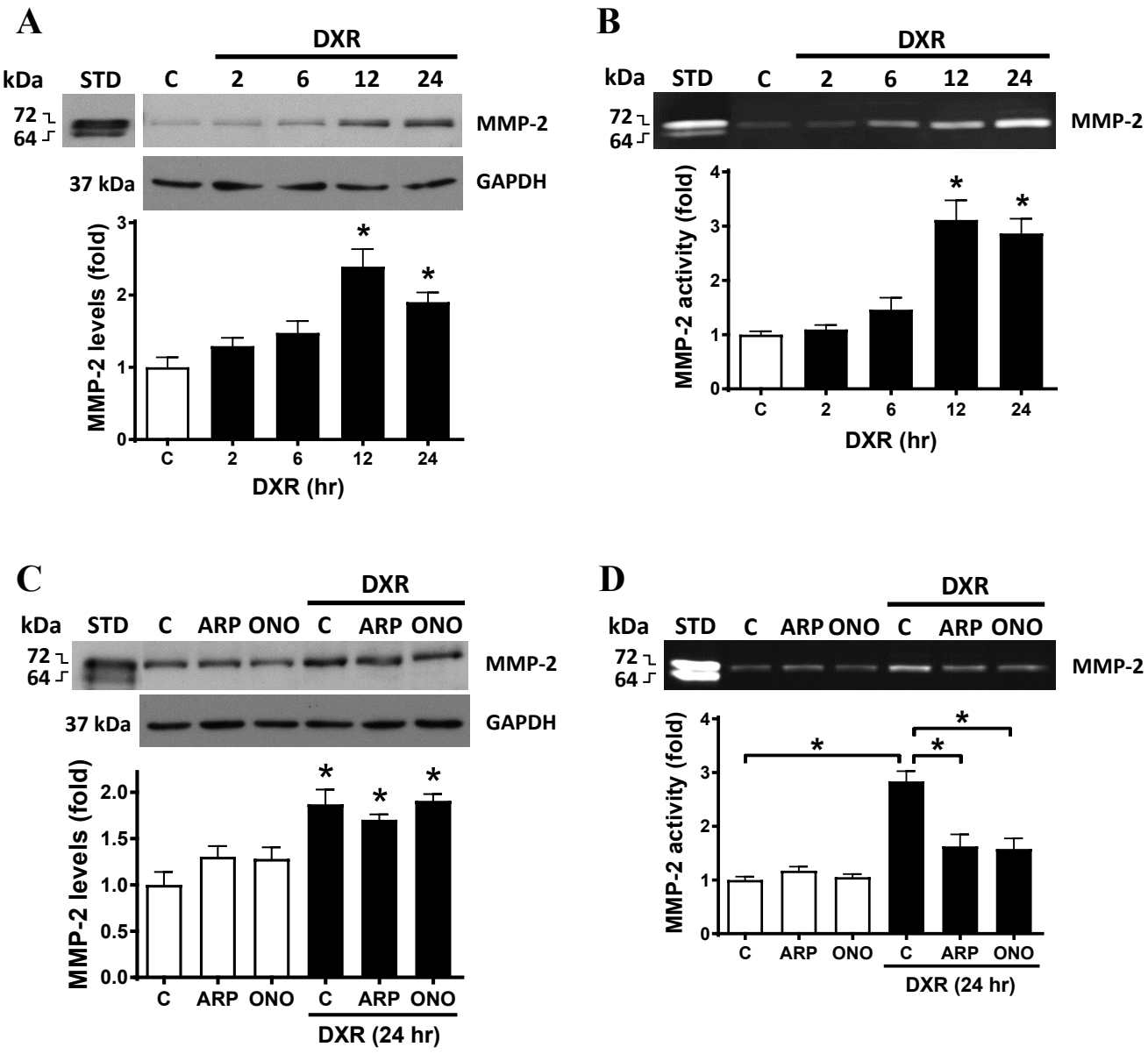

Figure 2.4: DXR increases MMP-2 activity and protein level NRVM lysates. (A) DXR (0.5 μM) increased MMP-2 protein level in NRVM lysates in a time-dependent manner, peaking at 12 hr (n=5). (B) DXR increased intracellular MMP-2 activity in a time-dependent manner (n=5). (C) MMP inhibitors ARP-100 and ONO-4817 (1 μM each) did not affect MMP-2 protein levels (n=5). (A-C): * $p<0.05$ versus vehicle control by one-way ANOVA followed by Dunnett's post hoc test. (D) ARP-100 and ONO-4817 attenuated DXR-induced increase in MMP-2 activity (n=7). * $p<0.05$ versus control by one-way ANOVA followed by Tukey's post hoc test. STD: HT-1080 cell conditioned medium. Bar graphs represent mean ± S.E.M.

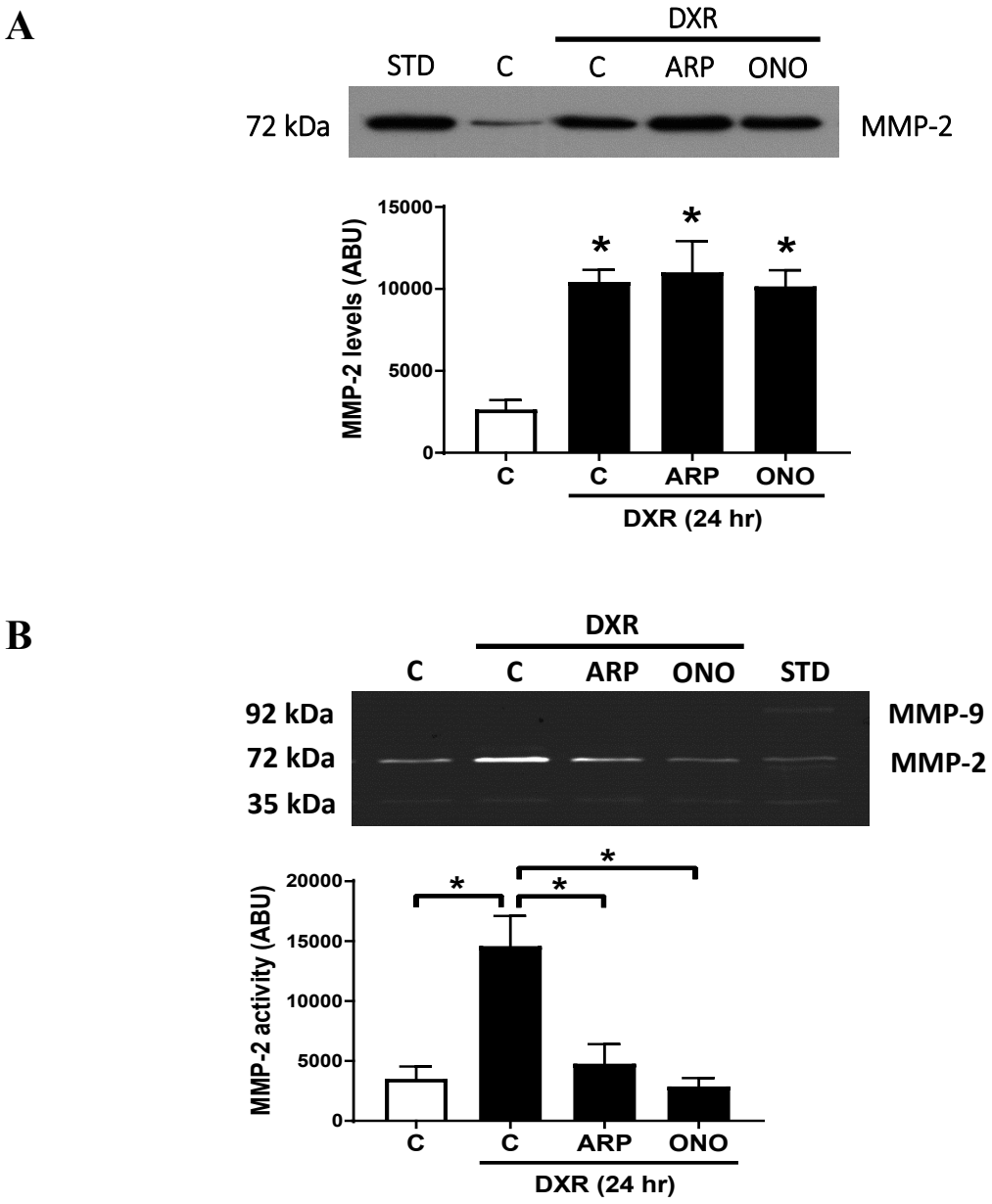

Figure 2.5: DXR increases secreted MMP-2 levels and activity from NRVM. (A) DXR (0.5 μM, 24 hr) increased levels of MMP-2 secreted into the conditioned media (n=4). * $p<0.05$ versus vehicle control by one-way ANOVA followed by Tukey's post hoc test. (B) DXR increased secreted MMP-2 activity, an effect that was reduced by ARP-100 and ONO-4817 (n=5). ABU: arbitrary units. Bar graphs represent mean ± S.E.M. * $p<0.05$ by one way ANOVA followed by Tukey's post hoc test.

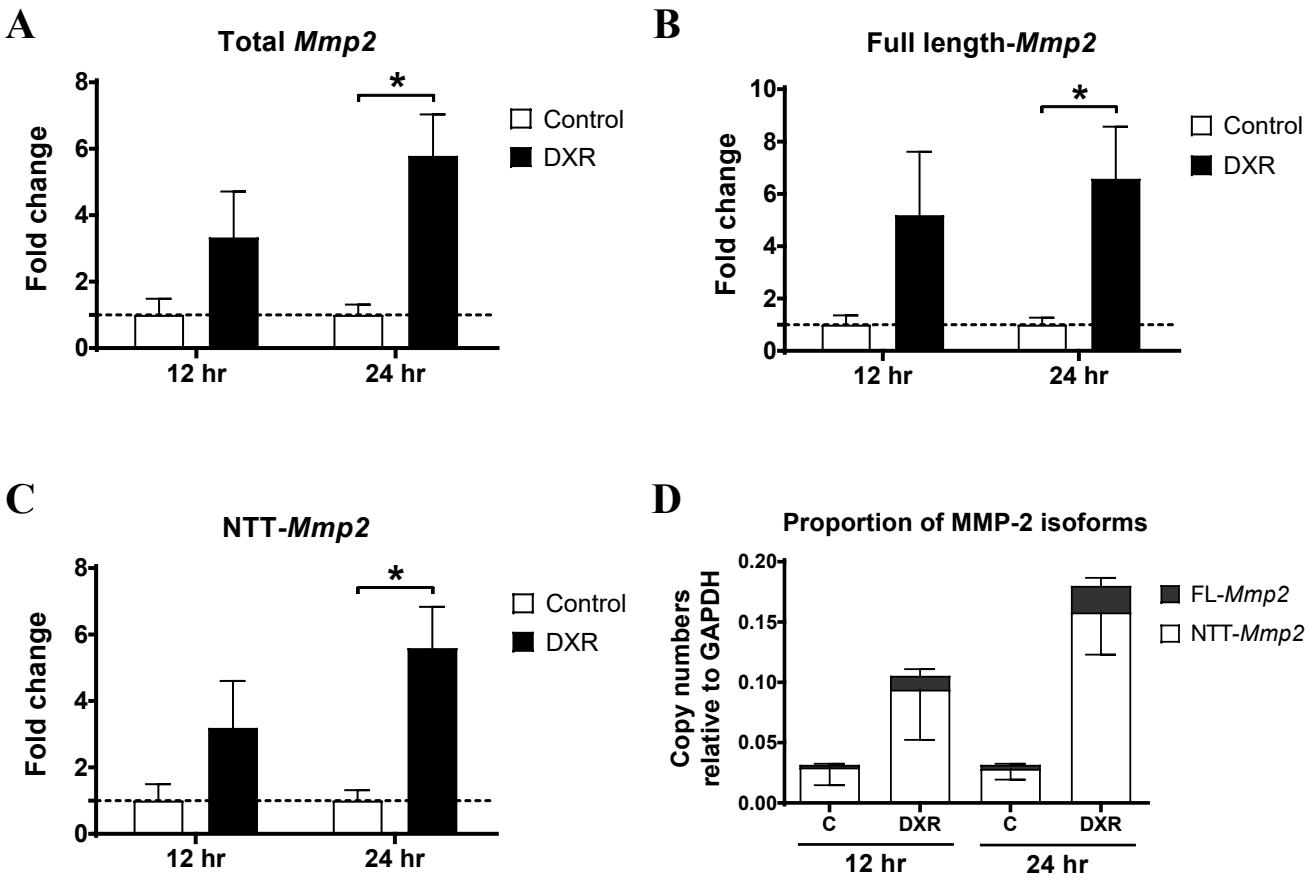

Figure 2.6: DXR enhances the expression of full length and N-terminal truncated (NTT) *Mmp2* in NRVM. (A) DXR (0.5 μM) increased expression of total *Mmp*2, (B) full length (72 kDa) *Mmp*2, and (C) NTT-*Mmp*2 isoforms in a time-dependent manner as measured by qPCR. (A-C): * $p<0.05$ by two-way ANOVA followed by Bonferroni's post hoc test. (D) The majority of DXR-induced *Mmp2* expression in NRVM was attributed to the NTT-MMP-2 isoform (n=6-8). Bar graphs represent mean ± S.E.M.

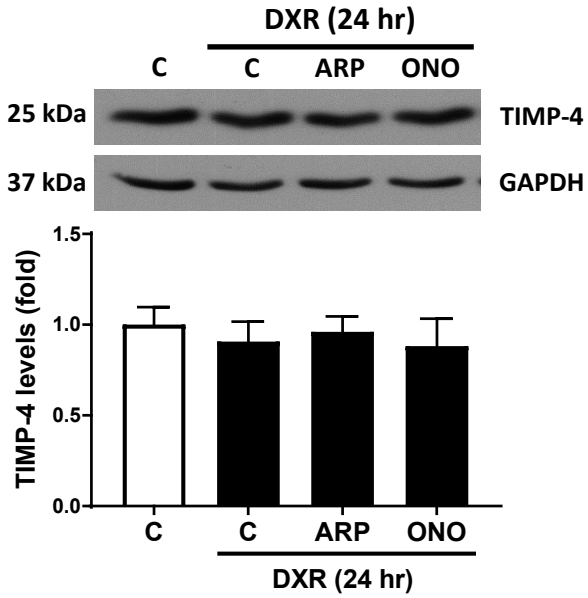

Figure 2.7: DXR did not alter TIMP-4 protein levels in NRVM lysates after 24 hr (n=6). Bar graphs represent mean ± S.E.M. $p>0.05$ by one-way ANOVA.

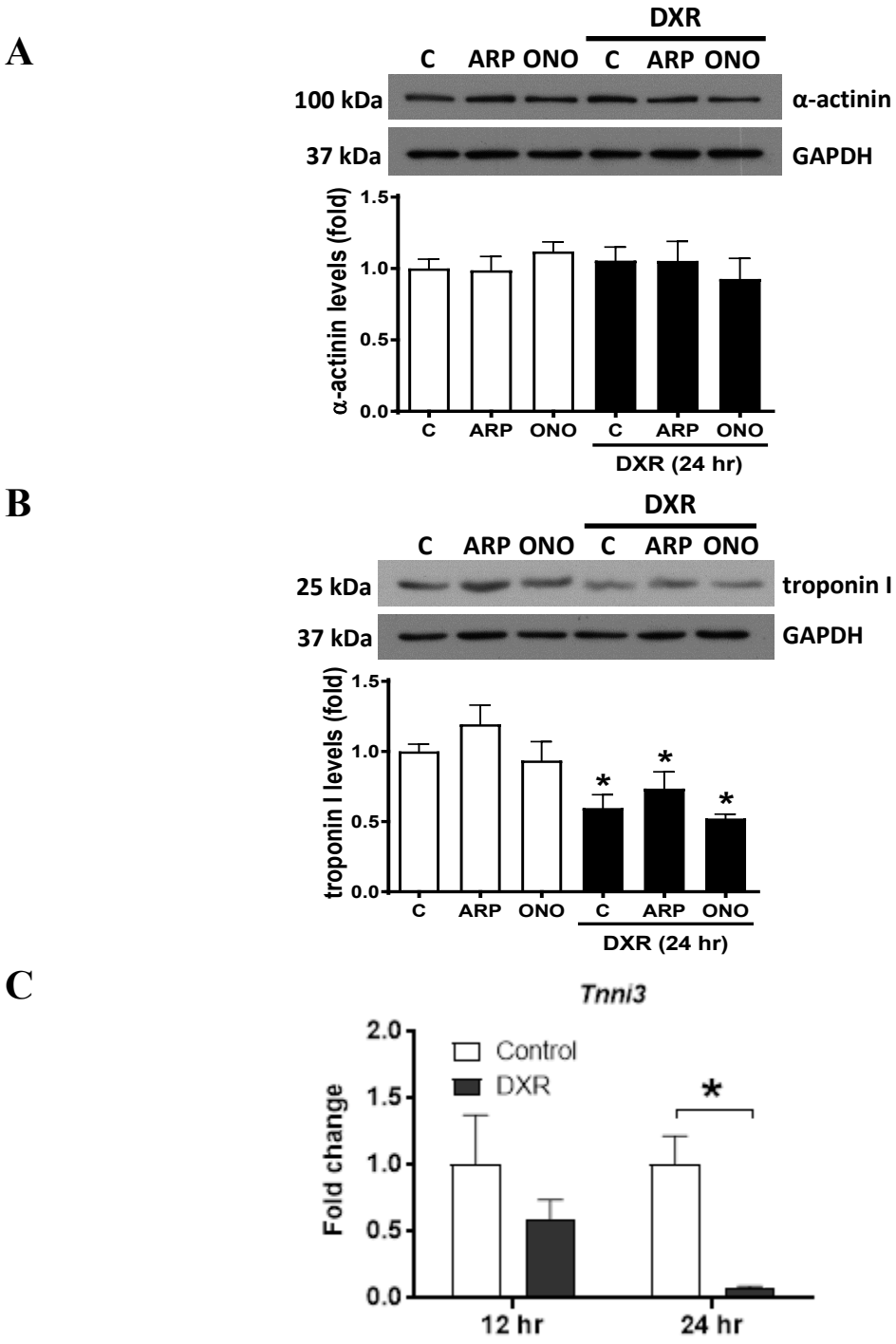

Figure 2.8: The effect of DXR on levels of sarcomeric proteins α-actinin and troponin I in NRVM. (A) DXR (0.5 μM) did not affect α-actinin levels after 24 hr (n=5). (B) In contrast, DXR reduced the levels of troponin I which was not prevented with MMP inhibitors ARP-100 and ONO-4817 (n=5). * $p<0.05$ by one-way ANOVA followed by Dunnett's post hoc test. (C) DXR reduced troponin I (*Tnni3*) mRNA expression after 24 hr (n=8). Bar graphs represent mean ± S.E.M. * $p<0.05$ by two-way ANOVA followed by Bonferroni's post hoc test.

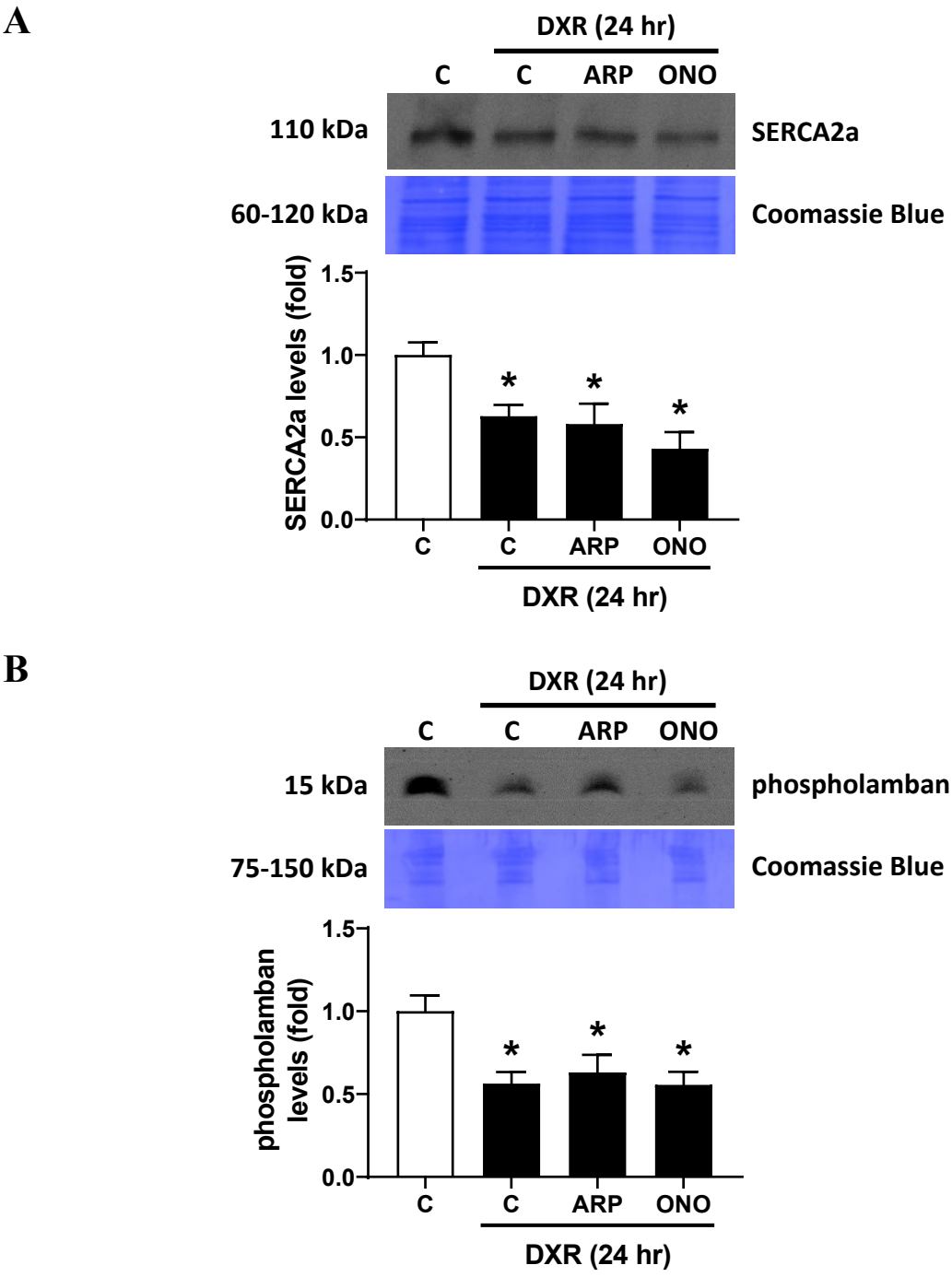

Figure 2.9: The effect of DXR on sarcoplasmic reticulum resident proteins SERCA2a and phospholamban in NRVM. DXR reduced the levels of (A) SERCA2a and (B) phospholamban, which were not prevented with MMP inhibitors ARP-100 and ONO-4817 (n=5). Bar graphs represent mean ± S.E.M. * $p<0.05$ by one-way ANOVA followed by Dunnett's post hoc test.

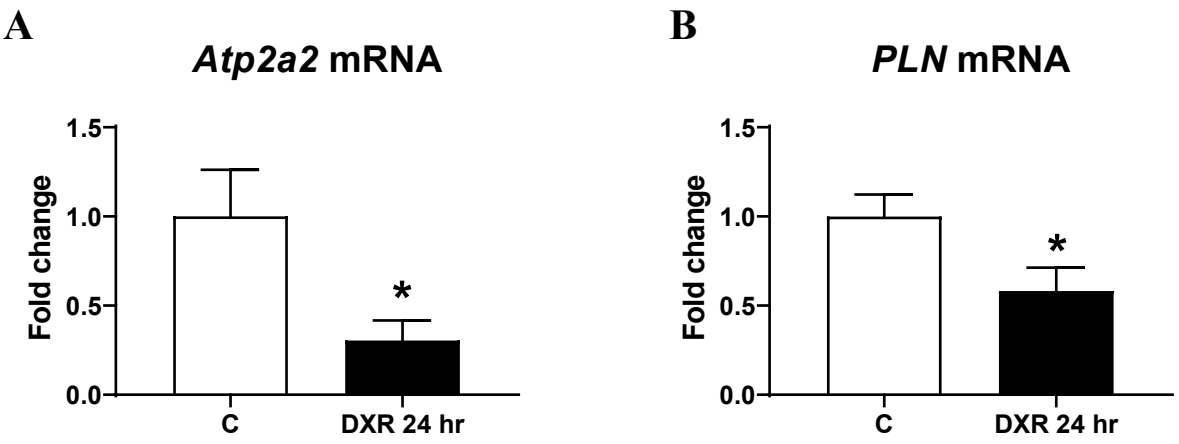

Figure 2.10: DXR decreased the expression of (A) *Atp2a2* and (B) *PLN*, which encode sarcoplasmic reticulum proteins SERCA2a and phospholamban, respectively (n=7). Bar graphs represent mean ± S.E.M. * $p<0.05$ versus control by paired two-tailed t-test.

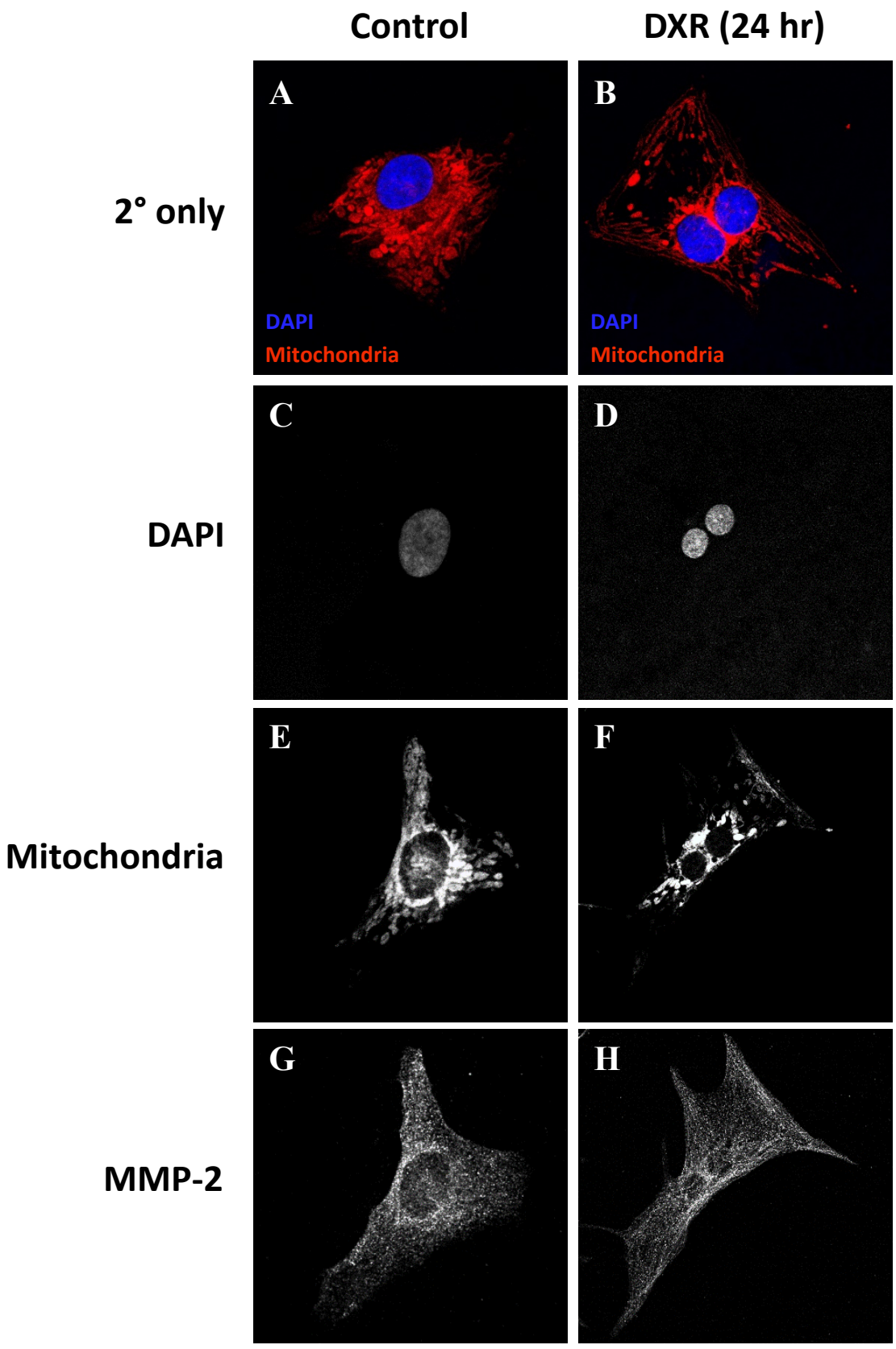
Control
DXR (24 hr)
2° only
DAPI
Mitochondria
MMP-2
A
B
C
D
E
F
G
H
DAPI
Mitochondria
DAPI
Mitochondria

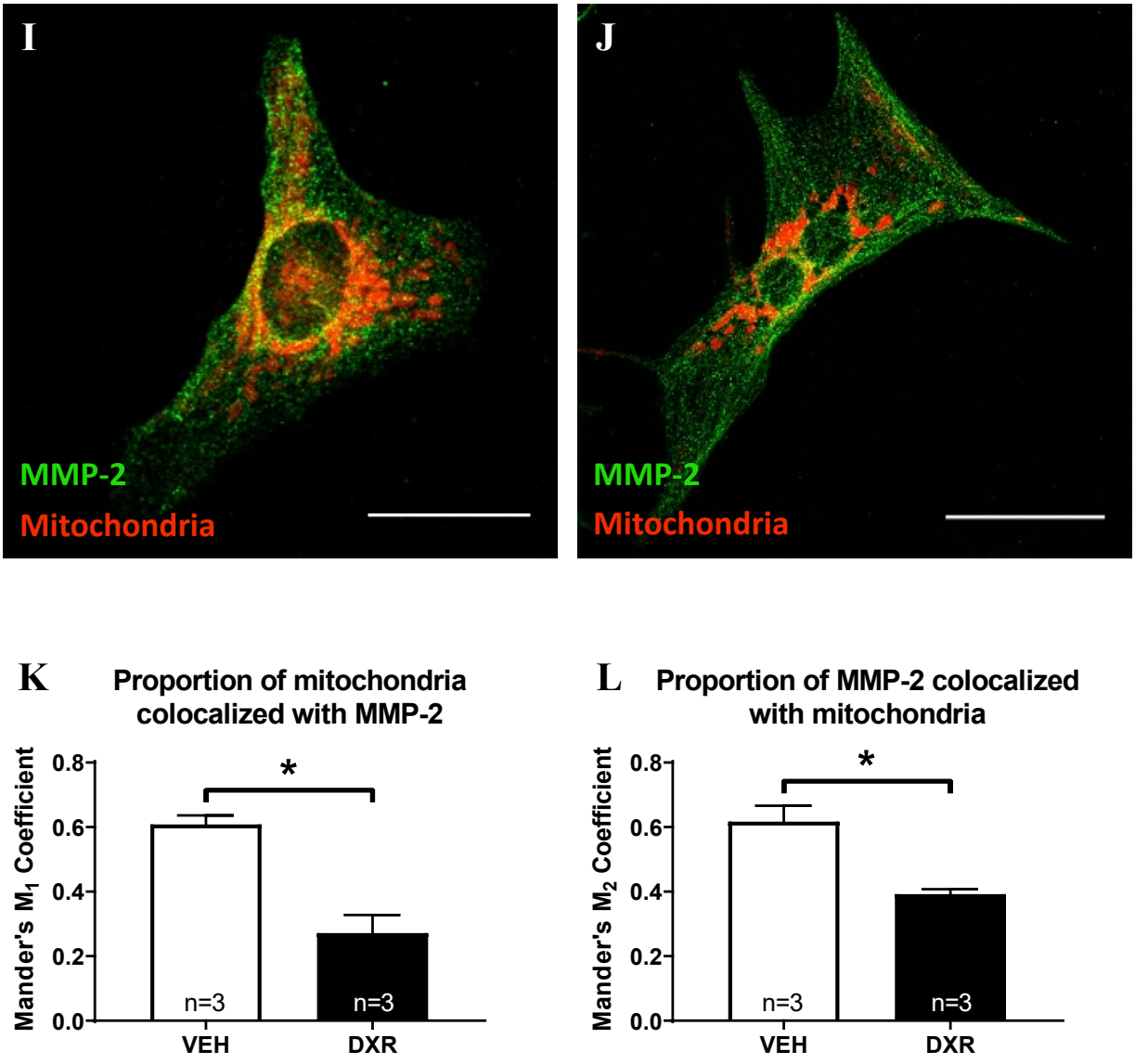

Figure 2.11: DXR caused a redistribution of intracellular MMP-2 from the mitochondria to the cytosol in NRVM. Non-specific binding from the secondary antibody was not observed in (A) Control or (B) DXR-treated NRVM. Control and DXR-treated NRVM were stained with (C,D) DAPI, (E,F) MitoTracker Red, and an (G,H) anti-MMP-2 antibody. (I,J) Representative merged images of MMP-2 and MitoTracker Red in Control and DXR-treated NRVM (co-localization seen as yellow). Scale bar = 20 µm. Co-localization of MMP-2 to the mitochondria was determined by Mander's Overlap Coefficient M_1 (K) and M_2 (L). MMP-2 is co-localized in mitochondria in Control NRVM. DXR reduced the localization of MMP-2 in the mitochondria. Bar graphs represent mean ± S.E.M. * $p<0.05$ versus control by paired two-tailed t-test.

CHAPTER 3

Matrix metalloproteinase inhibitors attenuate doxorubicin cardiotoxicity by preventing intracellular and extracellular matrix remodeling

A manuscript based on this chapter is in preparation:

Chan BYH, Roczkowsky R, Poirier M, Cho WJ, Sergi C, Granzier H, Schulz R. Matrix metalloproteinase inhibitors attenuate doxorubicin cardiotoxicity by preventing intracellular and extracellular matrix remodeling.

3.1 Introduction

Despite the advent of targeted cancer therapies, anthracyclines such as doxorubicin (DXR) are still used to treat over 50% of childhood cancers and adult malignancies[251]. Paradoxically, improvements in cancer survival have dramatically increased cardiovascular complications as a result of the severe, irreversible cardiotoxic side effects of many chemotherapeutic agents including anthracyclines, alkylating agents, taxanes, and immunotherapies[151, 168]. One in four patients develop asymptomatic left ventricular dysfunction and one in 20 patients develop overt heart failure when taking anthracyclines[163]. Prophylactic treatment with heart failure drugs (β-blockers, ACE inhibitors, angiotensin II receptor antagonists) have showed modest, short-term improvements in ejection fraction, but long-term cardiac remodeling was unabated[185, 186]. An adjuvant therapy is needed to prevent anthracycline cardiotoxicity.

Developing an adjuvant therapy has been challenging in part because the mechanism of DXR cardiotoxicity is multifactorial. Anthracyclines enhance oxidative stress which ultimately leads to cardiomyocyte death[168]. Important pathophysiological mechanisms linking these events include mitochondrial dysfunction[170], extracellular matrix remodeling[181], and degradation of sarcomeric proteins[129].

Matrix metalloproteinases (MMPs) are zinc-dependent proteases best recognized for their roles in tissue remodeling by proteolyzing extracellular matrix proteins in both physiological and pathophysiological processes. This includes angiogenesis, wound healing, cellular proliferation, cancer metastasis, atherosclerosis, and myocardial infarction[9]. In fact, broad spectrum MMP inhibitors such as batimastat and marimastat were developed as anticancer drugs. It has since been recognized that MMPs also target non-extracellular matrix substrates both inside[8, 11] and outside[252]

the cell. Of the 23 human MMPs, MMP-2 is localized in discrete subcellular compartments within cardiomyocytes including the sarcomere, cytoskeleton, nuclei, and mitochondria[218]. Oxidative stress increases MMP-2 expression by transcriptional upregulation[21] and/or triggers an alternative transcription start site to produce an intracellular N-terminal truncated (NTT)-MMP-2 that is devoid of a signal sequence[18]. Furthermore, oxidative stress directly activates intracellular MMP-2 by post-translational modification via the S-glutathiolation of a critical cysteine in its autoinhibitory domain[39]. Activated MMP-2 directly impairs cardiac contractile function by proteolyzing several sarcomeric proteins including troponin I, myosin light chain-1, and titin[63].

Titin is a giant myofilament protein which functions both as a scaffold for sarcomeric assembly and as a molecular spring in striated muscle cells[98]. Titin molecules are anchored at the Z-disc and extend to the M-line of the sarcomere (Fig. 1.5). Titin is composed of an extensible region and highly conserved inextensible regions, which secure the thin and thick filaments near the Z-disc and A-band region, respectively. In the cardiomyocyte, the extensible I-band region is spliced by RNA binding motif protein 20 (RBM20) to produce either N2B (~3 MDa) or N2BA (>3.3 MDa) titin isoform (Fig. 1.5)[104]. Cardiomyocytes that express higher levels of the smaller N2B titin isoform exhibit greater passive force than those that express more N2BA titin[99]. Alterations in titin isoform expression and titin proteolysis are implicated in dilated cardiomyopathy and ischemic heart injury[63, 125, 253]. Indeed, inhibition of MMP-2 activity ameliorated cardiac dysfunction in ischemic heart injury by preventing the degradation of sarcomeric proteins including titin[218]. Titin proteolysis[129] and upregulation of intracellular MMP-2[254] are implicated in DXR-induced cardiomyocyte injury. However, whether MMP-2 is responsible for titin proteolysis caused by the cardiotoxic side effects of anthracyclines remains unknown.

Given the roles of MMP-2 in intracellular and extracellular matrix remodeling, we determined whether titin is a target of MMP-2 and evaluated the effect of MMP inhibitors on left ventricular remodeling and cardiac dysfunction in DXR cardiotoxicity.

3.2 Methods

3.2.1 Reagents

Reagents used for this investigation were purchased from Sigma-Aldrich (Oakville, Ontario) unless stated otherwise. The MMP inhibitor ONO-4817 was a gift from Ono Pharmaceutical Co., Osaka, Japan.

3.2.2 Animal protocol

All experiments involving animals in this study were approved by the University of Alberta Institutional Animal Care and Use Committee, in accordance to the *Guide to the Care and Use of Experimental Animals* published by the Canadian Council on Animal Care (AUP protocol number 329).

3.2.3 Preparation of drugs

Doxorubicin hydrochloride (DXR, D1515, Sigma-Aldrich) was dissolved in sterile 0.9% saline to a final concentration of 1 mg/mL. The stock of DXR was then filtered through a 0.22 μm syringe filter, then aliquoted, and stored at -80°C until use. Doxycycline hyclate (Doxy, D9891, Sigma-Aldrich) was dissolved in sterile 0.9% saline containing 2% (w/v) carboxymethyl cellulose to a final concentration of 3.75 mg/mL. ONO-4817 was resuspended in sterile 0.9% saline containing 2% (w/v) carboxymethyl cellulose to a final concentration of 15 mg/mL. Doxy and ONO-4817 were prepared fresh daily before administering to the mice.

3.2.4 Doxorubicin cardiotoxicity protocol

The DXR and MMP inhibitor treatment regimen is outlined in Fig. 3.1. To avoid the sex-dependent sensitivities to DXR cardiotoxicity[151, 255], only male mice were used in this study. DXR was administered to male C57BL/6J mice at 8 weeks of age, once a week for 4 weeks (6 mg/kg/wk, i.p., cumulative dose of 24 mg/kg). This dose of DXR is clinically relevant as it reaches a therapeutic plasma concentration of 0.05 μM by 24 hr[256, 257]. Beginning on day 1, Control and DXR groups were treated daily with saline or MMP inhibitors 15 mg/kg Doxy[68] or 60 mg/kg ONO-4817 by oral gavage for 28 days. These MMP inhibitors have been tested at similar doses in different rodent models of disease for two weeks without any adverse effects[258-261]. Mice were randomly assigned to Control, Doxy, ONO-4817, DXR, DXR+Doxy, or DXR+ONO-4817 groups (n=10/group).

3.2.5 Echocardiography

Mice were anesthetized with 1.5 mg/kg isoflurane (inhalation) and *in vivo* cardiac contractile function and morphology were assessed by transthoracic 2D/M-mode echocardiography using a Vevo 770 high-resolution imaging system equipped with a 30 MHz transducer (RMV-707B; VisualSonics, Toronto, ON). M-mode images were obtained to measure left ventricular posterior wall and interventricular septum thickness. Complete systolic and diastolic parameters were measured at baseline (day 1) and at day 28 following treatment.

3.2.6 Blood sampling and plasma collection

Following echocardiography on day 28, the mice were euthanized with 240 mg/kg sodium pentobarbital (i.p., Bimeda-MTC Animal Health Inc, Cambridge, ON). Approximately 1 mL of whole blood was collected from the left ventricle of each mouse by cardiac puncture. 3.15% (w/v)

trisodium citrate solution was added to the blood in a 1:9 (v/v) ratio to prevent clotting. The blood was then centrifuged at 14,000 g for 4 min at 4°C to collect the plasma. The plasma was then flash frozen in liquid nitrogen and stored in -80°C until use.

3.2.7 Preparation of heart samples

Following bilateral thoracotomy, hearts were excised and then exsanguinated with PBS. The left ventricle was divided for qPCR and protein quantification experiments by sectioning with razor blades before being flash frozen in liquid nitrogen. Total cellular RNA was extracted from ventricular tissue using TRIzol reagent (10 μL TRIzol per mg tissue, Invitrogen), 5 mm stainless steel beads (Qiagen, Hilden, Germany), and the TissueLyzer II system (Qiagen). Ventricular extracts were prepared by homogenizing frozen ventricle in ice cold radioimmunoprecipitation assay (RIPA) buffer containing 1% proteinase inhibitor cocktail (10 μL buffer per mg tissue) by sonication using a microtip equipped Sonifier 250 (Branson Ultrasonics, Danbury, CT) for biochemical analyses. Ventricular extracts were centrifuged at 10,000 g for 10 min at 4°C to remove tissue debris. The supernatant was collected, flash frozen in liquid nitrogen, and stored at -80°C until use.

Left ventricular sections from the same heart were also prepared for histological analyses and electron microscopy. For histological analyses, left ventricular sections were fixed in 10% neutral buffered formalin at 4°C overnight before paraffin embedding (performed by the Alberta Diabetes Institute Histocore). For conventional electron microscopy, left ventricular sections were fixed in a mixture containing 3% glutaraldehyde and 3% paraformaldehyde in 0.1 M sodium cacodylate buffer (#15950, Electron Microscopy Sciences) overnight at 4°C. For immunoelectron microscopy, left ventricular sections were fixed in 4% paraformaldehyde (#15710, Electron Microscopy Sciences) in 0.1 M Sorensen's Phosphate Buffer (pH 7.2, #11600-05, Electron

Microscopy Sciences) overnight at 4°C.

3.2.8 Histology

Paraffin-embedded ventricular tissue was cut into 4 μm thick sections and mounted onto Superfrost Plus slides. Hematoxylin and eosin stain was performed at room temperature on rehydrated ventricular sections using Weigert's iron hematoxylin set (HT1079, Sigma-Aldrich). To determine the size of the nuclei in the ventricular sections, images were binarized by applying a threshold on ImageJ. Using ImageJ, the analyzing particles function was used to determine the average nuclear size and the total area of nuclei.

Collagen content in the ventricular sections was stained using picrosirius red solution (Direct Red 80, #365548, Sigma-Aldrich). The following procedure is performed at room temperature. Ventricular sections were dipped in 0.2% phosphomolybdic acid for 30 min, then stained in picrosirius red solution for 1 hr, rinsed in 0.2% acetic acid, then dehydrated in ethanol before mounting with Permount (Thermo Fisher Scientific). Collagen birefringence was viewed using both unpolarized and polarized light. Collagen type I exhibits a yellow, orange, or red color while collagen type III appears green under polarized light. Stained ventricular sections were imaged on a Zeiss Axio Imager M1 polarized light microscope (Zeiss, Oberkochen, Germany). Collagen area fraction was determined by binarizing the images before analyzing using ImageJ. Collagen area fraction was determined by dividing the area of collagen by the total tissue area of each image.

For both hematoxylin and eosin and picrosirius red staining, three images (technical replicates) were captured and analyzed for each left ventricular section. The mean from the technical replicates was determined for each biological replicate. Five to eight individual

biological replicates were analyzed in total.

3.2.9 Western blot analysis

Protein concentration of ventricular extracts was measured using the bicinchoninic acid assay (Sigma-Aldrich) using BSA (Pierce Life Technologies, Rockford, IL) as a standard. 30 µg of total protein from heart extracts were separated on 8% polyacrylamide gels. After electrophoresis, proteins were wet transferred onto polyvinylidene difluoride membranes (Bio-Rad). Membranes were immunoblotted with primary monoclonal antibodies against MMP-2 (ab92536; Abcam), TIMP-3 (sc-30075; Santa Cruz), TIMP-4 (ab58425; Abcam), and α-tubulin (ab7291; Abcam). α-tubulin was used as a loading control. Primary antibodies were then probed with the appropriate secondary antibody, either goat anti-rabbit (CLCC42007; Cedarlane) or goat anti-mouse (CLCC30007; Cedarlane). Protein bands were visualized using chemiluminescent detection reagent (Clarity Western ECL Substrate; Bio-Rad). Membranes were then exposed to autoradiography film. X-ray films were scanned using a Bio-Rad GS-800 densitometer and quantified using ImageJ.

3.2.10 Gelatin zymography

Gelatin zymography was performed to determine MMP-2/-9 activity in ventricular extracts prepared as per section 2.2.7 with the exception that 30 µg of protein was loaded for each sample.

3.2.11 qPCR

Total cellular RNA extracted from ventricular tissue was quantified using a NanoDrop ND8000 spectrophotometer. RNA integrity was determined using an Agilent 2100 Bioanalyzer (Agilent Technologies, Santa Clara, CA), in which RNA migrates through a microcapillary system and detects the ratio of 28S and 18S ribosomal RNA. Samples with RNA integrity numbers greater

than 6 (good: 6-8, excellent: 9-10) were used. To eliminate genomic DNA contamination, RNA was digested with 1 U of DNase I (Invitrogen) at room temperature for 15 min and then at 65°C for 10 min. Reverse transcription was performed using the qScript cDNA SuperMix (Quanta Biosciences, Beverly, MA). qPCR primers for *B2M*, *Mmp2*, NTT-*Mmp2*, and *Rbm20* are shown in Table 3.1. Primer sequences for *Mmp2*, NTT-*Mmp2*, and *Rbm20* were obtained from Kim et al[262] and Guo et al[104]. Each primer pair was verified directly by PCR product sequencing and by in silico (Primer-BLAST, NCBI) analysis for secondary structure, false priming sites, primer dimers, and off targets. Samples were analyzed in triplicate by qPCR using the SYBR Green I Master Mix (Roche Diagnostics) for 40 cycles (15s denaturation, 45s annealing, 60s extension) in a LightCycler 480 System (Roche Diagnostics). C_q values and melt curves were analyzed with the LightCycler 480 software v1.5.1. (Roche Diagnostics). A standard curve was generated to calculate copy numbers in the samples by loading increasing amounts of corresponding purified DNA standards of known concentration for each gene during each assay. mRNA expression of each gene was calculated by first normalizing the copy numbers of each sample to the reference gene *B2M* (encoding β_2-microglobulin) and then normalized to the Control group. B2M was used as the reference gene as it had the greatest stability index compared with those for β-actin, GAPDH, or HPRT1 (data not shown).

3.2.12 Detection of S-glutathiolated MMP-2 by co-immunoprecipitation

To determine whether MMP-2 is activated by oxidative stress-induced S-glutathiolation, ventricular extracts (50 μg protein/sample), diluted in RIPA buffer, were incubated with rabbit MMP-2 antibody (1:100, ab92536, Abcam) or rabbit IgG isotype control (ab27472, Abcam) on a rotator overnight at 4°C. 50 μL of Protein G Sepharose bead slurry (ab193259, Abcam) was added to each antibody-ventricular extract sample and incubated on a rotator for 4 hr at 4°C. The

suspension was centrifuged (2,000 g, 2 min, 4°C) and the precipitates were washed with wash buffer (150 mM NaCl, 10 mM Tris, 1 mM EDTA, 1 mM EGTA, 0.2 mM sodium orthovanadate, 1% (v/v) Triton X-100). The immunoprecipitates were resuspended in 2x Laemmli buffer, heat denatured at 95°C for 5 min, and separated on 8% polyacrylamide gels for western blot analysis. The proteins were then wet transferred onto PVDF membranes at 100 V for 1 hr at 4°C. The PVDF membranes were probed with a mouse glutathione antibody (1:2000, ab19534, Abcam) to detect S-glutathiolated MMP-2.

3.2.13 Determining cardiac titin isoforms and its degradation products

3.2.13.1 Preparation of titin solubilization buffer

Urea-thiourea titin solubilization buffer was prepared as follows: 48 g urea and 15.2 g thiourea (both ACS grade, Sigma-Aldrich) were dissolved in 40 mL H_2O on a hot plate. The solution temperature was kept below 40°C to prevent the formation of cyanate. 10 g of a mixed bed resin (AG 501-X8, Bio-Rad) was added to the urea-thiourea buffer with agitation at room temperature for 15 min. The solution was filtered and the resin was rinsed with 10 mL H_2O (total 90-100 mL). 0.605 g Trizma base and 3 g SDS were added to the filtrate and the pH was adjusted to 7.5 with 1 M HCl. 1.155 g dithiothreitol was added to the urea-thiourea buffer. Once the pH was readjusted to 6.8, 2-4 mg bromophenol blue was added. The solution was then transferred to a graduated cylinder and H_2O was added until the total volume reached 100 mL. The solution was filtered through a Millex HA 0.22 µm filter (Millipore) to remove any residual particulates. The final urea-thiourea solubilisation buffer was stored at room temperature. Before the buffer was added to ventricular samples, additional dithiothreitol was added to the urea-thiourea titin solubilization buffer until the final concentration reached 75 mM.

3.2.13.2 Preparation of 50% glycerol with protease inhibitors

50 mL ultrapure glycerol (MP Biomedicals, Santa Ana, CA) was diluted with 50 mL ultrapure mass-spec grade H_2O. Leupeptin (10 μM, ILP-4041, Peptides International, Louisville, KY), E-64 (10 μM, Sigma-Aldrich), and phenylmethylsulfonylfluoride (0.5 mM) were prepared in 50% glycerol and stored in -20°C until use.

3.2.13.3 Titin solubilization from left ventricular tissue

Approximately 15 mg of frozen ventricular tissue was pulverized in a 2 mL Kontes Dounce style homogenizer with 'A' and 'B' pestles. First, the 2 mL Dounce homogenizer and pestle 'A' were cooled in liquid nitrogen. The weighed ventricular tissue was transferred to the Dounce homogenizer and pulverized with pestle 'A' in liquid nitrogen for 2 min until the tissue was ground and smooth. The Dounce homogenizer containing the pulverized ventricular tissue was then brought to -20°C for 20 min.

Titin solubilization buffer containing 75 mM DTT was added to the pulverized ventricular tissue in the Dounce homogenizer at a 20 μL buffer:1 mg tissue ratio. An equivalent volume of 50% glycerol containing protease inhibitors (20 μL buffer: 1 mg tissue ratio) was added to the Dounce homogenizer. The Dounce homogenizer was then transferred to a 60°C water bath and gently mixed with pestle 'A' for 30 sec. The sample was then solubilized with pestle 'B' for 3.5 min at 60°C and remained incubated in the 60°C water bath for another 10 min. The solubilized tissue was transferred to 2 mL microfuge tubes and centrifuged at 10,000 g for 6 min at room temperature. The supernatant was collected and stored at -80°C until use.

3.2.13.4 Preparation of 1% agarose gels for titin analysis

A pair of 16 x 18 cm glass plates (Fisher Scientific) with a 1.5 mm spacer were secured onto a mounting stand. A 1-inch acrylamide plug was poured by adding 16% acrylamide, electrophoresis running buffer (50 mM Tris base, 0.384 M glycine, 0.1% SDS), H_2O, and polymerizing agents (tetramethylethylenediamine and 10% w/v ammonium persulfate diluted in H_2O). After polymerization, the glass plates were transferred into a 60°C incubator for 20 min.

To prepare a 1% (w/v) agarose gel solution, 1 g Seakem Gold Agarose (Lonza, Basel, Switzerland) was dissolved in 30 mL glycerol, 20 mL 5x electrophoresis running buffer (see Appendix), and 50 mL H_2O. The solution was heated on a hot plate until the agarose dissolved. Each gel required 30-40 mL of 1% agarose gel solution. 13-well 1.5 mm combs were inserted between the glass plates filled with agarose gel solution. The agarose gel was polymerized at room temperature and then stored at 4°C until use.

Before loading samples, each well was filled with electrophoresis running buffer (containing 10 mM β-mercaptoethanol). Each sample was run at five loading volumes (3, 4.5, 6, 7.5, and 9 µL). 1% agarose gels were electrophoresed at 15 mA/per gel (300-400 V) for 3 hr at 4°C on a Hoefer SE600 gel unit. After electrophoresis, the agarose gel was fixed in presoak solution (20% methanol, 10% acetic acid, 70% H_2O) for at least 1 hr at room temperature to prevent the large proteins from diffusing in the gel. Each gel was then stained with staining solution (8% w/v ammonium sulfate, 0.8% w/v Neuhoff's optimized Coomassie Brilliant Blue, 20% methanol) at room temperature overnight. Agarose gels were then destained with destaining solution (25% methanol, 75% H_2O) twice, 2 hr each, at room temperature on the shaker.

The agarose gels were scanned and the band densities were analyzed using 1D-scan

(Scanalytics Inc, Milwaukee, WI). The density of T1 titin (total of N2BA and N2B titin), T2 titin (cleaved titin), and myosin heavy chain (MHC) were normalized to the volume (3, 4.5, 6, 7.5, 9 μL) of sample loaded. A linear slope was determined for each sample by plotting the band density as a function of the volume of sample loaded. Titin proteolysis was determined by the ratio of titin degradation product (T2) to intact titin (T1).

3.2.14 Ultrastructural analysis by electron microscopy

3.2.14.1 Subcellular localization of MMP-2 by immunogold electron microscopy

For conventional transmission electron microscopy, left ventricular tissue was pre-fixed in a mixture of 3% paraformaldehyde and 3% glutaraldehyde in 0.1 M sodium cacodylate buffer (Cat. #15950, Electron Microscopy Sciences). The tissue was then post-fixed in a mixture of 2% osmium tetroxide (Cat. #19150, Electron Microscopy Sciences) and 1.5% potassium ferrocyanide (Cat. #25154-10, Electron Microscopy Sciences) in 0.1 M sodium cacodylate buffer (Cat. #11654, Electron Microscopy Sciences). The tissue was then dehydrated in a series of ethanol (30, 50, 70, 80, 90, 95, and 100% ethanol), embedded in Spurr's resin (Electron Microscopy Sciences), and thermally polymerized at 70°C. The polymerized tissue was longitudinally trimmed along the myofilaments and cut by an ultramicrotome (Leica EM UC7, Leica Microsystems, Wetzlar, Germany) and a diamond knife (DiATOME, Hatfield, PA). 70 nm ultrathin sections were sectioned and transferred to a 200 mesh bare copper grid. The ultrathin sections were contrasted by post-staining with UranyLess and lead citrate (Electron Microscopy Sciences). The ultrathin sections were observed with a transmission electron microscope (Hitachi H-7650 TEM, Hitachi High-Technologies Canada Inc., Toronto, ON) with an 11 megapixel EMCCD (Advanced Microscopy Techniques, Woburn, MA).

For immuno transmission electron microscopic study of the left ventricular myocardium, left ventricular tissue was fixed in 4% paraformaldehyde (#15710, Electron Microscopy Sciences) in 0.1 M Sorensen's Phosphate Buffer (pH 7.2, #11600-05, Electron Microscopy Sciences) for 24 hr at 4°C. Fixed left ventricular tissue was then rinsed in 0.1 M sodium phosphate buffer (pH 7.4) before dehydration in a graded alcohol series (30%, 50%, 70%, and 80% ethanol). The fixed tissue was embedded in London Resin White (Cat. #18181, Ted Pella Inc., Redding, CA) and polymerized under ultraviolet light. The entire immuno transmission electron microscopy sample preparation procedure was performed at 4°C to preserve antigenicity. The ultraviolet polymerized tissue was longitudinally sectioned along the myofilaments and 80 nm ultrathin sections were transferred to a 300 mesh bare nickel grid for immunolabeling.

Prior to incubation with antibodies, the grids were incubated in quenching buffer (80 mM glycine in 0.01 M Sorensen's PBS) for 15 min at room temperature. The grids were washed in wash buffer (0.5% BSA in 0.01 M Sorensen's PBS) for 6 min and then blocked with blocking buffer (5% BSA and 2% cold fish skin gelatin in 0.01 M Sorensen's PBS) for 30 min at room temperature. The grids were incubated with 10 µL of monoclonal mouse anti-MMP-2 IgG antibody (1:50, MAB3008, Millipore) diluted in 2% BSA and 2% cold fish skin gelatin in 0.01 M Sorensen's PBS, overnight at 4°C. The grids were then washed with washing buffer (0.5% BSA in 0.01 M PBS) for 6 x 2 min each at room temperature. The grids were then incubated with 18 nm diameter colloidal gold-conjugated donkey anti-mouse IgG secondary antibodies (1:10, #715-215-150, Jackson ImmunoResearch Laboratories, West Grove, PA) for 90 min at room temperature. Grids were washed with 0.01 M PBS (6 x 1 min each) followed by H_2O (4 x 1 min each) at room temperature. Contrast agent UranylLess (0.25x, #22409, Electron Microscopy Sciences) was applied to the grids for 1 min at room temperature. Contrast was further enhanced

by coating the grids with carbon (7 nm thick) using a high vacuum carbon evaporator (Leica EM ACE600, Leica Microsystems). The grids were then visualized using a Hitachi H-7650 transmission electron microscope equipped with a charged-couple device camera (Advanced Microscopy Techniques, Woburn, MA) at 60 kV.

3.2.14.2 Quantification of the subcellular localization of MMP-2

To determine the distribution and density of MMP-2 molecules in cardiomyocyte mitochondria and sarcomere, immunogold electron micrographs were analyzed on ImageJ. Cardiomyocytes were verified by the presence of sarcomeres. Six different images were acquired for each biological replicate. Within each image, 10 mitochondria and 10 sarcomeres were traced as individual Region of Interests (ROI). A total of 60 mitochondria and 60 sarcomeres were analyzed for each biological replicate. Each image was binarized by adjusting the threshold from 0-50 to visualize only immunogold particles. For 18 nm-colloidal gold-conjugated secondary antibodies, only particles with an area greater than 100 nm^2 were analyzed. For each mitochondrial and sarcomeric ROI, the number of gold particles were counted and normalized to the area (μm^2) of the ROI. From the 60 mitochondria and sarcomeres, the average number of MMP-2 molecules per μm^2 within the mitochondria and sarcomere was determined for each biological replicate. This was repeated across four independent biological replicates.

3.2.14.3 Ultrastructural analysis by conventional transmission electron microscopy

Sample preparation for conventional transmission electron microscopy was similar to immunogold electron microscopy (section 3.2.14.1) with the following exceptions. 1-2 mm^3 left ventricular tissue were fixed in ice-cold 3% glutaraldehyde and 3% formaldehyde in 0.1 M sodium cacodylate buffer (#15950, Electron Microscopy Sciences) for 24 hr at 4°C. Fixed left ventricular

samples were then briefly rinsed in 0.075 M sodium cacodylate buffer and osmicated with 1% osmium tetroxide (Electron Microscopy Sciences) in 0.05 M sodium cacodylate buffer for 2 hr at 4°C.

3.2.15 Statistical analysis

Data are expressed as mean ± SEM of *n* biological replicates (hearts). Echocardiography, histological analyses, qPCR, western blot, gelatin zymography, and titin proteolysis experiments were analyzed by one-way ANOVA followed by Sidak's post hoc test using GraphPad Prism 7 (GraphPad Software). Baseline (day 1) echocardiography was analyzed by one-way ANOVA using Tukey's post-hoc test. Quantification of electron micrographs were analyzed by paired two-tailed t-test. p values <0.05 were considered significant.

3.3 Results

3.3.1. The effect of DXR and MMP inhibitors on body weight

Control mice increased body weight over the 4 week course of the study (Fig. 3.2). In contrast, DXR, DXR+Doxy, and DXR+ONO-4817 mice did not gain body weight. At day 28, DXR and DXR+Doxy, but not DXR+ONO-4817, mice weighed significantly less than control mice.

3.3.2. MMP inhibitors ameliorate DXR-induced cardiac contractile dysfunction

Baseline echocardiography data (day 1) from all mice showed no significant differences in morphological or functional parameters between all groups (Table 3.2). The effects of Doxy and ONO-4817 alone on in vivo cardiac function (day 28) are summarized in Table 3.3. Doxy and ONO-4817 alone had no effect on cardiac function. Nearly all parameters were unaffected by the

MMP inhibitors with the exception of reduced systolic and diastolic interventricular septum thickness with ONO-4817 (Table 3.3).

DXR caused systolic dysfunction marked by a significant reduction in left ventricular fractional shortening (Fig. 3.3A) and ejection fraction (Fig. 3.3B) relative to control. DXR also caused diastolic dysfunction marked by a reduction in E′/A′ (Fig. 3.3C) and increased isovolumic contraction time (IVCT, Table 3.4) compared to control. Both MMP inhibitors attenuated DXR-impaired systolic and diastolic dysfunction by improving fractional shortening, ejection fraction, E′/A′, and IVCT. DXR reduced cardiac output, an effect that was prevented by ONO-4817, but not Doxy ($p=0.076$) (Fig. 3.3D). Full functional parameters measured by echocardiography at the end of the experiment (day 28) are summarized in Table 3.4.

3.3.3. Doxycycline attenuates cardiac remodeling in DXR cardiotoxicity

DXR caused significant remodeling of the heart including thinning of the left ventricular posterior wall (Fig. 3.4A) and interventricular septum measured during systole (Fig. 3.4B). DXR also increased the left ventricular internal diameter during systole (Fig. 3.4C) and expanded the left ventricular end-systolic volume (Fig. 3.4D). These adverse changes in cardiac morphology were prevented by Doxy but not ONO-4817. There were no significant differences in the thickness of the posterior wall, interventricular septum, nor the left ventricular internal diameter during diastole (Table 3.4). Full cardiac morphology parameters measured at the end of the experiment (day 28) are summarized in Table 3.4.

3.3.4. MMP inhibitors prevent myofibrillar remodeling in DXR cardiotoxicity

Left ventricular free wall sections were examined histologically from control, DXR, DXR+Doxy, and DXR+ONO-4817 treated mice. Hematoxylin and eosin staining revealed that

DXR hearts exhibit increased cardiomyocyte dropout and myofibrillar disorganization compared to control hearts (Fig. 3.5A,B). Moreover, some nuclei appear enlarged whereas some appear fragmented in the DXR hearts. Doxy and ONO-4817 prevented DXR-induced myofibrillar disarray and caused less cardiomyocyte dropout (Fig. 3.5C,D). The average size of nuclei was unchanged between groups (Fig. 3.5E). However, the total nuclear area relative to tissue area was significantly increased in DXR and DXR+Doxy hearts compared to control hearts (Fig. 3.5F).

3.3.5. DXR-induced interstitial fibrosis is prevented by MMP inhibition

Left ventricular interstitial fibrosis was detected by picrosirius red staining using both light (Fig. 3.6A-D) and polarized light (Fig. 3.6E-H). DXR increased interstitial fibrosis as seen by increased picrosirius red staining (Fig. 3.6B) and collagen birefringence (Fig. 3.6F) compared to control hearts. DXR increased both collagen type I (yellow-red) and type III (green) as visualized under polarized light (Fig. 3.6F). Quantification of the total collagen birefringence (Fig. 3.6E-H) showed that DXR increased collagen deposition by 347% of control and this was prevented with Doxy and ONO-4817 (Fig. 3.6I).

3.3.6. DXR cardiotoxicity is associated with enhanced MMP-2 level and activity

DXR significantly increased 72 kDa MMP-2 protein levels in the heart to ~150% of control, which was prevented with Doxy and ONO-4817 (Fig. 3.7A). Changes in MMP-2 protein levels were accompanied by a twofold increase in myocardial 72 kDa MMP-2 activity by gelatin zymography with no evidence of other gelatinolytic activities including 64 kDa MMP-2 or MMP-9 (Fig. 3.7B).

3.3.7. DXR elevates MMP-2 levels and activity in the plasma

MMP-2 protein and activity were also measured in plasma to determine changes in its

circulating levels as a possible biomarker of DXR cardiotoxicity. DXR increased MMP-2 protein levels, which was attenuated by ONO-4817 but not Doxy (Fig. 3.8A). These changes in MMP-2 protein levels were accompanied by an increase in MMP-2 gelatinolytic activity (Fig. 3.8B). ONO-4817 abolished the DXR-induced increase in MMP-2 activity in the plasma.

3.3.8. DXR does not affect TIMP-3/4 levels in the heart

MMP-2 activity is modulated by tissue inhibitor of metalloproteinases (TIMPs), namely TIMP-3 in the extracellular matrix and TIMP-4, the most abundant endogenous inhibitor of intracellular MMP activity found in cardiac myocytes[51]. TIMP-3 (Fig. 3.9A) and TIMP-4 (Fig. 3.9B) protein levels in the heart were not affected by DXR in the presence or absence of Doxy and ONO-4817.

3.3.9. Detection of S-glutathiolated MMP-2 in the heart

Reactive oxygen-nitrogen species in combination with cellular glutathione can activate MMP-2 by its S-glutathiolation[39]. S-glutathiolated MMP-2 in ventricular extracts was determined by immunoblot against glutathiolated proteins following immunoprecipitation of MMP-2. Glutathiolated MMP-2 was detected in the hearts of both control and DXR groups (Fig. 3.10). However, there did not appear to be differences in the amount of glutathiolated MMP-2 between control and DXR hearts. One consistent observation was reduced levels in a ~50 kDa protein from the MMP-2 immunoprecipitates of DXR hearts compared to control hearts.

3.3.10. DXR upregulates NTT-MMP-2 expression in the heart

As oxidative stress can also upregulate the expression of NTT-*Mmp2*, I measured the mRNA expression of NTT-*Mmp2* and 72 kDa *Mmp2* by qPCR. DXR increased NTT-*Mmp2* expression to ~200% of control (Fig. 3.11A). Doxy and ONO-4817 abolished the upregulation of

NTT-*Mmp2* caused by DXR to 105% and 74% of control, respectively (Fig. 3.11A). Interestingly, DXR did not affect mRNA levels of 72 kDa *Mmp2* (Fig. 3.11B).

3.3.11. The effect of DXR on inflammasome markers

The NTT-MMP-2 isoform is involved in the innate immune response and is associated with elevated levels of interleukin-6 (*IL6*) and chemokine (C-X-C) motif ligand 1 (*CXCL1*)[263]. I found that DXR-induced upregulation of NTT-*Mmp2* was accompanied by an increase in *IL6* (Fig. 3.12A), but not *CXCL1*, mRNA expression (Fig. 3.12B). Interestingly, ONO-4817 prevented increased *IL6* expression. There was a trend for Doxy to reduce DXR-enhanced *IL6* expression, however, this was not statistically significant (p=0.31 vs DXR).

3.3.12. Ultrastructure of the left ventricle by transmission electron microscopy

To understand the mechanism by which MMP-2 activity causes injury to myocytes in DXR cardiotoxicity, I evaluated ultrastructural damage in cardiomyocytes from left ventricular sections obtained from control and DXR mice. Transmission electron micrographs of longitudinal sections of the myofilaments revealed significant differences in the ultrastructure of the sarcomere and mitochondria between control (Fig. 3.13A,C) and DXR (Fig. 3.13B,D) left ventricular sections. Marked sarcomeric degeneration included reduced sarcomere lengths, more diffuse and less prominent Z-discs, disassembly of the M-line, and significant myofilament disorganization compared to control (Fig. 3.13A,B). Consistent with previous reports[164, 264], the mitochondria in DXR hearts appeared fragmented including disruption of cristae compared to control (Fig. 3.13C,D). Abnormal swelling/distention of T-tubules as well as increased glycogen particles around mitochondria were also observed in DXR hearts (Fig. 3.13E,F).

3.3.13. DXR increases the diameter of the thick filaments

Electron micrographs of longitudinal sections revealed that DXR caused significant disorganization of myofilament proteins but this view does not differentiate the thick from thin filaments. Cross-sections of the sarcomere revealed the crystal-like array of the thin (actin) and thick (myosin) filaments in both control and DXR hearts (Fig. 3.14A,B). I found significant differences in the contrast of the thick filaments, which were markedly increased in DXR hearts compared to control. This difference in contrast suggests there may be differences in the diameter of the thick filament. Indeed, the average diameter of myosin was greater in DXR hearts (22.8 ± 1.1 nm) than control hearts (15.6 ± 0.2 nm) (Fig. 3.14C). The distance between the thick filaments remained unchanged (Fig. 3.14D).

3.3.14. DXR increases MMP-2 levels in the sarcomere and mitochondria

To visualize the subcellular localization of MMP-2, I performed immunogold transmission electron microscopy on left ventricular sections of control and DXR hearts. A control where the primary antibody is omitted and only the colloidal gold secondary antibody was used showed an absence of non-specific binding in control (Fig. 3.15A) and DXR (Fig. 3.15B) hearts. Consistent with previous reports[84, 95], MMP-2 was localized in both the sarcomere and mitochondria in control and DXR hearts (Fig. 3.15C,D). Within the sarcomere, MMP-2 was localized to the Z-disc, I-band, A-band, and M-line. Previous studies have reported intracellular MMP-2 in the mitochondria and mitochondrial-associated membrane[95, 246]. I found abundant MMP-2 within the mitochondria and along the outer mitochondria membrane in both control and DXR hearts (Fig. 3.15C,D). Because the colloidal gold-conjugated secondary antibodies bind to the primary antibodies at a 1:1 stoichiometric ratio, I determined the number of MMP-2 molecules per square micron within the mitochondria or sarcomere. There was nearly twice the number of MMP-2 molecules per square

micron in the mitochondria than in the sarcomere in both control and DXR hearts (Fig. 3.15E,F). DXR treatment doubled the number of MMP-2 molecules per square micron in the sarcomere and mitochondria (Fig. 3.15E,F).

3.3.15. DXR cardiotoxicity induces titin proteolysis which is prevented by MMP inhibition

I then determined whether DXR-induced myofilament lysis is attributed to cardiac titin proteolysis. The levels of titin isoforms (N2BA and N2B), intact titin (T1=N2BA+N2B), and its major degradation product (T2) were measured in ventricular extracts by agarose gel electrophoresis. The ventricles from DXR-treated mice revealed three titin bands, including two full-length titin bands (>3 MDa), corresponding to N2BA and N2B titin, and a lower molecular weight degradation product, T2 (Fig. 3.16A). The ratio of T2 to T1 titin determines the degree of titin degradation. DXR significantly increased cardiac titin proteolysis, which was attenuated by ONO-4817 (Fig. 3.16A,B). Doxy trended to reduce DXR-induced titin proteolysis, but this was not statistically significant ($p=0.35$ vs DXR). DXR did not significantly change the ratio of total titin (T1+T2) to myosin heavy chain (MHC) compared to control hearts (Fig. 3.16C).

3.3.16. DXR does not alter cardiac titin isoform expression

Dilated cardiomyopathy is associated with changes in titin isoform expression[125]. However, there were no differences in the ratio of N2BA:N2B titin across all groups (Fig. 3.17A). This was confirmed by the absence of alterations in the expression of *Rbm20* (Fig. 3.17B), the splice factor of titin which dictates isoform expression[104].

3.4 Discussion

I demonstrated for the first time that two orally available MMP inhibitors Doxy and ONO-

4817 attenuate DXR cardiotoxicity in vivo. I established that DXR increases MMP-2 activity in the heart, in part, by upregulating NTT-MMP-2, an intracellular MMP-2 isoform which is expressed under conditions of oxidative stress. Blocking the activity of MMP-2 prevented myofilament lysis, titin proteolysis, and interstitial fibrosis in the heart. The combined actions of MMP inhibitors on extracellular and intracellular matrix remodeling improved functional and morphological parameters of the hearts which were impaired by DXR.

Prophylactic administration of drugs used to treat heart failure is the current treatment recommendation to alleviate chemotherapy-induced cardiotoxicity[183]. However, drugs such as angiotensin converting enzyme inhibitors, angiotensin II receptor antagonists, and β-blockers show at best modest improvement in ejection fraction and do not prevent chemotherapy-induced left ventricular remodeling[186], which typically precedes the development of heart failure[265]. Doxy was reported to reduce myocardial oxidative stress and apoptosis in DXR-treated mice[266]. However, the role of MMPs was not considered despite knowledge that Doxy is an MMP inhibitor already at sub-antimicrobial doses[68]. Our previous work demonstrated that Doxy and ONO-4817 improve cardiac contractile function following acute ischemia-reperfusion injury[63, 192], another cardiac pathology associated with enhanced oxidative stress. Doxy has also been shown to significantly reduce adverse left ventricular remodeling in myocardial infarct patients[73]. In accordance with those findings, I showed that either Doxy and ONO-4817 protected the hearts from DXR cardiotoxicity by attenuating both cardiac contractile dysfunction and remodeling, suggesting that MMPs are implicated in the detrimental effects of DXR on the heart.

MMP-2 is regulated by oxidative stress at both transcriptional and post-translational levels. Firstly, oxidative stress can upregulate MMP-2 expression[21] and trigger the de novo expression of NTT-MMP-2 through an alternative promoter within the first intron[18]. Secondly, intracellular

MMP-2 can be directly activated by peroxynitrite via *S*-glutathiolation of a critical cysteine residue in its autoinhibitory domain, exposing its catalytic site[39]. Our results reveal that DXR increases MMP-2 levels and activity in the heart, in part, by upregulating NTT-MMP-2 expression. This is consistent with our findings in cardiomyocytes that DXR enhances the expression of NTT-MMP-2 and 72 kDa MMP-2 protein and activity by increasing oxidative stress[254].

Hallmarks of cardiac pathology such as cardiomyocyte dropout, interstitial fibrosis, and inflammation are also signatures of DXR cardiotoxicity[267]. These dynamic changes take place in the extracellular matrix, which plays an important role in tissue architecture and cell signaling. Oxidative stress and inflammatory processes elevate MMP-2 activity in the injured myocardium, resulting in the degradation of the extracellular matrix[9]. Extracellular matrix degradation drives an inflammatory response causing myofibroblast proliferation and collagen deposition[268]. NTT-MMP-2 plays an important role in initiating a pro-inflammatory and pro-apoptotic innate immune response in myocardial injury[18, 231]. Expression of NTT-MMP-2 triggers the activation of NFAT and NF-κB signaling cascades and expression of a highly defined innate immunity transcriptome including IL6[231]. My results show that DXR cardiotoxicity is associated with increased NTT-*Mmp2* expression, *IL6* expression, and interstitial fibrosis. Interestingly, MMP inhibitors significantly prevented DXR-induced increased NTT-*Mmp2* and *IL6* expression. This is likely a result of the MMP inhibitors diminishing pathological degradation of the intra- and extra-cellular matrices, blocking inflammatory processes, and ultimately preventing the enhancement in MMP-2 expression.

Beyond the myocardial interstitium, MMP-2 is also elevated within cardiomyocytes in cardiomyopathy and oxidative stress injury[82, 218]. Intracellular MMP-2 activity directly affects cardiomyocyte structure and function by cleaving contractile proteins in the sarcomere[269]. Titin is

the third most abundant myofilament protein in the sarcomere and plays an important role in cardiac function and sarcomere integrity[98]. Degradation of titin or alteration in its splicing will have detrimental effects on cardiac contractile function[63, 125]. I show here for the first time that DXR increases the level of MMP-2 in the sarcomere, contributing to titin proteolysis and impairing cardiac contractile function. The increased titin T2/T1 ratio in DXR hearts was associated with reduced sarcomere length, myofilament lysis, and cardiac contractile dysfunction. This effect is likely attributed to increased MMP-2 activity, given that the T2/T1 ratio was markedly reduced when MMP activity was blocked by ONO-4817. There is emerging evidence that oxidative stress can directly result in titin proteolysis. Munkanatta Godage *et al*[270] recently reported that the lysine methyltransferase SMYD2 dissociates from the near Z-disc region of titin during oxidative stress, rendering titin susceptible to in vitro proteolysis by MMP-2 and calpains. Since oxidative stress contributes to DXR cardiotoxicity, it would be of significant interest to determine whether SMYD2 is glutathiolated under this condition, which may exacerbate titin proteolysis.

In addition to titin, DXR caused ultrastructural changes to the thick filaments including the dissolution of the M-line and increased the diameter of the thick filaments. Because there were no differences in myosin heavy chain protein levels as evaluated by agarose gel electrophoresis, the differences in the diameter of the thick filament may be related to alterations in the conformation of myosin. DXR is known to induce carbonylation and degradation of cardiac myosin binding proteins[245]. Myosin binding protein C regulates the structure of the thick filaments by binding to the S2 hinge regions of myosin[271]. Degradation of myosin binding protein C may alter conformation of the myosin, decreasing the force generated during cardiomyocyte contraction.

This study does not rule out that MMP-2 may target other sarcomeric proteins including troponin I, α-actinin, and myosin light chain-1, which are susceptible to proteolysis under

conditions of oxidative stress. I also determined whether altered titin isoform expression, which is a common characteristic in patients with dilated cardiomyopathy[125], is implicated in DXR cardiotoxicity. I found that DXR does not affect titin splicing as there were no differences in the expression of titin splice factor *Rbm20* nor on the ratio between N2BA and N2B titin.

In summary, I have demonstrated that two different orally available MMP inhibitors attenuate DXR cardiotoxicity through different mechanisms. Doxy, the only MMP-2 inhibiting drug currently approved for clinical use, prevented early remodeling of the heart. This is consistent with the findings from the TIPTOP trial where Doxy reduced adverse ventricular remodeling and improved left ventricular ejection fraction in ST-elevation myocardial infarction patients[73]. Tetracyclines such as minocycline and Doxy are known to accumulate in the heart[272]. The intracellular concentration of Doxy within cardiomyocytes compared to ONO-4817 remains unknown. However, ONO-4817 is a more potent MMP inhibitor and shows greater preference than Doxy for inhibiting gelatinases (MMP-2 and MMP-9)[62].

My results elucidate the role of MMP-2 in intracellular and extracellular matrix remodeling in DXR cardiotoxicity. Furthermore, I demonstrated that two orally available, selective MMP inhibitors ameliorate DXR-induced cardiac dysfunction and remodeling by attenuating titin proteolysis, myofilament lysis, and interstitial fibrosis. Prophylactic inhibition of MMP activity could be an effective means to prevent heart injury caused by anthracyclines in the treatment of cancer.

Table 3.1: Primer sequences used for qPCR in mouse left ventricular tissue.

Gene	Full name	Sequence (5' to 3')	GenBank ID	Amplicon size (bp)
B2M	beta-2-microglobulin	F: TGGTCTTTCTGGTGCTTGTCTC R: CCCGTTCTTCAGCATTTGGATTTC	NM_009735.3	170
Mmp2	matrix metalloproteinase-2	F: GACCTCTGCGGGTTCTCTGC R: TTGCAACTCTCCTTGGGGCAGC	NM_008610.3	163
NTT-*Mmp2*	N-terminal truncated *Mmp2*	F: GTGAATCACCCCACTGGTGGGTG R: TTGCAACTCTCCTTGGGGCAGC	N/A	229
Rbm20	RNA-binding motif 20	F: CCTGCCTTTGGGTCTCGGCTTAAC R: CCCTTTCACATGTAGCTCCCAGTC	NM_001170847	216
IL6	interleukin-6	F: TGTATGAACAACGATGATGCACTTG R: TACTCCAGGTAGCTATGGTACTCC	NM_031169.2	152
CXCL1	chemokine (C-X-C) motif ligand 1	F: AGCCACACTCAAGAATGGTC R: GAGCAGTCTGTCTTCTTTCTCC	NM_008176.3	120

Table 3.2: Baseline body weight, cardiac morphology, and function of each group of mice at the start of experiment before treatment (day 1).

Measures	**Control (n=10)**	**DXR (n=10)**	**DXR + Doxy (n=10)**	**DXR + ONO (n=10)**
Body weight, g	21.8±0.4	22.7±0.4	22.5±0.4	23.0±0.4
Heart rate, beats per minute	462±16	472±10	478±14	469±13
Morphology				
Interventricular septum thickness diastole, mm	0.72±0.03	0.77±0.02	0.75±0.02	0.75±0.02
Interventricular septum thickness systole, mm	1.08±0.04	1.18±0.04	1.22±0.05	1.10±0.04
LV posterior wall thickness diastole, mm	0.72±0.04	0.73±0.02	0.76±0.02	0.75±0.02
LV posterior wall thickness systole, mm	1.04±0.05	1.08±0.03	1.08±0.03	1.06±0.02
LV internal diameter diastole, mm	3.83±0.08	3.81±0.06	3.76±0.08	3.92±0.08
LV internal diameter systole, mm	2.70±0.11	2.62±0.06	2.44±0.09	2.69±0.06
Systolic function				
Ejection fraction, %	60.7±3.0	59.5±1.5	65.2±1.7	59.6±1.2
Fractional shortening, %	33.1±3.5	31.1±1.0	33.6±0.9	31.1±0.8
LV end-diastolic volume, μL	63.4±3.2	65.8±2.7	60.5±4.0	69.3±3.1
LV end-systolic volume, μL	27.7±2.6	25.9±1.6	21.3±2.0	27.8±1.4
Cardiac output, mL/min	16.9±0.8	18.8±0.8	18.8±1.3	19.4±0.9
Stroke volume, μL	35.7±1.1	39.8±1.6	39.3±2.4	41.5±2.1
Diastolic function				
E'/A' ratio	1.16±0.08	1.12±0.03	1.12±0.03	1.14±0.03
Mitral E velocity, mm/s	539±36	577±31	576±40	584±37
Mitral A velocity, mm/s	387±22	378±21	381±28	380±23
E/E'	-27.1±1.9	-26.4±2.2	-27.9±2.5	-26.5±1.9
Deceleration time, ms	20.2±2.2	18.8±1.4	21.5±1.8	20.9±2.3
IVRT, ms	18.9±0.8	17.1±0.8	17.8±0.9	17.4±0.7
IVCT, ms	13.7±0.9	12.0±0.7	13.2±0.6	12.0±0.5
TEI index	0.79±0.03	0.70±0.03	0.73±0.02	0.71±0.03

Table 3.3: Body weight, cardiac morphology, and function in control mice treated with doxycycline or ONO-4817 alone (day 28). a: $p<0.05$ by one-way ANOVA followed by Sidak's post hoc test.

Measures	Control (n=10)	Doxy (n=7)	ONO (n=7)
Body weight, g	25.1±0.5	24.8±0.8	26.3±0.5
Heart rate, beats per minute	466±13	458±18	463±11
Morphology			
Interventricular septum thickness diastole, mm	0.81±0.02	0.78±0.02	0.71±0.02 [a]
Interventricular septum thickness systole, mm	1.25±0.05	1.09±0.03	1.04±0.06 [a]
LV posterior wall thickness diastole, mm	0.78±0.02	0.76±0.02	0.70±0.02
LV posterior wall thickness systole, mm	1.16±0.04	1.11±0.04	1.04±0.01
LV internal diameter diastole, mm	3.92±0.07	3.90±0.12	3.96±0.09
LV internal diameter systole, mm	2.55±0.09	2.72±0.14	2.69±0.16
Systolic function			
Ejection fraction, %	63.9±2.3	58.1±2.9	57.1±2.5
Fractional shortening, %	34.5±1.7	30.8±1.7	29.6±1.7
LV end-diastolic volume, μL	66.6±2.6	67.4±5.3	69.5±3.3
LV end-systolic volume, μL	24.6±2.1	28.0±3.2	30.6±2.9
Cardiac output, mL/min	201±1.0	17.9±1.1	18.0±0.7
Stroke volume, μL	42.0±1.3	39.4±3.0	38.9±1.5
Diastolic function			
E'/A' ratio	1.07±0.04	1.13±0.06	1.11±0.04
Mitral E velocity, mm/s	522±28	528±46	506±47
Mitral A velocity, mm/s	383±22	324±32	337±35
E/E'	-27.0±1.4	-25.3±2.2	-29.2±2.7
Deceleration time, ms	19.3±1.8	19.5±2.4	18.6±2.1
IVRT, ms	18.7±0.7	19.7±0.9	18.9±1.3
IVCT, ms	12.6±0.9	12.8±0.8	14.1±0.8
TEI index	0.77±0.03	0.73±0.02	0.78±0.05

Table 3.4: Body weight, cardiac morphology, and function in DXR mice treated with or without MMP inhibitors doxycycline or ONO-4817 (day 28). a: $p<0.05$ vs Control, b: $p<0.05$ vs DXR by one-way ANOVA followed by Sidak's post hoc test.

Measures	**Control (n=10)**	**DXR (n=10)**	**DXR + Doxy (n=10)**	**DXR + ONO (n=10)**
Body weight, g	25.1±0.5	21.2±0.6 [a]	21.3±0.5	23.1±0.4 [b]
Heart rate, beats per minute	466±13	427±11	460±12	455±11
Morphology				
Interventricular septum thickness diastole, mm	0.81±0.02	0.69±0.03 [a]	0.77±0.04	0.71±0.03
Interventricular septum thickness systole, mm	1.25±0.05	0.95±0.06 [a]	1.19±0.06 [b]	1.04±0.05
LV posterior wall thickness diastole, mm	0.78±0.02	0.71±0.02	0.76±0.04	0.74±0.02
LV posterior wall thickness systole, mm	1.16±0.04	0.99±0.04 [a]	1.14±0.04 [b]	1.07±0.02
LV internal diameter diastole, mm	3.92±0.07	3.82±0.10	3.70±0.08	3.79±0.10
LV internal diameter systole, mm	2.55±0.09	2.93±0.09 [a]	2.58±0.09 [b]	2.64±0.11
Systolic function				
Ejection fraction, %	63.9±2.3	45.5±2.4 [a]	59.7±2.5 [b]	58.4±2.2 [b]
Fractional shortening, %	34.5±1.7	22.3±1.4 [a]	31.4±1.8 [b]	30.5±1.5 [b]
LV end-diastolic volume, µL	66.6±2.6	63.4±3.6	58.6±3.1	62.1±4.2
LV end-systolic volume, µL	24.6±2.1	33.6±2.5 [a]	23.9±2.0 [b]	26.26±2.8
Cardiac output, mL/min	20.1±1.0	12.8±1.1 [a]	15.87±1.0	16.2±0.7 [b]
Stroke volume, µL	42.0±1.3	29.8±2.2 [a]	34.7±2.3	35.89±1.8
Diastolic function				
E'/A' ratio	1.07±0.04	0.86±0.06 [a]	1.01±0.08	0.88±0.03
Mitral E velocity, mm/s	522±28	427±26	432±48	444±40
Mitral A velocity, mm/s	383±22	294±21	289±38	289±29
E/E'	-27.0±1.4	-29.2±2.0	-25.8±3.8	-29.3±2.9
Deceleration time, ms	19.3±1.8	25.1±1.8	20.6±1.9	18.2±1.6 [b]
IVRT, ms	18.7±0.7	21.2±0.7	19.1±0.6	17.5±0.9 [b]
IVCT, ms	12.6±0.9	16.1±1.0 [a]	14.2±1.1	12.0±0.9 [b]
TEI index	0.77±0.03	0.86±0.03	0.86±0.01	0.73±0.03 [b]

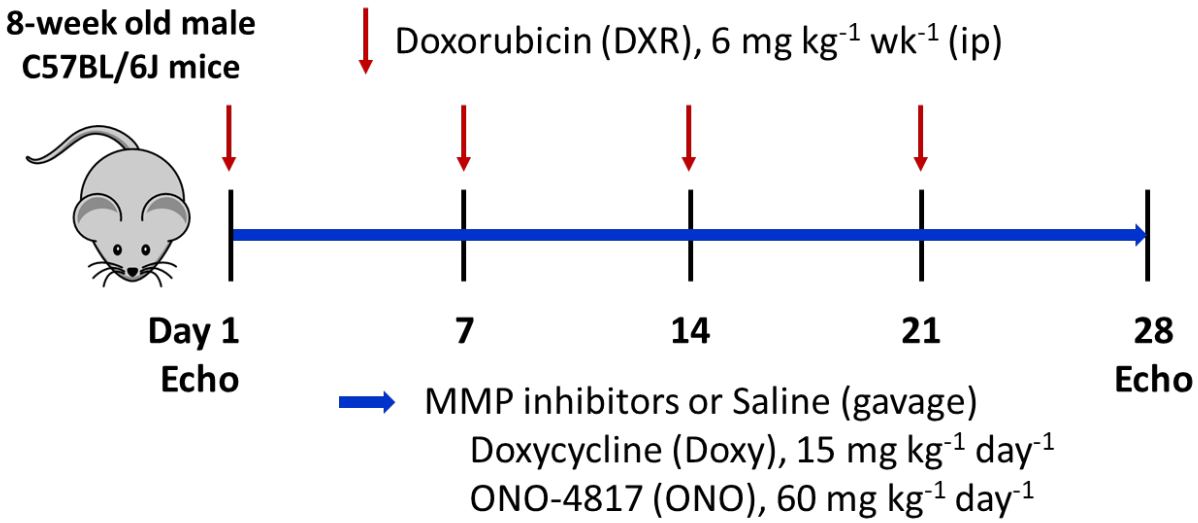

Figure 3.1: DXR and MMP inhibitor treatment regimen in 8-week old male C57BL/6J mice. DXR was administered weekly (6 mg/kg/wk, i.p.) with or without MMP inhibitors doxycycline (15 mg/kg/day, oral gavage) or ONO-4817 (60 mg/kg/day, oral gavage). Echocardiography was conducted on days 1 and 28. Hearts and plasma were collected on day 28 for biochemical and imaging analyses.

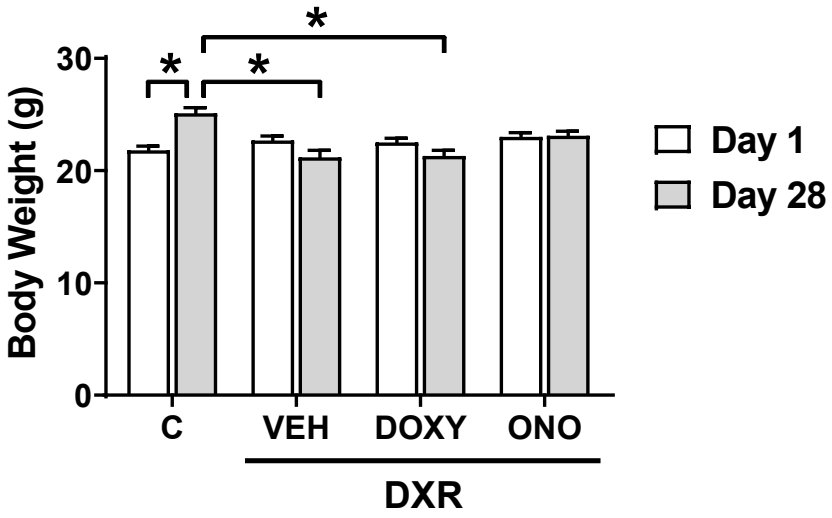

Figure 3.2: Body weight of mice treated with DXR with or without MMP inhibitors doxycycline (Doxy) or ONO-4817 (ONO) at day 1 and 28 (n=10). *p<0.05 by two-way ANOVA followed by Sidak's post hoc test. Bar graphs represent mean ± S.E.M.

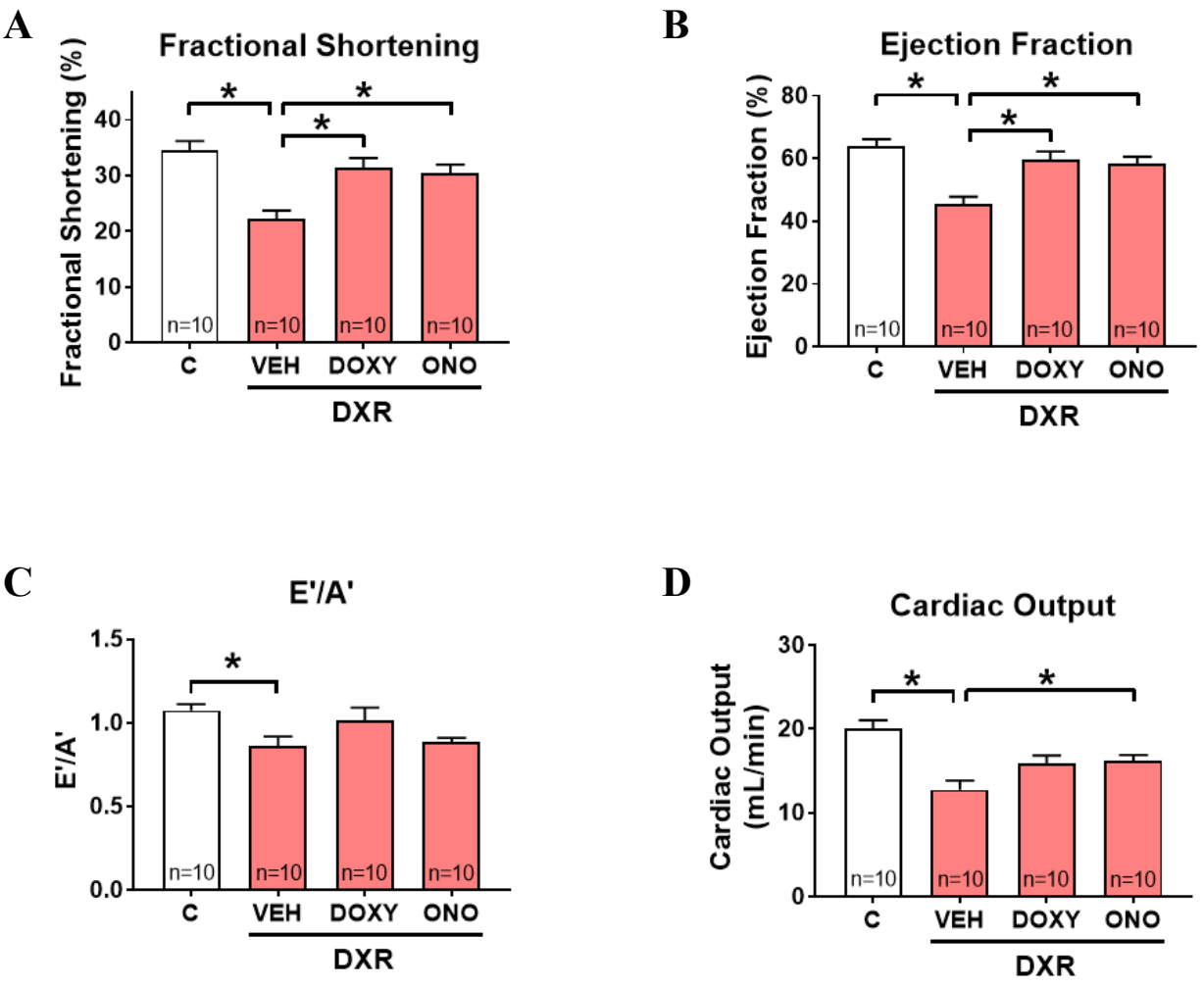

Figure 3.3: Cardiac function in doxorubicin (DXR) mice treated with MMP inhibitors Doxy or ONO. DXR impaired both (A,B) systolic and (C) diastolic function and reduced (D) cardiac output. Doxy and ONO rescued DXR-reduced fractional shortening and ejection fraction. *$p<0.05$ by one-way ANOVA followed by Sidak's post hoc test. Bar graphs represent mean ± S.E.M. Echocardiography was performed by Donna Beker.

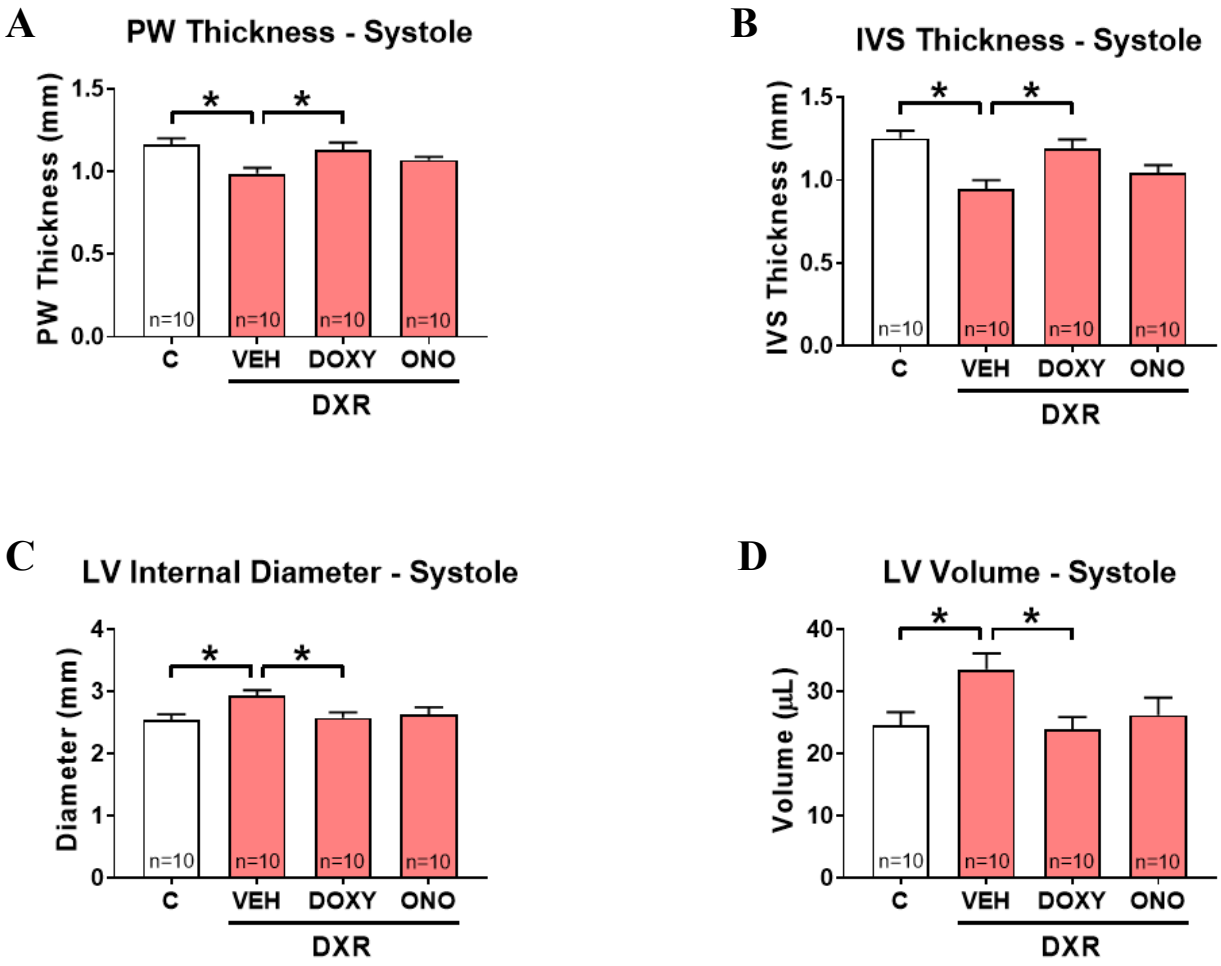

Figure 3.4: Cardiac morphology in mice treated with DXR with or without Doxy or ONO. DXR caused adverse cardiac remodeling marked by the thinning of the (A) posterior wall (PW) and (B) interventricular septum (IVS) and expansion of the (C,D) LV, which were attenuated by Doxy. *$p<0.05$ by one-way ANOVA followed by Sidak's post hoc test. Bar graphs represent mean ± S.E.M. Echocardiography was performed by Donna Beker.

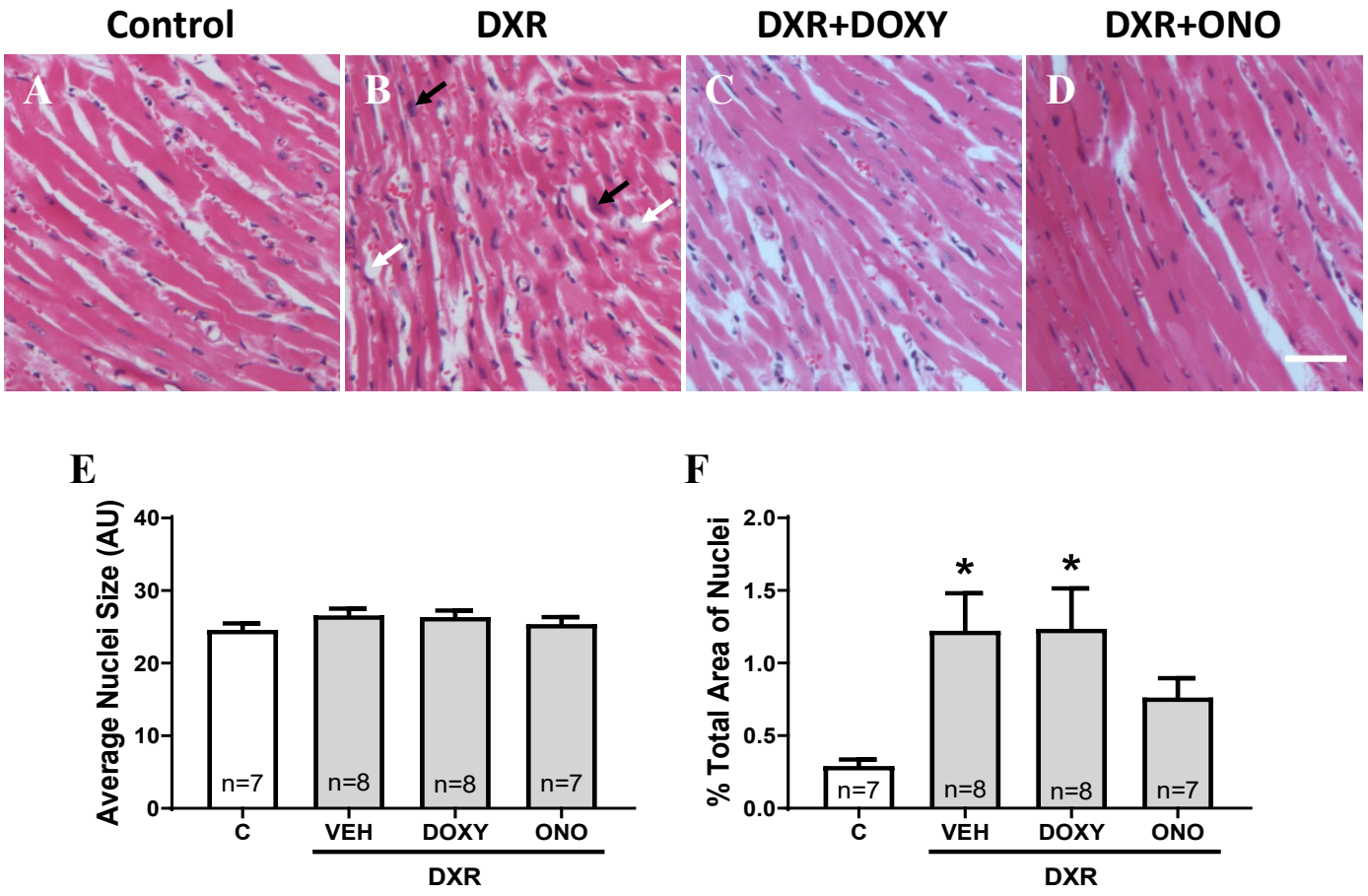

Figure 3.5: MMP inhibitors prevent histopathological cardiac remodeling in DXR cardiotoxicity. Hematoxylin and eosin stained sections of the left ventricular free wall from (A) Control, (B) DXR, (C) DXR+Doxy, and (D) DXR+ONO mice. DXR caused cardiomyocyte dropout (white arrows), crowding of the myofibrils, and enlarged nuclei (black arrows). Scale bar = 50 µm. (E) All groups exhibited similar average nuclear size. (F) DXR and DXR+Doxy hearts exhibited increased total nuclear area compared to control. *$p<0.05$ by one-way ANOVA followed by Dunnett' post hoc test. Bar graphs represent mean ± S.E.M.

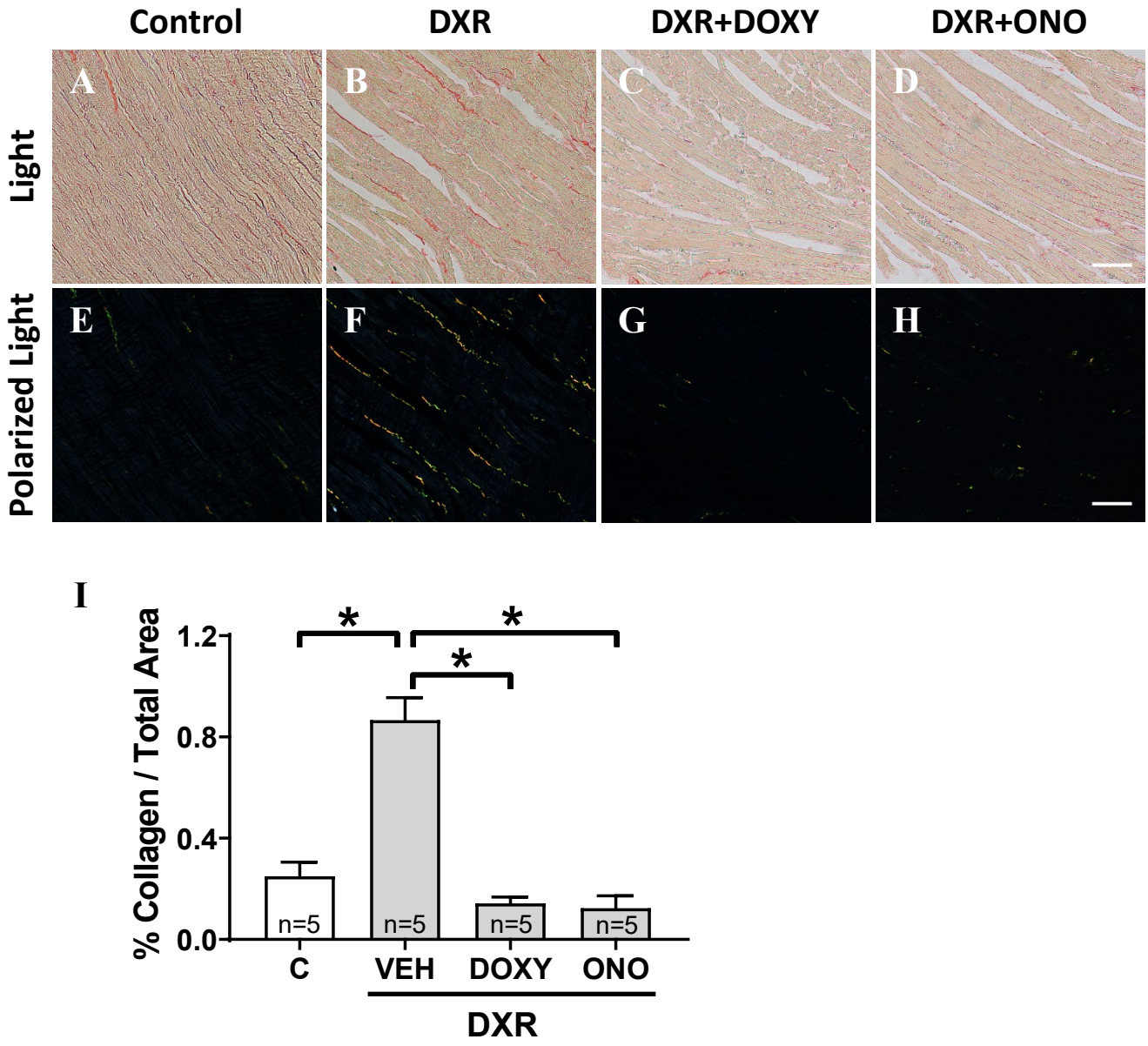

Figure 3.6: MMP inhibitors attenuate interstitial fibrosis in DXR cardiotoxicity. Representative images of left ventricular sections stained with Picrosirius Red examined under (A-D) light and (E-H) polarized light. Scale bar = 50 µm. (I) Doxy and ONO prevented DXR-induced left ventricular interstitial fibrosis as measured under polarized light microscopy. *$p<0.05$ by one-way ANOVA followed by Sidak's post hoc test. Bar graphs represent mean ± S.E.M.

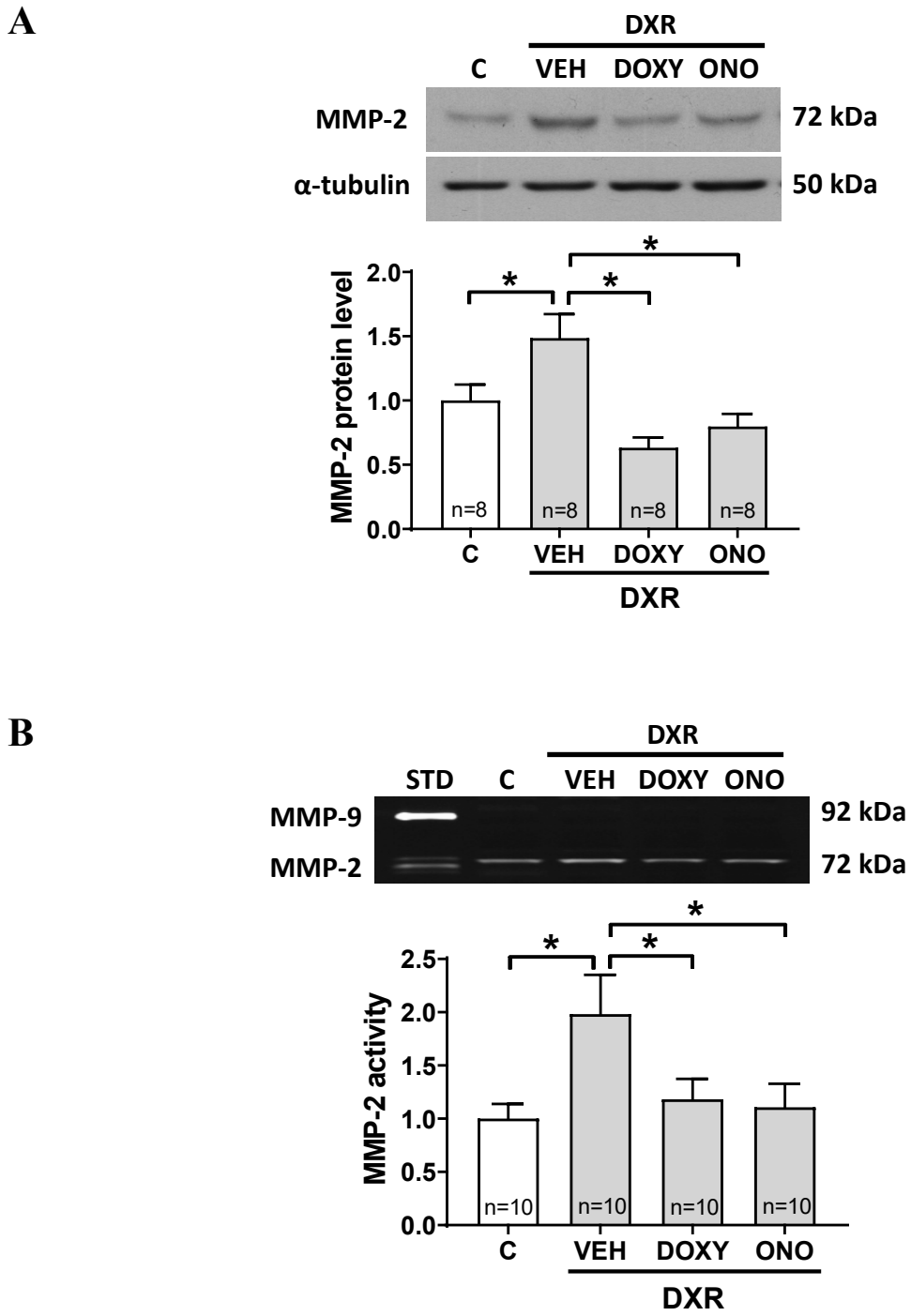

Figure 3.7: MMP-2 levels and activity in left ventricle from DXR mice treated with MMP inhibitors. DXR increased MMP-2 (A) protein levels and (B) activity in the heart, which were prevented by Doxy and ONO. *$p<0.05$ by one-way ANOVA followed by Sidak's post hoc test. Bar graphs represent mean ± S.E.M.

A

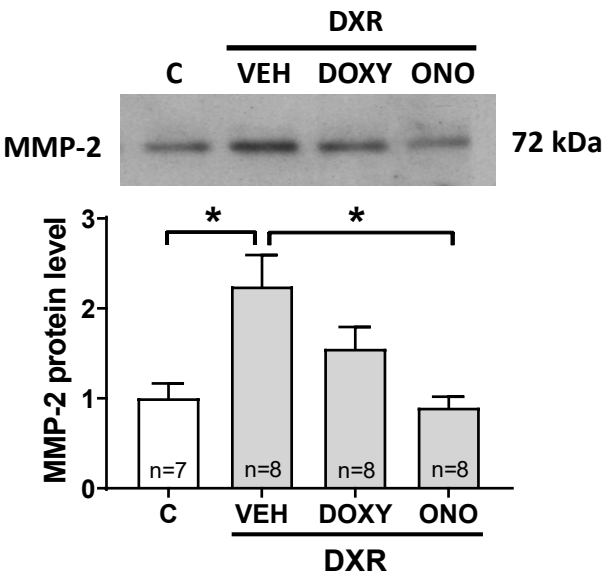

B

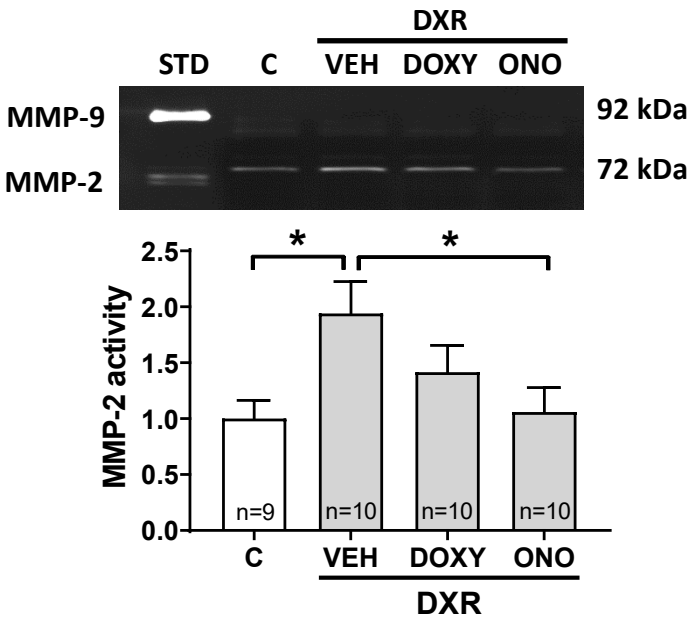

Figure 3.8: MMP-2 levels and activity in plasma from DXR mice treated with MMP inhibitors. DXR-treated mice exhibited increased levels of MMP-2 (A) protein and (B) activity in the plasma, which was prevented by ONO but not Doxy. *$p<0.05$ by one-way ANOVA followed by Sidak's post hoc test. Bar graphs represent mean ± S.E.M.

A

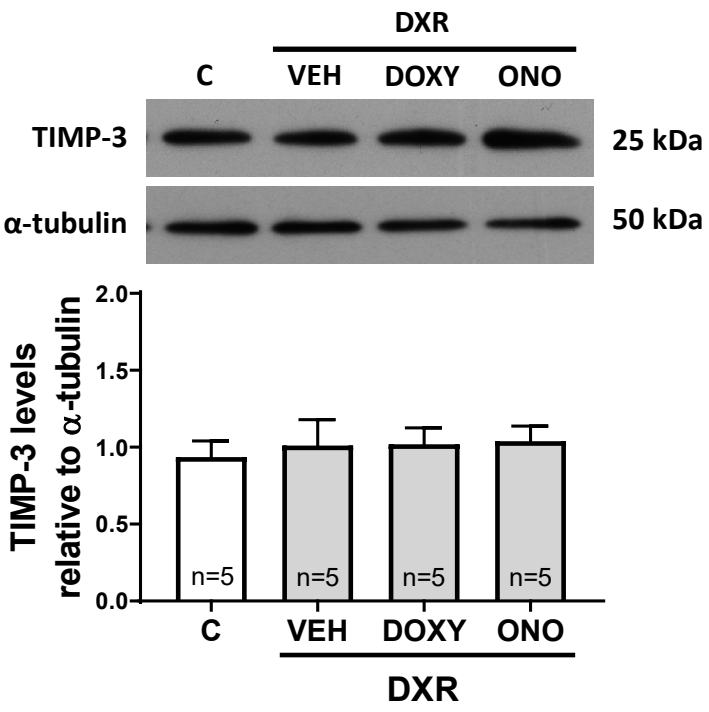

B

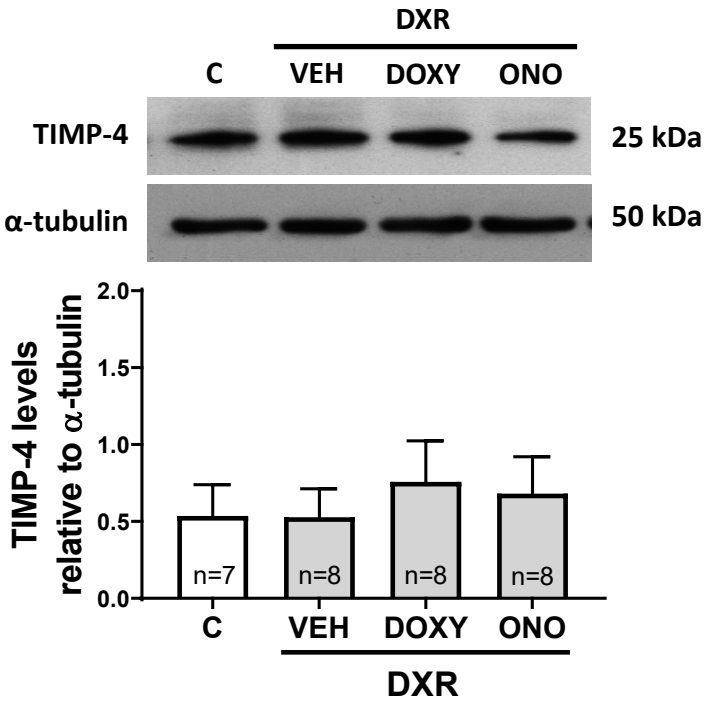

Figure 3.9: TIMP protein levels in the left ventricle. DXR nor MMP inhibitors Doxy and ONO affected (A) TIMP-3 or (B) TIMP-4 protein levels. $p>0.05$ by one-way ANOVA. Bar graphs represent mean ± S.E.M.

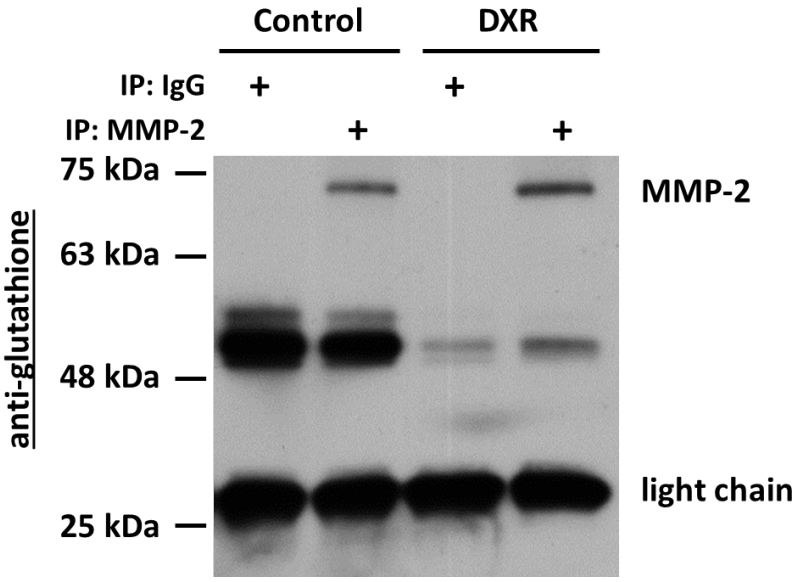

Figure 3.10: Detection of S-glutathiolated MMP-2 in left ventricular extracts. S-glutathiolated MMP-2 was detected by probing for glutathione in anti-MMP-2 immunoprecipitates in control and DXR left ventricular extracts. IgG was used as a negative control. Representative of three independent experiments.

A

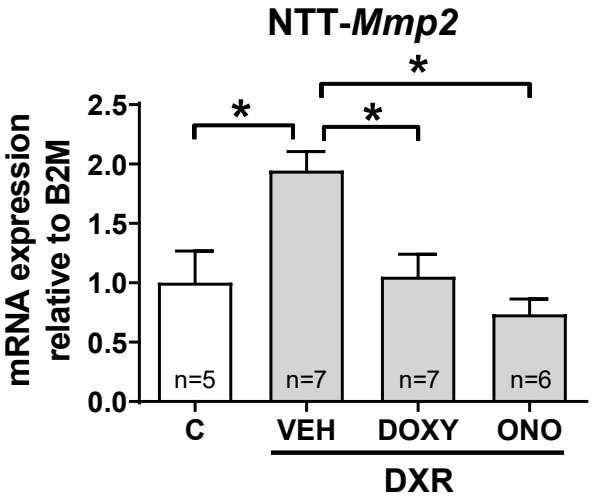

B

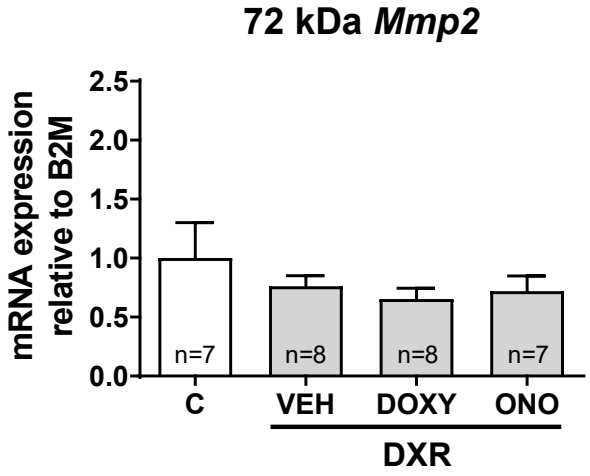

Figure 3.11: MMP-2 isoform expression in the left ventricle from DXR mice treated with or without MMP inhibitors. DXR upregulated (A) N-terminal truncated (NTT)-*Mmp2*, but did not affect (B) full-length (FL) *Mmp2* mRNA expression in the heart. (A,B) DXR-induced upregulation of NTT-*Mmp2* was prevented in mice treated with Doxy or ONO. *$p<0.05$ by one-way ANOVA followed by Sidak's post hoc test. Bar graphs represent mean ± S.E.M.

A

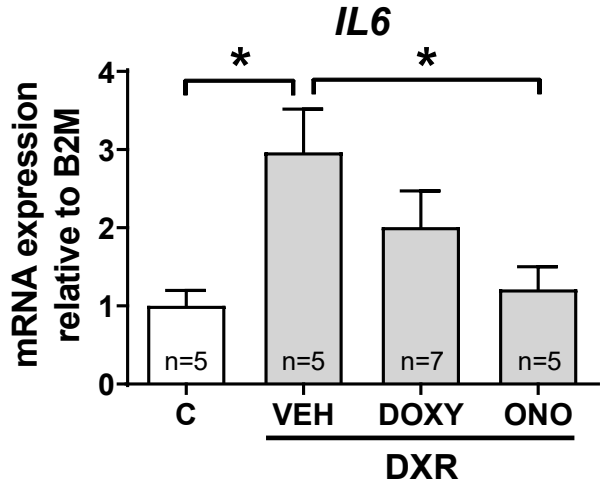

B

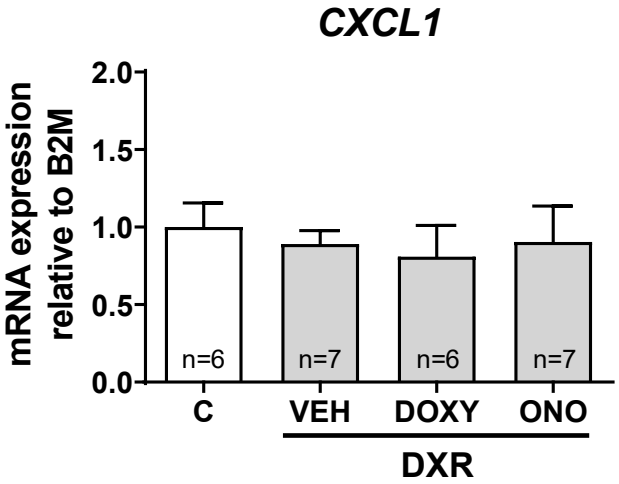

Figure 3.12: mRNA expression of inflammasome markers interleukin 6 (*IL6*) and chemokine (C-X-C) motif ligand 1 (*CXCL1*), which are associated with NTT-MMP-2 expression in the mouse heart. (A) DXR increased *IL6* expression in the heart, an effect that was prevented with ONO. (B) DXR did not affect *CXCL1* expression in the heart. $p>0.05$ by one-way ANOVA. Bar graphs represent mean ± S.E.M.

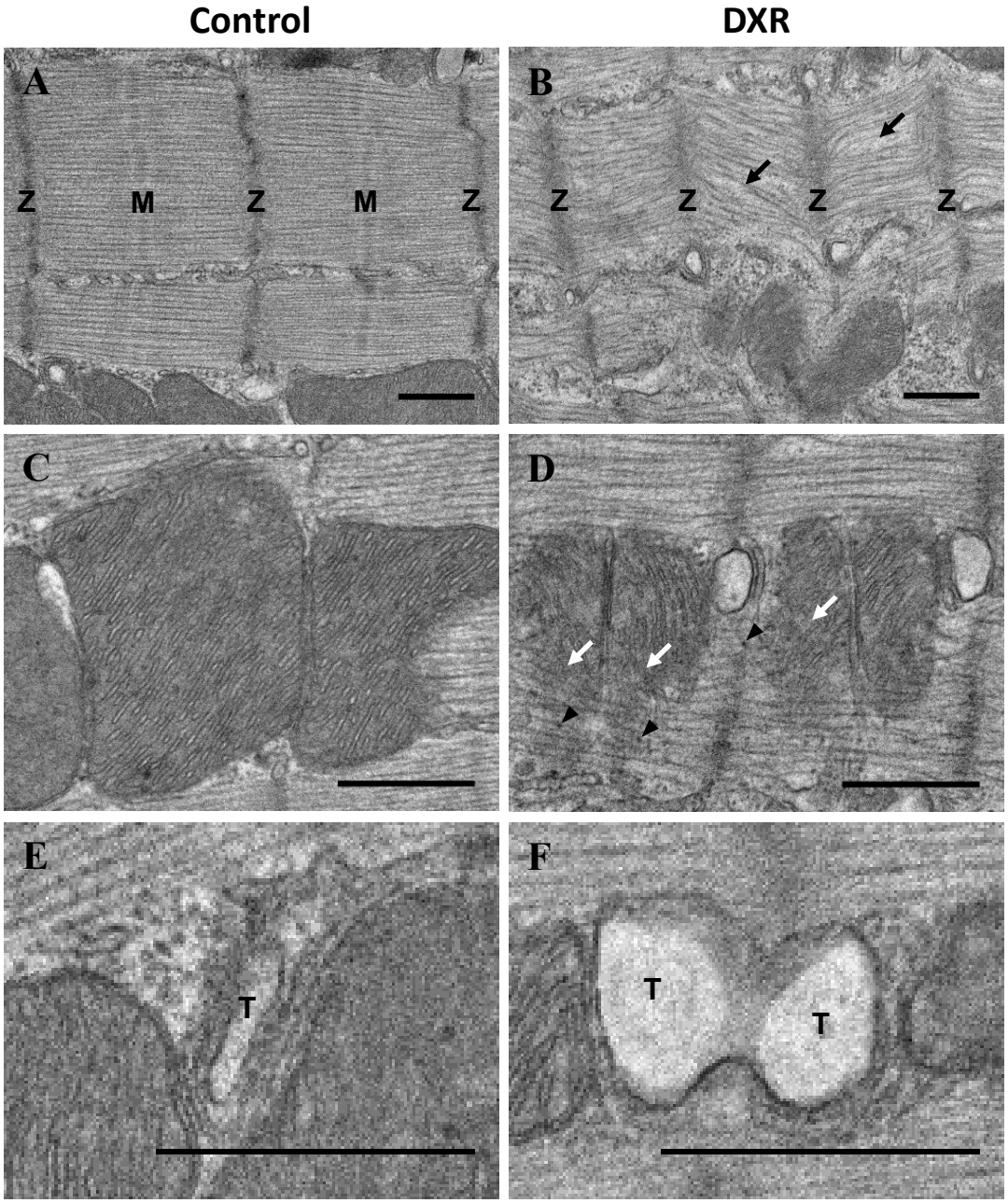

Figure 3.13: Transmission electron micrographs of cardiac myocytes from left ventricular sections of control and DXR treated mice. (A,C) Control hearts exhibit normal arrangement of myofilaments and mitochondrial cristae morphology. (B) The myocardium of DXR mice exhibits extensive myofilament disorganization, diffuse Z-discs (Z), and disassembly of M-line (M), shown by black arrows, compared to control. (D) DXR hearts exhibit mitochondrial degeneration (white arrows) and increased glycogen particles (arrowheads). (E,F) DXR also caused T-tubule (T) distention in the left ventricle compared to control. Representative of more than 50 images captured from 4 hearts from each group. Scale bar = 500 nm.

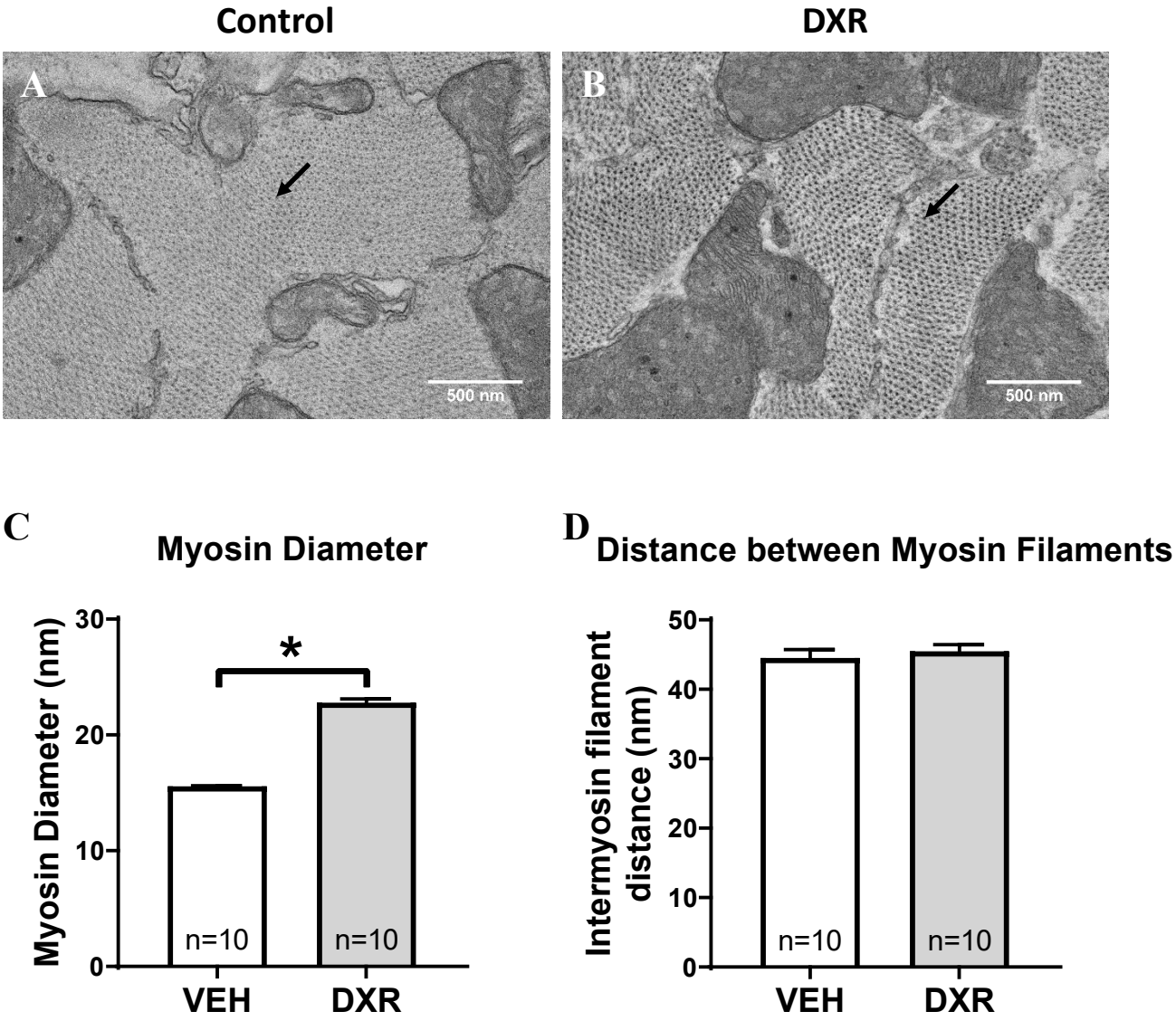

Figure 3.14: Electron micrographs of cross sections from the left ventricle of control and DXR treated mice. Cross-sectional views of the sarcomere of (A) control and (B) DXR hearts. Thick filaments are labelled with a black arrow. Scale bar = 500 μm. (C) The diameter of myosin are greater in DXR hearts than in control hearts. (D) The intermyosin filament distance between control and DXR hearts are similar. Ten separate images were captured and analyzed from each group. *$p<0.05$ by paired two-tailed t-test. Bar graphs represent mean ± S.E.M.

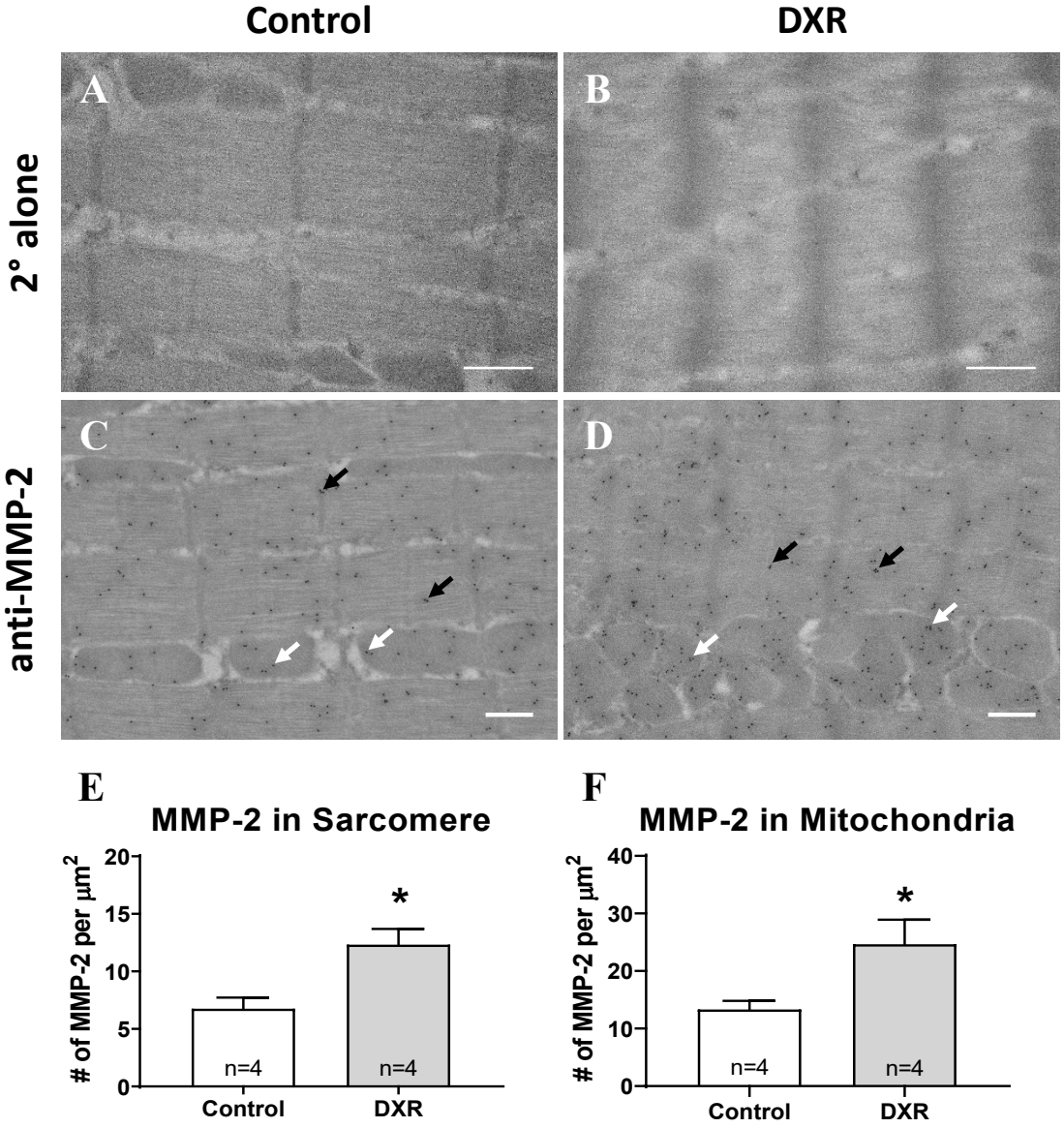

Figure 3.15: Determination of mitochondrial and sarcomeric MMP-2 in the left ventricle of control and DXR mice. Non-specific binding from the secondary antibody was not observed in the left ventricular sections of (A) control or (B) DXR mice. Representative immunogold electron micrographs of MMP-2 in the sarcomere (black arrows) and mitochondria (white arrows) from (C) control and (D) DXR hearts. Scale bar = 500 nm. Quantification of immunogold particles, conjugated to anti-MMP-2 antibody that were localized within the (E) sarcomere and (F) mitochondria. A total of 24 images were captured and analyzed from 4 separate hearts from each group. *$p<0.05$ by paired two-tailed t-test. Bar graphs represent mean ± S.E.M.

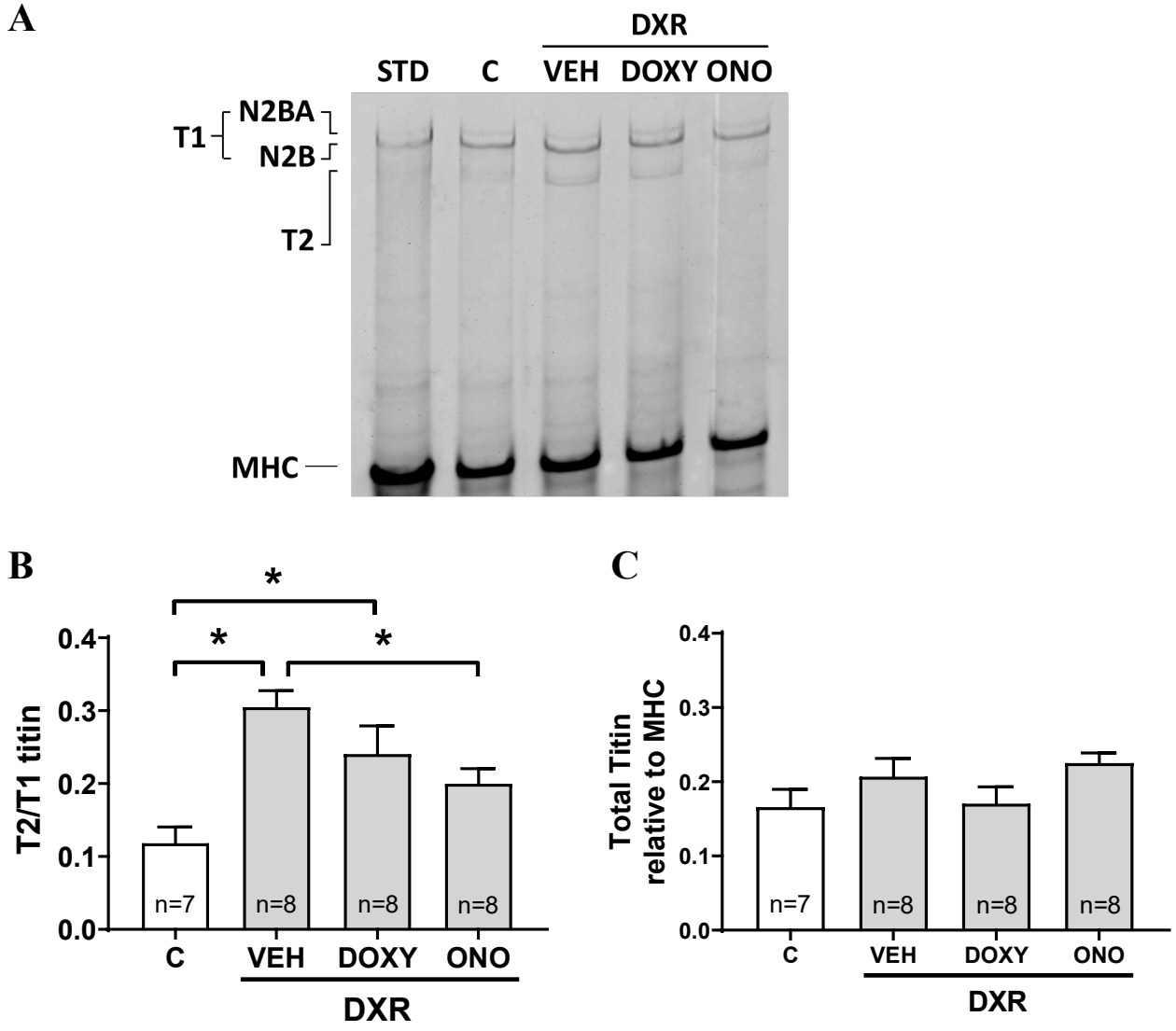

Figure 3.16: Cardiac titin proteolysis in DXR cardiotoxicity. (A) Representative Coomassie blue stained agarose gel showing titin levels in ventricular extracts. Ratio of titin degradation product (T2) to N2BA and N2B titin (T1) in ventricular extracts from control, DXR, DXR+Doxy, and DXR+ONO groups. Myosin heavy chain (MHC) was used as a loading control. (B) Cardiac titin proteolysis, represented by the T2 to T1 titin ratio, was significantly increased in DXR and DXR+Doxy mice. DXR-induced titin proteolysis was prevented with ONO. (C) Ratio of total titin (T1+T2) MHC content was unchanged between groups. *$p<0.05$ by one-way ANOVA followed by Sidak's post hoc test. Bar graphs represent mean ± S.E.M.

A

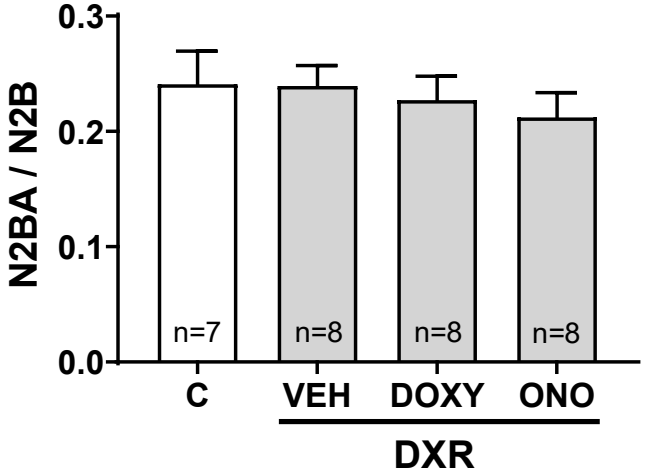

B

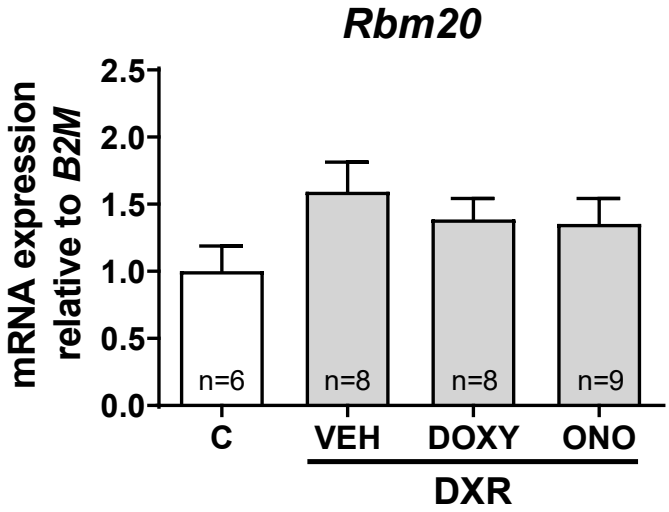

Figure 3.17. Cardiac titin isoform expression in DXR cardiotoxicity. DXR did not alter cardiac titin isoform expression, seen by the absence of changes in (A) N2BA to N2B titin ratio and (B) *Rbm20* mRNA expression. $p>0.05$ by one-way ANOVA. Bar graphs represent mean ± S.E.M.

CHAPTER 4

Junctophilin-2 is a target of matrix metalloproteinase-2 in myocardial ischemia-reperfusion injury

A manuscript based on this chapter is in preparation:

Chan BYH*, Roczkowsky R*, Poirier M, Lee TYT, Mahmud Z, Schulz R. Junctophilin-2 is a target of matrix metalloproteinase-2 in myocardial ischemia-reperfusion injury.

4.1 Introduction

Ischemic heart disease is one of the leading causes of global mortality and morbidity[187]. While timely restoration of blood flow to the heart critically limits the ischemic insult, there are no treatments to prevent heart injury caused by reperfusion. Myocardial ischemia-reperfusion (IR) injury disrupts excitation-contraction coupling, resulting in reduced myocardial contractility[273]. Increased oxidative stress[190], intracellular calcium overload[187], and damage to dyadic junctions[134] are amongst several important mechanisms which underlie defective excitation-contraction coupling and impaired cardiac contractile function in IR injury.

Cardiac excitation-contraction coupling is the critical process in which an action potential is converted into the mechanical contraction of the heart[137]. Cardiomyocyte contraction is tightly controlled by calcium-induced calcium release, whereby extracellular calcium enters through voltage-gated L-type calcium channels, which then activates calcium efflux from the sarcoplasmic reticulum through type 2 ryanodine receptors[138, 140]. Calcium-induced calcium release depends on the propinquity between T-tubules and the terminal cisternae of the sarcoplasmic reticulum network[141, 142]. The T-tubule-sarcoplasmic reticulum junction is anchored by a family of proteins known as junctophilin (JPH)[130]. Of the four known members of the JPH family[136], JPH-2 is the predominant isoform expressed in the heart[130].

JPH-2 is a structural membrane protein which tethers T-tubules across a ~15 nm junctional cleft to the sarcoplasmic reticulum to allow for coordinated calcium-induced calcium release in cardiomyocytes[130, 143]. JPH-2 consists of eight membrane occupation and recognition nexus (MORN) motifs in the amino-terminal region and a transmembrane domain in its C-terminal which anchor to the plasma membrane and sarcoplasmic reticulum, respectively (Fig. 1.6)[130]. JPH-2 is

localized near the Z-disc region of the sarcomere in close spatial proximity to type 2 ryanodine receptors[131]. Cardiac-specific knockdown of JPH-2 reduced the number of junctional membrane complexes, impaired cardiac contractility, and caused heart failure in mice[146]. Similarly, reduced levels of JPH-2 have been reported in heart failure and this was associated with ultrastructural uncoupling between the T-tubule-sarcoplasmic reticulum junction and cardiac contractile dysfunction[145, 147, 274-277]. More recently, loss of JPH-2 was reported in acute myocardial IR injury[134, 135]. This was attributed to the proteolytic activity of calpains with the use of the calpain inhibitor MDL-28170[134]. However, MDL-28170 is also a potent inhibitor of MMP-2[149], raising the possibility that MMP-2 is responsible for JPH-2 proteolysis in myocardial IR injury.

Matrix metalloproteinase-2 (MMP-2) is an intra- and extracellular protease best known for its canonical function in remodeling extracellular matrix proteins[269]. However, MMP-2 is also localized in many subcellular locales within the cardiomyocyte including the sarcomere, nucleus, mitochondria, mitochondria-associated membrane, sarcoplasmic reticulum, and caveolae[218]. During reperfusion, a burst of reactive oxygen and nitrogen species including peroxynitrite is generated in the ischemic myocardium[189]. Oxidative stress by increased generation of peroxynitrite activates MMP-2[39], where it proteolyzes structural and contractile sarcomeric proteins such as α-actinin, myosin light chain-1, troponin I, and titin[63, 84-86, 269]. Inhibition of MMP-2 prevented the degradation of sarcomeric proteins and improved the recovery of cardiac contractile function during reperfusion[63, 84, 85, 218].

Given that MMP-2 and JPH-2 are enriched along the Z-disc of the sarcomere in cardiomyocytes[63, 131], I determined whether JPH-2 is a target of MMP-2 in myocardial IR injury. In this study, I determined that MMP-2 contributes to JPH-2 proteolysis in IR injury, an effect that was prevented with an MMP inhibitor. Preventing JPH-2 proteolysis by MMP inhibition was

associated with improved cardiac contractile function during IR. In vitro proteolysis studies and in silico analysis identified multiple putative MMP-2 cleavage sites in JPH-2.

4.2 Methods

4.2.1 Preparation of ARP-100 for use in working heart perfusions

ARP-100 (Cayman Chemical) was purchased at exact weight (10 mg). DMSO (Fisher Scientific) was added to the vial containing ARP-100 to prepare a 20 mM ARP-100 stock solution. This stock solution was divided into 20 µL aliquots and stored at -80°C until use.

4.2.2 Isolated working rat heart perfusion

Male Sprague-Dawley rats (300-400 g), purchased from Charles River Laboratories (Saint-Constant, QC), were kept in the animal facility for 7 days to acclimatize under light-dark cycle control and received food and water *ad libitum*. Rats were anesthetized with 240 mg/kg sodium pentobarbital (i.p.). Hearts were excised, rinsed in ice cold Krebs-Henseleit solution (118 mM NaCl, 25 mM $NaHCO_3$, 4.7 mM KCl, 1.2 mM $MgSO_4$, 1.2 mM KH_2PO_4, 11 mM glucose, 0.5 mM EDTA, and 3 mM $CaCl_2$). Hearts were then cannulated at the aorta and perfused in Langendorff mode for 10 min (pre-equilibration time) at constant pressure (60 mmHg) with oxygenated Krebs-Henseleit solution (95% O_2, 5% CO_2) at 37°C. During this time, non-cardiac tissue was removed from the heart and the left atria was cannulated. Hearts were then perfused in working mode with recirculating Krebs-Henseleit solution (100 mL volume) with the addition of 100 µU insulin (Humulin R, Lilly, Indianapolis, IN), 0.1% BSA (Equitech-Bio Inc, Kerrville, TX), and 5 mM sodium pyruvate. Hearts were maintained at 37°C for the duration of the experiment by enclosure in a water-jacketed glass heart chamber. Perfusate entered the left atria with a hydrostatic preload pressure of 15 mmHg and was then ejected from the left ventricle against a hydrostatic afterload

pressure of 75 mmHg. Cardiac output and aortic flow were measured with in-line ultrasonic flow probes (Transonic Systems Inc, Ithaca, NY) in the left atrial in-flow and aortic outflow lines, respectively. Heart rate and peak systolic pressure were measured using a pressure transducer (Harvard Apparatus, Holliston, MA) in the aortic outflow line. Cardiac work, the product of cardiac output and peak systolic pressure, was used as an index of mechanical function. Hearts were equilibrated for at least 10 min before starting the timed perfusion experiment, designated as t = 0 min.

Beginning at t = 0 min, control hearts were perfused aerobically for 70 min. IR hearts were perfused aerobically for 20 min and then subjected to 20 min global, no-flow ischemia, followed by 30 min aerobic perfusion. To test the effect of an MMP inhibitor drug, either 10 μM ARP-100 or its vehicle (0.05% v/v DMSO) were added at t = 10 min perfusion to the recirculating perfusate. A schematic diagram of the isolated working rat heart perfusion protocol is illustrated in Fig. 4.1.

4.2.3 Preparation of heart samples

After 70 min of perfusion, the left atrial in-flow and aortic out-flow perfusate lines were clamped and the ventricles were squeezed with Wollenberger clamps (cooled to liquid nitrogen temperature) and then immersed in liquid nitrogen. To assess protein levels, the frozen ventricles were pulverized in liquid nitrogen using a mortar and pestle. A portion of the pulverized ventricular tissue was weighed and homogenized in 1:10 (w/v) RIPA buffer (150 mM NaCl, 1.0% IGEPAL CA-630, 0.5% sodium deoxycholate, 0.1% SDS and 50 mM Tris, 0.1% proteinase inhibitor cocktail, pH 8.0) using a PRO200 tissue homogenizer (Bio-Gen, Cambridge, MA) for 2 min (in cycles of 15 seconds on, 15 seconds off) at 4°C. The homogenate was then centrifuged at 10,000 g for 10 min at 4°C. The supernatant was collected, aliquoted and stored at -80°C. Total protein concentration was measured by bicinchoninic acid assay using BSA as a standard.

A separate series of identical heart perfusions were performed in order to provide left ventricular samples for in situ zymography and immunohistochemistry experiments. Immediately after perfusion, the left ventricle of each heart was isolated and fixed at 4°C for 24 hr in either zinc fixative (36.7 mM $ZnCl_2$, 27.3 mM zinc acetate dihydrate, 0.63 mM calcium acetate, and 0.1 M Tris, pH 7.6) for in situ zymography or in 4% paraformaldehyde in 0.1 M Sorensen's phosphate buffered solution (Electron Microscopy Sciences) for immunohistochemistry. After 24 hr, zinc-fixed left ventricles were embedded in paraffin and stored at 4°C until use. After 24 hr, paraformaldehyde-fixed left ventricles were cryopreserved in 30% (w/v) sucrose in 0.1 M Sorenson's phosphate buffered solution at 4°C for 24 hr. Cryopreserved ventricular tissue were snap frozen in Tissue-Tek Optimal Cutting Temperature compound (OCT, VWR, Radnor, PA) cooled in liquid nitrogen and stored at -80°C until use.

4.2.4 Western blot analysis

Ventricular extracts (10 μg of total protein) were separated on 8% polyacrylamide gels by electrophoresis. Proteins were wet transferred onto polyvinylidene difluoride membranes (Bio-Rad) as described in Section 2.2.8. Membranes were immunoblotted with primary antibodies against JPH-2 (#40-5300, Thermo Fisher Scientific) and GAPDH (2118S, Cell Signaling Technology). Primary antibodies were then probed with secondary goat anti-rabbit IgG antibodies (CLCC42007, Cedarlane). Protein bands were visualized using chemiluminescent detection reagent Clarity™ ECL western substrate (Bio-Rad) and exposed to autoradiography film. These were scanned with a Bio-Rad GS-800 densitometer and quantified on ImageJ v1.48.

4.2.5 Immunoprecipitation

To determine whether MMP-2 interacts with JPH-2 in the heart, ventricular extracts (25

μg/sample) were diluted in RIPA buffer to a final volume of 200 μL and incubated with rabbit MMP-2 antibody (1:200, ab92536, Abcam) or rabbit IgG isotype control (ab27472, Abcam) under rotatory agitation overnight at 4°C. 50 μL of Protein G Sepharose bead slurry (ab193259, Abcam) was then added to each antibody-homogenate sample and incubated on a rotator for 4 hr at 4°C. The suspension was centrifuged (3,000 g, 2 min, 4°C) and the beads were washed with wash buffer (150 mM NaCl, 10 mM Tris, 1 mM EDTA, 1 mM EGTA, 0.2 mM sodium orthovanadate, 1% Triton X-100, pH 7.4) three times at room temperature. The beads were resuspended in 2x Laemmli buffer, heat denatured at 95°C for 5 min, and separated on 8% polyacrylamide gels for western blot analysis. After transfer, the PVDF membranes were probed with JPH-2 antibody (#40-5300, Thermo Fisher Scientific) to determine whether MMP-2 is associated with JPH-2.

4.2.6 In situ zymography

Paraffin embedded, zinc-fixed left ventricular tissue was cut into 4 μm thick sections and mounted onto Superfrost Plus glass slides (Fisher Scientific) at room temperature. Slides were deparaffinized in an ethanol series (100% to 70%) and then in water at room temperature. DQ gelatin is fluorescein-labeled gelatin substrate that is internally quenched unless it is cleaved by gelatinases such as MMP-2/-9. Each ventricular section was incubated with 50 μL of 50 μg/mL of DQ gelatin (Thermo Fisher Scientific) diluted in zymographic activity buffer (50 mM Tris-HCl, 150 mM NaCl, 5 mM $CaCl_2 \cdot 2H_2O$, and 0.05% NaN_3, pH 7.6) at 37ºC or 4ºC (autofluorescence control) for 4 hr. Ventricular sections were also incubated with DQ gelatin substrate in the presence of MMP inhibitor EDTA (20 mM) at 37°C to determine the contribution of MMP activity to detectable gelatinolytic activity[278]. After incubation with DQ gelatin, nuclei were stained with 1 μg/mL DAPI (Sigma-Aldrich). Slides were washed with PBS before mounting with coverslips using Vectashield mounting medium (H-1400, Vector Laboratories).

Gelatinolytic activity was visualized with a Leica TSC SP5 confocal laser scanning microscope (Leica). DAPI was visualized using a 405 nm diode laser (20%) with a bandpass 425-485 nm filter. Fluorescein was captured using an argon ion laser (488 nm, 20%) with a band pass 508-558 nm filter. Images were collected in sequential mode with a line average of 4 at a resolution of 1024 x 1024 pixels. Three fields of view were acquired from each left ventricle. Three individual left ventricles from separate rats were analyzed for each group. MMP activity was quantified by the following equation:

$$MMP\ activity\ per\ \mu m^2 = \frac{(DQ_{37°C}) - (DQ_{37°C}EDTA) - (DQ_{4°C})}{tissue\ area\ (\mu m^2)}$$

MMP activity was quantified by determining the amount of gelatinolytic activity that is inhibited by EDTA ($DQ_{37°C}$ – $DQ_{37°C}$EDTA). This value was then subtracted by the fluorescence contributed by autofluorescence ($DQ_{4°C}$) and then normalized to the area of tissue (μm^2). The tissue area was determined by applying a threshold on ImageJ. The MMP activity from a single left ventricle was determined from an average across three randomly selected field of views. This was performed for three separate left ventricles from each experimental group.

4.2.7 Immunohistochemistry

Fixed, frozen left ventricular tissue embedded in OCT was cut at -20°C into 4 µm thick sections and mounted onto Superfrost Plus slides. Sections were rehydrated in PBS for 10 min at room temperature. Antigen retrieval was performed by incubating sections in 1x Target Retrieval Solution (Dako, Carpinteria, CA) at 95°C for 30 min, then placed at room temperature for 20 min, and then rinsed in running H_2O for 10 min. Sections were quenched with PBS containing 0.4 M glycine for 15 min at room temperature. Sections were then incubated with blocking buffer (Image-iT FX signal enhancer, Invitrogen) for 1 hr at room temperature. Double immunolabeling was

performed by incubating sections with an MMP-2 antibody (mouse anti-MMP-2 IgG_1, 1:100, MAB3308, Millipore), diluted in PBS containing 10% goat serum (Sigma-Aldrich), overnight at 4°C. After washing with PBS (3 x 10 min), sections were incubated with a JPH-2 antibody (rabbit anti-JPH-2 IgG, 1:100, #40-5300, Thermo Fisher Scientific), diluted in PBS containing 10% goat serum (Sigma-Aldrich), overnight at 4°C. After washing with PBS (3 x 10 min), sections were incubated with secondary antibodies conjugated to fluorescent dyes (Alexa Fluor 555 goat anti-mouse IgG1, 1:500, A21127, Invitrogen; Alexa Fluor 488 goat anti-rabbit IgG, 1:500, A11008, Invitrogen), diluted in PBS containing 10% goat serum, for 1 hr at room temperature. After washing with PBS (3 x 10 min), nuclei were stained with 1 μg/mL DAPI solution at room temperature for 15 min. The slides were mounted with coverslips using ProLong Diamond Antifade Mountant (Invitrogen) and cured at room temperature for 24 hr before imaging.

Immunolabelled ventricular sections were visualized with a Leica SP5 laser scanning confocal microscope. DAPI was visualized using a 405 nm diode laser (40%) with a bandpass 410-460 nm filter. Alexa Fluor 488 was captured using an argon ion laser (488 nm, 40%) with a band pass 498-538 nm filter. Alexa Fluor 555 was captured using a Green HeNe laser (543 nm, 40%) with a band pass 553-613 nm filter. Images were collected in sequential mode with a line average of 4 at a resolution of 2048 x 2048 pixels. 5 field of views were examined from each left ventricle.

4.2.8 In vitro proteolysis

4.2.8.1 4-aminophenylmercuric acetate activation of MMP-2

4-aminophenylmercuric acetate (APMA) activates the MMP-2 zymogen by disrupting the sulfhydryl bond between Cys102 and the catalytic zinc ion[279]. Human full length MMP-2 purified from TIMP-2 knockout human fibrosarcoma cells (HT1080 cell line, ATCC) prepared in our lab

(0.2 mg/mL) was added to activity buffer (150 mM NaCl, 50 mM Tris-HCl, 5 mM $CaCl_2$, pH 7.6) containing 1 mM APMA to a final volume of 200 µL. The reaction was incubated at 37°C for 2 hr. APMA activated MMP-2 was aliquoted and stored at -80°C. APMA activated MMP-2 was diluted to 1 ng/mL in RIPA buffer and its activity was confirmed by gelatin zymography (see Appendix).

4.2.8.2 In vitro proteolysis of endogenous JPH-2 within ventricular extracts

Note that purified JPH-2 is not commercially available. Ventricular extracts (4 µg of protein) were incubated with increasing amounts of activated human recombinant MMP-2 (0-100 ng) in the presence or absence of 30 µM ARP-100 for 1 hr at 37°C. 4 µg of ventricular homogenate was also incubated with 10 ng of APMA-activated MMP-2 at 37°C for 15, 30, 45, and 60 min. The reaction products were then separated on a 10% polyacrylamide gel, transferred, and immunoblotted for JPH-2 as described above.

4.2.9 In silico predicted JPH-2 cleavage sites by MMP-2

In silico prediction of JPH-2 cleavage sites by MMP-2 was performed using online cleavage prediction server CleavPredict (http://cleavpredict.sanfordburnham.org)[280]. This online tool is optimized for matrix metalloproteinases and can predict the substrate cleavage sites for 11 MMPs including MMP-2 by using position weight matrix (PWM). There is currently no 3D crystal structure of JPH-2 available in Protein Data Bank (PDB). Therefore, the rat JPH-2 FASTA sequence (UniProt ID - Q2PS20) was entered into the CleavPredict query sequence section and MMP-2 was selected as the protease. The datasets from CleavPredict used a high throughout proteomic technique and proteome identification of protease cleavage sites (PICS) to determine the substrate specificity profiling of MMP-2[280].

4.2.10 Statistical analysis

Data are expressed as mean ± SEM of *n* independent experiments. Working heart functional data, in vitro degradation, and western blot data were analyzed by one-way ANOVA followed by Dunnett's or Tukey's post-hoc test using GraphPad Prism 7 (GraphPad Software). *p* values <0.05 were considered significant.

4.3 Results

4.3.1 MMP inhibitor ARP-100 improves cardiac contractile function in IR injury

Fig. 4.1 illustrates the isolated working rat heart protocol for Aerobic, Aerobic+ARP, IR, and IR+ARP groups. Aerobic hearts exhibited no loss of contractile function, measured by cardiac work, for the entire 70 min of perfusion (Fig. 4.2). A summary of the contractile parameters measured at the end of perfusion are detailed in Table 4.1. ARP-100 had no effect on the contractile function of Aerobic hearts (Table 4.1). IR hearts exhibited impaired recovery of contractile function during reperfusion compared to Aerobic hearts (Fig. 4.2). ARP-100 significantly improved the recovery of cardiac work, cardiac output, and coronary flow during reperfusion compared to IR hearts (Fig. 4.2, Table 4.1).

4.3.2 ARP-100 inhibits in situ myocardial MMP-2 activity

In situ zymography was performed on left ventricular sections from Aerobic, IR, and IR+ARP hearts to visualize the distribution of myocardial MMP-2 activity. Aerobic, IR, and IR+ARP ventricular sections incubated with DQ in the presence of EDTA (pan-MMP inhibitor) exhibited no gelatinolytic activity confirming this activity is MMP-dependent (Fig. 4.3A-C). Brightfield images revealed that IR hearts exhibited myofibrillar disorganization compared to

Aerobic hearts (Fig. 4.3D,E). IR+ARP hearts showed normal myofibrillar organization similar to Aerobic hearts (Fig. 4.3F). In situ zymography revealed abundant MMP activity within the cardiomyocytes of Aerobic and IR hearts, which was abolished in IR+ARP hearts (Fig. 4.3G-I). In particular, MMP activity was localized to the Z-disk of the sarcomere in Aerobic hearts (Fig. 4.3G,J), whereas this activity was redistributed as intracellular clusters in IR hearts (Fig. 4.3H,K) and abolished in IR+ARP hearts (Fig. 4.3I-M). I performed gelatin zymography on the ventricular extracts of each heart to determine whether MMP-2 or MMP-9 is contributing to MMP activity. In situ zymography and gelatin zymography detect different levels of MMP activity due to the inherent separation of ARP-100 from MMP-2 during electrophoresis. More importantly, gelatin zymography specifically shows abundant MMP-2 activity, but no detectable MMP-9 activity in the ventricular extracts (Fig. 4.3N). This suggests that the proteolytic activity measured by in situ zymography is attributed to MMP-2.

4.3.3 MMP-2 contributes to JPH-2 proteolysis in IR injury

To determine whether MMP-2 contributes to JPH-2 proteolysis in myocardial IR injury, JPH-2 levels in ventricular extracts from Aerobic, IR, and IR+ARP hearts were assessed by immunoblot. JPH-2 levels were unchanged between the three groups (Fig. 4.4A). Increased exposure of the immunoblots revealed a lower molecular weight band (~63 kDa) representing a putative JPH-2 degradation product in the ventricular extracts from each group (Fig. 4.4B). More importantly, IR hearts exhibited a fivefold increase in JPH-2 degradation compared to Aerobic hearts (Fig. 4.4B), which was attenuated in the IR+ARP hearts.

4.3.4 MMP-2 binds to JPH-2 in Aerobic and IR hearts

In order to detect a possible interaction between MMP-2 and JPH-2 in the rat heart, MMP-

2 was immunoprecipitated from ventricular extracts and then probed for JPH-2 by immunoblot. Full length JPH-2, JPH-2 aggregates, and a putative lower molecular weight (~55 kDa) JPH-2 degradation product were detected in both Aerobic and IR hearts (Fig. 4.5).

4.3.5 MMP-2 is co-localized to JPH-2 in the heart

Given that MMP-2 and JPH-2 are both enriched in the Z-disc region of the sarcomere[63, 131], colocalization of MMP-2 and JPH-2 was assessed by immunofluorescence. Myofibrillar and nuclear morphology was visualized by brightfield microscopy and DAPI staining, respectively, in Aerobic and IR left ventricular tissue (Fig. 4.6 A,B,F,G). There were no differences in myofibrillar (Fig. 4.6A,B) and nuclear morphology between Aerobic and IR groups (Fig. 4.6 F,G). JPH-2 staining in the left ventricle was consistent with Z-disc sarcomeric structures in both Aerobic and IR groups (Fig. 4.6C,H). MMP-2 was primarily localized to the Z-disc of the sarcomere and, to a lesser degree, between adjacent Z-discs in both Aerobic and IR rat hearts (Fig. 4.6 D, I). The staining between the Z-discs is likely localized in the cytosol and/or the M-line region of the sarcomere. When MMP-2 and JPH-2 signals were merged, MMP-2 was strongly co-localized to JPH-2 in Aerobic and IR rat hearts (Fig. 4.6E,J).

4.3.6 JPH-2 is susceptible to proteolysis by MMP-2

As purified JPH-2 is not commercially available, in order to test the susceptibility of JPH-2 to proteolysis by MMP-2, I incubated ventricular extracts prepared from an Aerobic heart with increasing amounts of APMA-activated MMP-2 for 30 min. A JPH-2 immunoblot revealed that MMP-2 reduced JPH-2 levels in a concentration-dependent manner (Fig. 4.7A). JPH-2 proteolysis was abolished by ARP-100. A longer exposure of the immunoblot detected three lower molecular weight putative JPH-2 degradation products (75, 65, and 55 kDa) (Fig. 4.7B). At the highest

concentration of MMP-2 (500 ng), the 75 and 65 kDa bands were further proteolyzed. Degradation of these JPH-2 fragments was prevented by ARP-100.

4.3.7 In silico prediction of MMP-2 cleavage sites in JPH-2

Using CleavPredict, I identified 30 potential cleavage sites in JPH-2 by MMP-2 along with their predicted secondary structure and corresponding mass of both N-terminal and C-terminal cleavage fragments. I tabulated the ten cleavage sites with the highest PWM score (Table 4.2). As expected, no cleavage sites were predicted within the highly structured regions of JPH-2, namely the α-helix domain and the transmembrane domain within the sarcoplasmic reticulum (Table 4.2, Fig. 1.6). Most of the cleavage sites were predicted to lie within the MORN motifs. I then aligned the predicted cleavage sites with the active site specificity profiling dataset of MMP-2 determined by CleavPredict[281] to determine its similarity to the substrate amino acid specificity from P3-P3′. There was an average of 57% sequence homology to the PICS sequence specificity profile of MMP-2 from P3-P3′ position (Table 4.2).

According to its primary amino acid sequence, JPH-2 has a theoretical molecular weight of 75 kDa. However, the apparent molecular weight of JPH-2 observed in gel electrophoresis is 97 kDa[134, 135]. I adjusted the theoretical N- and C-terminal masses of the predicted cleavage products by 1.54 (97 kDa / 63 kDa) to predict which cleavage sites may produce a ~63 kDa degradation product as observed in the IR hearts. Of interest, two cleavage sites, P1 at 350 and 372, resulted in degradation products with an apparent molecular weight of around 63 kDa (Table 4.2).

4.4 Discussion

Elucidating the mechanism of JPH-2 proteolysis is essential to understanding impaired

myocardial contractility in IR injury. In this study, I demonstrated that JPH-2, a key structural component of the dyadic junction, is a target of MMP-2 in acute myocardial IR injury. In situ zymography analysis revealed that MMP-2 is localized to the Z-disc region of the sarcomere in Aerobic rat hearts. IR hearts exhibited disrupted Z-discs and clusters of intracellular MMP-2 activity. In silico analysis identified multiple, specific, putative MMP-2 cleavage sites in the MORN motifs and the divergent region of JPH-2. Indeed, endogenous JPH-2 in ventricular extracts was susceptible to proteolysis by MMP-2 in vitro. Inhibition of MMP-2 by ARP-100 not only improved the recovery of cardiac contractile function after IR in isolated rat hearts, but also attenuated the increase in JPH-2 degradation caused by IR injury. This indicates that JPH-2 proteolysis as a result of IR injury is reduced upon the inhibition of MMP activity.

Although MMPs have been extensively studied for their roles in remodeling extracellular matrix proteins in long term (days to weeks) remodeling processes[9], MMPs also target non-matrix substrates[10] including intracellular proteins[218] in acute (seconds to minutes) pathophysiological processes. MMP-2 is maximally activated within minutes of ischemia-reperfusion. Inhibition of MMP activity with o-phenanthroline, doxycycline, and ONO-4817 improved the recovery of cardiac contractile function in IR injury by preventing the degradation of sarcomeric (troponin I, titin, and myosin light chain-1)[63, 84, 85] and cytoskeletal (α-actinin)[86] proteins. Consistent with previous reports, MMP inhibition with ARP-100, the most selective MMP-2 preferring inhibitor available, improved cardiac work following IR injury. Although ARP-100 also inhibits MMP-3 (K_i = 4500 nM) and MMP-9 (K_i = 200 nM)[60, 66], MMP-2 is the major protease inhibited by ARP-100 as MMP-3 is not found in cardiomyocytes and MMP-9 activity was not detected in ventricular extracts.

Immunofluorescence and subcellular fractionation studies have localized MMP-2 in

many subcellular locales, most prominently near the Z-disc region of the sarcomere in cardiomyocytes[63]. For the first time, I show that MMP-2 activity is localized to the Z-disc region in cardiomyocytes in the isolated rat heart by in situ zymography. Furthermore, immunohistochemistry with an MMP-2 antibody showed MMP-2 staining consistent with Z-disc sarcomeric structures in the rat left ventricular tissue. This observation was consistent with previous studies which reported the localization of MMP-2 to the Z-disc and degradation of titin[63] and α-actinin, the cytoskeletal protein which connects thin filaments from adjacent sarcomeres at the Z-disc, in peroxynitrite infused isolated rat hearts[86]. Interestingly, the striated pattern of the staining of the cardiac myofibrils from Aerobic hearts were not observed in IR hearts. This difference was accompanied by a redistribution of intracellular MMP-2 activity which appeared clustered in the cytosolic compartment within the cardiomyocyte. IR+ARP hearts showed little to no MMP-2 activity and normal myofibrillar morphology. These results suggest that the Z-disc region of the sarcomere is an important target of MMP-2 activity in myocardial IR injury.

JPH-2 is the structural membrane protein which plays an important role in the molecular organization of the juncture of the T-tubule with the sarcoplasmic reticulum in cardiac muscle cells[130]. JPH-2 plays an important role in the coupling between L-type calcium channels and type 2 ryanodine receptors in calcium-induced calcium release[146, 274]. Alterations in JPH-2 expression have deleterious consequences on myocardial contractility by reducing density of dyadic junctions and decreasing the efficiency of excitation-contraction coupling[145, 274, 282]. Furthermore, loss of JPH-2 is consistently found in several types of progressive heart failure including dilated, hypertrophic, and ischemic cardiomyopathy[145, 274, 275]. Recent studies have suggested the JPH-2 levels are reduced in acute myocardial IR injury[134, 135]. Guo et al[134] found that loss of JPH-2 was prevented by the calpain inhibitor MDL-28170, which also inhibits MMP-2 activity[149]. However,

these studies did not report any JPH-2 degradation products in the ventricular extracts without the addition of exogenous calcium or calpain[134, 135]. I found that IR injury caused JPH-2 degradation, marked by an increase in the levels of a 63 kDa JPH-2 fragment. JPH-2 degradation and IR-induced cardiac contractile dysfunction was ameliorated by ARP-100. This indicates that preventing JPH-2 proteolysis with MMP inhibitors contributes to the recovery of cardiac contractile function. The structural integrity of JPH-2 is essential for coordinated calcium-induced calcium release in cardiomyocytes. Cleavage of JPH-2 by MMP-2 may disrupt intracellular calcium homeostasis in IR injury. Protecting the structural integrity of JPH-2 in the heart may be an important determinant of whether an ischemic insult is reversible or irreversible.

Although JPH binds to sphingomyelin and phosphatidylcholine, no proteins have yet been found to be associated with JPH by immunoaffinity purification[130]. In this study, immunofluorescence showed that MMP-2 is strongly co-localized with JPH-2 in both Aerobic and IR rat hearts. Immunoprecipitation studies revealed that MMP-2 is associated with full-length JPH-2 and a putative 55 kDa JPH-2 fragment in the heart. The 63 kDa JPH-2 degradation product found in the ventricular extracts was not associated with MMP-2 by immunoprecipitation. Interestingly, Murphy et al[135] reported the presence of a 75 kDa putative JPH-1 fragment released into the incubation buffer from extensor digitorum longus muscles stimulated with caffeine in vitro. Similarly, this 75 kDa JPH-2 degradation product may diffuse from the ventricular extracts and into the wash buffer during immunoprecipitation. Alternatively, MMP-2 may not be bound to the JPH-2 fragment after proteolysis and this would not be detected by immunoprecipitation using an MMP-2 antibody.

I then tested the susceptibility of JPH-2 to proteolysis by MMP-2 by incubating the ventricular extracts from Aerobic hearts to increasing concentrations of MMP-2. MMP-2 not only

directly cleaved JPH-2, but it also further proteolyzed other putative JPH-2 degradation products. Cleavage prediction software identified multiple putative MMP-2 cleavage sites in JPH-2. Due to the differences in the theoretical and the apparent molecular weight in gel electrophoresis, I predicted the JPH-2 cleavage sites that would correspond to a 63 kDa degradation product by estimating its apparent molecular weights from the calculated molecular weights of the N-terminal and C-terminal products. Two cleavage sites, P1 at 350 and 372, resulted in degradation products with an apparent molecular weight of around 63 kDa (Table 4.2). These cleavage sites are localized between the MORN motifs and the α-helix region. JPH-2 has eight MORN motifs in the amino-terminal region which interact with phospholipids, particularly sphingomyelin and phosphatidylcholine in the plasma membrane[130]. Cleavage of the MORN motifs in JPH-2 would disrupt the dyadic junction between the plasma membrane and the sarcoplasmic reticulum. While the function of the divergent region remains unclear[132], its susceptibility to proteolysis by MMP-2 may vary across different isoforms. Most notably, no cleavage sites were predicted in the cytosolic α-helix domain and the sarcoplasmic reticulum transmembrane domain, both of which are highly structured regions that are likely inaccessible for proteolytic degradation.

This study adds to the growing repertoire of intracellular MMP-2 substrates and increases our understanding of the role of MMP-2 in ischemic heart disease. These data provide compelling evidence that MMP-2 contributes to JPH-2 proteolysis in the pathogenesis of myocardial IR injury. Given that importance of JPH-2 in calcium-induced calcium release and cardiac excitation-contraction coupling, inhibiting its proteolysis by MMP-2 may be protective in ischemic heart disease.

Table 4.1: Cardiac performance parameters at the end of perfusion for the four groups of isolated working rat hearts. *p<0.05 vs Aerobic, ‡p<0.05 vs IR by one-way ANOVA followed by Tukey's post hoc test.

End of perfusion (70 min)	**Aerobic (n=9)**	**Aerobic+ARP (n=5)**	**IR (n=11)**	**IR+ARP (n=9)**
Cardiac output (mL/min)	68.8±3.4	60.8±9.1	23.5±5.7*	46.1±3.1‡
Aortic flow (mL/min)	46.6±2.6	39.2±8.7	9.6±3.1*	24.9±3.3‡
Coronary flow (mL/min)	22.2±1.6	21.6±1.5	13.8±3.1	21.2±1.9
Heart rate (bpm)	276±7	258±15	123±31*	203±16
Peak systolic pressure (mmHg)	118±3	110±4	83±16	120±4
Cardiac work ($mmHg \cdot mL \cdot min^{-1} \cdot 10^{-3}$)	7.4±0.5	6.1±1.1	2.5±0.65*	5.0±0.4‡

Table 4.2: Top 10 positional weight matrix (PWM) score for MMP-2 cleavage sites within the cytoplasmic region of rat JPH-2 according to CleavPredict. The predicted cleavage sites were aligned with the active site specificity profiling dataset of MMP-2[281] to determine the percent homology to MMP-2 cleavage motifs. Cleavage sites P1 350 and 372 (in bold) were predicted to produce degradation products with a similar molecular weight observed in IR hearts by gel electrophoresis.

P1	Residues	PWM Score	N-mass (kDa)	C-mass (kDa)	P3-P3' (% homology)
165	LSS-LRS	7.24	17.9	56.3	50%
201	LSL-LAT	3.40	21.5	52.7	50%
213	PGL-FTR	4.50	22.6	51.6	50%
222	LGR-LRR	5.91	23.6	50.6	33%
241	LSF-LKS	6.78	25.8	48.4	50%
350	**VLP-LKS**	**5.07**	**37.6**	**36.6**	**67%**
372	**AAA-IAR**	**3.79**	**40.0**	**34.3**	**83%**
555	VAL-YRG	4.07	59.4	14.8	50%
594	PSP-VSA	4.94	63.7	10.5	83%
640	ARG-LSK	3.96	68.6	5.6	50%
				Average	**57%**

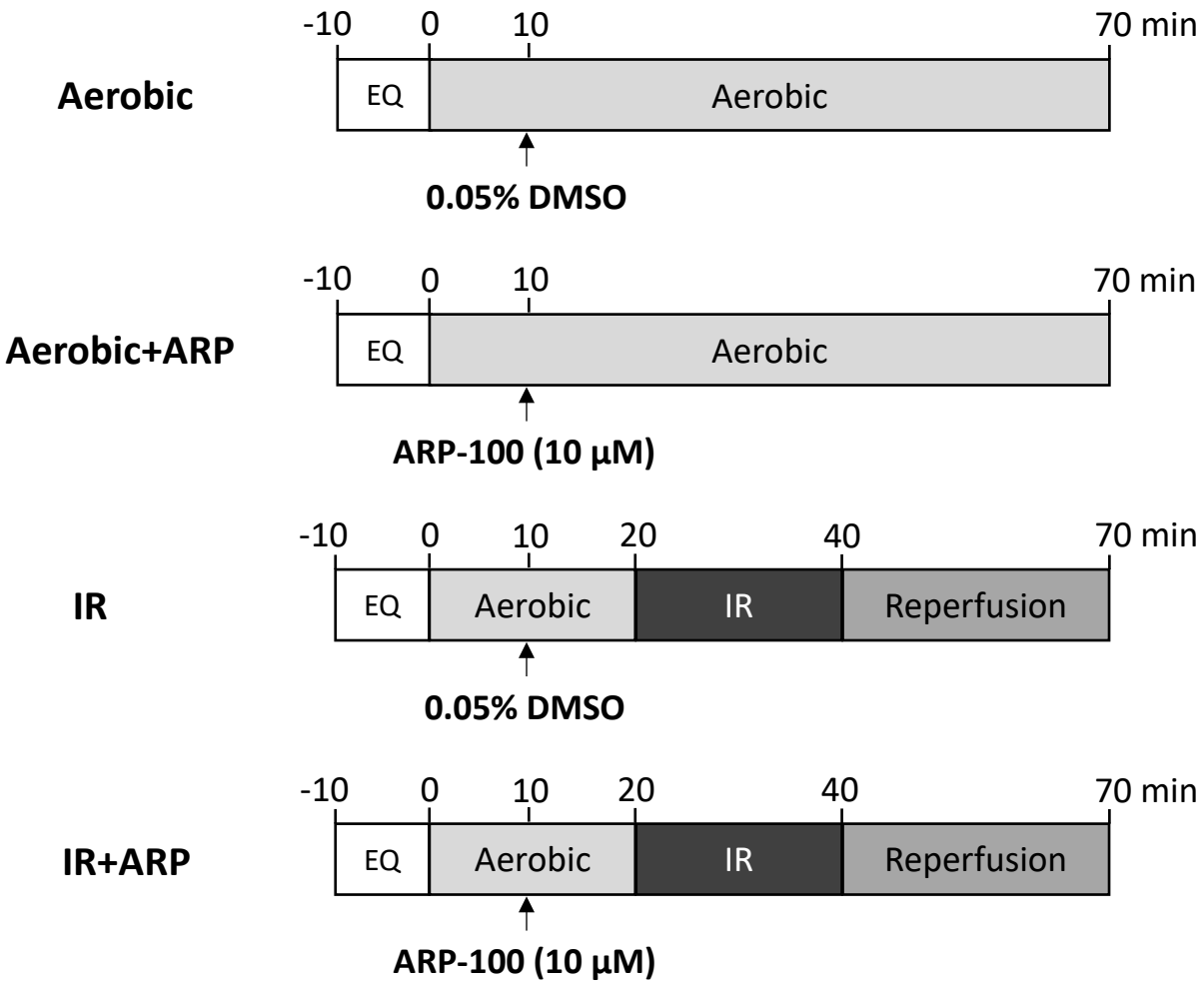

Figure 4.1: Schematic diagram of the working heart perfusion protocol in Aerobic, Aerobic+ARP, ischemic-reperfused (IR), and IR+ARP rat hearts. IR hearts were subject to 20 min global, no flow ischemia, followed by 30 min of aerobic reperfusion. 10 µM ARP-100 or 0.05% DMSO (vehicle) was added to the recirculating buffer 10 min into perfusion.

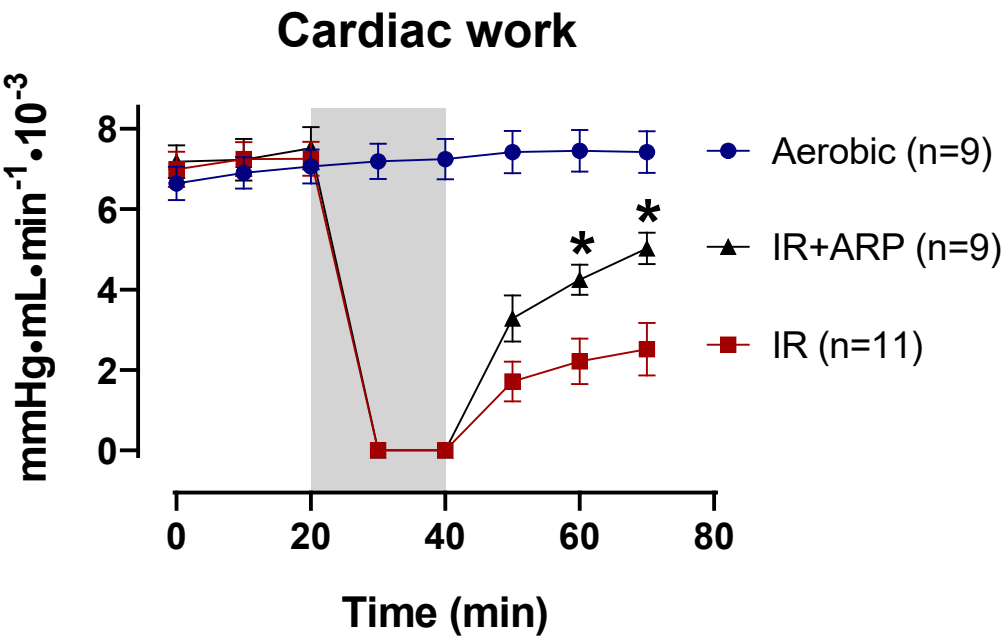

Figure 4.2: Cardiac contractile performance determined by cardiac work in IR hearts perfused with ARP-100. Cardiac work is the product of peak systolic pressure and cardiac output. IR hearts were subjected to 30 min global, no-flow ischemia (indicated by grey box) followed by 30 min reperfusion in the presence or absence of ARP-100 (10 μM). ARP-100 significantly improved the recovery of cardiac work compared to IR hearts at the end of reperfusion. *$p<0.05$ vs IR by two-way ANOVA followed by Tukey's post hoc test. Hearts were perfused by Andrej Roczkowsky.

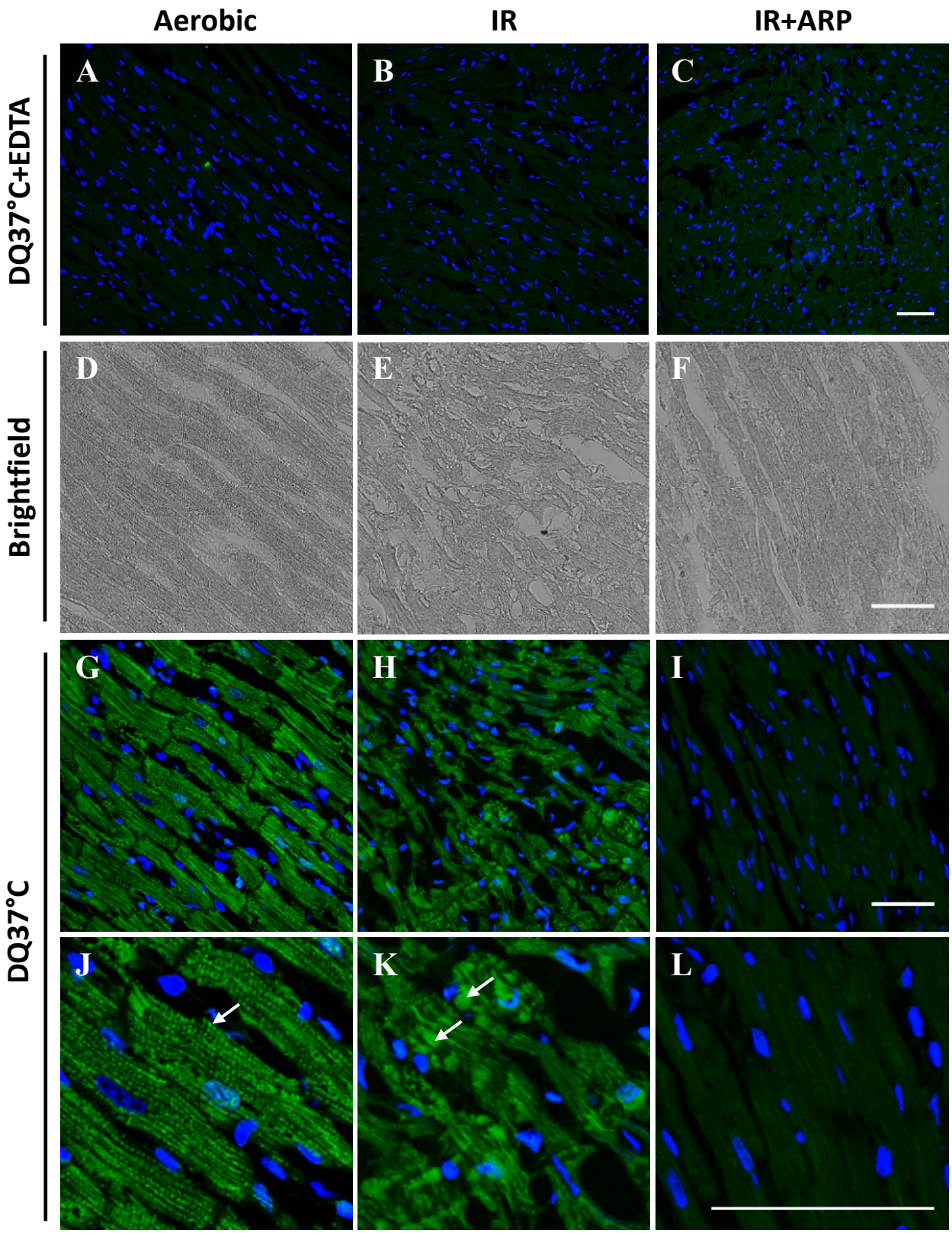
Aerobic
IR
IR+ARP
DQ37°C+EDTA
Brightfield
DQ37°C
A
B
C
D
E
F
G
H
I
J
K
L

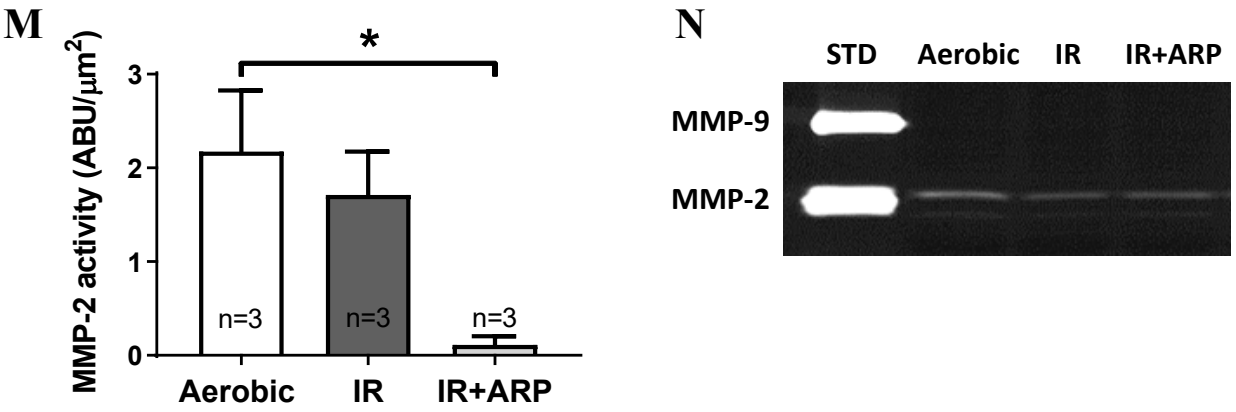

Figure 4.3: IR injury causes a redistribution of myocardial MMP-2 activity in situ. (A-C) Representative in situ zymography images show that MMP activity from ventricular sections incubated with DQ gelatin was blocked with a pan-MMP inhibitor EDTA (20 mM). (D-F) Brightfield images revealed that IR hearts exhibited abnormal myofibrillar morphology compared to Aerobic and IR+ARP hearts. (G-I) In situ zymography localized MMP-2 gelatinolytic activity within cardiomyocytes in Aerobic and IR hearts, which was attenuated in IR+ARP hearts. (J-L) Higher magnification revealed that MMP-2 activity exhibited a striated pattern (arrows) in Aerobic hearts, whereas MMP-2 activity appeared redistributed and clustered in IR hearts. Scale bar = 50 μm. (M) Myocardial MMP-2 activity normalized to tissue area (μm^2) by in situ zymography was quantified. *$p<0.05$ by one-way ANOVA followed by Tukey's post hoc test. Bar graphs represent mean ± S.E.M. (N) Gelatin zymography detected 72 kDa MMP-2, but no MMP-9 activity in the ventricular extracts. STD: HT-1080 cell conditioned medium.

A

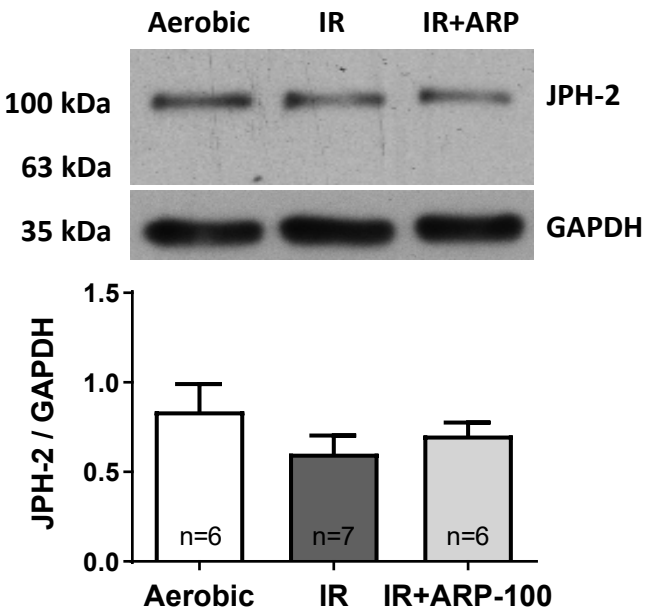

B

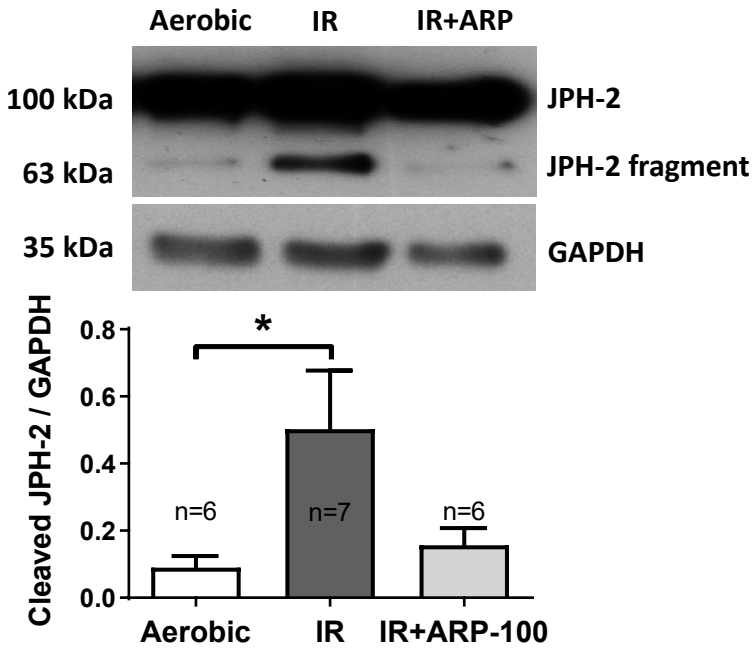

Figure 4.4: Levels of JPH-2 and its degradation product in ventricular extracts from isolated rat hearts. (A) JPH-2 protein levels were unchanged between Aerobic, IR, and IR+ARP hearts. (B) IR hearts exhibited a significant increase in a 63 kDa JPH-2 degradation product, an effect that was prevented by ARP-100. *$p<0.05$ by one way ANOVA followed by Tukey's post hoc test. Bar graphs represent mean ± S.E.M.

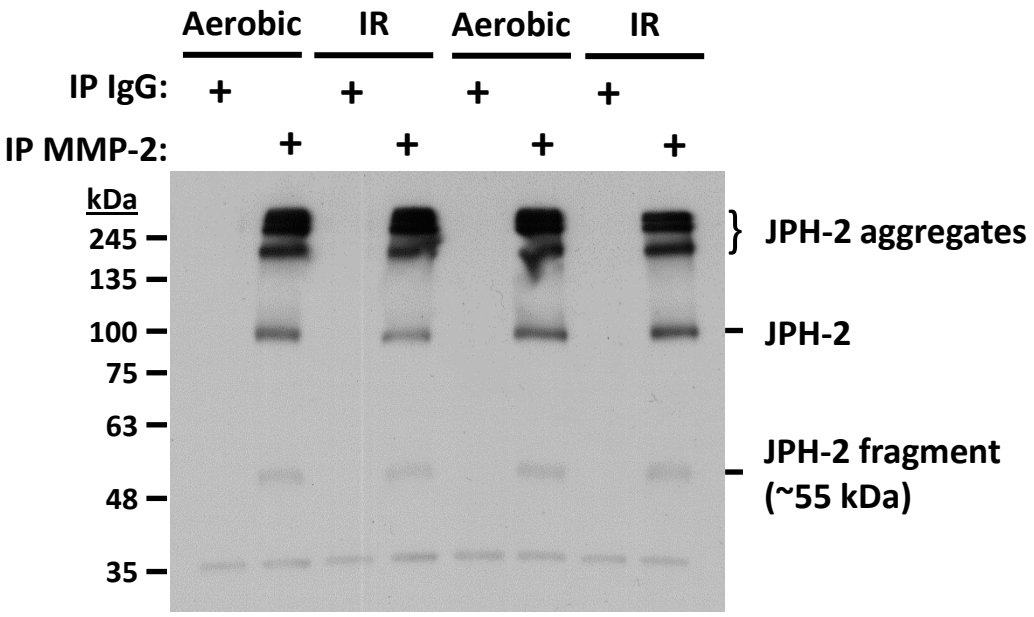

Figure 4.5: MMP-2 binds to JPH-2 in the heart. A JPH-2 immunoblot on MMP-2 immunoprecipitates from Aerobic and IR hearts revealed that MMP-2 is bound to JPH-2 aggregates, JPH-2 monomer, and a putative JPH-2 degradation product. Representative of three independent experiments.

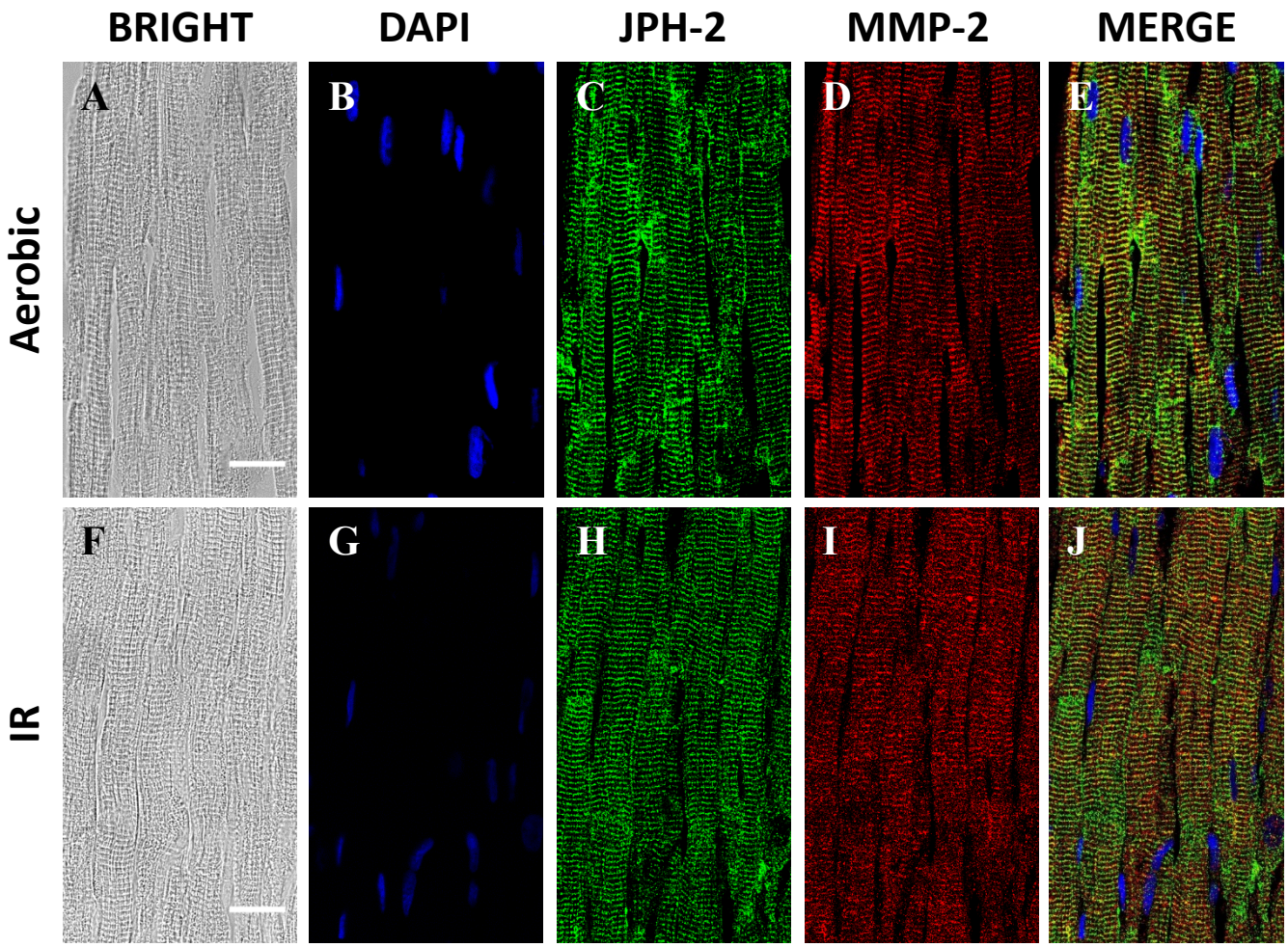

Figure 4.6: MMP-2 is co-localized to JPH-2 in Aerobic and IR rat hearts. (A,F) Representative brightfield images of left ventricular tissue from Aerobic and IR rat hearts. Left ventricular tissue sections from Aerobic and IR rat hearts were stained with (B,G) DAPI, (C,H) an anti-JPH-2 antibody, and an (D,I) anti-MMP-2 antibody. (E,J) Representative merged images of MMP-2, JPH-2, and DAPI in Aerobic and IR rat hearts (co-localization seen as yellow). Scale bar = 20 µm.

A

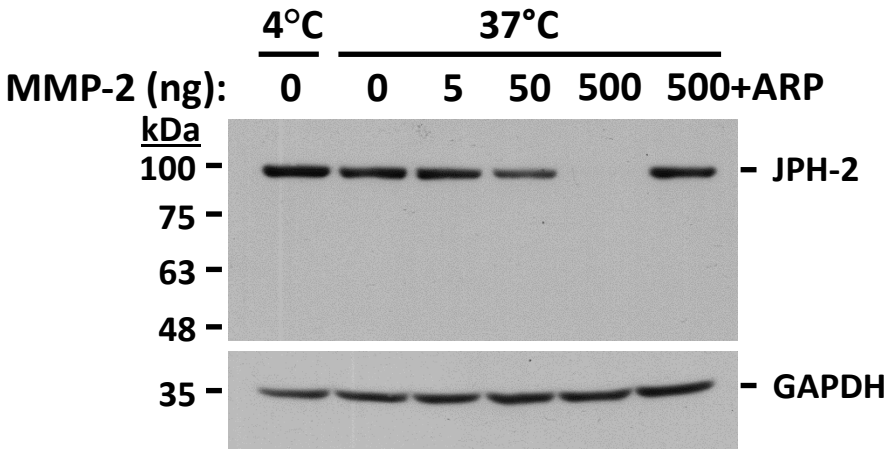

B

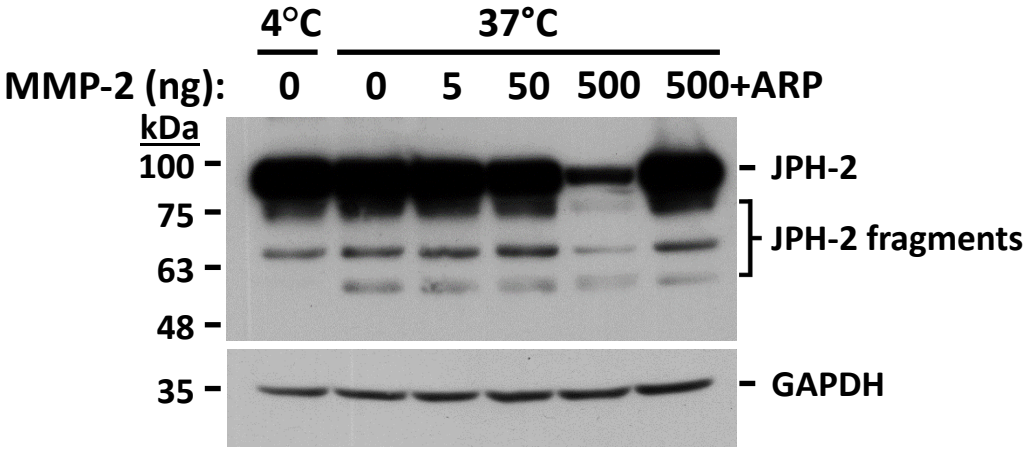

Figure 4.7: JPH-2 is susceptible to proteolysis by MMP-2. (A) A JPH-2 immunoblot of ventricular extracts (20 µg) from an Aerobic heart following incubation with MMP-2 (5-500 ng) for 30 min at 37°C. MMP-2 cleaves JPH-2 in a concentration-dependent manner, which is prevented with ARP-100 (ARP). (B) Increased exposure of the JPH-2 immunoblot revealed the presence of lower molecular weight JPH-2 degradation products (75, 65, and 55 kDa). Position of molecular weight markers shown on left. Representative of three independent experiments.

CHAPTER 5

CONCLUSIONS

5.1 General conclusions

Ischemic heart disease and cancer are the two leading causes of mortality worldwide[150, 283]. An estimated 27.5 million people die each year from either cardiovascular disease or cancer, each accounting for 31% and 16% of global mortality, respectively[284, 285]. The global economic burden of cardiovascular disease and cancer is increasingly taxing, costing nearly a combined $2 trillion each year[285, 286]. Cancer and the heart were once thought to be almost mutually exclusive research topics due to the extremely rare occurrence of heart cancers. However, cancer and its treatment can affect the heart in other ways. Many anticancer drugs possess side-effects which damage the heart. This often goes undetected during treatment and does not become apparent until years after treatment. Unfortunately many cancer patients end up as cardiology patients. In order to develop more effective therapies to protect the heart, a better understanding of the mechanisms of heart disease is needed.

MMPs have become an important target in heart disease and cancer given their active roles in remodeling the extracellular matrix in a multitude of pathophysiological processes. In recent years, the discovery of intracellular MMPs and their substrates demonstrated that MMPs are not limited to long-term processes but can also have cellular functions on a time scale of seconds to minutes. As such, this thesis examined the role of MMP-2 and the effect of pharmacological MMP inhibitors in acute ischemic heart injury and chronic anthracycline cardiotoxicity.

In Chapter 2, I provided at least two mechanisms by which anthracyclines activate intracellular MMP-2 in cardiomyocytes. First, DXR increased oxidative stress and both the levels and activity of 72 kDa MMP-2 in cardiomyocytes. Previous studies have shown that approximately

half of nascent MMP-2 remains intracellular due to the inefficient targeting of the signal peptide for secretion[17]. Intracellular 72 kDa MMP-2 activity can be enhanced by oxidative stress via its S-glutathiolation[39]. Second, DXR also enhanced the expression of NTT-MMP-2, which is an active protease. This chapter determined that approximately 90% of the MMP-2 transcripts encode NTT-MMP-2 in NRVM. It remains unknown why NTT-MMP-2 is expressed under physiological conditions. However, it is known that isolated cardiomyocytes are under low levels of oxidative stress which regulates the release of intracellular calcium and the force of contraction[287, 288]. It is possible that the low levels of RONS under basal conditions of cell culture are sufficient to trigger the expression of NTT-MMP-2 in cardiomyocytes. The mitochondria and MAM are significant subcellular organelles where NTT-MMP-2 and 72 kDa MMP-2 are found[18, 95]. Interestingly, this study showed that DXR caused MMP-2 to redistribute from the mitochondria to the cytosol and was accompanied by the concomitant increased release of MMP-2 into the culture medium. The secretion of MMP-2 may be a protective mechanism to diminish enhanced MMP-2 activity inside cardiomyocytes[192].

Titin, the molecular spring of the sarcomere, was first identified as a target of MMP-2 in acute myocardial IR injury[63]. Inhibition of MMP-2 activity prevented titin degradation and subsequently improved the recovery of cardiac contractile function during reperfusion[63]. Chapter 3 examined the role of MMP-2 in intracellular and extracellular matrix remodeling in anthracycline cardiotoxicity. In accordance with the findings in Chapter 2, DXR increased NTT-*Mmp2* mRNA expression and increased MMP-2 levels in the heart. DXR increased the localization of intracellular MMP-2 to specific regions of the sarcomere including the Z-disc and M-line. DXR-induced MMP-2 activity was associated with myofilament lysis and titin proteolysis. More importantly, inhibition of MMP-2 activity by ONO-4817 ameliorated DXR-induced cardiac

contractile dysfunction by preventing titin proteolysis.

I also demonstrated that Doxy, the only clinically approved MMP-2 inhibiting drug, prevented DXR-induced cardiac remodeling. DXR-induced cardiac remodeling is attributed, in part, to increased interstitial fibrosis, an effect that was prevented by Doxy and ONO-4817. This is consistent with the findings from the TIPTOP trial which showed that Doxy reduced adverse ventricular remodeling and improved left ventricular ejection fraction in ST-elevation myocardial infarction patients[73]. A recent clinical trial showed that heart failure pharmacotherapy with ACE inhibitors and β-blockers did not abate chemotherapy-induced left ventricular remodeling[186]. This chapter highlights the protective effects of MMP inhibitors against DXR-induced cardiac remodeling. Perhaps ACE inhibitors and β-blockers should be supplemented with MMP inhibitors such as Doxy to ameliorate DXR-induced cardiac contractile dysfunction and long-term left ventricular remodeling.

It is also important to note that first generation broad spectrum MMP inhibitors such as batimastat and marimastat showed excellent anticancer efficacy from preclinical studies and went into clinical trials. However, off-target effects including inhibition of non-MMPs and MMP-1 caused undesirable side effects including musculoskeletal pain[58-60]. Some believe that MMP inhibitors which are more selective for on-target effects and avoid off-target effects would achieve great therapeutic efficacy in cancer chemotherapy[61]. It may be that the same MMP inhibitor properties used for chemotherapy would also be cardioprotective. Since then, many selective MMP inhibitors have been developed and Doxy was found to have good MMP-2 inhibitory properties and poor affinity to MMP-1. MMP inhibitors as an adjuvant therapy should be considered not only to protect the heart from chemotherapy cardiotoxicity, but may also enhance the efficacy of anticancer drugs.

Given that MMP-2 and JPH-2 are both localized to the Z-disc region of the sarcomere, Chapter 4 investigated JPH-2 as a novel target of MMP-2 in IR injury. Using the techniques of immunohistochemistry and immunoprecipitation, I found discrete co-localization between MMP-2 and JPH-2 in the Z-disc region of the sarcomere in cardiomyocytes of isolated rat heart ventricular tissue. JPH-2 in ventricular extracts was susceptible to proteolysis when incubated with MMP-2 in a concentration-dependent manner, an effect that was prevented with MMP inhibition. Isolated rat hearts subject to IR injury exhibited impaired myocardial contractility associated with increased JPH-2 degradation. Inhibition of MMP activity with ONO-4817 attenuated IR-induced JPH-2 degradation and improved the recovery of cardiac contractile function. Previous studies have conclusively demonstrated that MMP-2 is localized to the cardiac sarcomere and proteolyzes specific myofilament proteins upon its activation during IR injury[63, 84, 85]. In corroboration with those studies, MMP-2 dependent JPH-2 proteolysis may provide a link between myofilament lysis and impaired calcium handling in IR-induced cardiac contractile dysfunction. In addition, MMP-2 dependent JPH-2 proteolysis may also be implicated in ischemic, dilated, and hypertrophic cardiomyopathies which are associated with loss of JPH-2 and T-tubule damage[145].

5.2 Limitations

My thesis presents novel findings which open doors not only in the field of MMP biology and cardiovascular research, but also in the emerging field of cardio-oncology. However, each investigation should be subject to critical analysis of the limitations associated with my experimental approach. This evaluation is essential to avoid misinterpretation of data while identifying areas of improvement for future studies.

5.2.1 Limitations of Chapter 2

In Chapter 2, I demonstrated that MMP-2 activation is an early event in DXR-treated NRVM. MMP-2 activity from cell lysates and conditioned media was assessed by gelatin zymography. Although this technique is highly sensitive to detect MMP-2 and reproducible, its use comes with several limitations. Tissue/cell homogenization and gelatin zymography separates MMPs from their endogenous protein inhibitor complexes with TIMPs. Furthermore, the latent forms of MMP-2 and MMP-9 are chemically activated by gelatin zymography. The results of gelatin zymography may be more reflective of protein levels than activity. Although kinetic MMP assays based on the use of fluorogenic substrates are available, they do not differentiate MMP-2 from MMP-9 activity. The main objective of this study was to identify whether MMP-2 activation is an early event in DXR-induced cardiomyocyte injury and which of its subtypes are involved. Thus, gelatin zymography was used to assess MMP-2 activity. To address this limitation, the Schulz lab is currently developing Förster resonance energy transfer[289] based MMP-2 biosensors which will enable the measurement of intracellular MMP-2 activity in live cells.

Neonatal rat ventricular myocytes were the primary cells used to determine the effect of DXR on MMP-2 expression and activity. To understand mechanisms related to anthracycline cardiotoxicity in adults, it would be preferable to study cardiomyocytes isolated from adult animals. However, they are more unstable than NRVM in culture and their sarcomeric integrity is compromised over time while in culture. Of most significance, previous studies in our lab have found that the rigorous digestive process in isolating adult myocytes depletes the cells, at least temporarily, of MMP-2. This would compromise the ability to detect cellular changes in MMP-2, leaving neonatal myocytes as the primary option, which are superior to immortalized cardiac muscle cell lines (HL-1 and H9C2). Despite NRVM being more robust in culture and showing

spontaneous contractile activity, they are immature cells which exhibit disorganized myofibrils[290] and express both slow skeletal and cardiac troponin I isoforms[291, 292]. Whether MMP-2 localizes to the thin myofilaments of NRVM and is able to proteolyze slow skeletal troponin I or other sarcomeric proteins remains unclear.

5.2.2 Limitations of Chapter 3

In Chapter 3, young adult male mice were treated with DXR with or without two orally available MMP inhibitors to evaluate the cardioprotective effects of MMP inhibition against anthracycline-induced cardiotoxicity. Although this model of anthracycline-induced cardiotoxicity is well established, it does not fully emulate what is observed clinically. First, cancer patients treated with anthracyclines typically develop dilated cardiomyopathy as a result of the cardiotoxic side effects of anthracycline treatment. In mice treated with anthracyclines, the hearts do not become hypertrophic and dilated. Instead, the size of the myocardium becomes much smaller compared to control. Some studies were designed to include the administration of angiotensin II after the termination of anthracycline treatment to trigger a hypertrophic phenotype. Note that angiotensin II is an important trigger of increased MMP-2 expression in cells[293]. Given my findings on the effect of MMP inhibition on DXR-induced interstitial fibrosis in the heart, this would be of significant interest to investigate. The relationship between cancer and cachexia is well documented[294]. Cancer causes additional stress to the heart that can result in cardiac and skeletal muscle wasting[295]. This condition is not replicated in healthy mice. Without the use of tumor-bearing mice, I cannot fully evaluate the cardioprotective effects of MMP inhibitors on the heart nor would I be able to determine the potential anti-tumor effects of selective MMP inhibitors.

Immunoblot was performed to estimate the levels of specific proteins including MMP-2. However, like many techniques, immunoblot relies on the use of antibodies and interpretation of

data depends on the specificity of primary and secondary antibodies. In this study, two MMP-2 isoforms were detected by qPCR whereas only one isoform, 72 kDa MMP-2, was detected by immunoblot. However, not all mRNA transcripts are translated to protein. Therefore, observations by qPCR do not always reflect protein levels. It is also possible that the anti-MMP-2 antibody used has a greater affinity for the 72 kDa MMP-2 isoform over the NTT-MMP-2 isoform. This may explain the discrepancy between my observations from qPCR and immunoblot experiments.

5.2.3 Limitations of Chapter 4

In Chapter 4, hearts isolated from young adult male rat were perfused ex vivo in working mode and subject to global, no flow ischemia to investigate the role of MMP-2 in myocardial IR injury. This technique is useful for assessing the acute effects of pharmacological interventions on cardiac contractile function. Despite its advantages, this method has its limitations. The isolated working rat heart lacks neurohormonal regulation, which may result in observations different than those observed in vivo. Perfusion of the isolated heart with a crystalloid buffer only partially substitutes the ionic and energy substrate content of blood, but does not replace all components of blood. Lastly, global, no-flow ischemia is a simplification of myocardial IR injury. Decreased blood flow in the heart usually takes place in a sub-region of the coronary arteries as a result of the formation of a thrombus, resulting in a focal injury. In acute coronary syndrome, only focal regions of the myocardium become ischemic which vary in degree of injury ranging from reversible to irreversible (cell death) injury[188].

There are limitations with the degradation assay used to assess the susceptibility of JPH-2 to proteolysis in vitro. Typically, an in vitro degradation assay consists of incubating a purified recombinant protein in the presence of a protease. However, recombinant full-length JPH-2 is not commercially available. To test the susceptibility of JPH-2 to proteolysis by MMP-2, ventricular

extracts were incubated with MMP-2 and an immunoblot with an anti-JPH-2 antibody was performed to detect degradation products. Only products recognized by the JPH-2 antibody would be detected. This approach also makes it difficult to perform mass spectrometry to fully map MMP-2 cleavage sites in JPH-2 given the plethora of proteins in ventricular extracts. It is also possible that other proteases in ventricular extracts proteolyze JPH-2 and/or may be proteolytically activated by MMP-2. However, I was able to determine that JPH-2 proteolysis is abolished by the MMP-2 preferring inhibitor ARP-100, which does not possess calpain inhibitory activity[97].

Loss of JPH-2 reduces myocardial contractility by disrupting calcium-induced calcium release. My study investigated the relationship between MMP-dependent JPH-2 proteolysis and cardiac contractile function. Future studies determining the effect of MMP inhibitors on IR injury induced change in calcium-induced calcium release are warranted.

5.3 Future directions

One of my recent preliminary studies details the loss of JPH-2 protein in DXR-treated NRVM (see Appendix). This study was inspired by my findings in isolated rat hearts whereby JPH-2 was identified as a putative target of MMP-2 in IR injury. Impaired intracellular calcium handling has been characterized in DXR-induced cardiotoxicity. Consistent with my findings, this was commonly attributed to reduced levels of SERCA2a and phospholamban[296]. However, alterations in JPH-2 have not yet been implicated in DXR-induced cardiotoxicity. Interestingly, MMP inhibitors attenuated the loss of JPH-2 caused by DXR. This result suggests that JPH-2 is degraded in an MMP-dependent manner in DXR-treated NRVM. Decreased amplitude and frequency of calcium transients have been reported in DXR-treated isolated cardiomyocytes[173, 234]. It would be of significant interest to determine whether MMP inhibitors ameliorate DXR-induced

depressed calcium transients in NRVM.

My discovery that titin, the molecular spring of the sarcomere, being a target of MMP-2 in DXR-induced cardiotoxicity in vivo is an exciting discovery that opens many avenues for future investigation. Titin is a major determinant of systolic and diastolic function in the heart. Degradation of titin would have significant effects on the compliance of the myocardium. While echocardiography can only identify differences in baseline cardiac function between groups, I predict the differences between DXR and control mice would be even greater if the hearts were stressed. This would reveal the effect of DXR on the compliance of the myocardium. This could be achieved by performing pressure volume analysis, which measures the elastance of the left ventricle by determining the end-diastolic and end-systolic pressure-volume relationship. To clearly elucidate the role of MMP-2 in anthracycline cardiotoxicity, transgenic mice with cardiac-specific overexpression of 72 kDa MMP-2[230, 246] or NTT-MMP-2[231, 246], and MMP-2 knockout mice should be used. Of greater clinical significance, cardioprotection by MMP inhibitors should be evaluated in DXR treated tumor-bearing mice. This would determine whether inhibition of MMP-2 has additional anti-tumor efficacy in conjunction to anthracyclines while protecting against its cardiotoxic side effects.

Finally, identifying JPH-2 as a novel target of MMP-2 in IR injury provides new insights to the pathophysiological role of MMP-2 in myocardial oxidative stress injury. The investigation on the role of MMP-2 in JPH-2 proteolysis need to be extrapolated in an in vivo model of IR injury. This could be performed by subjecting MMP-2 knockout mice or cardiac-specific 72 kDa MMP-2 transgenic mice[230, 246] to left anterior descending coronary artery ligation. Further investigation is required to delineate the consequences of MMP-2 mediated JPH-2 proteolysis and cardiac contractile dysfunction in IR injury. Ultrastructural examination by immunogold electron

microscopy would reveal whether MMP-2 is localized to damaged T-tubules in IR hearts. The effect of JPH-2 proteolysis on calcium-induced calcium release could be investigated by measuring calcium transients in isolated adult myocytes from the hearts of these mice. These future directions would reveal the role of MMP-2 on impaired intracellular calcium homeostasis in myocardial IR injury.

5.4 Final words

In light of the studies in my thesis, I have shown that activation of MMP-2 plays an important role in the initiation and propagation of acute and chronic oxidative stress injury to the heart. Identification of other novel intracellular and extracellular substrates of MMP-2 will help us better understand its pathophysiological role in the mechanisms which underlie a gamut of heart diseases. Finally, this thesis highlights the protective mechanisms of pharmacological MMP inhibition against myocardial oxidative stress injury. Prophylactic use of orally available MMP inhibitors may be a potential therapeutic strategy to prevent heart injury/disease in patients.

REFERENCES

1. Gross J and Lapiere CM. Collagenolytic activity in amphibian tissues: a tissue culture assay. *Proc Natl Acad Sci USA*. 1962;48:1014-22.

2. Bornstein P, Kang AH and Piez KA. The limited cleavage of native collagen with chymotrypsin, trypsin, and cyanogen bromide. *Biochemistry*. 1966;5:3803-12.

3. Goldberg GI, Wilhelm SM, Kronberger A, Bauer EA, Grant GA and Eisen AZ. Human fibroblast collagenase. Complete primary structure and homology to an oncogene transformation-induced rat protein. *J Biol Chem*. 1986;261:6600-5.

4. Page-McCaw A, Ewald AJ and Werb Z. Matrix metalloproteinases and the regulation of tissue remodelling. *Nat Rev Mol Cell Biol*. 2007;8:221-33.

5. Liotta LA, Abe S, Robey PG and Martin GR. Preferential digestion of basement membrane collagen by an enzyme derived from a metastatic murine tumor. *Proc Natl Acad Sci USA*. 1979;76:2268-72.

6. Collier IE, Wilhelm SM, Eisen AZ, Marmer BL, Grant GA, Seltzer JL, Kronberger A, He CS, Bauer EA and Goldberg GI. H-ras oncogene-transformed human bronchial epithelial cells (TBE-1) secrete a single metalloprotease capable of degrading basement membrane collagen. *J Biol Chem*. 1988;263:6579-87.

7. Okada Y, Morodomi T, Enghild JJ, Suzuki K, Yasui A, Nakanishi I, Salvesen G and Nagase H. Matrix metalloproteinase 2 from human rheumatoid synovial fibroblasts. Purification and activation of the precursor and enzymic properties. *Eur J Biochem*. 1990;194:721-30.

8. Schulz R. Intracellular targets of matrix metalloproteinase-2 in cardiac disease: rationale and therapeutic approaches. *Annu Rev Pharmacol Toxicol*. 2007;47:211-42.

9. Spinale FG. Myocardial matrix remodeling and the matrix metalloproteinases: influence on cardiac form and function. *Physiol Rev*. 2007;87:1285-342.

10. McCawley LJ and Matrisian LM. Matrix metalloproteinases: they're not just for matrix anymore! *Curr Opin Cell Biol*. 2001;13:534-40.

11. Cauwe B and Opdenakker G. Intracellular substrate cleavage: a novel dimension in the biochemistry, biology and pathology of matrix metalloproteinases. *Crit Rev Biochem Mol Biol*. 2010;45:351-423.

12. Iyer RP, Patterson NL, Fields GB and Lindsey ML. The history of matrix metalloproteinases: milestones, myths, and misperceptions. *Am J Physiol Heart Circ Physiol*. 2012;303:H919-30.

13. Hidalgo M and Eckhardt SG. Development of matrix metalloproteinase inhibitors in cancer therapy. *J Natl Cancer Inst*. 2001;93:178-93.

14. Kleiner DE and Stetler-Stevenson WG. Matrix metalloproteinases and metastasis. *Cancer Chemother Pharmacol*. 1999;43 Suppl:S42-51.

15. Morgunova E, Tuuttila A, Bergmann U, Isupov M, Lindqvist Y, Schneider G and Tryggvason K. Structure of human pro-matrix metalloproteinase-2: activation mechanism revealed. *Science*. 1999;284:1667-70.

16. Tallant C, Marrero A and Gomis-Ruth FX. Matrix metalloproteinases: fold and function of their catalytic domains. *Biochim Biophys Acta*. 2010;1803:20-8.

17. Ali MA, Chow AK, Kandasamy AD, Fan X, West LJ, Crawford BD, Simmen T and Schulz R. Mechanisms of cytosolic targeting of matrix metalloproteinase-2. *J Cell Physiol*. 2012;227:3397-404.

18. Lovett DH, Mahimkar R, Raffai RL, Cape L, Maklashina E, Cecchini G and Karliner JS. A novel intracellular isoform of matrix metalloproteinase-2 induced by oxidative stress activates innate immunity. *PLoS One*. 2012;7:e34177.

19. Chakraborti S, Mandal M, Das S, Mandal A and Chakraborti T. Regulation of matrix metalloproteinases: an overview. *Mol Cell Biochem*. 2003;253:269-85.

20. Bergman MR, Cheng S, Honbo N, Piacentini L, Karliner JS and Lovett DH. A functional activating protein 1 (AP-1) site regulates matrix metalloproteinase 2 (MMP-2) transcription by cardiac cells through interactions with JunB-Fra1 and JunB-FosB heterodimers. *Biochem J*. 2003;369:485-96.

21. Alfonso-Jaume MA, Bergman MR, Mahimkar R, Cheng S, Jin ZQ, Karliner JS and Lovett DH. Cardiac ischemia-reperfusion injury induces matrix metalloproteinase-2 expression through the AP-1 components FosB and JunB. *Am J Physiol Heart Circ Physiol*. 2006;291:H1838-46.

22. Qin H, Sun Y and Benveniste EN. The transcription factors Sp1, Sp3, and AP-2 are required for constitutive matrix metalloproteinase-2 gene expression in astroglioma cells. *J Biol Chem*. 1999;274:29130-7.

23. Harendza S, Lovett DH and Stahl RA. The hematopoietic transcription factor PU.1 represses gelatinase A transcription in glomerular mesangial cells. *J Biol Chem*. 2000;275:19552-9.

24. Matsumoto K, Abiko S and Ariga H. Transcription regulatory complex including YB-1 controls expression of mouse matrix metalloproteinase-2 gene in NIH3T3 cells. *Biol Pharm Bull*. 2005;28:1500-4.

25. Bian J and Sun Y. Transcriptional activation by p53 of the human type IV collagenase (gelatinase A or matrix metalloproteinase 2) promoter. *Mol Cell Biol*. 1997;17:6330-8.

26. Xie TX, Wei D, Liu M, Gao AC, Ali-Osman F, Sawaya R and Huang S. Stat3 activation regulates the expression of matrix metalloproteinase-2 and tumor invasion and metastasis. *Oncogene*. 2004;23:3550-60.

27. Felx M, Guyot MC, Isler M, Turcotte RE, Doyon J, Khatib AM, Leclerc S, Moreau A and Moldovan F. Endothelin-1 (ET-1) promotes MMP-2 and MMP-9 induction involving the transcription factor NF-κB in human osteosarcoma. *Clinical Sci*. 2006;110:645-54.

28. Galis ZS, Muszynski M, Sukhova GK, Simon-Morrissey E and Libby P. Enhanced expression of vascular matrix metalloproteinases induced in vitro by cytokines and in regions of human atherosclerotic lesions. *Ann N Y Acad Sci*. 1995;748:501-7.

29. Grandas OH, Mountain DH, Kirkpatrick SS, Cassada DC, Stevens SL, Freeman MB and Goldman MH. Regulation of vascular smooth muscle cell expression and function of matrix metalloproteinases is mediated by estrogen and progesterone exposure. *J Vasc Surg*. 2009;49:185-91.

30. Goldman S, Lovett DH and Shalev E. Mechanisms of matrix metalloproteinase-2 (mmp-2) transcriptional repression by progesterone in jar choriocarcinoma cells. *Reprod Biol Endocrinol*. 2009;7:41.

31. Hu SI, Klein M, Carozza M, Rediske J, Peppard J and Qi JS. Identification of a splice variant of neutrophil collagenase (MMP-8). *FEBS Lett*. 1999;443:8-10.

32. Tardif G, Dupuis M, Reboul P, Geng CS, Pelletier JP, Ranger P and Martel-Pelletier J. Identification and differential expression of human collagenase-3 mRNA species derived from internal deletion, alternative splicing, and different polyadenylation and transcription initiation sites. *Osteoarthr Cartil*. 2003;11:524-37.

33. Matsumoto S, Katoh M, Saito S, Watanabe T and Masuho Y. Identification of soluble type of membrane-type matrix metalloproteinase-3 formed by alternatively spliced mRNA. *Biochim Biophys Acta*. 1997;1354:159-70.

34. Ross HH and Fillmore HL. Identification of a novel human MT5-MMP transcript variant in multipotent NT2 cells. *FEBS Lett*. 2007;581:5923-8.

35. Strongin AY, Collier I, Bannikov G, Marmer BL, Grant GA and Goldberg GI. Mechanism of cell surface activation of 72-kDa type IV collagenase. Isolation of the activated form of the membrane metalloprotease. *J Biol Chem*. 1995;270:5331-8.

36. Nishida Y, Miyamori H, Thompson EW, Takino T, Endo Y and Sato H. Activation of matrix metalloproteinase-2 (MMP-2) by membrane type 1 matrix metalloproteinase through an artificial receptor for proMMP-2 generates active MMP-2. *Cancer Res*. 2008;68:9096-104.

37. Okamoto T, Akaike T, Nagano T, Miyajima S, Suga M, Ando M, Ichimori K and Maeda H. Activation of human neutrophil procollagenase by nitrogen dioxide and peroxynitrite: a novel mechanism for procollagenase activation involving nitric oxide. *Arch Biochem Biophys*. 1997;342:261-74.

38. Okamoto T, Akaike T, Sawa T, Miyamoto Y, van der Vliet A and Maeda H. Activation of matrix metalloproteinases by peroxynitrite-induced protein S-glutathiolation via disulfide S-oxide formation. *J Biol Chem*. 2001;276:29596-602.

39. Viappiani S, Nicolescu AC, Holt A, Sawicki G, Crawford BD, Leon H, van Mulligen T and Schulz R. Activation and modulation of 72 kDa matrix metalloproteinase-2 by peroxynitrite and glutathione. *Biochem Pharmacol*. 2009;77:826-34.

40. Sariahmetoglu M, Crawford BD, Leon H, Sawicka J, Li L, Ballermann BJ, Holmes C, Berthiaume LG, Holt A, Sawicki G and Schulz R. Regulation of matrix metalloproteinase-2 (MMP-2) activity by phosphorylation. *Faseb J*. 2007;21:2486-95.

41. Filipiak K, Kubinski K, Hellman U, Ramos A and de Pascual-Teresa B. Human protein kinase CK2 phosphorylates matrix metalloproteinase 2 and inhibits its activity. *Chembiochem*. 2014;15:1873-6.

42. Sariahmetoglu M, Skrzypiec-Spring M, Youssef N, Jacob-Ferreira AL, Sawicka J, Holmes C, Sawicki G and Schulz R. Phosphorylation status of matrix metalloproteinase 2 in myocardial ischaemia-reperfusion injury. *Heart*. 2012;98:656-62.

43. Koo BH, Kim YH, Han JH and Kim DS. Dimerization of matrix metalloproteinase-2 (MMP-2): functional implication in MMP-2 activation. *J Biol Chem*. 2012;287:22643-53.

44. Williamson RA, Marston FA, Angal S, Koklitis P, Panico M, Morris HR, Carne AF, Smith BJ, Harris TJ and Freedman RB. Disulphide bond assignment in human tissue inhibitor of metalloproteinases (TIMP). *Biochem J*. 1990;268:267-74.

45. Brew K, Dinakarpandian D and Nagase H. Tissue inhibitors of metalloproteinases: evolution, structure and function. *Biochim Biophys Acta*. 2000;1477:267-83.

46. Baker AH, Edwards DR and Murphy G. Metalloproteinase inhibitors: biological actions and therapeutic opportunities. *J Cell Sci*. 2002;115:3719-27.

47. Chua CC, Hamdy RC and Chua BH. Angiotensin II induces TIMP-1 production in rat heart endothelial cells. *Biochim Biophys Acta*. 1996;1311:175-80.

48. Li YY, McTiernan CF and Feldman AM. Proinflammatory cytokines regulate tissue inhibitors of metalloproteinases and disintegrin metalloproteinase in cardiac cells. *Cardiovasc Res*. 1999;42:162-72.

49. Yu WH, Yu S, Meng Q, Brew K and Woessner JF, Jr. TIMP-3 binds to sulfated glycosaminoglycans of the extracellular matrix. *J Biol Chem*. 2000;275:31226-32.

50. Fedak PW, Altamentova SM, Weisel RD, Nili N, Ohno N, Verma S, Lee TY, Kiani C, Mickle DA, Strauss BH and Li RK. Matrix remodeling in experimental and human heart failure: a possible regulatory role for TIMP-3. *Am J Physiol Heart Circ Physiol*. 2003;284:H626-34.

51. Schulze CJ, Wang W, Suarez-Pinzon WL, Sawicka J, Sawicki G and Schulz R. Imbalance between tissue inhibitor of metalloproteinase-4 and matrix metalloproteinases during acute myocardial ischemia-reperfusion injury. *Circulation*. 2003;107:2487-2492.

52. Radomski A, Jurasz P, Sanders EJ, Overall CM, Bigg HF, Edwards DR and Radomski MW. Identification, regulation and role of tissue inhibitor of metalloproteinases-4 (TIMP-4) in human platelets. *Br J Pharmacol*. 2002;137:1330-8.

53. Frears ER, Zhang Z, Blake DR, O'Connell JP and Winyard PG. Inactivation of tissue inhibitor of metalloproteinase-1 by peroxynitrite. *FEBS Lett*. 1996;381:21-4.

54. Donnini S, Monti M, Roncone R, Morbidelli L, Rocchigiani M, Oliviero S, Casella L, Giachetti A, Schulz R and Ziche M. Peroxynitrite inactivates human-tissue inhibitor of metalloproteinase-4. *FEBS Lett*. 2008;582:1135-40.

55. Macaulay VM, O'Byrne KJ, Saunders MP, Braybrooke JP, Long L, Gleeson F, Mason CS, Harris AL, Brown P and Talbot DC. Phase I study of intrapleural batimastat (BB-94), a matrix metalloproteinase inhibitor, in the treatment of malignant pleural effusions. *Clin Cancer Res*. 1999;5:513-20.

56. Nemunaitis J, Poole C, Primrose J, Rosemurgy A, Malfetano J, Brown P, Berrington A, Cornish A, Lynch K, Rasmussen H, Kerr D, Cox D and Millar A. Combined analysis of studies of the effects of the matrix metalloproteinase inhibitor marimastat on serum tumor markers in advanced cancer: selection of a biologically active and tolerable dose for longer-term studies. *Clin Cancer Res*. 1998;4:1101-9.

57. Rosenbaum E, Zahurak M, Sinibaldi V, Carducci MA, Pili R, Laufer M, DeWeese TL and Eisenberger MA. Marimastat in the treatment of patients with biochemically relapsed prostate cancer: a prospective randomized, double-blind, phase I/II trial. *Clin Cancer Res*. 2005;11:4437-43.

58. Peterson JT. The importance of estimating the therapeutic index in the development of matrix metalloproteinase inhibitors. *Cardiovasc Res*. 2006;69:677-87.

59. Fingleton B. MMPs as therapeutic targets--still a viable option? *Semin Cell Dev Biol*. 2008;19:61-8.

60. Tuccinardi T, Martinelli A, Nuti E, Carelli P, Balzano F, Uccello-Barretta G, Murphy G and Rossello A. Amber force field implementation, molecular modelling study, synthesis and MMP-1/MMP-2 inhibition profile of (R)- and (S)-N-hydroxy-2-(N-isopropoxybiphenyl-4-ylsulfonamido)-3-methylbutanamides. *Bioorganic Med Chem*. 2006;14:4260-76.

61. Fisher JF and Mobashery S. Recent advances in MMP inhibitor design. *Cancer Metastasis Rev*. 2006;25:115-36.

62. Yamada A, Uegaki A, Nakamura T and Ogawa K. ONO-4817, an orally active matrix metalloproteinase inhibitor, prevents lipopolysaccharide-induced proteoglycan release from the joint cartilage in guinea pigs. *Inflamm Res*. 2000;49:144-6.

63. Ali MA, Cho WJ, Hudson B, Kassiri Z, Granzier H and Schulz R. Titin is a target of matrix metalloproteinase-2: implications in myocardial ischemia/reperfusion injury. *Circulation*. 2010;122:2039-47.

64. Shimoyama T, Tabuchi N, Chung J, Koyama T and Sunamori M. Matrix metalloproteinase inhibitor (ONO-4817) attenuates ischemia-reperfusion injury in rat lung. *Med Sci Monit*. 2006;12:BR51-6.

65. Shirahane K, Yamaguchi K, Koga K, Watanabe M, Kuroki S and Tanaka M. Hepatic ischemia/reperfusion injury is prevented by a novel matrix metalloproteinase inhibitor, ONO-4817. *Surgery*. 2006;139:653-64.

66. Rossello A, Nuti E, Orlandini E, Carelli P, Rapposelli S, Macchia M, Minutolo F, Carbonaro L, Albini A, Benelli R, Cercignani G, Murphy G and Balsamo A. New N-arylsulfonyl-N-alkoxyaminoacetohydroxamic acids as selective inhibitors of gelatinase A (MMP-2). *Bioorganic Med Chem*. 2004;12:2441-50.

67. Golub LM, Lee HM, Ryan ME, Giannobile WV, Payne J and Sorsa T. Tetracyclines inhibit connective tissue breakdown by multiple non-antimicrobial mechanisms. *Adv Dent Res*. 1998;12:12-26.

68. Lee HM, Ciancio SG, Tuter G, Ryan ME, Komaroff E and Golub LM. Subantimicrobial dose doxycycline efficacy as a matrix metalloproteinase inhibitor in chronic periodontitis patients is enhanced when combined with a non-steroidal anti-inflammatory drug. *J Periodontol*. 2004;75:453-63.

69. Uitto VJ, Firth JD, Nip L and Golub LM. Doxycycline and chemically modified tetracyclines inhibit gelatinase A (MMP-2) gene expression in human skin keratinocytes. *Ann N Y Acad Sci*. 1994;732:140-51.

70. Caton J and Ryan ME. Clinical studies on the management of periodontal diseases utilizing subantimicrobial dose doxycycline (SDD). *Pharmacol Res*. 2011;63:114-20.

71. Berman B, Perez OA and Zell D. Update on rosacea and anti-inflammatory-dose doxycycline. *Drugs Today*. 2007;43:27-34.

72. Smith GN, Jr., Mickler EA, Hasty KA and Brandt KD. Specificity of inhibition of matrix metalloproteinase activity by doxycycline: relationship to structure of the enzyme. *Arthritis Rheum*. 1999;42:1140-6.

73. Cerisano G, Buonamici P, Valenti R, Sciagrà R, Raspanti S, Santini A, Carrabba N, Dovellini EV, Romito R, Pupi A, Colonna P and Antoniucci D. Early short-term doxycycline therapy in patients with acute myocardial infarction and left ventricular dysfunction to prevent the ominous progression to adverse remodelling: the TIPTOP trial. *Eur Heart J*. 2014;35:184-191.

74. Giannelli G, Falk-Marzillier J, Schiraldi O, Stetler-Stevenson WG and Quaranta V. Induction of cell migration by matrix metalloprotease-2 cleavage of laminin-5. *Science*. 1997;277:225-8.

75. Kenny HA, Kaur S, Coussens LM and Lengyel E. The initial steps of ovarian cancer cell metastasis are mediated by MMP-2 cleavage of vitronectin and fibronectin. *J Clin Invest*.

2008;118:1367-79.

76. Fernandez-Patron C, Radomski MW and Davidge ST. Vascular matrix metalloproteinase-2 cleaves big endothelin-1 yielding a novel vasoconstrictor. *Circ Res*. 1999;85:906-11.

77. Fernandez-Patron C, Stewart KG, Zhang Y, Koivunen E, Radomski MW and Davidge ST. Vascular matrix metalloproteinase-2-dependent cleavage of calcitonin gene-related peptide promotes vasoconstriction. *Circ Res*. 2000;87:670-6.

78. McQuibban GA, Gong JH, Tam EM, McCulloch CA, Clark-Lewis I and Overall CM. Inflammation dampened by gelatinase A cleavage of monocyte chemoattractant protein-3. *Science*. 2000;289:1202-6.

79. Dean RA, Butler GS, Hamma-Kourbali Y, Delbe J, Brigstock DR, Courty J and Overall CM. Identification of candidate angiogenic inhibitors processed by matrix metalloproteinase 2 (MMP-2) in cell-based proteomic screens: disruption of vascular endothelial growth factor (VEGF)/heparin affin regulatory peptide (pleiotrophin) and VEGF/Connective tissue growth factor angiogenic inhibitory complexes by MMP-2 proteolysis. *Mol Cell Biol*. 2007;27:8454-65.

80. Ito A, Mukaiyama A, Itoh Y, Nagase H, Thogersen IB, Enghild JJ, Sasaguri Y and Mori Y. Degradation of interleukin 1β by matrix metalloproteinases. *J Biol Chem*. 1996;271:14657-60.

81. Yu Q and Stamenkovic I. Cell surface-localized matrix metalloproteinase-9 proteolytically activates TGF-β and promotes tumor invasion and angiogenesis. *Genes Dev*. 2000;14:163-76.

82. Rouet-Benzineb P, Buhler JM, Dreyfus P, Delcourt A, Dorent R, Perennec J, Crozatier B, Harf A and Lafuma C. Altered balance between matrix gelatinases (MMP-2 and MMP-9) and their tissue inhibitors in human dilated cardiomyopathy: potential role of MMP-9 in myosin-heavy chain degradation. *Eur J Heart Fail*. 1999;1:337-52.

83. Coker ML, Doscher MA, Thomas CV, Galis ZS and Spinale FG. Matrix metalloproteinase synthesis and expression in isolated LV myocyte preparations. *Am J Physiol Heart Circ Physiol*. 1999;277:H777-87.

84. Wang W, Schulze CJ, Suarez-Pinzon W, Dyck J, Sawicki S and Schulz R. Intracellular action of matrix metalloproteinase-2 accounts for acute myocardial ischemia and reperfusion injury. *Circulation*. 2002;106:1543-1549.

85. Sawicki G, Leon H, Sawicka J, Sariahmetoglu M, Schulze CJ, Scott PG, Szczesna-Cordary D and Schulz R. Degradation of myosin light chain in isolated rat hearts subjected to ischemia-reperfusion injury: a new intracellular target for matrix metalloproteinase-2. *Circulation*. 2005;112:544-52.

86. Sung MM, Schulz CG, Wang W, Sawicki G, Bautista-Lopez NL and Schulz R. Matrix metalloproteinase-2 degrades the cytoskeletal protein alpha-actinin in peroxynitrite

mediated myocardial injury. *J Mol Cell Cardiol*. 2007;43:429-36.

87. Buchholz B, Perez V, Siachoque N, Miksztowicz V, Berg G, Rodríguez M, Donato M and Gelpi RJ. Dystrophin proteolysis: a potential target for MMP-2 and its prevention by ischemic preconditioning. *Am J Physiol Heart Circ Physiol*. 2014;307:H88-96.

88. Lalu MM, Csonka C, Giricz Z, Csont T, Schulz R and Ferdinandy P. Preconditioning decreases ischemia/reperfusion-induced release and activation of matrix metalloproteinase-2. *Biochem Biophys Res Commun*. 2002;296:937-41.

89. Kwan JA, Schulze CJ, Wang W, Leon H, Sariahmetoglu M, Sung M, Sawicka J, Sims DE, Sawicki G and Schulz R. Matrix metalloproteinase-2 (MMP-2) is present in the nucleus of cardiac myocytes and is capable of cleaving poly (ADP-ribose) polymerase (PARP) in vitro. *Faseb J*. 2004;18:690-2.

90. Si-Tayeb K, Monvoisin A, Mazzocco C, Lepreux S, Decossas M, Cubel G, Taras D, Blanc JF, Robinson DR and Rosenbaum J. Matrix metalloproteinase 3 is present in the cell nucleus and is involved in apoptosis. *Am J Pathol*. 2006;169:1390-401.

91. Eguchi T, Kubota S, Kawata K, Mukudai Y, Uehara J, Ohgawara T, Ibaragi S, Sasaki A, Kuboki T and Takigawa M. Novel transcription-factor-like function of human matrix metalloproteinase 3 regulating the CTGF/CCN2 gene. *Mol Cell Biol*. 2008;28:2391-413.

92. Zuo X, Pan W, Feng T, Shi X and Dai J. Matrix metalloproteinase 3 promotes cellular anti-dengue virus response via interaction with transcription factor NFκB in cell nucleus. *PLoS One*. 2014;9:e84748.

93. Hill JW, Poddar R, Thompson JF, Rosenberg GA and Yang Y. Intranuclear matrix metalloproteinases promote DNA damage and apoptosis induced by oxygen-glucose deprivation in neurons. *Neuroscience*. 2012;220:277-90.

94. Zimowska M, Swierczynska M and Ciemerych MA. Nuclear MMP-9 role in the regulation of rat skeletal myoblasts proliferation. *Biol Cell*. 2013;105:334-44.

95. Hughes BG, Fan X, Cho WJ and Schulz R. MMP-2 is localized to the mitochondria-associated membrane of the heart. *Am J Physiol Heart Circ Physiol*. 2014;306: H764-H770.

96. Lin HB, Sharma K, Bialy D, Wawrzynska M, Purves R, Cayabyab FS, Wozniak M and Sawicki G. Inhibition of MMP-2 expression affects metabolic enzyme expression levels: proteomic analysis of rat cardiomyocytes. *J Proteom*. 2014;106:74-85.

97. Roczkowsky A, Chan BYH, Lee TYT, Mahmud Z, Hartley B, Julien O, Armanious G, Young HS and Schulz R. Myocardial MMP-2 contributes to SERCA2a proteolysis during cardiac ischemia-reperfusion injury. *Cardiovasc Res*. 2019;Under revision.

98. LeWinter MM and Granzier H. Cardiac titin: a multifunctional giant. *Circulation*. 2010;121:2137-45.

99. Granzier HL and Labeit S. The giant protein titin: a major player in myocardial mechanics, signaling, and disease. *Circ Res*. 2004;94:284-95.

100. Labeit S, Lahmers S, Burkart C, Fong C, McNabb M, Witt S, Witt C, Labeit D and Granzier H. Expression of distinct classes of titin isoforms in striated and smooth muscles by alternative splicing, and their conserved interaction with filamins. *J Mol Biol*. 2006;362:664-81.

101. Lahmers S, Wu Y, Call DR, Labeit S and Granzier H. Developmental control of titin isoform expression and passive stiffness in fetal and neonatal myocardium. *Circ Res*. 2004;94:505-13.

102. Methawasin M, Strom JG, Slater RE, Fernandez V, Saripalli C and Granzier H. Experimentally Increasing the Compliance of Titin Through RNA Binding Motif-20 (RBM20) Inhibition Improves Diastolic Function In a Mouse Model of Heart Failure With Preserved Ejection Fraction. *Circulation*. 2016;134:1085-1099.

103. Methawasin M, Hutchinson KR, Lee EJ, Smith JE, 3rd, Saripalli C, Hidalgo CG, Ottenheijm CA and Granzier H. Experimentally increasing titin compliance in a novel mouse model attenuates the Frank-Starling mechanism but has a beneficial effect on diastole. *Circulation*. 2014;129:1924-36.

104. Guo W, Schafer S, Greaser ML, Radke MH, Liss M, Govindarajan T, Maatz H, Schulz H, Li S, Parrish AM, Dauksaite V, Vakeel P, Klaassen S, Gerull B, Thierfelder L, Regitz-Zagrosek V, Hacker TA, Saupe KW, Dec GW, Ellinor PT, MacRae CA, Spallek B, Fischer R, Perrot A, Ozcelik C, Saar K, Hubner N and Gotthardt M. RBM20, a gene for hereditary cardiomyopathy, regulates titin splicing. *Nat Med*. 2012;18:766-73.

105. Watanabe K, Nair P, Labeit D, Kellermayer MS, Greaser M, Labeit S and Granzier H. Molecular mechanics of cardiac titin's PEVK and N2B spring elements. *J Biol Chem*. 2002;277:11549-58.

106. Li H, Linke WA, Oberhauser AF, Carrion-Vazquez M, Kerkvliet JG, Lu H, Marszalek PE and Fernandez JM. Reverse engineering of the giant muscle protein titin. *Nature*. 2002;418:998-1002.

107. Kellermayer MS, Smith SB, Bustamante C and Granzier HL. Complete unfolding of the titin molecule under external force. *J Struct Biol*. 1998;122:197-205.

108. Trombitas K, Redkar A, Centner T, Wu Y, Labeit S and Granzier H. Extensibility of isoforms of cardiac titin: variation in contour length of molecular subsegments provides a basis for cellular passive stiffness diversity. *Biophys J*. 2000;79:3226-34.

109. Wu Y, Cazorla O, Labeit D, Labeit S and Granzier H. Changes in titin and collagen underlie diastolic stiffness diversity of cardiac muscle. *J Mol Cell Cardiol*. 2000;32:2151-62.

110. Cazorla O, Freiburg A, Helmes M, Centner T, McNabb M, Wu Y, Trombitas K, Labeit S and Granzier H. Differential expression of cardiac titin isoforms and modulation of cellular

stiffness. *Circ Res*. 2000;86:59-67.

111. Zou P, Pinotsis N, Lange S, Song YH, Popov A, Mavridis I, Mayans OM, Gautel M and Wilmanns M. Palindromic assembly of the giant muscle protein titin in the sarcomeric Z-disk. *Nature*. 2006;439:229-33.

112. Obermann WM, Gautel M, Steiner F, van der Ven PF, Weber K and Furst DO. The structure of the sarcomeric M band: localization of defined domains of myomesin, M-protein, and the 250-kD carboxy-terminal region of titin by immunoelectron microscopy. *J Cell Biol*. 1996;134:1441-53.

113. Pernigo S, Fukuzawa A, Bertz M, Holt M, Rief M, Steiner RA and Gautel M. Structural insight into M-band assembly and mechanics from the titin-obscurin-like-1 complex. *Proc Natl Acad Sci U S A*. 2010;107:2908-13.

114. Kontrogianni-Konstantopoulos A and Bloch RJ. The hydrophilic domain of small ankyrin-1 interacts with the two N-terminal immunoglobulin domains of titin. *J Biol Chem*. 2003;278:3985-91.

115. Furukawa T, Ono Y, Tsuchiya H, Katayama Y, Bang ML, Labeit D, Labeit S, Inagaki N and Gregorio CC. Specific interaction of the potassium channel beta-subunit minK with the sarcomeric protein T-cap suggests a T-tubule-myofibril linking system. *J Mol Biol*. 2001;313:775-84.

116. Gautel M, Goulding D, Bullard B, Weber K and Furst DO. The central Z-disk region of titin is assembled from a novel repeat in variable copy numbers. *J Cell Sci*. 1996;109 (Pt 11):2747-54.

117. Sorimachi H, Freiburg A, Kolmerer B, Ishiura S, Stier G, Gregorio CC, Labeit D, Linke WA, Suzuki K and Labeit S. Tissue-specific expression and alpha-actinin binding properties of the Z-disc titin: implications for the nature of vertebrate Z-discs. *J Mol Biol*. 1997;270:688-95.

118. Trinick J. Titin and nebulin: protein rulers in muscle? *Trends Biochem Sci*. 1994;19:405-9.

119. Fujita H, Labeit D, Gerull B, Labeit S and Granzier HL. Titin isoform-dependent effect of calcium on passive myocardial tension. *Am J Physiol Heart Circ Physiol*. 2004;287:H2528-34.

120. Labeit D, Watanabe K, Witt C, Fujita H, Wu Y, Lahmers S, Funck T, Labeit S and Granzier H. Calcium-dependent molecular spring elements in the giant protein titin. *Proc Natl Acad Sci U S A*. 2003;100:13716-21.

121. Linke WA, Kulke M, Li H, Fujita-Becker S, Neagoe C, Manstein DJ, Gautel M and Fernandez JM. PEVK domain of titin: an entropic spring with actin-binding properties. *J Struct Biol*. 2002;137:194-205.

122. Freiburg A and Gautel M. A molecular map of the interactions between titin and myosin-

binding protein C. Implications for sarcomeric assembly in familial hypertrophic cardiomyopathy. *Eur J Biochem*. 1996;235:317-23.

123. Muhle-Goll C, Habeck M, Cazorla O, Nilges M, Labeit S and Granzier H. Structural and functional studies of titin's fn3 modules reveal conserved surface patterns and binding to myosin S1--a possible role in the Frank-Starling mechanism of the heart. *J Mol Biol*. 2001;313:431-47.

124. Makarenko I, Opitz CA, Leake MC, Neagoe C, Kulke M, Gwathmey JK, del Monte F, Hajjar RJ and Linke WA. Passive stiffness changes caused by upregulation of compliant titin isoforms in human dilated cardiomyopathy hearts. *Circ Res*. 2004;95:708-16.

125. Nagueh SF, Shah G, Wu Y, Torre-Amione G, King NM, Lahmers S, Witt CC, Becker K, Labeit S and Granzier HL. Altered titin expression, myocardial stiffness, and left ventricular function in patients with dilated cardiomyopathy. *Circulation*. 2004;110:155-62.

126. Hein S, Scholz D, Fujitani N, Rennollet H, Brand T, Friedl A and Schaper J. Altered expression of titin and contractile proteins in failing human myocardium. *J Mol Cell Cardiol*. 1994;26:1291-306.

127. Morano I, Hadicke K, Grom S, Koch A, Schwinger RH, Bohm M, Bartel S, Erdmann E and Krause EG. Titin, myosin light chains and C-protein in the developing and failing human heart. *J Mol Cell Cardiol*. 1994;26:361-8.

128. Dhiman M, Nakayasu ES, Madaiah YH, Reynolds BK, Wen JJ, Almeida IC and Garg NJ. Enhanced nitrosative stress during Trypanosoma cruzi infection causes nitrotyrosine modification of host proteins: implications in Chagas' disease. *Am J Pathol*. 2008;173:728-40.

129. Lim CC, Zuppinger C, Guo X, Kuster GM, Helmes M, Eppenberger HM, Suter TM, Liao R and Sawyer DB. Anthracyclines induce calpain-dependent titin proteolysis and necrosis in cardiomyocytes. *J Biol Chem*. 2004;279:8290-8299.

130. Takeshima H, Komazaki S, Nishi M, Iino M and Kangawa K. Junctophilins: a novel family of junctional membrane complex proteins. *Mol Cell*. 2000;6:11-22.

131. Ziman AP, Gomez-Viquez NL, Bloch RJ and Lederer WJ. Excitation-contraction coupling changes during postnatal cardiac development. *J Mol Cell Cardiol*. 2010;48:379-86.

132. Beavers DL, Landstrom AP, Chiang DY and Wehrens XH. Emerging roles of junctophilin-2 in the heart and implications for cardiac diseases. *Cardiovasc Res*. 2014;103:198-205.

133. Woo JS, Srikanth S, Nishi M, Ping P, Takeshima H and Gwack Y. Junctophilin-4, a component of the endoplasmic reticulum-plasma membrane junctions, regulates Ca^{2+} dynamics in T cells. *Proc Natl Acad Sci USA*. 2016;113:2762-7.

134. Guo A, Hall D, Zhang C, Peng T, Miller JD, Kutschke W, Grueter CE, Johnson FL, Lin RZ and Song LS. Molecular determinants of calpain-dependent cleavage of junctophilin-2

protein in cardiomyocytes. *J Biol Chem*. 2015;290:17946-55.

135. Murphy RM, Dutka TL, Horvath D, Bell JR, Delbridge LM and Lamb GD. Ca^{2+}-dependent proteolysis of junctophilin-1 and junctophilin-2 in skeletal and cardiac muscle. *J Physiol*. 2013;591:719-29.

136. Garbino A, van Oort RJ, Dixit SS, Landstrom AP, Ackerman MJ and Wehrens XH. Molecular evolution of the junctophilin gene family. *Physiol Genomics*. 2009;37:175-86.

137. Eisner DA, Caldwell JL, Kistamas K and Trafford AW. Calcium and excitation-contraction coupling in the heart. *Circ Res*. 2017;121:181-195.

138. Bers DM. Cardiac excitation-contraction coupling. *Nature*. 2002;415:198-205.

139. Bers DM. Calcium cycling and signaling in cardiac myocytes. *Annu Rev Physiol*. 2008;70:23-49.

140. Wang SQ, Song LS, Lakatta EG and Cheng H. Ca^{2+} signalling between single L-type Ca^{2+} channels and ryanodine receptors in heart cells. *Nature*. 2001;410:592-6.

141. Pinali C, Bennett H, Davenport JB, Trafford AW and Kitmitto A. Three-dimensional reconstruction of cardiac sarcoplasmic reticulum reveals a continuous network linking transverse-tubules: this organization is perturbed in heart failure. *Circ Res*. 2013;113:1219-30.

142. Hayashi T, Martone ME, Yu Z, Thor A, Doi M, Holst MJ, Ellisman MH and Hoshijima M. Three-dimensional electron microscopy reveals new details of membrane systems for Ca^{2+} signaling in the heart. *J Cell Sci*. 2009;122:1005-13.

143. Franzini-Armstrong C and Protasi F. Ryanodine receptors of striated muscles: a complex channel capable of multiple interactions. *Physiol Rev*. 1997;77:699-729.

144. Kaprielian RR, Stevenson S, Rothery SM, Cullen MJ and Severs NJ. Distinct patterns of dystrophin organization in myocyte sarcolemma and transverse tubules of normal and diseased human myocardium. *Circulation*. 2000;101:2586-94.

145. Zhang HB, Li RC, Xu M, Xu SM, Lai YS, Wu HD, Xie XJ, Gao W, Ye H, Zhang YY, Meng X and Wang SQ. Ultrastructural uncoupling between T-tubules and sarcoplasmic reticulum in human heart failure. *Cardiovasc Res*. 2013;98:269-76.

146. van Oort RJ, Garbino A, Wang W, Dixit SS, Landstrom AP, Gaur N, De Almeida AC, Skapura DG, Rudy Y, Burns AR, Ackerman MJ and Wehrens XH. Disrupted junctional membrane complexes and hyperactive ryanodine receptors after acute junctophilin knockdown in mice. *Circulation*. 2011;123:979-88.

147. Xu M, Zhou P, Xu SM, Liu Y, Feng X, Bai SH, Bai Y, Hao XM, Han Q, Zhang Y and Wang SQ. Intermolecular failure of L-type Ca^{2+} channel and ryanodine receptor signaling in hypertrophy. *PLoS Biol*. 2007;5:e21.

148. Wei S, Guo A, Chen B, Kutschke W, Xie YP, Zimmerman K, Weiss RM, Anderson ME, Cheng H and Song LS. T-tubule remodeling during transition from hypertrophy to heart failure. *Circ Res*. 2010;107:520-31.

149. Ali MA, Stepanko A, Fan X, Holt A and Schulz R. Calpain inhibitors exhibit matrix metalloproteinase-2 inhibitory activity. *Biochem Biophys Res Commun*. 2012;423:1-5.

150. Fitzmaurice C, Allen C, Barber RM, Barregard L, Bhutta ZA, Brenner H, Dicker DJ, Chimed-Orchir O, Dandona R, Dandona L, Fleming T, Forouzanfar MH, Hancock J, Hay RJ, Hunter-Merrill R, Huynh C, Hosgood HD, Johnson CO, Jonas JB, Khubchandani J, Kumar GA, Kutz M, Lan Q, Larson HJ, Liang X, Lim SS, Lopez AD, MacIntyre MF, Marczak L, Marquez N, Mokdad AH, Pinho C, Pourmalek F, Salomon JA, Sanabria JR, Sandar L, Sartorius B, Schwartz SM, Shackelford KA, Shibuya K, Stanaway J, Steiner C, Sun J, Takahashi K, Vollset SE, Vos T, Wagner JA, Wang H, Westerman R, Zeeb H, Zoeckler L, Abd-Allah F, Ahmed MB, Alabed S, Alam NK, Aldhahri SF, Alem G, Alemayohu MA, Ali R, Al-Raddadi R, Amare A, Amoako Y, Artaman A, Asayesh H, Atnafu N, Awasthi A, Saleem HB, Barac A, Bedi N, Bensenor I, Berhane A, Bernabe E, Betsu B, Binagwaho A, Boneya D, Campos-Nonato I, Castaneda-Orjuela C, Catala-Lopez F, Chiang P, Chibueze C, Chitheer A, Choi JY, Cowie B, Damtew S, das Neves J, Dey S, Dharmaratne S, Dhillon P, Ding E, Driscoll T, Ekwueme D, Endries AY, Farvid M, Farzadfar F, Fernandes J, Fischer F, TT GH, Gebru A, Gopalani S, Hailu A, Horino M, Horita N, Husseini A, Huybrechts I, Inoue M, Islami F, Jakovljevic M, James S, Javanbakht M, Jee SH, Kasaeian A, Kedir MS, Khader YS, Khang YH, Kim D, Leigh J, Linn S, Lunevicius R, El Razek HMA, Malekzadeh R, Malta DC, Marcenes W, Markos D, Melaku YA, Meles KG, Mendoza W, Mengiste DT, Meretoja TJ, Miller TR, Mohammad KA, Mohammadi A, Mohammed S, Moradi-Lakeh M, Nagel G, Nand D, Le Nguyen Q, Nolte S, Ogbo FA, Oladimeji KE, Oren E, Pa M, Park EK, Pereira DM, Plass D, Qorbani M, Radfar A, Rafay A, Rahman M, Rana SM, Soreide K, Satpathy M, Sawhney M, Sepanlou SG, Shaikh MA, She J, Shiue I, Shore HR, Shrime MG, So S, Soneji S, Stathopoulou V, Stroumpoulis K, Sufiyan MB, Sykes BL, Tabares-Seisdedos R, Tadese F, Tedla BA, Tessema GA, Thakur JS, Tran BX, Ukwaja KN, Uzochukwu BSC, Vlassov VV, Weiderpass E, Wubshet Terefe M, Yebyo HG, Yimam HH, Yonemoto N, Younis MZ, Yu C, Zaidi Z, Zaki MES, Zenebe ZM, Murray CJL and Naghavi M. Global, regional, and national cancer Incidence, mortality, years of life lost, years lived with disability, and disability-adjusted life-years for 32 cancer groups, 1990 to 2015: a systematic analysis for the global burden of disease study. *JAMA Oncol*. 2017;3:524-548.

151. Bloom MW, Hamo CE, Cardinale D, Ky B, Nohria A, Baer L, Skopicki H, Lenihan DJ, Gheorghiade M, Lyon AR and Butler J. Cancer therapy-related cardiac dysfunction and heart failure: part 1: definitions, pathophysiology, risk factors, and imaging. *Circ Heart Fail*. 2016;9:e002661.

152. Moslehi JJ. Cardiovascular toxic effects of targeted cancer therapies. *N Engl J Med*. 2016;375:1457-1467.

153. Carver JR, Shapiro CL, Ng A, Jacobs L, Schwartz C, Virgo KS, Hagerty KL, Somerfield MR and Vaughn DJ. American Society of Clinical Oncology clinical evidence review on the

ongoing care of adult cancer survivors: cardiac and pulmonary late effects. *J Clin Oncol*. 2007;25:3991-4008.

154. Hanrahan EO, Gonzalez-Angulo AM, Giordano SH, Rouzier R, Broglio KR, Hortobagyi GN and Valero V. Overall survival and cause-specific mortality of patients with stage T1a,bN0M0 breast carcinoma. *J Clin Oncol*. 2007;25:4952-60.

155. Silber JH, Cnaan A, Clark BJ, Paridon SM, Chin AJ, Rychik J, Hogarty AN, Cohen MI, Barber G, Rutkowski M, Kimball TR, Delaat C, Steinherz LJ and Zhao H. Enalapril to prevent cardiac function decline in long-term survivors of pediatric cancer exposed to anthracyclines. *J Clin Oncol*. 2004;22:820-8.

156. Ewer MS and Lippman SM. Type II chemotherapy-related cardiac dysfunction: time to recognize a new entity. *J Clin Oncol*. 2005;23:2900-2.

157. Blum RH and Carter SK. Adriamycin. A new anticancer drug with significant clinical activity. *Ann Intern Med*. 1974;80:249-59.

158. McGowan JV, Chung R, Maulik A, Piotrowska I, Walker JM and Yellon DM. Anthracycline chemotherapy and cardiotoxicity. *Cardiovasc Drug Ther*. 2017;31:63-75.

159. Altena R, Perik PJ, van Veldhuisen DJ, de Vries EG and Gietema JA. Cardiovascular toxicity caused by cancer treatment: strategies for early detection. *Lancet Oncol*. 2009;10:391-9.

160. Von Hoff DD, Layard MW, Basa P, Davis HLJ, Von Hoff AL, Rozencweig M and Muggia FM. Risk factors for doxorubicin-induced congestive heart failure. *Ann Intern Med*. 1979;91:710-7.

161. Lefrak EA, Pitha J, Rosenheim S and Gottlieb JA. A clinicopathologic analysis of adriamycin cardiotoxicity. *Cancer*. 1973;32:302-14.

162. Chatterjee K, Zhang J, Honbo N and Karliner JS. Doxorubicin cardiomyopathy. *Cardiology*. 2010;115:155-62.

163. Yeh ET and Bickford CL. Cardiovascular complications of cancer therapy: incidence, pathogenesis, diagnosis, and management. *J Am Coll Cardiol*. 2009;53:2231-47.

164. Zhou S, Starkov A, Froberg MK, Leino RL and Wallace KB. Cumulative and irreversible cardiac mitochondrial dysfunction induced by doxorubicin. *Cancer Res*. 2001;61:771-7.

165. Sardao VA, Oliveira PJ, Holy J, Oliveira CR and Wallace KB. Morphological alterations induced by doxorubicin on H9c2 myoblasts: nuclear, mitochondrial, and cytoskeletal targets. *Cell Biol Toxicol*. 2009;25:227-43.

166. Mukhopadhyay P, Rajesh M, Bátkai S, Kashiwaya Y, Haskó G, Liaudet L, Szabó C and Pacher P. Role of superoxide, nitric oxide, and peroxynitrite in doxorubicin-induced cell death in vivo and in vitro. *Am J Physiol Heart Circ Physiol*. 2009;296:H1466-83.

167. Sawyer D. Anthracyclines and heart failure. *N Engl J Med*. 2013;368:1154-6.

168. Singal P and Iliskovic N. Doxorubicin-induced cardiomyopathy. *N Engl J Med*. 1998;339:900-905.

169. Zhang S, Liu X, Bawa-Khalfe T, Lu LS, Lyu YL, Liu LF and Yeh ET. Identification of the molecular basis of doxorubicin-induced cardiotoxicity. *Nat Med*. 2012;18:1639-42.

170. Carvalho FS, Burgeiro A, Garcia R, Moreno AJ, Carvalho RA and Oliveira PJ. Doxorubicin-induced cardiotoxicity: from bioenergetic failure and cell death to cardiomyopathy. *Med Res Rev*. 2014;34:106-135.

171. Doroshow JH. Anthracycline antibiotic-stimulated superoxide, hydrogen peroxide, and hydroxyl radical production by NADH dehydrogenase. *Cancer Res*. 1983;43:4543-51.

172. Balanehru S and Nagarajan B. Intervention of adriamycin induced free radical damage. *Biochem Int*. 1992;28:735-44.

173. Jiang J, Temma K and Akera T. Doxorubicin-induced changes in intracellular Ca^{2+} transients observed in cardiac myocytes isolated from guinea-pig heart. *Can J Physiol Pharmacol*. 1994;72:622-31.

174. Wang YX and Korth M. Effects of doxorubicin on excitation-contraction coupling in guinea pig ventricular myocardium. *Circ Res*. 1995;76:645-653.

175. Olson RD, Gambliel HA, Vestal RE, Shadle SE, Charlier HAJ and Cusack BJ. Doxorubicin cardiac dysfunction: effects on calcium regulatory proteins, sarcoplasmic reticulum, and triiodothyronine. *Cardiovasc Toxicol*. 2005;5:269-83.

176. Hanna AD, Lam A, Tham S, Dulhunty AF and Beard NA. Adverse effects of doxorubicin and its metabolic product on cardiac RyR2 and SERCA2A. *Mol Pharmacol*. 2014;86:438-49.

177. Ito H, Miller SC, Billingham ME, Akimoto H, Torti SV, Wade R, Gahlmann R, Lyons G, Kedes L and Torti FM. Doxorubicin selectively inhibits muscle gene expression in cardiac muscle cells in vivo and in vitro. *Proc Natl Acad Sci USA*. 1990;87:4275-9.

178. Nikitovic D, Juranek I, Wilks MF, Tzardi M, Tsatsakis A and Tzanakakis GN. Anthracycline-dependent cardiotoxicity and extracellular matrix remodeling. *Chest*. 2014;146:1123-1130.

179. Kizaki K, Ito R, Okada M, Yoshioka K, Uchide T, Temma K, Mutoh K, Uechi M and Hara Y. Enhanced gene expression of myocardial matrix metalloproteinases 2 and 9 after acute treatment with doxorubicin in mice. *Pharmacol Res*. 2006;53:341-6.

180. Spallarossa P, Altieri P, Garibaldi S, Ghigliotti G, Barisione C, Manca V, Fabbi P, Ballestrero A, Brunelli C and Barsotti A. Matrix metalloproteinase-2 and -9 are induced differently by doxorubicin in H9c2 cells: The role of MAP kinases and NAD(P)H oxidase.

Cardiovasc Res. 2006;69:736-45.

181. Goetzenich A, Hatam N, Zernecke A, Weber C, Czarnotta T, Autschbach R and Christiansen S. Alteration of matrix metalloproteinases in selective left ventricular adriamycin-induced cardiomyopathy in the pig. *J Heart Lung Transplant*. 2009;28:1087-93.

182. Ivanova M, Dovinova I, Okruhlicova L, Tribulova N, Simoncikova P, Barte-kova M, Vlkovicova J and Barancik M. Chronic cardiotoxicity of doxorubicin involves activation of myocardial and circulating matrix metalloproteinases in rats. *Acta Pharmacol Sin*. 2012;33:459-69.

183. Curigliano G, Cardinale D, Suter T, Plataniotis G, de Azambuja E, Sandri MT, Criscitiello C, Goldhirsch A, Cipolla C and Roila F. Cardiovascular toxicity induced by chemotherapy, targeted agents and radiotherapy: ESMO Clinical Practice Guidelines. *Ann Oncol*. 2012;23 Suppl 7:vii155-vii166.

184. Gulati G, Heck SL, Ree AH, Hoffmann P, Schulz-Menger J, Fagerland MW, Gravdehaug B, von Knobelsdorff-Brenkenhoff F, Bratland A, Storas TH, Hagve TA, Rosjo H, Steine K, Geisler J and Omland T. Prevention of cardiac dysfunction during adjuvant breast cancer therapy (PRADA): a 2 x 2 factorial, randomized, placebo-controlled, double-blind clinical trial of candesartan and metoprolol. *Eur Heart J*. 2016;37:1671-80.

185. Bosch X, Rovira M, Sitges M, Domenech A, Ortiz-Perez JT, de Caralt TM, Morales-Ruiz M, Perea RJ, Monzo M and Esteve J. Enalapril and carvedilol for preventing chemotherapy-induced left ventricular systolic dysfunction in patients with malignant hemopathies: the OVERCOME trial (preventiOn of left Ventricular dysfunction with Enalapril and caRvedilol in patients submitted to intensive ChemOtherapy for the treatment of Malignant hEmopathies). *J Am Coll Cardiol*. 2013;61:2355-62.

186. Pituskin E, Mackey JR, Koshman S, Jassal D, Pitz M, Haykowsky MJ, Pagano JJ, Chow K, Thompson RB, Vos LJ, Ghosh S, Oudit GY, Ezekowitz JA and Paterson DI. Multidisciplinary approach to novel therapies in cardio-oncology research (MANTICORE 101-Breast): a randomized trial for the prevention of trastuzumab-associated cardiotoxicity. *J Clin Oncol*. 2017;35:870-877.

187. Hausenloy DJ and Yellon DM. Myocardial ischemia-reperfusion injury: a neglected therapeutic target. *J Clin Invest*. 2013;123:92-100.

188. Eisen A, Giugliano RP and Braunwald E. Updates on acute coronary syndrome: a review. *JAMA Cardiol*. 2016;1:718-30.

189. Yasmin W, Strynadka KD and Schulz R. Generation of peroxynitrite contributes to ischemia-reperfusion injury in isolated rat hearts. *Cardiovasc Res*. 1997;33:422-32.

190. Ferdinandy P and Schulz R. Nitric oxide, superoxide, and peroxynitrite in myocardial ischaemia-reperfusion injury and preconditioning. *Br J Pharmacol*. 2003;138:532-43.

191. Ambrosio G, Flaherty JT, Duilio C, Tritto I, Santoro G, Elia PP, Condorelli M and Chiariello

M. Oxygen radicals generated at reflow induce peroxidation of membrane lipids in reperfused hearts. *J Clin Invest*. 1991;87:2056-66.

192. Cheung PY, Sawicki G, Wozniak M, Wang W, Radomski MW and Schulz R. Matrix metalloproteinase-2 contributes to ischemia-reperfusion injury in the heart. *Circulation*. 2000;101:1833-9.

193. Van Eyk JE, Powers F, Law W, Larue C, Hodges RS and Solaro RJ. Breakdown and release of myofilament proteins during ischemia and ischemia/reperfusion in rat hearts: identification of degradation products and effects on the pCa-force relation. *Circ Res*. 1998;82:261-71.

194. Beckman JS. Parsing the effects of nitric oxide, S-nitrosothiols, and peroxynitrite on inducible nitric oxide synthase-dependent cardiac myocyte apoptosis. *Circ Res*. 1999;85:870-1.

195. Turer AT and Hill JA. Pathogenesis of myocardial ischemia-reperfusion injury and rationale for therapy. *Am J Cardiol*. 2010;106:360-8.

196. Smith GL, Donoso P, Bauer CJ and Eisner DA. Relationship between intracellular pH and metabolite concentrations during metabolic inhibition in isolated ferret heart. *J Physiol*. 1993;472:11-22.

197. Murphy E, Perlman M, London RE and Steenbergen C. Amiloride delays the ischemia-induced rise in cytosolic free calcium. *Circ Res*. 1991;68:1250-8.

198. Hartmann M and Decking UK. Blocking Na^+-H^+ exchange by cariporide reduces Na^+-overload in ischemia and is cardioprotective. *J Mol Cell Cardiol*. 1999;31:1985-95.

199. Tani M and Neely JR. Role of intracellular Na^+ in Ca^{2+} overload and depressed recovery of ventricular function of reperfused ischemic rat hearts. Possible involvement of H^+-Na^+ and Na^+-Ca^{2+} exchange. *Circ Res*. 1989;65:1045-56.

200. Garcia-Dorado D, Ruiz-Meana M, Inserte J, Rodriguez-Sinovas A and Piper HM. Calcium-mediated cell death during myocardial reperfusion. *Cardiovasc Res*. 2012;94:168-80.

201. Matsumura Y, Saeki E, Inoue M, Hori M, Kamada T and Kusuoka H. Inhomogeneous disappearance of myofilament-related cytoskeletal proteins in stunned myocardium of guinea pig. *Circ Res*. 1996;79:447-54.

202. Griffiths EJ and Halestrap AP. Mitochondrial non-specific pores remain closed during cardiac ischaemia, but open upon reperfusion. *Biochem J*. 1995;307 (Pt 1):93-8.

203. Thibault H, Piot C, Staat P, Bontemps L, Sportouch C, Rioufol G, Cung TT, Bonnefoy E, Angoulvant D, Aupetit JF, Finet G, Andre-Fouet X, Macia JC, Raczka F, Rossi R, Itti R, Kirkorian G, Derumeaux G and Ovize M. Long-term benefit of postconditioning. *Circulation*. 2008;117:1037-44.

204. Staat P, Rioufol G, Piot C, Cottin Y, Cung TT, L'Huillier I, Aupetit JF, Bonnefoy E, Finet G, Andre-Fouet X and Ovize M. Postconditioning the human heart. *Circulation*. 2005;112:2143-8.

205. Lonborg J, Kelbaek H, Vejlstrup N, Jorgensen E, Helqvist S, Saunamaki K, Clemmensen P, Holmvang L, Treiman M, Jensen JS and Engstrom T. Cardioprotective effects of ischemic postconditioning in patients treated with primary percutaneous coronary intervention, evaluated by magnetic resonance. *Circ Cardiovasc Interv*. 2010;3:34-41.

206. Hu L, Wang J, Zhu H, Wu X, Zhou L, Song Y, Zhu S, Hao M, Liu C, Fan Y, Wang Y and Li Q. Ischemic postconditioning protects the heart against ischemia-reperfusion injury via neuronal nitric oxide synthase in the sarcoplasmic reticulum and mitochondria. *Cell Death Dis*. 2016;7:e2222.

207. Freixa X, Bellera N, Ortiz-Perez JT, Jimenez M, Pare C, Bosch X, De Caralt TM, Betriu A and Masotti M. Ischaemic postconditioning revisited: lack of effects on infarct size following primary percutaneous coronary intervention. *Eur Heart J*. 2012;33:103-12.

208. Sorensson P, Saleh N, Bouvier F, Bohm F, Settergren M, Caidahl K, Tornvall P, Arheden H, Ryden L and Pernow J. Effect of postconditioning on infarct size in patients with ST elevation myocardial infarction. *Heart*. 2010;96:1710-5.

209. Engstrom T, Kelbaek H, Helqvist S, Hofsten DE, Klovgaard L, Clemmensen P, Holmvang L, Jorgensen E, Pedersen F, Saunamaki K, Ravkilde J, Tilsted HH, Villadsen A, Aaroe J, Jensen SE, Raungaard B, Botker HE, Terkelsen CJ, Maeng M, Kaltoft A, Krusell LR, Jensen LO, Veien KT, Kofoed KF, Torp-Pedersen C, Kyhl K, Nepper-Christensen L, Treiman M, Vejlstrup N, Ahtarovski K, Lonborg J and Kober L. Effect of ischemic postconditioning during primary percutaneous coronary intervention for patients with ST-segment elevation myocardial infarction: a randomized clinical trial. *JAMA Cardiol*. 2017;2:490-497.

210. Gotberg M, Olivecrona GK, Koul S, Carlsson M, Engblom H, Ugander M, van der Pals J, Algotsson L, Arheden H and Erlinge D. A pilot study of rapid cooling by cold saline and endovascular cooling before reperfusion in patients with ST-elevation myocardial infarction. *Circ Cardiovasc Interv*. 2010;3:400-7.

211. Erlinge D, Gotberg M, Lang I, Holzer M, Noc M, Clemmensen P, Jensen U, Metzler B, James S, Botker HE, Omerovic E, Engblom H, Carlsson M, Arheden H, Ostlund O, Wallentin L, Harnek J and Olivecrona GK. Rapid endovascular catheter core cooling combined with cold saline as an adjunct to percutaneous coronary intervention for the treatment of acute myocardial infarction. The CHILL-MI trial: a randomized controlled study of the use of central venous catheter core cooling combined with cold saline as an adjunct to percutaneous coronary intervention for the treatment of acute myocardial infarction. *J Am Coll Cardiol*. 2014;63:1857-65.

212. Mewton N, Croisille P, Gahide G, Rioufol G, Bonnefoy E, Sanchez I, Cung TT, Sportouch C, Angoulvant D, Finet G, Andre-Fouet X, Derumeaux G, Piot C, Vernhet H, Revel D and Ovize M. Effect of cyclosporine on left ventricular remodeling after reperfused myocardial infarction. *J Am Coll Cardiol*. 2010;55:1200-5.

213. Piot C, Croisille P, Staat P, Thibault H, Rioufol G, Mewton N, Elbelghiti R, Cung TT, Bonnefoy E, Angoulvant D, Macia C, Raczka F, Sportouch C, Gahide G, Finet G, Andre-Fouet X, Revel D, Kirkorian G, Monassier JP, Derumeaux G and Ovize M. Effect of cyclosporine on reperfusion injury in acute myocardial infarction. *N Engl J Med*. 2008;359:473-81.

214. Lonborg J, Kelbaek H, Vejlstrup N, Botker HE, Kim WY, Holmvang L, Jorgensen E, Helqvist S, Saunamaki K, Terkelsen CJ, Schoos MM, Kober L, Clemmensen P, Treiman M and Engstrom T. Exenatide reduces final infarct size in patients with ST-segment-elevation myocardial infarction and short-duration of ischemia. *Circ Cardiovasc Interv*. 2012;5:288-95.

215. Lonborg J, Vejlstrup N, Kelbaek H, Botker HE, Kim WY, Mathiasen AB, Jorgensen E, Helqvist S, Saunamaki K, Clemmensen P, Holmvang L, Thuesen L, Krusell LR, Jensen JS, Kober L, Treiman M, Holst JJ and Engstrom T. Exenatide reduces reperfusion injury in patients with ST-segment elevation myocardial infarction. *Eur Heart J*. 2012;33:1491-9.

216. Cung TT, Morel O, Cayla G, Rioufol G, Garcia-Dorado D, Angoulvant D, Bonnefoy-Cudraz E, Guerin P, Elbaz M, Delarche N, Coste P, Vanzetto G, Metge M, Aupetit JF, Jouve B, Motreff P, Tron C, Labeque JN, Steg PG, Cottin Y, Range G, Clerc J, Claeys MJ, Coussement P, Prunier F, Moulin F, Roth O, Belle L, Dubois P, Barragan P, Gilard M, Piot C, Colin P, De Poli F, Morice MC, Ider O, Dubois-Rande JL, Unterseeh T, Le Breton H, Beard T, Blanchard D, Grollier G, Malquarti V, Staat P, Sudre A, Elmer E, Hansson MJ, Bergerot C, Boussaha I, Jossan C, Derumeaux G, Mewton N and Ovize M. Cyclosporine before PCI in patients with acute myocardial infarction. *N Engl J Med*. 2015;373:1021-31.

217. Kandasamy AD, Chow AK, Ali MAM and Schulz R. Matrix metalloproteinase-2 and myocardial oxidative stress injury: beyond the matrix. *Cardiovasc Res*. 2010;85:413-423.

218. Hughes BG and Schulz R. Targeting MMP-2 to treat ischemic heart injury. *Basic Res Cardiol*. 2014;109:424.

219. Quick AP, Landstrom AP, Wang Q, Beavers DL, Reynolds JO, Barreto-Torres G, Tran V, Showell J, Philippen LE, Morris SA, Skapura D, Bos JM, Pedersen SE, Pautler RG, Ackerman MJ and Wehrens XH. Novel junctophilin-2 mutation A405S is associated with basal septal hypertrophy and diastolic dysfunction. *JACC Basic Transl Sci*. 2017;2:56-67.

220. Unverferth B, Magorien R, Balcerzak S, Leier C and Unverferth D. Early changes in human myocardial nuclei after doxorubicin. *Cancer*. 1983;52:215-221.

221. Myers C, Bonow R, Palmeri S, Jenkins J, Corden B, Locker G, Doroshow J and Epstein S. A randomized controlled trial assessing the prevention of doxorubicin cardiomyopathy by N-acetylcysteine. *Semin Oncol*. 1983;10:53-5.

222. Martin E, Thougaard AV, Grauslund M, Jensen PB, Bjorkling F, Hasinoff BB, Tjornelund J, Sehested M and Jensen LH. Evaluation of the topoisomerase II-inactive bisdioxopiperazine ICRF-161 as a protectant against doxorubicin-induced cardiomyopathy. *Toxicology*. 2009;255:72-9.

223. Herman EH, Zhang J, Rifai N, Lipshultz SE, Hasinoff BB, Chadwick DP, Knapton A, Chai J and Ferrans VJ. The use of serum levels of cardiac troponin T to compare the protective activity of dexrazoxane against doxorubicin- and mitoxantrone-induced cardiotoxicity. *Cancer Chemother Pharmacol*. 2001;48:297-304.

224. Ichikawa Y, Ghanefar M, Bayeva M, Wu R, Khechaduri A, Naga Prasad SV, Mutharasan RK, Naik TJ and Ardehali H. Cardiotoxicity of doxorubicin is mediated through mitochondrial iron accumulation. *J Clin Invest*. 2014;124:617-30.

225. Green PS and Leeuwenburgh C. Mitochondrial dysfunction is an early indicator of doxorubicin-induced apoptosis. *Biochim Biophys Acta*. 2002;1588:94-101.

226. Bai P, Mabley JG, Liaudet L, Virag L, Szabó C and Pacher P. Matrix metalloproteinase activation is an early event in doxorubicin-induced cardiotoxicity. *Oncol Rep*. 2004;11:505-8.

227. Peterson JT, Hallak H, Johnson L, Li H, O'Brien PM, Sliskovic DR, Bocan TM, Coker ML, Etoh T and Spinale FG. Matrix metalloproteinase inhibition attenuates left ventricular remodeling and dysfunction in a rat model of progressive heart failure. *Circulation*. 2001;103:2303-9.

228. Spinale F. Matrix metalloproteinases: regulation and dysregulation in the failing heart. *Circ Res*. 2002;90:520-530.

229. DeCoux A, Lindsey ML, Villarreal F, Garcia RA and Schulz R. Myocardial matrix metalloproteinase-2: inside out and upside down. *J Mol Cell Cardiol*. 2014;77:64-72.

230. Bergman MR, Teerlink JR, Mahimkar R, Li L, Zhu BQ, Nguyen A, Dahi S, Karliner JS and Lovett DH. Cardiac matrix metalloproteinase-2 expression independently induces marked ventricular remodeling and systolic dysfunction. *Am J Physiol Heart Circ Physiol*. 2007;292:H1847-60.

231. Lovett DH, Mahimkar R, Raffai RL, Cape L, Zhu BQ, Jin ZQ, Baker AJ and Karliner JS. N-terminal truncated intracellular matrix metalloproteinase-2 induces cardiomyocyte hypertrophy, inflammation and systolic heart failure. *PLoS One*. 2013;8:e68154.

232. Dodd DA, Atkinson JB, Olson RD, Buck S, Cusack BJ, Fleischer S and Boucek RJ, Jr. Doxorubicin cardiomyopathy is associated with a decrease in calcium release channel of the sarcoplasmic reticulum in a chronic rabbit model. *J Clin Invest*. 1993;91:1697-705.

233. Kim SY, Kim SJ, Kim BJ, Rah SY, Chung SM, Im MJ and Kim U. Doxorubicin-induced reactive oxygen species generation and intracellular Ca^{2+} increase are reciprocally modulated in rat cardiomyocytes. *Exp Mol Med*. 2006;38:535-45.

234. Maeda A, Honda M, Kuramochi T and Takabatake T. Doxorubicin cardiotoxicity: diastolic cardiac myocyte dysfunction as a result of impaired calcium handling in isolated cardiac myocytes. *Jpn Circ J*. 1998;62:505-11.

235. Keung EC, Toll L, Ellis M and Jensen RA. L-type cardiac calcium channels in doxorubicin cardiomyopathy in rats morphological, biochemical, and functional correlations. *J Clin Invest*. 1991;87:2108-13.

236. Stammers AN, Susser SE, Hamm NC, Hlynsky MW, Kimber DE, Kehler DS and Duhamel TA. The regulation of sarco(endo)plasmic reticulum calcium-ATPases (SERCA). *Can J Physiol Pharmacol*. 2015;93:843-54.

237. MacLennan DH and Kranias EG. Phospholamban: a crucial regulator of cardiac contractility. *Nat Rev Mol Cell Biol*. 2003;4:566-77.

238. Baghirova S, Hughes BG, Poirier M, Kondo MY and Schulz R. Nuclear matrix metalloproteinase-2 in the cardiomyocyte and the ischemic-reperfused heart. *J Mol Cell Cardiol*. 2016;94:153-161.

239. Chow AK, Cena J, El-Yazbi AF, Crawford BD, Holt A, Cho WJ, Daniel EE and Schulz R. Caveolin-1 inhibits matrix metalloproteinase-2 activity in the heart. *J Mol Cell Cardiol*. 2007;42:896-901.

240. Hausladen A and Fridovich I. Superoxide and peroxynitrite inactivate aconitases, but nitric oxide does not. *J Biol Chem*. 1994;269:29405-8.

241. Csont T, Viappiani S, Sawicka J, Slee S, Altarejos JY, Batinić-Haberle I and Schulz R. The involvement of superoxide and iNOS-derived NO in cardiac dysfunction induced by pro-inflammatory cytokines. *J Mol Cell Cardiol*. 2005;39:833-840.

242. Greene RF, Collins JM, Jenkins JF, Speyer JL and Myers CE. Plasma pharmacokinetics of adriamycin and adriamycinol: implications for the design of in vitro experiments and treatment protocols. *Cancer Res*. 1983;43:3417-21.

243. Weinstein DM, Mihm MJ and Bauer JA. Cardiac peroxynitrite formation and left ventricular dysfunction following doxorubicin treatment in mice. *J Pharmacol Exp Ther*. 2000;294:396-401.

244. Octavia Y, Tocchetti CG, Gabrielson KL, Janssens S, Crijns HJ and Moens AL. Doxorubicin-induced cardiomyopathy: from molecular mechanisms to therapeutic strategies. *J Mol Cell Cardiol*. 2012;52:1213-25.

245. Aryal B, Jeong J and Rao VA. Doxorubicin-induced carbonylation and degradation of cardiac myosin binding protein C promote cardiotoxicity. *Proc Natl Acad Sci USA*. 2014;111:2011-6.

246. Lovett DH, Chu C, Wang G, Ratcliffe MB and Baker AJ. A N-terminal truncated intracellular isoform of matrix metalloproteinase-2 impairs contractility of mouse myocardium. *Front Physiol*. 2014;5:363.

247. Leco KJ, Apte SS, Taniguchi GT, Hawkes SP, Khokha R, Schultz GA and Edwards DR. Murine tissue inhibitor of metalloproteinases-4 (*Timp*-4): cDNA isolation and expression in

adult mouse tissues. *FEBS Lett*. 1997;401:213-7.

248. Gilchrist JS, Cook T, Abrenica B, Rashidkhani B and Pierce GN. Extensive autolytic fragmentation of membranous versus cytosolic calpain following myocardial ischemia-reperfusion. *Can J Physiol Pharmacol*. 2010;88:584-94.

249. Singh RB, Chohan PK, Dhalla NS and Netticadan T. The sarcoplasmic reticulum proteins are targets for calpain action in the ischemic-reperfused heart. *J Mol Cell Cardiol*. 2004;37:101-10.

250. Ascensao A, Lumini-Oliveira J, Machado NG, Ferreira RM, Goncalves IO, Moreira AC, Marques F, Sardao VA, Oliveira PJ and Magalhaes J. Acute exercise protects against calcium-induced cardiac mitochondrial permeability transition pore opening in doxorubicin-treated rats. *Clinical Sci*. 2011;120:37-49.

251. Smith LA, Cornelius VR, Plummer CJ, Levitt G, Verrill M, Canney P and Jones A. Cardiotoxicity of anthracycline agents for the treatment of cancer: systematic review and meta-analysis of randomised controlled trials. *BMC Cancer*. 2010;10:337.

252. Rodriguez D, Morrison CJ and Overall CM. Matrix metalloproteinases: what do they not do? New substrates and biological roles identified by murine models and proteomics. *Biochim Biophys Acta*. 2010;1803:39-54.

253. Neagoe C, Kulke M, del Monte F, Gwathmey JK, de Tombe PP, Hajjar RJ and Linke WA. Titin Isoform Switch in Ischemic Human Heart Disease. *Circulation*. 2002;106:1333-1341.

254. Chan BYH, Roczkowsky A, Moser N, Poirier M, Hughes BG, Ilarraza R and Schulz R. Doxorubicin induces de novo expression of N-terminal-truncated matrix metalloproteinase-2 in cardiac myocytes. *Can J Physiol Pharmacol*. 2018;96:1238-1245.

255. Moulin M, Piquereau J, Mateo P, Fortin D, Rucker-Martin C, Gressette M, Lefebvre F, Gresikova M, Solgadi A, Veksler V, Garnier A and Ventura-Clapier R. Sexual dimorphism of doxorubicin-mediated cardiotoxicity: potential role of energy metabolism remodeling. *Circ Heart Fail*. 2015;8:98-108.

256. Barpe DR, Rosa DD and Froehlich PE. Pharmacokinetic evaluation of doxorubicin plasma levels in normal and overweight patients with breast cancer and simulation of dose adjustment by different indexes of body mass. *Eur J Pharm Sci*. 2010;41:458-63.

257. Johansen PB. Doxorubicin pharmacokinetics after intravenous and intraperitoneal administration in the nude mouse. *Cancer Chemother Pharmacol*. 1981;5:267-70.

258. Castro MM, Rizzi E, Figueiredo-Lopes L, Fernandes K, Bendhack LM, Pitol DL, Gerlach RF and Tanus-Santos JE. Metalloproteinase inhibition ameliorates hypertension and prevents vascular dysfunction and remodeling in renovascular hypertensive rats. *Atherosclerosis*. 2008;198:320-31.

259. Hariya A, Takazawa K, Yamamoto T and Amano A. ONO-4817, a novel matrix

metalloproteinase inhibitor, attenuates allograft vasculopathy in a rat cardiac transplant. *J Heart Lung Transplant*. 2004;23:1163-9.

260. Naito Y, Takagi T, Kuroda M, Katada K, Ichikawa H, Kokura S, Yoshida N, Okanoue T and Yoshikawa T. An orally active matrix metalloproteinase inhibitor, ONO-4817, reduces dextran sulfate sodium-induced colitis in mice. *Inflamm Res*. 2004;53:462-8.

261. Yaras N, Sariahmetoglu M, Bilginoglu A, Aydemir-Koksoy A, Onay-Besikci A, Turan B and Schulz R. Protective action of doxycycline against diabetic cardiomyopathy in rats. *Br J Pharmacol*. 2008;155:1174-84.

262. Kim SS, Shin N, Bae SS, Lee MY, Rhee H, Kim IY, Seong EY, Lee DW, Lee SB, Kwak IS, Lovett DH and Song SH. Enhanced expression of two discrete isoforms of matrix metalloproteinase-2 in experimental and human diabetic nephropathy. *PLoS One*. 2017;12:e0171625.

263. Joshi SK, Lee L, Lovett DH, Kang H, Kim HT, Delgado C and Liu X. Novel intracellular N-terminal truncated matrix metalloproteinase-2 isoform in skeletal muscle ischemia-reperfusion injury. *J Orthop Res*. 2015;34:502-509.

264. Khiati S, Dalla Rosa I, Sourbier C, Ma X, Rao VA, Neckers LM, Zhang H and Pommier Y. Mitochondrial topoisomerase I (Top1mt) is a novel limiting factor of doxorubicin cardiotoxicity. *Clin Cancer Res*. 2014;20:4873-81.

265. Cohn JN, Ferrari R and Sharpe N. Cardiac remodeling--concepts and clinical implications: a consensus paper from an international forum on cardiac remodeling. *J Am Coll Cardiol*. 2000;35:569-82.

266. Lai HC, Yeh YC, Ting CT, Lee WL, Lee HW, Wang LC, Wang KY, Lai HC, Wu A and Liu TJ. Doxycycline suppresses doxorubicin-induced oxidative stress and cellular apoptosis in mouse hearts. *Eur J Pharmacol*. 2010;644:176-187.

267. Ma Y, Zhang X, Bao H, Mi S, Cai W, Yan H, Wang Q, Wang Z, Yan J, Fan GC, Lindsey ML and Hu Z. Toll-like receptor (TLR) 2 and TLR4 differentially regulate doxorubicin induced cardiomyopathy in mice. *PLoS One*. 2012;7:e40763.

268. Cleutjens JP, Kandala JC, Guarda E, Guntaka RV and Weber KT. Regulation of collagen degradation in the rat myocardium after infarction. *J Mol Cell Cardiol*. 1995;27:1281-92.

269. Ali MAM, Fan F and Schulz R. Cardiac sarcomeric proteins: novel intracellular targets of matrix metalloproteinase-2 in heart disease. *Trends Cardiovasc Med*. 2011;21:112-8.

270. Munkanatta Godage DNP, VanHecke GC, Samarasinghe KTG, Feng HZ, Hiske M, Holcomb J, Yang Z, Jin JP, Chung CS and Ahn YH. SMYD2 glutathionylation contributes to degradation of sarcomeric proteins. *Nat Commun*. 2018;9:4341.

271. Flashman E, Redwood C, Moolman-Smook J and Watkins H. Cardiac myosin binding protein C: its role in physiology and disease. *Circ Res*. 2004;94:1279-89.

272. Romero-Perez D, Fricovsky E, Yamasaki KG, Griffin M, Barraza-Hidalgo M, Dillmann W and Villarreal F. Cardiac uptake of minocycline and mechanisms for in vivo cardioprotection. *J Am Coll Cardiol*. 2008;52:1086-94.

273. Louch WE, Ferrier GR and Howlett SE. Changes in excitation-contraction coupling in an isolated ventricular myocyte model of cardiac stunning. *Am J Physiol Heart Circ Physiol*. 2002;283:H800-10.

274. Landstrom AP, Kellen CA, Dixit SS, van Oort RJ, Garbino A, Weisleder N, Ma J, Wehrens XH and Ackerman MJ. Junctophilin-2 expression silencing causes cardiocyte hypertrophy and abnormal intracellular calcium-handling. *Circ Heart Fail*. 2011;4:214-23.

275. Minamisawa S, Oshikawa J, Takeshima H, Hoshijima M, Wang Y, Chien KR, Ishikawa Y and Matsuoka R. Junctophilin type 2 is associated with caveolin-3 and is down-regulated in the hypertrophic and dilated cardiomyopathies. *Biochem Biophys Res Commun*. 2004;325:852-6.

276. Wagner E, Lauterbach MA, Kohl T, Westphal V, Williams GS, Steinbrecher JH, Streich JH, Korff B, Tuan HT, Hagen B, Luther S, Hasenfuss G, Parlitz U, Jafri MS, Hell SW, Lederer WJ and Lehnart SE. Stimulated emission depletion live-cell super-resolution imaging shows proliferative remodeling of T-tubule membrane structures after myocardial infarction. *Circ Res*. 2012;111:402-14.

277. Woo JS, Hwang JH, Ko JK, Weisleder N, Kim DH, Ma J and Lee EH. S165F mutation of junctophilin 2 affects Ca^{2+} signalling in skeletal muscle. *Biochem J*. 2010;427:125-34.

278. Hadler-Olsen E, Solli AI, Hafstad A, Winberg JO and Uhlin-Hansen L. Intracellular MMP-2 activity in skeletal muscle is associated with type II fibers. *J Cell Physiol*. 2015;230:160-9.

279. Itoh Y, Binner S and Nagase H. Steps involved in activation of the complex of pro-matrix metalloproteinase 2 (progelatinase A) and tissue inhibitor of metalloproteinases (TIMP)-2 by 4-aminophenylmercuric acetate. *Biochem J*. 1995;308 (Pt 2):645-51.

280. Kumar S, Ratnikov BI, Kazanov MD, Smith JW and Cieplak P. CleavPredict: a platform for reasoning about matrix metalloproteinases proteolytic events. *PLoS One*. 2015;10:e0127877.

281. Eckhard U, Huesgen PF, Schilling O, Bellac CL, Butler GS, Cox JH, Dufour A, Goebeler V, Kappelhoff R, Keller UAD, Klein T, Lange PF, Marino G, Morrison CJ, Prudova A, Rodriguez D, Starr AE, Wang Y and Overall CM. Active site specificity profiling of the matrix metalloproteinase family: proteomic identification of 4300 cleavage sites by nine MMPs explored with structural and synthetic peptide cleavage analyses. *Matrix Biol*. 2016;49:37-60.

282. Wu HD, Xu M, Li RC, Guo L, Lai YS, Xu SM, Li SF, Lu QL, Li LL, Zhang HB, Zhang YY, Zhang CM and Wang SQ. Ultrastructural remodelling of Ca^{2+} signalling apparatus in failing heart cells. *Cardiovasc Res*. 2012;95:430-8.

283. Roth GA, Johnson C, Abajobir A, Abd-Allah F, Abera SF, Abyu G, Ahmed M, Aksut B, Alam T, Alam K, Alla F, Alvis-Guzman N, Amrock S, Ansari H, Arnlov J, Asayesh H, Atey TM, Avila-Burgos L, Awasthi A, Banerjee A, Barac A, Barnighausen T, Barregard L, Bedi N, Belay Ketema E, Bennett D, Berhe G, Bhutta Z, Bitew S, Carapetis J, Carrero JJ, Malta DC, Castaneda-Orjuela CA, Castillo-Rivas J, Catala-Lopez F, Choi JY, Christensen H, Cirillo M, Cooper L, Jr., Criqui M, Cundiff D, Damasceno A, Dandona L, Dandona R, Davletov K, Dharmaratne S, Dorairaj P, Dubey M, Ehrenkranz R, El Sayed Zaki M, Faraon EJA, Esteghamati A, Farid T, Farvid M, Feigin V, Ding EL, Fowkes G, Gebrehiwot T, Gillum R, Gold A, Gona P, Gupta R, Habtewold TD, Hafezi-Nejad N, Hailu T, Hailu GB, Hankey G, Hassen HY, Abate KH, Havmoeller R, Hay SI, Horino M, Hotez PJ, Jacobsen K, James S, Javanbakht M, Jeemon P, John D, Jonas J, Kalkonde Y, Karimkhani C, Kasaeian A, Khader Y, Khan A, Khang YH, Khera S, Khoja AT, Khubchandani J, Kim D, Kolte D, Kosen S, Krohn KJ, Kumar GA, Kwan GF, Lal DK, Larsson A, Linn S, Lopez A, Lotufo PA, El Razek HMA, Malekzadeh R, Mazidi M, Meier T, Meles KG, Mensah G, Meretoja A, Mezgebe H, Miller T, Mirrakhimov E, Mohammed S, Moran AE, Musa KI, Narula J, Neal B, Ngalesoni F, Nguyen G, Obermeyer CM, Owolabi M, Patton G, Pedro J, Qato D, Qorbani M, Rahimi K, Rai RK, Rawaf S, Ribeiro A, Safiri S, Salomon JA, Santos I, Santric Milicevic M, Sartorius B, Schutte A, Sepanlou S, Shaikh MA, Shin MJ, Shishehbor M, Shore H, Silva DAS, Sobngwi E, Stranges S, Swaminathan S, Tabares-Seisdedos R, Tadele Atnafu N, Tesfay F, Thakur JS, Thrift A, Topor-Madry R, Truelsen T, Tyrovolas S, Ukwaja KN, Uthman O, Vasankari T, Vlassov V, Vollset SE, Wakayo T, Watkins D, Weintraub R, Werdecker A, Westerman R, Wiysonge CS, Wolfe C, Workicho A, Xu G, Yano Y, Yip P, Yonemoto N, Younis M, Yu C, Vos T, Naghavi M and Murray C. Global, regional, and national burden of cardiovascular diseases for 10 causes, 1990 to 2015. *J Am Coll Cardiol*. 2017;70:1-25.

284. Collaborators GMaCoD. Global, regional, and national age-sex specific all-cause and cause-specific mortality for 240 causes of death, 1990-2013: a systematic analysis for the global burden of disease study 2013. *Lancet*. 2015;385:117-71.

285. Knaul FM, Arreola-Ornelas H, Méndez O, Alsan M, Seinfeld J, Marx A and Atun R. The global economics burden of cancer. In: B. W. Stewart and C. P. Wild, eds. *World Cancer Report 2014* Lyon: World Health Organization; 2014: 576-82.

286. Bloom DE, Cafiero ET, Jané-Llopis E, Abrahams-Gessel S, Bloom LR, Fathima S, Feigl AB, Gaziano T, Mowafi M, Pandya A, Prettner K, Rosenberg L, Seligman B, Stein AZ and Weinstein C. The global economic burden of noncommunicable diseases. 2011:1-48.

287. Gorlach A, Bertram K, Hudecova S and Krizanova O. Calcium and ROS: a mutual interplay. *Redox Biol*. 2015;6:260-71.

288. Smith MA and Reid MB. Redox modulation of contractile function in respiratory and limb skeletal muscle. *Respir Physiol Neurobiol*. 2006;151:229-41.

289. Ai HW, Hazelwood KL, Davidson MW and Campbell RE. Fluorescent protein FRET pairs for ratiometric imaging of dual biosensors. *Nat Methods*. 2008;5:401-3.

290. Peter AK, Bjerke MA and Leinwand LA. Biology of the cardiac myocyte in heart disease. *Mol Biol Cell*. 2016;27:2149-60.

291. Hunkeler NM, Kullman J and Murphy AM. Troponin I isoform expression in human heart. *Circ Res*. 1991;69:1409-14.

292. Murphy AM, Jones L, 2nd, Sims HF and Strauss AW. Molecular cloning of rat cardiac troponin I and analysis of troponin I isoform expression in developing rat heart. *Biochemistry*. 1991;30:707-12.

293. Arenas IA, Xu Y, Lopez-Jaramillo P and Davidge ST. Angiotensin II-induced MMP-2 release from endothelial cells is mediated by TNF-α. *Am J Physiol Cell Physiol*. 2004;286:C779-84.

294. Fearon K, Strasser F, Anker SD, Bosaeus I, Bruera E, Fainsinger RL, Jatoi A, Loprinzi C, MacDonald N, Mantovani G, Davis M, Muscaritoli M, Ottery F, Radbruch L, Ravasco P, Walsh D, Wilcock A, Kaasa S and Baracos VE. Definition and classification of cancer cachexia: an international consensus. *Lancet Oncol*. 2011;12:489-95.

295. Murphy KT. The pathogenesis and treatment of cardiac atrophy in cancer cachexia. *Am J Physiol Heart Circ Physiol*. 2016;310:H466-77.

296. Zhang Y, Chen Y, Zhang M, Tang Y, Xie Y, Huang X and Li Y. Doxorubicin induces sarcoplasmic reticulum calcium regulation dysfunction via the decrease of SERCA2 and phospholamban expressions in rats. *Cell Biochem Biophys*. 2014;70:1791-1798.

297. Octavia Y, Tocchetti CG, Gabrielson KL, Janssens S, Crijns HJ and Moens AL. Doxorubicin-induced cardiomyopathy: from molecular mechanisms to therapeutic strategies. *J Mol Cell Cardiol*. 2012;52:1213-25.

298. Solcia E, Ballerini L, Bellini O, Magrini U, Bertazzoli C, Tosana G, Sala L, Balconi F and Rallo F. Cardiomyopathy of doxorubicin in experimental animals, factors affecting the severity, distribution and evolution of myocardial lesions. *Tumori*. 1981;67:461-72.

299. Llach A, Mazevet M, Mateo P, Villejouvert O, Ridoux A, Rucker-Martin C, Ribeiro M, Fischmeister R, Crozatier B, Benitah JP, Morel E and Gomez AM. Progression of excitation-contraction coupling defects in doxorubicin cardiotoxicity. *J Mol Cell Cardiol*. 2019;126:129-139.

300. Takemura G and Fujiwara H. Doxorubicin-induced cardiomyopathy from the cardiotoxic mechanisms to management. *Prog Cardiovasc Dis*. 2007;49:330-52.

APPENDIX

A1.1 Introduction

In anthracycline cardiotoxicity, oxidative stress activates intracellular proteases including calpains[129] and MMP-2[254] within cardiomyocytes. In Chapter 4, JPH-2 was identified as a substrate of MMP-2 and its degradation was associated with reduced contractile function in myocardial IR injury. Proteolytic cleavage of JPH-2 reduces myocardial contractility by impairing intracellular calcium homeostasis involving disruptions the junction between the T-tubules and sarcoplasmic reticulum in cardiomyocytes[134]. Similarly, DXR causes T-tubule distention[162, 297, 298] and reduced calcium transients[173, 234], thereby impairing cardiomyocyte contraction. DXR-induced alterations in intracellular calcium homeostasis within cardiomyocytes precedes the onset of myocardial dysfunction[299]. Thus, understanding the mechanisms of impaired calcium handling is essential for understanding the development of DXR cardiotoxicity. Interestingly, JPH-2 proteolysis has not been investigated in DXR cardiotoxicity.

In this preliminary study, I determined whether JPH-2 proteolysis is implicated in DXR-induced cardiomyocyte injury and whether it is preventable by MMP inhibitors.

A1.2 Methods

A1.2.1 Cell culture

NRVM were isolated as per Section 2.2.1 and treated with MMP inhibitors ARP-100 or ONO-4817 (1 μM each) as per Section 2.2.3.

A1.2.2 Western blot analysis

Cell lysate samples (5 μg protein each) were diluted in 6x Laemmli buffer and in RIPA buffer to a final volume of 20 μL. Samples were heat denatured at 95°C for 5 min and separated

on 8% polyacrylamide gels by electrophoresis at 100 V for 80 min. Proteins were wet transferred onto PVDF membranes and blocked as per Section 2.2.8. PVDF membranes were then immunoblotted with rabbit anti-JPH-2 (1:2000, #40-5300, ThermoFisher Scientific) overnight at 4°C. Loading controls were conducted by splitting PVDF membranes to immunoblot for GAPDH (1:15000, 2118S, Cell Signaling Technology, Danvers, MA) overnight at 4°C. PVDF membranes were incubated with secondary antibodies as per Section 2.2.8. Protein bands were visualized using chemiluminescent detection reagent Clarity ECL western substrate (Bio-Rad) and exposed to autoradiography film. Films were developed using an Optimax X-Ray film processor and scanned with a Bio-Rad GS-800 densitometer. Bands were then quantified on ImageJ.

A1.3 Results

A1.3.1 MMP inhibitors prevent DXR-induced loss of JPH-2 in NRVM

JPH-2 protein levels were measured by western blot in control and DXR-treated NRVM treated with or without ARP-100 or ONO-4817. 24 hr DXR treatment reduced 97 kDa JPH-2 protein levels in NRVM lysates by ~50% compared to control (Fig. A1.1). ARP-100 and ONO-4817 prevented DXR-induced loss of JPH-2 in NRVM. No potential lower molecular weight JPH-2 degradation products were detected, at least under this exposure.

A1.4 Discussion

Anthracycline-induced cardiomyopathy is associated with myocardial ultrastructural changes including swelling of T-tubules and the sarcoplasmic reticulum[300]. These ultrastructural alterations are accompanied with defective excitation-contraction coupling in anthracycline cardiotoxicity[299]. Cardiomyocytes isolated from rats subjected to chronic DXR treatment exhibited

increased peak L-type calcium current compared to control[235]. L-type calcium current plays a key role in calcium-induced calcium release from the sarcoplasmic reticulum. Increased calcium influx through the activation of dormant L-type calcium channels was suggested to be a protective mechanism to compensate for the partial loss of the T-tubular system[235]. Despite a larger calcium influx, DXR dampened calcium transients and reduced cardiomyocyte contractility[234]. Defective calcium-induced calcium release may be attributed to damage to the junctional membrane complex between the T-tubule and the sarcoplasmic reticulum[235]. Accordingly, my preliminary finding suggests that reduced JPH-2 levels may contribute to DXR-induced impaired intracellular calcium homeostasis in cardiomyocytes. The protective effect of ARP-100 and ONO-4817 suggest that MMPs may be involved in the loss of JPH-2. Further investigation is needed to fully elucidate the potential role of MMP-2 in impaired intracellular calcium handling in DXR-induced cardiomyocyte injury.

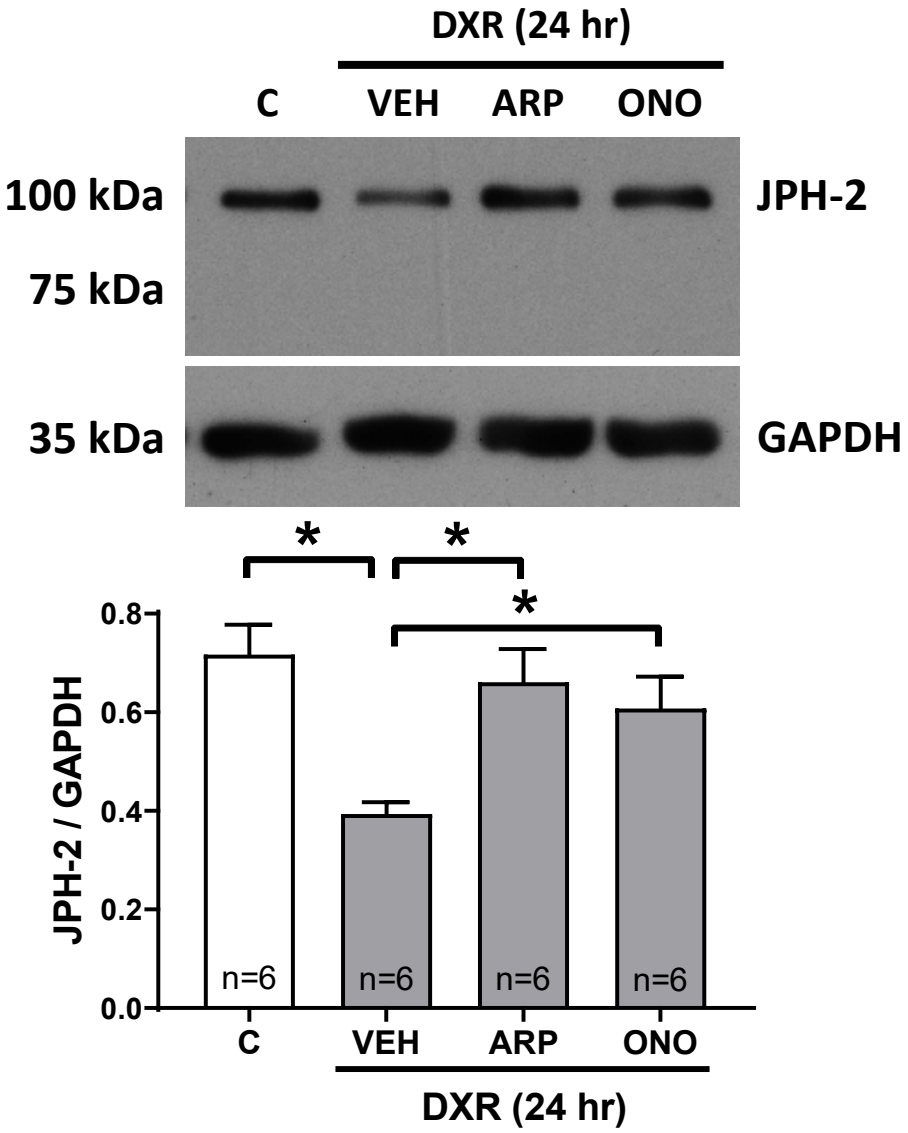

Figure A1.1: MMP inhibitors prevent DXR-induced loss of JPH-2 in NRVM. DXR reduced the levels of JPH-2 in NRVM, an effect that was prevented by ARP-100 and ONO-4817 (n=6). Bar graphs represent mean ± S.E.M. * $p<0.05$ by one-way ANOVA followed by Tukey's post hoc test.

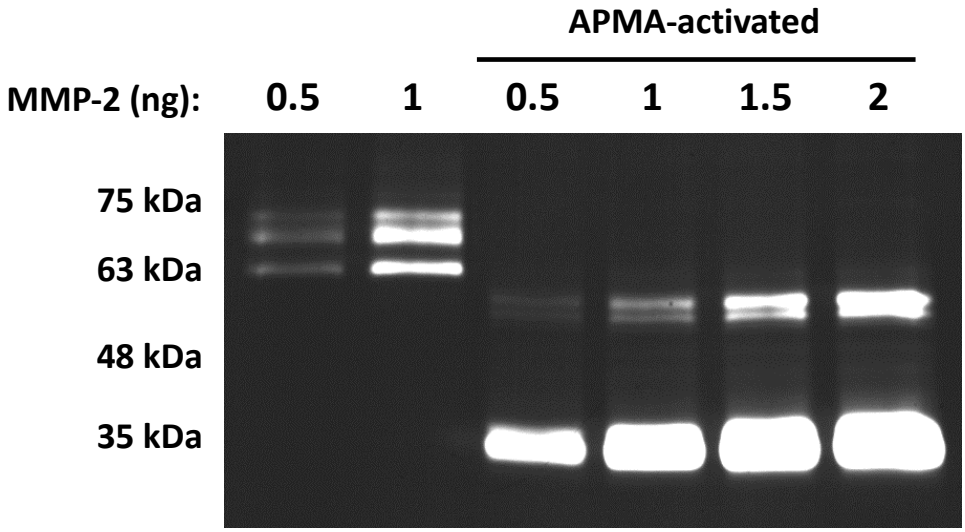

Figure A1.2: APMA activation of purified human MMP-2. MMP-2 activity was assessed by gelatin zymography. APMA causes 72 and 64 kDa MMP-2 to autoproteolyze, resulting in a ~55 kDa intermediate MMP-2 product and the 35 kDa MMP-2 catalytic domain.

GEL ELECTROPHORESIS SOLUTIONS

Western blot

6x Laemmli buffer: 0.25 M Tris (pH 6.8), 30% (v/v) glycerol, 10% (w/v) sodium dodecyl sulfate, 0.6 M dithiothreitol, and 0.012% (w/v) bromophenol blue.

Towbin buffer: 20% (v/v) methanol, 25 mM Tris, 192 mM glycine, and 0.005% (w/v) sodium dodecyl sulfate.

TBS-T: 0.1 M NaCl, 0.01 M Tris, pH 7.6, and 0.1% (v/v) Tween

Gelatin zymography

Nonreducing loading buffer: 0.5 M Tris (pH 6.8), 30% (v/v) glycerol, 10% (w/v) sodium dodecyl sulfate, and 0.012 % (w/v) bromophenol blue.

Zymography incubation buffer: 50 mM Tris, pH 7.6, 150 mM NaCl, 5 mM $CaCl_2$, and 0.05% (w/v) NaN_3.

Coomassie zymography staining solution: 0.05% (w/v) Coomassie Brilliant Blue G-250, 25% (v/v) methanol, 10% (v/v) acetic acid.

Agarose gels for titin analysis

5x electrophoresis running buffer: 0.25 M Tris-base, 1.92 M glycine, and 0.5% (w/v) sodium dodecyl sulfate

SDS-PAGE GELS

Tris-glycine SDS-PAGE 8% separating gel (prepares one 1.5 mm thick gel)

Solution	Volume (mL)
40% (w/v) acrylamide / 3.3% (w/v) bis-acrylamide 29:1	1.50
0.5 M Tris / 0.4% (w/v) SDS, pH 6.8	1.875
H_2O	4.125
10% (w/v) ammonium persulfate	0.025
Tetramethylethylenediamine (TEMED)	0.005

Tris-tricine SDS-PAGE 16% separating gel (prepares one 1.5 mm thick gel)

Solution	Volume (mL)
46.5% (w/v) acrylamide / 3% (w/v) bis-acrylamide	3.300
3 M Tris / 3% (w/v) SDS, pH 8.45	3.750
glycerol	1.000
H_2O	2.400
10% (w/v) ammonium persulfate	0.033
TEMED	0.004

Tris-tricine SDS-PAGE 10% spacing layer (prepares one 1.5 mm thick gel)

Solution	Volume (mL)
48% (w/v) acrylamide / 1.5% (w/v) bis-acrylamide	1.000
3 M Tris / 3% (w/v) SDS, pH 8.45	1.650
H_2O	2.350
10% (w/v) ammonium persulfate	0.025
TEMED	0.003

Tris-tricine SDS-PAGE 4% stacking layer (prepares one 1.5 mm thick gel)

Solution	Volume (mL)
48% (w/v) acrylamide / 1.5% (w/v) bis-acrylamide	0.330
3 M Tris / 3% (w/v) SDS, pH 8.45	1.000
H_2O	2.670
10% (w/v) ammonium persulfate	0.030
TEMED	0.003

Gelatin zymography 8% separating gel (prepares 1 0.75 mm thick gel)

Solution	Volume (mL)
40% (w/v) acrylamide / 3.3% (w/v) bis-acrylamide 29:1	3.00
0.5 M Tris / 0.4% (w/v) SDS, pH 6.8	3.75
gelatin (20 mg/mL)	1.50
H_2O	6.75
10% (w/v) ammonium persulfate	0.05
TEMED	0.01

AGAROSE GELS FOR TITIN ANALYSIS

12% acrylamide solution

Reagent	Volume
H_2O (mL)	3.89
30% acrylamide (mL)	4
5x electrophoresis running buffer (mL)	2
10% ammonium persulfate (µL)	100
TEMED (µL)	8.75

*Pour 4 mL acrylamide solution per gel

Agarose solution (prepares one 1.5 mm thick gel)

Reagent	Volume
Glycerol (mL)	15
5x electrophoresis running buffer (mL)	10
H_2O (mL)	25
Seakem Gold Agarose (g)	0.5
Final volume (mL)	50